2808914305

REFERENCE ONLY

UNIVERSITY OF LONDON THESIS

Degree PhD Year 2006 Name of Author GAVIOLI GIANCARLO

COPYRIGHT
This is a thesis accepted for a Higher Degree of the University of London. It is an unpublished typescript and the copyright is held by the author. All persons consulting the thesis must read and abide by the Copyright Declaration below.

COPYRIGHT DECLARATION
I recognise that the copyright of the above-described thesis rests with the author and that no quotation from it or information derived from it may be published without the prior written consent of the author.

LOANS
Theses may not be lent to individuals, but the Senate House Library may lend a copy to approved libraries within the United Kingdom, for consultation solely on the premises of those libraries. Application should be made to: Inter-Library Loans, Senate House Library, Senate House, Malet Street, London WC1E 7HU.

REPRODUCTION
University of London theses may not be reproduced without explicit written permission from the Senate House Library. Enquiries should be addressed to the Theses Section of the Library. Regulations concerning reproduction vary according to the date of acceptance of the thesis and are listed below as guidelines.

A. Before 1962. Permission granted only upon the prior written consent of the author. (The Senate House Library will provide addresses where possible).

B. 1962 - 1974. In many cases the author has agreed to permit copying upon completion of a Copyright Declaration.

C. 1975 - 1988. Most theses may be copied upon completion of a Copyright Declaration.

D. 1989 onwards. Most theses may be copied.

This thesis comes within category D.

☐ This copy has been deposited in the Library of UCL

☐ This copy has been deposited in the Senate House Library, Senate House, Malet Street, London WC1E 7HU.

C:\Documents and Settings\lproctor\Local Settings\Temporary Internet Files\OLK8\Copyright - thesis (2).doc

y
binders
965
s.com

Investigation of the regenerative and cascadability properties of optical signal processing devices at high bit-rates

Giancarlo Gavioli

A thesis submitted to the University of London for the degree of
Doctor of Philosophy (Ph.D.)

Department of Electronic and Electrical Engineering
University College London
February 2006

ProQuest LLC
789 East Eisenhower Parkway
P.O. Box 1346
Ann Arbor, MI 48106-1346

To my parents
and
to Elena

Abstract

This thesis investigates the use of Semiconductor Optical Amplifiers (SOA) for 10 and 40Gb/s all-optical 3R signal regeneration and wavelength conversion for application to advanced high-speed all-optical WDM networks.

Detailed experimental characterisation of the magnitude and the time scales of inter-band nonlinear effects in SOA is carried out. The regenerative properties of SOA gates are theoretically investigated and related to the SOA physical parameters by means of deriving the SOA gate transfer function.

A novel configuration for all-optical regeneration based on Polarisation Switching in an SOA-assisted Sagnac Interferometer (PSSI) is proposed and used to demonstrate, for the first time, multi-channel simultaneous 3R regeneration. This scheme allows to significantly enhance the switching frequency of the SOA, demonstrating error-free regeneration of 40Gb/s signal with long PRBS sequences using an SOA with carrier lifetime exceeding 250ps. The reshaping and retiming ability of the scheme are also assessed experimentally at bit-rate of 40Gb/s, to show the largest distortion tolerance range published to date for regeneration. The scheme is also used to demonstrate 40 to 10Gb/s demultiplexing.

The cascadability of optical regenerators and wavelength converters is also investigated experimentally. The impact of varying the inter-regenerator spacing in transmission with cascaded wavelength conversion and 3R regeneration over transoceanic distances, is experimentally investigated for the first time, using a novel reconfigurable fibre loop. These results show that a trade-off exists between the transmission signal Q-factor and the inter-regenerator spacing, which depends on the regenerator transfer function characteristics, and thus can be predicted from the SOA parameters. In 40Gb/s transmission with optical regeneration it was demonstrated that the use of an optical regenerator before the electrical receiver increases the power margin and maximum error-free transmission distance at 40Gb/s in excess of 100km.

Finally a novel concept for multi-channel wavelength conversion and regeneration is presented utilising an integrated SOA array in a novel configuration to demonstrate, for the first time, simultaneous regenerative wavelength conversion of 10Gb/s signals. This also shows the potential for large scale monolithic integration for optical processing applications in WDM networks.

Acknowledgements

First, I would like to thank my supervisor Prof. Polina Bayvel whose continuous guidance, encouragement and support were crucial for the progress of my work. I am very grateful to her for giving me the opportunity of working in a word-class research laboratory and for the unrestricted academic freedom she offered me.

I would like to thank Chris Park, Piero Gambini and Agilent technologies for providing the studentship which supported a significant part of this project.

I wish to thank Martin Zirngibl, Lucent Bell laboratories, for the valuable collaboration and for the many opportunities he gave me to visit his labs and to discuss my work with him and his colleagues. In particular, I would like to acknowledge Chris Doerr, for providing the SOA array used in the multi-wavelength optical processing experiments and K. Dreyer for providing the ultra-long SOA used in the 40Gb/s regeneration experiments.

I am very grateful to Prof. Juerg Leuthold (University of Karlsruhe) for very useful discussions which provided valuable inputs throughout the course of this project and for providing several SOAs for my experiments.

I would also like to thank Craig Tombling, Tony Kelley and Kamelian Ltd. for providing the SOAs used in the transmission with optical regeneration experiments and Alistair Poustie (CIP) for lending the mode-lock laser used in first SOA characterisation experiments.

I wish to thank all my friends and colleagues at UCL for their support during my postgraduate studies. In particular, I would like to thank Michael Düser for his constant encouragement and advice during my studies, Vitaly Mikhailov and Shamil Appathurai for contributing to this work through experimental advice and assistance in the laboratory, Benn Thomsen for the SOA characterisation experiments and for many interesting discussions on SOA nonlinearities, Christian Weber for his contributions to the SOA modelling results and Robert Killey for reading and correcting this thesis.

Finally, I would like to thank IEEE LEOS for the award of the 2005 Postgraduate Studentship.

Contents

List of figures

List of tables

Chapter 1 Introduction

The aim of this chapter is to introduce the concept of optical gates, their physical implementation and their applications in telecommunication networks.

Section (1.1) describes the physical characteristics of the telecommunication networks where optical gates are likely to be employed. This includes a brief overview on recent developments in high bit-rate transmission systems.

In section (1.2) the different candidate optical nonlinear materials for the implementation of optical gates are presented and compared. A particular attention, among the nonlinear optical material, will be given to SOA which are at the core of the research presented in this thesis.

The techniques proposed in literature to exploit the different nonlinearities in SOA are then discussed, and their performances compared.

In section (1.3) some potential applications for optical gates in transmission systems are described. In particular, the principles of operation of optical regeneration, demultiplexing and wavelength conversion are presented. Finally the motivations for the research presented in this thesis are summarised followed by the description of the thesis structure.

1.1 High bit-rate WDM RZ systems

It is well known that the telecommunications industry has experienced a remarkably constant increase in the demand for capacity.

Today's state-of-the-art transmission networks operate with electronic switching systems, interconnected by optical fibre links, where the fibre loss is overcome by optical amplification, up to a maximum capacity of 10Gb/s [Kei99]. Attention is now focused world-wide on the application and the deployment of optical multiplexing systems to further increase the transmission capacity toward the maximum transmission capacity of optical fibre. Indeed toward the end of this study, commercial wavelength division multiplexed systems at 40Gb/s per channel have become commercially available.

WDM (Wavelength Division Multiplexing) and OTDM (Optical Time Division Multiplexing) techniques have been proposed to increase the capacity of optical transmission system. In a WDM system, signals on different wavelengths are launched simultaneously into the optical fibre. In OTDM systems the signals are coded into a format comprising short RZ optical pulses (Return to Zero) which are interleaved in time. The appropriate time slot is used to identify each data signal. To increase the point-to-point capacity to terabit-per-second transmission, both multiplexing techniques have been utilised on the same fibre link [Ona96] [Gna96] [Mor96] [Chr98]. Transmission of up to 3Tb/s (19 channels x 160Gb/s) was demonstrated with WDM/OTDM multiplexing [Kav99].

The advantage of WDM is that it allows to fully exploit the wide bandwidth of the optical amplifiers and optical fibres. The advantage of using OTDM multiplexing on each WDM channel is to exceed the bit-rate per channel further beyond the highest available electronics processing speed; to date up to 1.28Tb/s per channel have been achieved with OTDM [Nak00] with respect to 80Gb/s for electrical multiplexing (ETDM) [Win05]. Furthermore OTDM employs RZ pulse coding which has been found to be most tolerant intensity modulation format to nonlinear distortion in fibre [Bre97]. Figure 1-1 shows a typical WDM/OTDM transmission system. The OTDM transmitter (TX) consists of a single source of short optical pulses replicated and modulated by the incoming data sequence and interleaved in time.

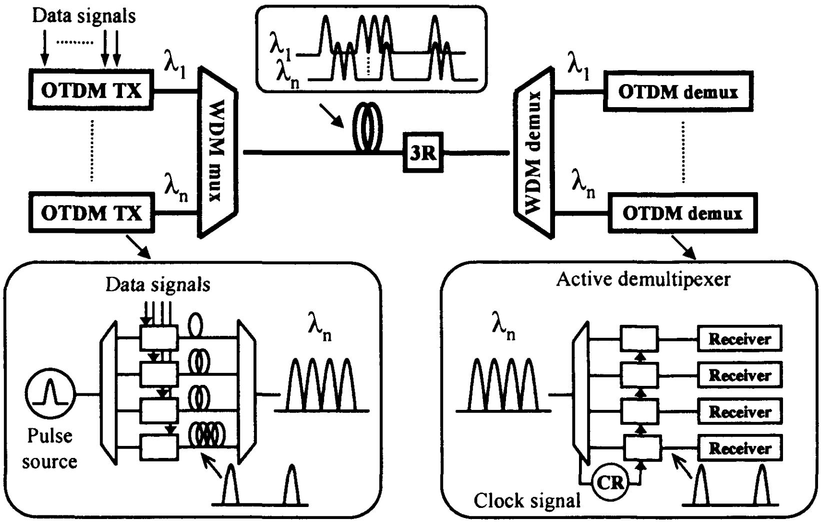

Figure 1-1 WDM OTDM transmission system block diagram

The OTDM signals are generated at different wavelength, passively multiplexed and routed along a single fibre. At the receiving terminal, wavelength selective passive optical components are used to demultiplex each individual wavelength which is then routed to an individual active OTDM demultiplexer prior to photo detection in the conventional manner. 3R (Re-timing Re-shaping and Re-amplification) regenerators are employed along the transmission line to suppress the distortion accumulated by the signal in fibre, allowing trans-oceanic transmission distances.

The success of future WDM/OTDM networks still depends on the development of practical technology to perform the various transmission functionalities. The enabling technologies for WDM systems were the development of the Erbium-Doped Fibre Amplifier (EDFA) and the invention of the phased array grating providing a practical wavelength multiplexer. Today EDFAs are designed to provide amplification exceeding 40dB with noise figures of 4-5dB. Gain-shifted EDFAs make the 1.57 to 1.60μm region also accessible [Mas90].

Key technologies needed for the current transition from WDM to WDM/OTDM system are short-pulse generation, dispersion-slope compensation, all-optical multiplexing and clock recovery from high-speed OTDMs [Ell97].

Several methods have been studied to generate short optical pulses (few picoseconds) that are synchronised with a master clock. Examples are mode-locked laser diode [Ray92], external modulation of continuous wave (CW) light by an electro-absorption modulator [Suz93], and harmonically mode locking of Er-doped fibre ring lasers [Tak90]. Dispersion-slope compensation techniques have become essential at the highest bit-rates, since dispersion and fibre-nonlinearity tolerances decrease with increasing bit-rates.

All-optical devices are necessary to perform the various bit-level processing on the aggregated signal which can not be performed electronically due to the bandwidth limitation. Among these functionalities are: time division demultiplexing, wavelength conversion, 3R regeneration and clock recovery.

All-optical processing devices are based on ultra-fast nonlinear effects in optical materials for switching at high frequencies. All-optical processing has several advantages over electrical processing; with the following recently demonstrated:

- Enables ultra-fast operations: All optical switching at 10GHz with 200fs switching window [Nak98a], 160Gb/s wavelength conversion [Leu05], 366:10Gb/s demultiplexing [Nak02] and 320Gb/s clock recovery [Boe05] have been demonstrated.

- A single all-optical device can perform multiple functionalities at ultra-fast bit-rate such as 3R regeneration with wavelength conversion and demultiplexing with clock recovery [Lud96] [Bux98].
- Enables the implementation of 3R regenerators beyond 40Gb/s [Kel99] [Leu05].
- All-optical processing has shown advanced optical logic functionalities at up to 100Gb/s [Ham02].
- Permits signal processing with storage functions [Pou97].
- All-optical devices allow simultaneous multiple wavelength optical processing; 3R regeneration, wavelength conversion and clock recovery [Gav04a] [Gav03c] [Mik01a].

In conclusion, WDM OTDM systems are already in an advanced experimental stage. Great effort has been dedicated in the development of optical components to perform the different OTDM functionalities at high bit-rates.

However, the performance of real transmission systems and networks employing optical gates for signal processing is yet to be investigated in detail.

This thesis presents novel devices for application to multi-channel signal 3R regeneration and wavelength conversion, novel techniques to characterisation their reshaping and switching performance at 40Gb/s and results from the investigation of their performance in realistic transmission scenarios.

1.2 All-optical devices

The classification of the different concepts used as the basis for all-optical signal processing is shown in Figure 1-2. Optical devices for signal processing can be distinguished with respect to their nonlinear material (optical fibre, SOAs, material with a strong second order nonlinearity χ^2), to the technique used to exploit the nonlinearities (Cross Phase Modulation "XPM", Cross Gain Modulation "XGM", Four-Wave Mixing "FWM", Different Frequency Generation "DFG") and to the configurations (fibre loops, interferometers, single SOA) which define the device functionality (3R regeneration, wavelength conversion, demultiplexing).

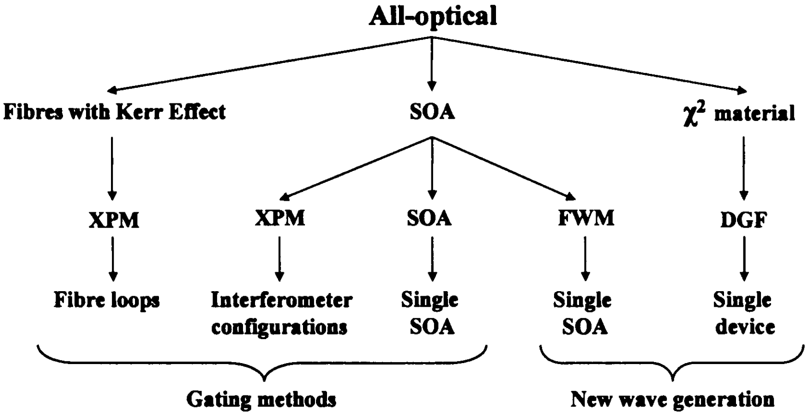

Figure 1-2 Classification of all optical concepts [Leu99]

In the following sections, the optical materials and techniques proposed to implement optical gates will be briefly reviewed.

1.2.1 Categories of nonlinear materials

In general, three different classes of material provide optical nonlinearities sufficient for all-optical processing operation: Optical fibres with Kerr effect, SOAs and materials with a strong second-order nonlinear susceptibility χ^2.

Nonlinear effects in optical fibre are due either to a change in the refractive index by intense light or scattering processes (Brillouin and Raman). The power dependence of the refractive index is of particular interest, since it can be exploited for switching in an interferometer configuration. Phenomena, where the refractive index changes Δn

are caused by an optical intensity I, are generally referred as Kerr effects and can be described by:

$$\Delta n = I \cdot n_2 \qquad (1\text{-}1)$$

with the second-order nonlinear refractive index n_2. Typical values of n_2 in non-dispersion-shifted single-mode fibres at 1.55μm are given in Table 1-1.

Kerr-based nonlinearities in fibres are extremely fast. However, it was recognized that the use of active nonlinear elements like SOAs provided much larger nonlinearities [Eis92]. SOAs exhibit at least three different nonlinear regimes. The strongest nonlinearities are due to carrier-related refractive index changes from gain saturation. In order to compare the Kerr effect in optical fibres with the refractive index changes in a SOA we represent the SOA nonlinearity in terms of n_2 in Table 1-1. This shows that the carrier-related refractive index changes in SOAs are several orders of magnitude larger than in fibre. Other nonlinearities in SOAs are either due to gain compression (Spectral Hole Burning, Carrier Heating, ...) or due to Kerr effects. These later effects are usually weaker. Furthermore SOAs allow for optical integrated circuitry of small size and low power consumption.

However, it is important to notice that the physical processes behind nonlinear effects in SOA and fibre are different, and thus their physical characteristics need to be considered when referring to Table 1-1. In fact, as discussed in the later chapters, the nonlinear refractive index in the SOA is mainly due to carrier-dependent processes. The relaxation time of the dominant carrier dynamics (inter-band) are in the range of nanoseconds. Therefore, for an optical pulse shorter than the carrier relaxation time it is the pulse energy (or the number of photons registed within the pulse width time interval) rather than its intensity that determines the nonlinear refractive index change. Thus, the refractive index nonlinearities in SOA can be defined as energy-dependent nonlinearities.

Conversely, the origin of the nonlinear refractive index response in fibre is mainly due to the Kerr effect which is related to the anharmonic motion of bound electrons under influence of an applied field [Agr05]. The Kerr effect has an instantaneous time response, and thus, the refractive index nonlinearities in fibre can be defined as intensity-dependent nonlinearities [Agr05].

Recently, AlGaAs waveguide devices have been produced with alternating crystal orientation such that type-II phase matching for different frequency generation (DGF) was obtained [Yoo98]. However large pump power was required for switching and low conversion efficiency was obtained.

		n_2 [cm^2/W]	**Relaxation Times [ps]**
Opt. Kerr Effect of a Standard Fibre		$n_2 = 2.2\text{-}3.4\ 10^{-16}$ [Dor88]	< 1
SOA (at band-gap)	**Carrier Effect**	$n_2 = 1.0\ 10^{-9}$	$\tau_c < 50 - 10000$ [Sto91]
	Gain Compression	$n_2 = 6.0\ 10^{-10}$	< 1
	Kerr Effect	$n_2 = 1.0\ 10^{-12}$	< 1

Table 1-1 Comparison between fibre and SOA nonlinearities at 1.55µm [Leu99]

Thus, SOAs show the largest nonlinearities among optical nonlinear materials around the wavelength range of interest for telecommunications transmission systems. This property, together with the potential for integrability in large optical circuits, makes SOAs one of the most promising solutions for the implementation of optical gates.

1.2.2 Techniques to exploit SOA nonlinearities for switching

In this section the most promising techniques proposed in literature to exploit SOA nonlinearities for optical switching are reviewed [Stu97] [Dur96].

In the Cross-Phase Modulation (XPM) technique, an optical signal is used to modulate the phase of another signal within an interferometer configuration. The interferometer is used to convert the optically induced phase shift into amplitude modulation. Figure 1-3 (a) shows a Mach-Zehnder interferometer with an SOA in each arm [Dur94]. Without the control signal $\mathbf{P_c}$, the clock signal $\mathbf{P_{ck}}$ is directed toward the cross output port $\mathbf{P_x}$. When the control signal is introduced into one arm of the MZI, the phase relationship within the SOA on the respective MZI arm changes and the input signal is directed from the cross into the bar output port $\mathbf{P_=}$. For full switching a phase shift of π radians must be attained by choosing the control signal power correspondingly. XPM based devices can achieve lossless, polarisation insensitive, high bit-rate switching (in excess of 40GHz) with low control signal power (few milliwatts) [Nak02] and high switching contrasts (up to 20dB) that are only limited by noise [Leu98b]. They can also operate over a wide wavelength range of 60nm [Leu97]. Advantageous features of XPM devices are the extinction ratio enhancement [Idl95] and the noise reduction which are due to the interferometer transfer function [Mik96].

(a) Cross-Phase Modulation (XPM)

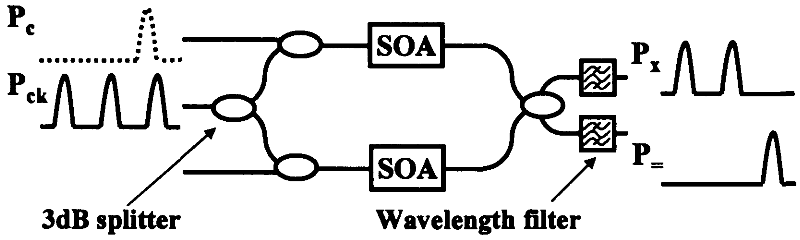

(b) Cross-Gain Modulation (XGM)

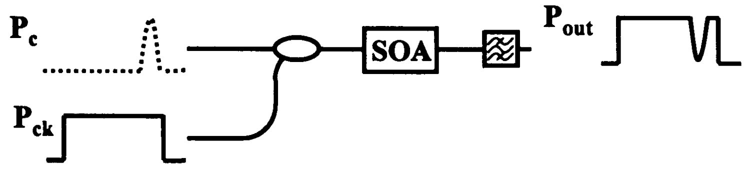

(c) Four-wave mixing (FWM)

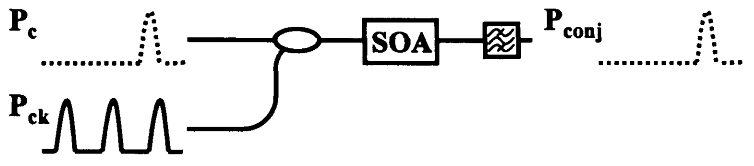

Figure 1-3 Different techniques to exploit the SOA nonlinearities

In the Cross-Gain Modulation (XGM) technique, the control signal $\mathbf{P_c}$ is used to modulate the carrier density and thus the gain of an SOA and, thereby, to modulate the intensity of the clock signal $\mathbf{P_{ck}}$, as shown in Figure 1-3 (b). This switching technique was demonstrated to operate at 40Gb/s [Dan96], however it inverts the pulse polarity due to carrier depletion. Operations at 160Gb/s maintaining pulse polarity was also demonstrated using an advanced XGM-based configurations (SOA-DI) [Leu05]. Problems associated with XGM are extinction ratio degradation [Wie93] and chirp produced by the phase modulation that necessarily accompanies gain modulation in the SOA [Per94].

Four-Wave Mixing (FWM) is a coherent wave-generation technique where intra-band nonlinearities are exploited to generate a new waveform $\mathbf{P_{conj}}$ from an input signal $\mathbf{P_{ck}}$ and a strong pump signal $\mathbf{P_c}$. The principal set-up is depicted in Figure 1-3 (c). FWM is extremely fast (sub-picoseconds) [Kaw97] and transparent to signal formats. In addition, it allows multi-channel operation [Wat98] and provides phase conjugation, which is an efficient method to solve the dispersion problem in fibre [Mar97b]. However, polarisation sensitivity, wavelength dependence of the conversion efficiency, amplifier spontaneous noise (ASE) of the SOA and the low conversion efficiency are problems which must be solved. Some of these can be solved using advanced configurations. For example, polarisation insensitive operation can be achieved by using 2 orthogonally polarised pump sources for switching [Has93]. Conversion efficiencies above 0dB have been achieved by using long SOA cavities [Dot96]. However, signal-to-noise ratio issues (in the range of 20dB/0.1nm) and high power requirements (usually in excess of 10mW) remain significant [Lu00].

A comparison of the experimental results obtained for the different techniques, described here, are summarised in Table 1-2. In conclusion, the XPM technique is probably the most promising method to exploit SOA nonlinearities, since it combines advantages such as high speed, low extinction ratio penalty, low power consumption requirements, polarisation insensitivity and high switching contrast. Different configurations have been proposed to exploit XPM and will be described in detail in the next chapter.

	XPM	XGM	FWM
Fastest experiment	366:10Gb/s [Nak02]	40Gb/s [Dan96]	100GHz [Kaw97]
Gain	dyn. 0dB [Leu98a]	-1.5dB [Dan96]	normally -10dB 0dB [Dot96]
Pump power	weak ($P \approx 1mW$)	moderate ($P < 10mW$)	strong
Polarisation independence	yes	yes	yes with 2 pumps [Has93]
Extinction ratio	ideal [Leu98b]	limited [Wie93]	ideal
Reshaping	yes [Id195]	yes [Che96]	
Noise reduction	yes [Mik96]	moderate	no
Chirp	weak	high	phase conjugation [Mar97b]
3dB wavelength dependency of P_c	~ 60nm [Leu97]	~ 60nm	~ 2nm
Transparent to modulation format	no	no	yes [Ger97]
Multi-channel operation	yes using an SOA array [Gav03c]	yes using an SOA array [Gav04b]	yes [Ger97]
Complexity	moderate	low	low

Table 1-2 Comparison of the different techniques to exploit SOA nonlinearities

1.3 Applications of SOA gates in RZ WDM networks

As shown in the previous section different techniques have been investigated to take advantage of nonlinear effects in SOAs so to implement an optically controlled intensity modulator, referred to as SOA gates.

SOA gates have been proposed to perform most of the bit-level processing functionalities required in transmission, which to date are carried out electrically. These include: signal 3R regeneration, wavelength conversion, time-division demultiplexing and clock recovery. This section briefly describes how these functionalities have been implemented with optical SOA gates.

1.3.1 Optical 3R regeneration with SOA gates

Figure 1-4 shows the generic configuration of an optical regenerator of the type studied in this thesis [Lec03]. The regenerator consists of an optical clock recovery unit and of a decision circuit. The optical clock recovery unit is responsible for the generation of a high quality optical RZ pulse train. Optical clock recovery circuits can be implemented with all optical techniques based on mode locking a self pulsating laser [Ray92] [Tak90], or with hybrid techniques where an electrical clock recovery circuit synchronises an optical pulse source to the input signal [Suz93]. The decision circuit, the SOA-gate, performs reshaping and retiming. Figure 1-4 shows the principle of operation of such an optical 3R regenerator.

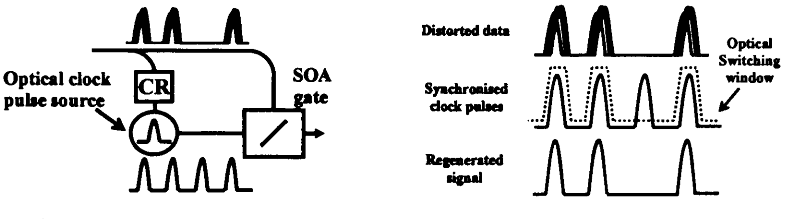

Figure 1-4 3R regeneration with an SOA gate: principle of operation

The incoming and distorted input signal triggers the nonlinear gate, hence generating a switching window which is applied to the newly generated optical clock signal so as to encode the input data stream onto the new optical carrier. The ultimate application of optical regeneration is in a transmission system where regenerators, placed periodically in the transmission path, compensate for the signal distortion accumulated over fibre, allowing ultra-long transmission distances.

1.3.2 Optical demultiplexing with SOA gates

Figure 1-5 shows the generic configuration of an optical demultiplexer with an SOA nonlinear gate [Ell95]. The demultiplexer consists of an optical clock recovery unit and an on-off gate. The optical clock recovery unit is responsible for the generation of a high quality optical RZ pulse train, known as the control signal, synchronised to and at the repetition rate of the tributary channel to be demultiplexed.

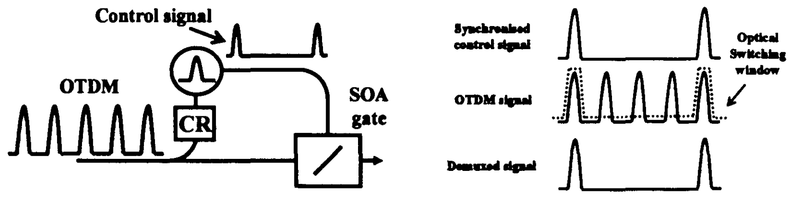

Figure 1-5 OTDM demultiplexing with an SOA gate: principle of operation

The control signal triggers the nonlinear gate, hence generating a switching window which extracts the desired channel from the OTDM input signal. In high-speed OTDM transmission, optical demultiplexing is necessary prior to optical to electrical converters where electrical processing is performed on the tributary channels, which is the case for most of the network nodes involved with signal routing.

1.3.3 Optical wavelength conversion with SOA gates

Figure 1-6 shows the generic configuration of an optical wavelength converter based on SOA nonlinear gates. The wavelength converter consists of a decision circuit and of a tuneable CW (Continuous Wave) light source [Dur96].

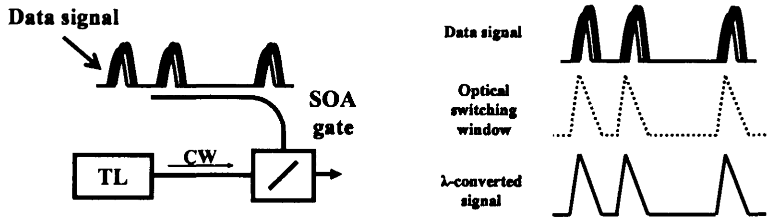

Figure 1-6 Wavelength conversion with an SOA gate: principle of operation

The CW light source generates the optical carrier at the desired wavelength. The data signal triggers the nonlinear gate, hence generating a switching window which modulates the CW light. The wavelength converted pulse shape depends entirely on the SOA gate switching window. The applications of wavelength conversion are multiple; from network signal routing [Gam98] to 3R regeneration. This is because most of all-optical processing techniques such as 3R regeneration, demultiplexing, clock recovery and all-optical routing, have inherent wavelength dependence, and thus wavelength conversion must be used to optimise or enable their operations.

Thesis aims

The aim of the work presented in this thesis is to study all-optical SOA gates for application to 3R regeneration in multi-channel transmission systems at bit-rates of up to 40Gb/s. To date, several configurations based on SOA nonlinearities have demonstrated signal regeneration at high bit-rates (≥40Gb/s). However, several questions have either not yet been addressed or resolved. These include:

- The relationship between the reshaping properties, the regenerator configuration characteristics and the SOA physical parameters has not yet been studied in detail. This is of fundamental importance to determine what configuration and which SOA parameters are required for 3R regeneration at a certain bit-rate.
- Techniques for multi-channel optical 3R regeneration and wavelength conversion have not been yet demonstrated. However, multi-channel regeneration and wavelength conversion are necessary to implement all-optical WDM networks with high channel density.
- The reshaping and retiming properties of SOA gates regenerators have only been partially assessed at 40Gb/s. Quantification of the regenerator tolerance to timing and intensity jitter is still to be verified.
- The cascadability properties of optical gates have not yet been investigated experimentally. Most of the transmission experiments with cascaded optical regeneration have been limited to demonstrate the enhancement of the transmission distance, however the relationship between the regenerator spacing and the transmission distance needs be addressed.

The above points are the subject of the research work presented in this thesis.

Thesis structure

This thesis describes novel SOA gates configurations and novel concepts in the study of their switching properties for application to all-optical processing in high bit-rate transmission systems. The main achievements of the work are:

- Detailed theoretical analysis of the reshaping properties of SOA gates based on XGM and XPM configurations, as a function of the SOA physical parameters (chapter 3) [13].
- Experimental demonstration of a novel fully integrable configuration for multi-wavelength signal wavelength conversion (chapter 4) [9].
- The experimental demonstration of a novel configurations for 40Gb/s all-optical signal regeneration, wavelength conversion and demultiplexing, capable of operating with multiple channels simultaneously (chapter 5) [4-7].
- Experimental quantification of the reshaping and retiming capability of the proposed optical 3R regenerator at up to 40Gb/s (chapter 5) [8].
- The definition of the cascadability principles of SOA gates and the assessment of the performance of transmission with optical 3R regeneration cascaded with different inter-regenerator spacing (chapter 6) [10-13].

An overview of the published research on the different SOA gates configurations and their experimental characterisation is given in **chapter 2**.

Chapter 3 presents the theoretical investigation of the switching properties of SOA gates based on both XPM and XGM techniques. The concept of the nonlinear transfer function is introduced to assess the SOA gate optical switching contrast and signal reshaping properties. The trade-off between the SOA gate switching properties and the switching frequency is investigated and related to the SOA physical parameters.

In the first part of **chapter 4**, a detailed experimental characterisation of the magnitude and dynamics of inter-band nonlinear effects in SOA is carried out to determine the α-factor, the gain recovery time and the chirp of the SOA used in the experiments presented this thesis. These results are used to support the experimental

investigation of the switching properties of XGM-based SOA gates (chapter 4) and of SOA-assisted interferometers (chapter 5).
In the second part of chapter 4, the performance of XGM-based wavelength conversion based the SOA-DI (delay interferometer) and SOA-OF (off-set filtering) configurations is experimentally investigated at 10 and 40Gb/s and compared to the SOA characterisation experimental results. A novel technique for simultaneous regenerative wavelength conversion of multiple 10Gbit/s signals is also demonstrated utilising a SOA array and a multi-channel optical equaliser.

In **chapter 5**, a novel configuration for all-optical regeneration based on Polarisation Switching in an SOA-assisted Sagnac Interferometer (PSSI) is presented. The scheme allows to significantly enhance the switching frequency of the SOA demonstrating error-free regeneration of 40Gb/s signal with long PRBS sequences using an SOA with carrier lifetime exceeding 250ps. Characterisation of the intensity jitter tolerance (reshaping) and retiming ability of the scheme are also assessed experimentally at bit rate of 10 and 40Gb/s, to show the largest distortion tolerance range published to date for optical regeneration. The scheme is also used to demonstrate simultaneous regeneration of multiple 10Gb/s channels and 40 to 10Gb/s demultiplexing.

In **chapter 6**, a transmission experiment with cascaded all-optical 3R regeneration, based on the PSSI configuration, is reported using a novel reconfigurable fibre loop to investigate, for the first time, the impact of varying the inter-regenerator spacing on long distance 10Gb/s transmission. The concept of the regenerator Q-factor gain is introduced to measure the regenerator noise suppression properties in transmission. This is the first assessment of the noise suppression properties of an optical regenerator while this is cascaded in a chain. Results show that a trade-off exists between the transmission signal Q-factor and the inter-regenerator spacing, which depends on the regenerator transfer function characteristics, and thus can be predicted from the SOA parameters. The effect of a single regenerator placed at the end of the transmission line prior to the electrical receiver at 10 and 40Gb/s is also studied to show that this can enhance the maximum transmission distance and the receiver sensitivity.

Chapter 7 draws the main conclusion of the work and discuses the implications of the results on the design of WDM optical transmission system with cascaded optical 3R regeneration. Future directions of research are also discussed.

Publications and conference presentations

The following is a list of publications that arose as a result of the research described in this thesis.

[1] G. Gavioli and P. Bayvel, "High-speed synchoronisation for optical packet networks", in Proc. London Communication Symposium 2000 (LCS 2000), 14-15 Sept. 2000, London (UK), Pages: 17-22

[2] G. Gavioli and P. Bayvel, "High-speed synchronisation for optical packet networks", in Proc. Postgraduate Research in Electronics and Photonics 2001 (PREP 2001), 9-11 Apr. 2001, Keele (UK), Pages: 81-82

[3] G. Gavioli and P. Bayvel, "Investigation and comparison of high-speed synchronisation techniques for optical packet networks", in Proc. Network and Optical Communications 2001 (NOC 2001), 10 June 2001, Ipswich (UK), Pages: 311-316

[4] G. Gavioli and P. Bayvel, "A novel high-stability 3R all-optical regenerator based on polarisation switching in semiconductor optical amplifier", in Proc. European Conference on Optical Communication (ECOC 2002), 8-12 Sept. 2002, Copenhagen (Dk), Paper We.7.3.2

[5] G. Gavioli and P. Bayvel, "Novel, 3R regenerator based on polarisation switching in a semiconductor optical amplifier-assisted fibre Sagnac interferometer", IEEE Photonics Technology Letters, Volume 15, Number 9, Sept. 2003, Pages: 1261-1263

[6] G. Gavioli, V. Mikhailov and P. Bayvel, "Novel, all-optical demultiplexer based on polarisation switching in a semiconductor optical amplifier", In Proc. Conference on Laser and Electro-Optics (CLEO 2003), 23-27 June 2003, Baltimore (USA), Paper CThQ7

[7] G. Gavioli and P. Bayvel, "Multichannel All-optical Regenerative Wavelength Conversion using an Integrated Semiconductor optical Amplifier Array", In Proc. Annual meeting of the IEEE Lasers and Electro-Optics Society (LEOS 2003), 26-30 October 2003, Tucson (USA), Paper ThO5

[8] G. Gavioli and P. Bayvel, "Amplitude jitter suppression using a patterning–tolerant, all-optical 3R regenerator", Electronics Letters, Volume 40, Number 11, May 2004, Pages: 688 - 690

[9] G. Gavioli, V. Mikhailov, P. Bayvel, "Multichannel wavelength conversion and regeneration using an array of SOA and a multichannel optical equalizer", in Proc. 30th European Conference on Optical Communication (ECOC 2004), 5-9 September 2004, Stockholm (Sweden), Paper Tu4.4.4

[10] G. Gavioli, V. Mikhailov, B. Thomsen and P. Bayvel, "Investigation of transmission with cascaded all-optical 3R regenerators and variable inter-regenerator spacing", Electronics Letters, Volume 41, Number 3, Feb. 2005, Pages: 146 – 148

[11] G. Gavioli, V. Mikhailov, B. Thomsen and P. Bayvel, "Investigation of Cascadability and Optimum Inter-Regenerator Spacing in Transmission with All-Optical 3R Regeneration", In Proc. Conference on Laser and Electro-Optics (CLEO 2005), 24-26 May 2005, Baltimore (USA), Paper CMQ5

[12] G. Gavioli, V. Mikhailov, B. Thomsen and P. Bayvel, "Investigation of fibre launch power margin in 40 Gb/s transmission with all-optical regeneration", in Proc. European Conference on Optical Communication (ECOC 2005), 25-29 Sept. 2005, Glasgow (Scotland), Paper Tu3.3.2

[13] G. Gavioli, V. Mikhailov, B. Thomsen and P. Bayvel, "Investigation of Cascadability and Optimum Inter-Regenerator Spacing in Transmission with All-Optical 3R Regeneration", in preparation for submission to Journal of Lightwave Technology

Chapter 2 Literature review: SOA gates and performance characterisation

Among the optical nonlinear materials, the largest optical nonlinearities, around the transmission bandwidth (1460-1625nm), are found in SOAs. XPM and XGM techniques have been suggested to exploit the SOA nonlinearities for all-optical processing.

Various configurations have also been proposed, in the literature, to take advantage of SOA nonlinearities for switching, and will be described in the first part of this chapter.

Since the refractive index and gain are coupled, XPM and XGM occur simultaneously in the SOA and both will contribute to the switching process. However, in this thesis, XGM configurations are referred to as those where gain saturation is the dominant nonlinearity and similarly XPM configurations as those where refractive index modulation is the dominant nonlinearity.

In the second part of this chapter, the experimental techniques proposed to characterise the SOA gates reshaping and cascadability properties for application to optical 3R regeneration are reviewed. This chapter also includes contributions from the work presented in this thesis.

2.1 Configurations

The choice of a configuration is frequently related to the SOA gate functionality or to the SOA physical characteristics.

XPM configurations are based on SOA-assisted interferometers and are usually employed for 3R regeneration and signal demultiplexing, due to their reshaping characteristics and short switching windows. The characteristics of switching in the different interferometer geometries have been extensively investigated [Tol00] [Sch02]. The SOAs with a large α-factor (≥ 4) are better suited for this application.

XGM configurations, instead, are usually employed for wavelength conversion, as they have demonstrated ultra-fast operations but have limited signal regenerative abilities. SOAs with a large dynamic gain response are better suited for this application.

2.1.1 Optical switching with SOA-assisted interferometers

As outlined earlier, XPM is the most power efficient technique to make use of the strong SOA nonlinearities. XPM potentially allows for high bit-rate switching with extinction ratios that are only limited by noise [Leu98b]. However there are several challenges in using SOAs as nonlinear optical elements in interferometer configurations.

First the SOA nonlinear refractive index and gain are related [Agr98]; thus, a refractive index change results also in a gain change. Variation of the transmittance of a SOA operating as a nonlinear phase modulator in an interferometer can cause significant switching contrast penalties [Leu98b]. Therefore, to achieve high on-off ratios within an interferometer configuration, both the intensities as well as the phases of the interfering signals have to be controlled within the configuration.

The second limiting factor lies in the operation speed. The photo-induced modulation effects in SOA are intrinsically limited in speed by the gain recovery time, which is a function of the carrier lifetime and the injection current [Dav95a]. Thus, for the case of a recovery time larger than the bit period, the SOA gate output pulses will be affected by pattern-dependent distortion. Pattern-dependent distortion in an interferometer is defined as the variation of the signal intensity (sometimes referred to as amplitude jitter) caused by variations of the interfering pulses phase and intensities which depend on the logical bit sequence of the control signal, and occur when the switching period is shorter than the SOA gain recovery time. Although most SOAs have a carrier lifetime in the range of several hundreds picoseconds [Sto91], it had been shown that the recovery time could be decreased to few tens of picoseconds by clamping the SOA gain with optical power to a nearly saturated gain level [Man94a] [Man94b] [Usa98]. However, reducing the recovery time by gain clamping also reduces the SOA gain and refractive index nonlinear dynamic response, and thus reduces the interferometer dynamic extinction ratio. Therefore, switching with a SOA involves a trade-off between a large nonlinearity and speed. For this reason the optimisation of the SOA phase and gain dynamic response is required to operate at high bit-rates.

This section reviews the various SOA-assisted interferometer configurations published in the literature showing the different advantages and disadvantages. These configurations are the Sagnac interferometer (TOAD), the Michelson interferometer

(MI), the Mach-Zehnder interferometer (MZI) and the polarisation discriminator interferometers (UNI, PSSI).

Terahertz Optical Asymmetric Demultiplexer (TOAD): For historical reasons, we start with the TOAD configuration, which was the first example of an SOA-assisted interferometer gate. The TOAD configuration, shown in Figure 2-1, is based on a fibre Sagnac interferometer and was realised, for the first time, in 1993 for all-optical demultiplexing [Sok93] and signal regeneration applications [Eis93].

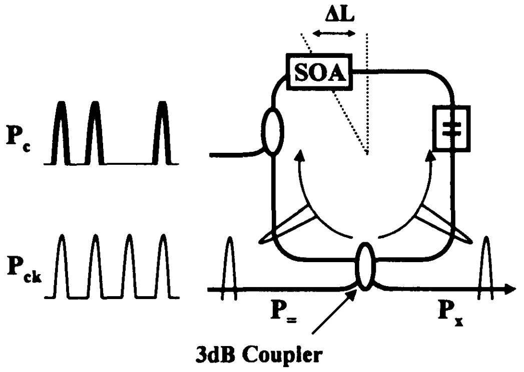

Figure 2-1 SOA-based Sagnac interferometer switch (TOAD)

The clock pulse train $\mathbf{P_{ck}}$ is split into a clockwise and counter-clockwise propagating pulse trains. When the control signal $\mathbf{P_c}$ is introduced in the clockwise propagating direction, it co-propagates simultaneously with the clockwise clock pulse through the SOA and changes its phase, whereas the counter-propagating clock signal reaches the SOA with time delay $\Delta t = c/\Delta L$. If the control signal power is sufficiently high, the pulse that is propagating with the control signal experiences a phase shift of π radians and is coupled into the output port $\mathbf{P_x}$. When there is no control signal, the input signals are mirrored back into the clock input port $\mathbf{P_=}$.

The advantages of the TOAD configuration are in the simplicity of controlling the switching window and in the operating stability. The interferometer optical switching window duration can be easily varied (up to the data bit period) by controlling the position of the SOA in the fibre loop mirror using an optical delay line (ODL). Due to the counter-propagating geometry both clock components travel trough the same path, and thus the TOAD configuration can be build in fibre without the need for temperature stabilisation circuitry. This leads to low switching energy requirements (sub-picojoule). Polarisation independent operation can also be achieved at the cost of operating the pump and probe signal on different wavelengths [Pie96], which is undesirable for 3R regeneration applications.

However, switching with the TOAD has two fundamental limitations which preclude high bit-rate operations. First is the poor switching contrast due to XGM between the control and the clock signal. Referring to Figure 2-1, the clock interfering components are differentially phase and intensity modulated by the control pulse in the SOA. However, in a TOAD the intensities of the clock interfering signals can not be controlled within the configuration at the interfering coupler. Thus, significant switching contrast penalties due to XGM are expected in the TOAD configuration [Eis95].

Secondly, due to the counter-propagating operation the optical switching window shape is asymmetric [Tol00] and the temporal width is limited by the SOA length [Hal99]. To date the fastest switching frequency demonstrated was 10Gb/s [Dav95b]. The asymmetry in the switching window shape can be understood from the phase response of SOA. Figure 2-3(a) shows a diagram of the phase change with time seen by the co-propagating and counter-propagating clock components (φ_{cp}, φ_{ccp}) travelling through the SOA, for $\Delta t = t_{SOA}/2$ where t_{SOA} is the propagation time through the SOA. The effect of the clock and control pulse width is neglected in this figure. The phase change seen by the co-propagating pulse exhibits, as will be described in the later chapters, a fast rising transition and a slower recovery tail. However, the phase change seen by the counter-propagating component shows a slow rising transition, which equals to twice the t_{SOA} period, followed by the slower recovery tail. Thus, the resultant differential phase modulation, which determines the switching window shape, is significantly asymmetric.

Furthermore, due to the counter-propagating operations, the TOAD scheme works well when the data pulse period T is longer than twice the propagation time through the SOA. In fact, when the SOA propagation time is more than half the bit period, a single control pulse will interact with more than one counter-propagating clock pulse component and impart an unwanted differential phase shift. This control pulse interaction with multiple clock pulse components leads to partial switching of unwanted clock pulses and degrades the fidelity of the switched out stream [Hall99]. For a 1mm long SOA, with refractive index n = 3.25, the propagation time through the amplifier is 10.8ps, and switching performance is expected to start degrading for data rates of 50 Gbit/s and higher. Such limitation is of fundamental importance for application to optical demultiplexing where the width of the switching window of the optical gate is not limited by the SOA phase dynamics (ie its recovery time). Conversely, for 3R regeneration the phase dynamic response of the SOA will introduces switching frequency limitations at bit-rates lower than 50Gb/s, as is shown in chapter 4.

Differential Operation Mode Mach-Zehnder (DOM-MZI): The configuration based on the Mach-Zehnder interferometer (MZI), is shown in Figure 2-2 [Lav02].

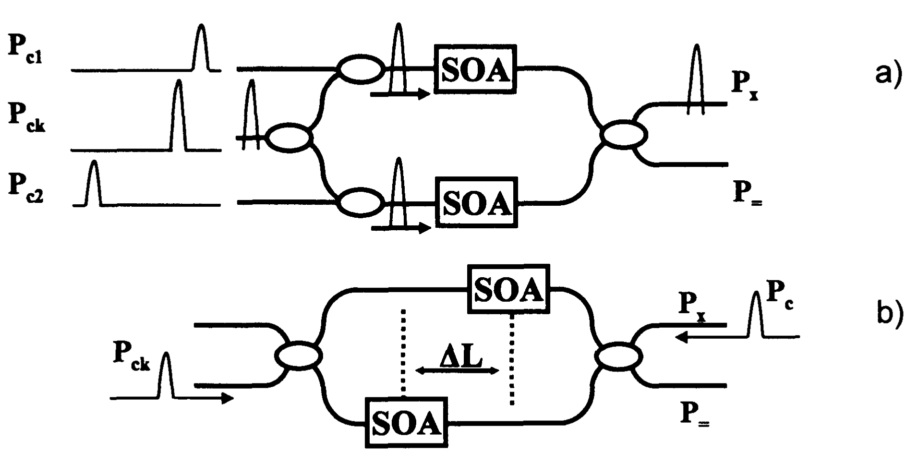

Figure 2-2 SOA-based Mach-Zehnder configurations for switching with fast resonant excitation; (a) Consecutive optical control pulses configuration (DOM-MZI), (b) Asymmetrically displaced SOAs configuration

To overcome the speed limitations of the SOA recovery time, an arrangement with two consecutive optical control pulses was proposed [Taj93]. This approach, also referred to as Differential Operation Mode (DOM), makes it possible to successfully operate at switching frequency in excess of the SOA recovery time [Fis99]. A first control signal $\mathbf{P_{c1}}$ is introduced into the SOA_1 to induce the necessary π radians phase shift for switching, as shown in Figure 2-2 (a). The second control signal $\mathbf{P_{c2}}$ is then introduced with a time delay into SOA_2. This is used to induce the same phase shift in the second MZI arm and, thereby, reset the switch. In this way the "*switch-off*" as well the "*switch-on*" time is controlled by the fast optical excitation process. Another solution consists in displacing the SOA along the propagation direction of the light and using counter-propagating control input signals [Kan95]. In this way the control signal induces the refractive index changes at different times in the MZI arms, thereby setting a phase-shift difference of π radians with the first control signal and resetting it with the second control signal as shown in Figure 2-2 (b). Unfortunately, this switching scheme allows only counter-propagating operation, which limits the switching speed [Leu99]. A graphical comparison of the TOAD and DOM-MZI switching window is shown in Figure .

In a DOM-MZI the two SOA compensate for the long SOA recovery time generating a switching window shorter than the switching bit period (T). In a TOAD, instead, the finite length of the SOA significantly affects the switching window shape and length, due to the counter-propagating operation. The DOM-MZI on the other hand, is not limited by the length of the SOA(s) in the gate, because the control and clock pulses all co-propagate through the gate. Thus, with identical SOA parameters the DOM-MZI, is capable of generating a shorter switching window.

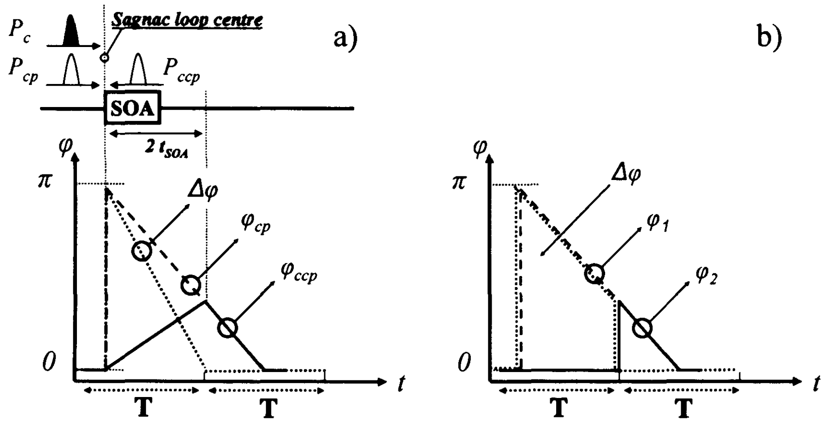

Figure 2-3 Comparison of TOAD (a) and DOM -MZI (b) differential phase modulation ($\Delta\varphi$) indicative of the switching window; φ_1 and φ_2 are the SOA nonlinear phase shift of P_{C1} and P_{C2} respectively. T is the bit period.

To achieve high on-off ratios (>20dB [Leu99]) within an interferometer configuration, both the phases as well as the intensities of the clock interfering signals have to be properly controlled within the configuration. However, the strong optical signal which modulates the phase of the clock components also modulates their intensity, degrading the MZI switching contrast. The penalty on the switching contrast in a MZI due to XGM differential gain modulation between the two interfering components can be estimated from the MZI transfer function.

The MZI transfer function can be expressed as:

$$I_o = I_1 + I_2 + 2\sqrt{I_1 I_2}\cos(\Delta\varphi) \qquad (2\text{-}1)$$

where I_0 is the interferometer output signal intensity, $\Delta\varphi$ is the differential phase shift between the interfering clock components with intensities I_1 and I_2. Defining the differential gain modulation as $\Delta G = I_1/I_2$, then equation (2-1) can be expressed for $\Delta\varphi = 0$ as:

$$I_o' = I_2\left(\sqrt{\Delta G} + 1\right)^2 \qquad (2\text{-}2)$$

Thus, as the control pulse saturates the SOA, the differential phase shift is reduced to zero ($\Delta\varphi = 0$), however ΔG increases, due to XGM, and the interferometer switching contrast is reduced. The penalty on the MZI switching contrast is plotted as a function of the differential gain (ΔG) in Figure 2-3. As the differential gain ΔG increases the MZI switching contrast decreases.

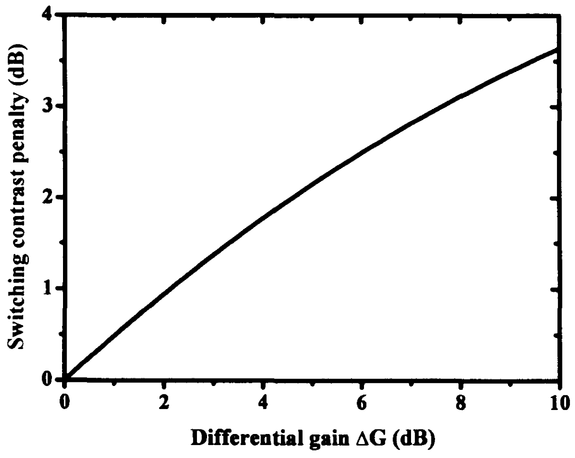

Figure 2-3 Switching contrast penalty as a function of the differential gain ΔG for the DOM-MZI

Figure shows the phase and transmittance dynamics of the 2 SOA of a DOM-MZI configuration [Max02] when operating as a 40Gb/s regenerator (T = 25ps). The measurements were taken with the experimental set-up described in chapter 4. As shown in the figure, the optical switching window can be significantly reduced using the DOM technique; however the differential gain modulation occurring between the two SOAs, here measured to be 3dB, will lead to switching contrast penalty of 1.5dB.

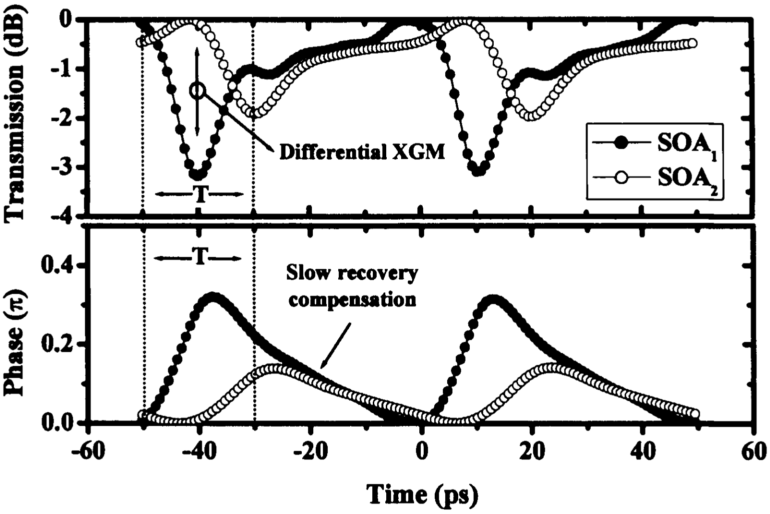

Figure 2-5 Experimentally measured SOAs dynamics of a 40Gb/s regenerator based on the DOM-MZI configuration

It was shown in [Leu98b] that asymmetries are needed to overcome the extinction ratio limitations in MZI all-optical switches caused by cross-gain modulation. An example for such asymmetries is given in Figure 2-4.

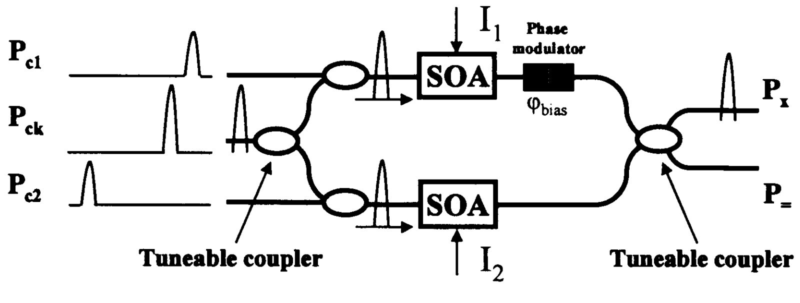

Figure 2-4 SOA-based Mach-Zehnder configurations with integrated asymmetries to obtain high extinction ratios; I_1 and I_2 are the SOA bias currents

The configuration contains asymmetrically biased SOAs ($I_1 \neq I_2$) and asymmetric couplers. A phase shifter is used to compensate the phase offset introduced by the asymmetrically biased SOAs. When the control signal P_{C1} is introduced into the SOA$_1$, the amplifier saturates. But since a higher current bias was applied relative to SOA$_2$, the saturation of the two SOAs relative to each other remains small and higher extinctions are obtained (>20dB [Leu99]). Similarly tuneable couplers are used to equalise the intensity of the interfering clock pulses so to minimise differential gain penalties.

A MZI device with asymmetries can, in principle, attain ideal extinction ratios [Leu98] when the control signal is a train of optical pulses, such as for demultiplexing applications. However, when the control signal is a randomly modulated pulse train, as for 3R regeneration applications, then the switching contrast will be limited by pattern-dependent distortion [Bis02b], which can only be partially compensated with asymmetries. Pattern-dependent distortion are caused by variations of the interfering pulses phase and intensities which depend on the logical bit sequence of the control signal, and occur when the switching period is shorter than the SOA gain recovery time.

In conclusion, the DOM-MZI configuration has demonstrated important features in the generation of ultra-short optical switching window with high contrast. Recently, a switching contrast of 17dB was demonstrated at 80Gb/s [Uen01]. Furthermore this configuration allows for co-propagating direction switching at any wavelength of the gain spectrum, including when the pump and prove have the same signal wavelength.

However, the DOM-MZ requires a minimum of 2 SOAs per switch, which have to be integrated on a planar waveguide to compensate for temperature-dependent instabilities which could occur between the two MZ arms.

Implementation with a planar waveguide has the disadvantage of having a higher insertion loss than with fibre. Thus, multiple gain elements (linear SOA) are usually integrated in the MZI switch to boost the signal power at the input and/or output of the nonlinear SOAs used for switching [Lav00]. The most recently reported integrated DOM-MZI devices operate with a minimum of 4 SOAs [Max02].

Furthermore implementing asymmetries of the kind depicted in Figure 2-4 significantly increase the device complexity. Tuneable couplers have not yet been implemented in DOM-MZI, and usually the effects of couplers asymmetries are partially emulated optimising the power of the two control pulses $\mathbf{P_{c1}}$ and $\mathbf{P_{c2}}$. However the range of tuneability is clearly limited and thus switching contrast penalties only partially compensated, furthermore the complexity of operating and tuning the device is significantly increased.

Polarisation discriminator interferometers (UNI, PSSI): To date, two configurations based on polarisation rotation in an SOA-assisted interferometer have been proposed and investigated in literature. The first is based on polarisation switching in a linear interferometer geometry (UNI) [Taj95], the second in a Sagnac interferometer geometry (PSSI) [Gav02]. With polarisation discriminator interferometers it is possible to control the phase and intensity of the interfering clock components and thus to achieve large extinction ratios at high bit-rates. When compared to the DOM-MZI, both configurations require a significantly simpler implementation operating with a single SOA in a fibre based interferometer. The Ultra-fast Nonlinear Interferometer (UNI) is shown in Figure 2-5 [Phi98]. To date, the highest bit-rate performance for all-optical regeneration with long pattern length has been achieved with the UNI, which demonstrated up to 80Gb/s operation [Kel99].

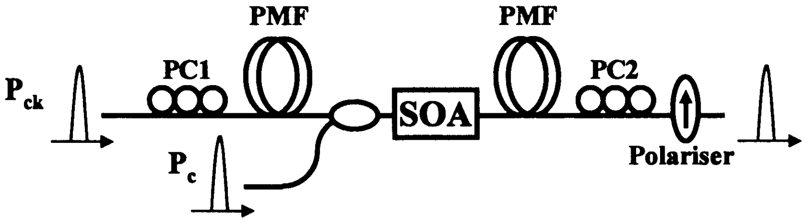

Figure 2-5 UNI configuration

The UNI operates as follows; at the input, the clock signal $\mathbf{P_{ck}}$ is split into two orthogonally polarised pulses by launching it at 45° to the axes of a polarisation maintaining fibre (PMF) or birefringent crystal. After traversing the PM fibre, the two orthogonal pulses are separated in time before they pass through a polarisation insensitive SOA. The separation in time allows to influence the clock pulse components inside the SOA individually by controlling the time arrival of the control pulse $\mathbf{P_c}$ in the SOA. The pulse pair is then launched at 45° into a second PM fibre or birefringent crystal, where the delay between the two clock pulses is reversed and the two components recombine on passage though a fibre polariser. The second length of PM fibre is wound onto a piezo-electric transducer, allowing simple adjustment of the interferometer bias. The control signal is then launched into the SOA via a 3dB coupler so that it co-propagates with the clock pulses. As the high energy control pulse (usually $\mathbf{P_c} \leq 1\text{pJ}$) passes through the SOA of the UNI a rapid transition in its refractive index occurs. The control pulse enters the SOA the instant the leading clock pulse has passed though the SOA, so that the trailing clock pulse component will be subject to a nonlinear phase shift and intensity modulation as a result of XPM and

XGM effects. The differential phase and intensity modulation of the two clock pulse components causes the polarisation of the recombined clock signal to rotate to an orthogonal state in the presence of the control pulse. A polarisation discriminator (Polariser) is then used to interfere the clock pulse components at the interferometer output. In a UNI the switching window depends on the differential delay accumulated between the two clock pulse components, and thus on the length of the PM fibre.

The UNI operates as a MZI with couplers asymmetries as shown in Figure 2-4. In fact, the power of the two orthogonal clock components can be tuned at the SOA input by simply varying the polarisation state of the clock signal $\mathbf{P_{ck}}$ at the PM fibre input using the polarisation controller PC1. Similarly PC2 allows to optimise the power of the interfering clock components at the polariser input and thus to achieve high switching contrasts [Phi98].

Thus, the advantage of the UNI over a DOM-MZI configuration operating either without or with limited coupling asymmetries is in the enhanced switching contrast. This characteristic makes the UNI a good candidate for applications to 3R regeneration.

However, because of the linear interferometer geometry, the UNI operates with a fixed non-tuneable switching window and requires active phase stabilisation techniques to minimise temperature-dependent phase fluctuations in the PM fibres. Both parameters are of fundamental importance to ensure stable operations and to maximise the retiming ability of the regenerator, especially for operation at high bit-rate [Jin94] [Gav01]. Temperature stabilisation can be achieved utilising a piezo-electric transducer to control the fibre length form temperature fluctuations, however this imposes a significant complexity increase in the configuration implementation. The switching window can not be dynamically tuned unless replacing the fibre. The UNI also require a polarisation independent SOA to operate. This precludes to use the UNI with an SOA array, which can enable multiple wavelength optical processing functionalities [Mik03a] [Gav03c] but usually has large polarisation dependent loss (PDL). Furthermore, the use of PM fibre does not allow the UNI configuration to be monolithically integrated in a single optical circuit.

To solve the problems just mentioned a new configuration based on polarisation switching in a Sagnac interferometer (PSSI) was proposed and demonstrated, for the first time, in this thesis. The PSSI, shown in Figure 2-6, operates as follows; the optical clock signal $\mathbf{P_{ck}}$ is launched 45° polarised at the input of the polarisation beam splitter (PBS), used to split the signal into two orthogonally polarised pulses which counter-propagate in the loop and recombine at the output port of the polarisation beam splitter, to interfere in a polariser. As in a conventional TOAD scheme, the SOA is offset from the loop centre, so that the clock pulses are separated in time, and do not overlap as they travel through the SOA. The control signal pulse $\mathbf{P_c}$, synchronised to the local clock signal, is coupled into the co-propagating arm of the interferometer, so to reach the SOA immediately after the counter-propagating clock pulse and just before the co-propagating pulse has passed through it. The co-propagating pulse experiences nonlinear cross phase and intensity modulation induced in the SOA by the control pulse, which causes the two clock pulses to recombine to a different polarisation state at the polarisation beam splitter output.

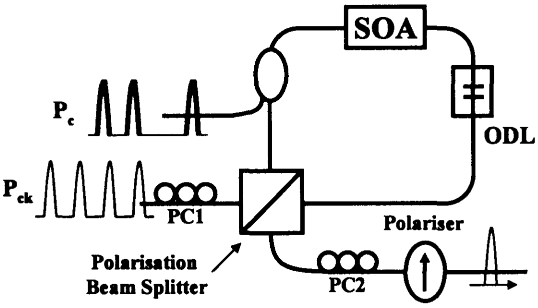

Figure 2-6 PSSI configuration

As the UNI, the PSSI also operates as a MZI with coupling asymmetries. In fact, the combination of PC1 and the polarisation beam splitter allows to tune the coupling ratio of the clock signal components launched into the SOA, while PC2 allows to optimise the power of the interfering components at the polariser input so to achieve high switching contrasts.

To date, 3R regeneration with the PSSI configuration has been demonstrated at bit-rates up to 40Gb/s [Gav04a]. The advantages of using a Sagnac interferometer over a linear interferometer geometry [Phi98] are in the simplicity of controlling the switching window and in the operating stability. The regenerator optical switching window can be easily tuned by controlling the position of the SOA in the fibre loop mirror using an optical delay line (ODL). The regenerator is inherently stable as the counter-propagating clock pulses split and recombine in the same beam splitter after travelling through the same fibre, including all random phase shifts induced by temperature effects on fibre, difficult to compensate in the linear geometry.

Furthermore, it has been shown that nonlinear cross modulation between counter-propagating wavelengths is weaker than for the case of co-propagating wavelengths due to spatially localised nonlinearity in the SOA [Top99]. The cross gain modulation imparted on a co-propagating wavelength was shown to be more than twice as strong as on a counter-propagating wavelength [Fen02]. Thus, using a counter-propagating configuration enhances the differential phase shift between the interfering clock components with respect to the case of a co-propagating configuration such as the UNI, increasing the regenerator switching contrast.

Furthermore the PSSI can also work with a polarisation sensitive SOA; these unique features allowed to operate this configuration with an integrated SOA array to perform, for the first time, multiple wavelengths signal regeneration [Gav03c].

2.1.2 Optical switching based on XGM in SOA

Switching based on XGM in SOA has demonstrated, to date, the record switching frequency of 160Gb/s all-optical wavelength conversion [Nak01] [Leu05]. However, as will be shown in chapter 3, due to the limited regenerative ability of the SOA gain nonlinearities, XGM-based techniques mainly find applications in high-speed wavelength conversion. In this section the most promising XGM-based configurations published in literature are reviewed.

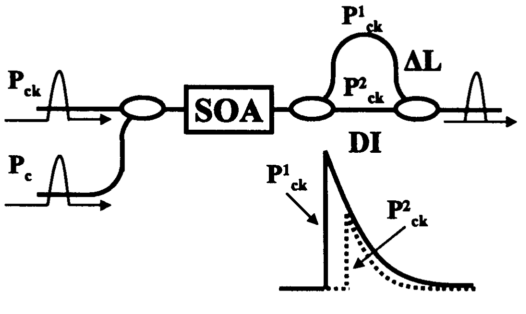

Figure 2-7 Delayed-interferometer configuration (SOA-DI)

SOA with a Delay Interferometer (SOA-DI): The SOA-DI configuration, shown in Figure 2-7, consists of one SOA and a Mach-Zehnder Interferometer [Leu01]. As the differential delay between the 2 arms of the MZ interferometer is in the range of the pulse width the MZI is usually referred to as a bit-delay interferometer (DI). The control signal pulse $\mathbf{P_c}$ modulates the gain and phase of the SOA, the co-propagating clock signal pulse $\mathbf{P_{ck}}$ experiences these phase shifts before it is guided into the MZI. There, $\mathbf{P_{ck}}$ is split and directed into the straight through and delayed MZI arms. When the clock pulses recombine at the output, the two signals interfere constructively until the pulse which is delayed by $\Delta t = c / \Delta L$ arrives carrying the same phase shift as the signal from the straight through MZI arm. The advantage of this concept is that it is simple and that it allows switching with the fast transients. The same concept was implemented using PM fibre rather than a DI interferometer as described in [Pat94] [Uen98].

SOA with a Pulse Reformatting Optical Filter (SOA-PROF): The SOA-PROF configuration, shown in Figure 2-8, consists of one SOA followed by a pulse reformatting optical filter, designed to exploit the chirp induced on the clock signal by the SOA for switching [Leu04]. The chirp is defined as the variation of the optical signal frequency with time [Agr02].

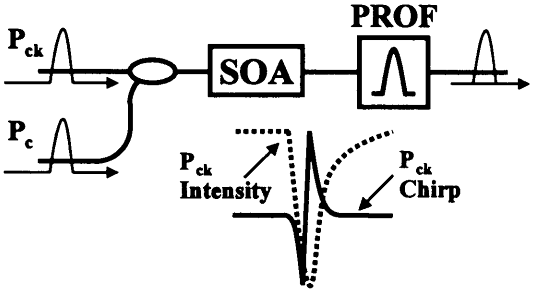

Figure 2-8 PROF configuration

The chirp profile of the wavelength converted pulse at the SOA output shows a red-shift on the rising edge and a blue shift on the falling edge. The PROF filter splits off the red-chirped form the blue chirped-part and recombine the two spectra components while introducing different time delays. By controlling the delay between the components the wavelength converter pulse can be shaped to RZ or NRZ format. Furthermore by taking advantage of both XPM and XGM, this configuration has shown the best conversion efficiency in terms of switching power and Q-factor published to date for wavelength conversion. However the implementation of the

PROF filter is sophisticated and, to date, has required the use of a reconfigurable microelectromechanical (MEMs) based filter.

Other techniques based only on filtering either the red or the blue chirped spectral component of the SOA output signal have shown similar performance with reduced conversion efficiency [Nie03a].

A comparison of the different configurations performance, based on published experimental results, is summarised in Table 2-1.

		TOAD	SOA-DI	DOM-MZI	UNI	PSSI
Demultiplexing	**Highest bit-rate**	250:10Gb/s [Gle94]		336:10Gb/s [Nak02]	160:10Gb/s [Sch01]	40:10Gb/s [Gav03b]
	switching window	4ps FWHM		<3ps FWHM	4.5ps FWHM	12ps FWHM
	Switching contrast	6dB		12dB	18dB	15dB
	Switching energy	800fJ		$P_1 = 200$fJ $P_2 = 1$fJ	10pJ	140fJ
40Gb/s regeneration	**Modulation format**		2^{31}-1 RZ [Leu01]	2^{23}-1 RZ [Lav02]	2^{31}-1 RZ [Phi98]	2^{31}-1 RZ [Gav04a]
	Switching energy		320fJ		60fJ	50pJ
	Switching contrast		18dB [Leu02a]			13dB
	Polarisation dependency		minimal	no	no	no for $\lambda_{ck} \neq \lambda_c$
λ-conversion	**Fastest experiment**	10Gb/s [Wan01]	160Gb/s [Leu05]	84Gb/s [Uen01]	80Gb/s [Kel99]	40Gb/s [Gav04a]
	Modulation format	RZ to NRZ NRZ to NRZ	RZ to RZ RZ to NRZ	RZ to RZ RZ to NRZ	RZ to RZ	RZ to RZ RZ to NRZ
	Sensitivity penalty	4dB	6dB	3dB	3dB	1dB
	Wavelength range		~ 60nm	~ 60nm		~ 60nm

Table 2-1 summary of the most significant characteristics and relevant experimental results for the different SOA gates configurations

At this stage is important to make a distinction between intra-band and inter-band nonlinearities. As explained in chapter 3, the SOA gain and refractive index nonlinearities are governed by free-carrier dynamics resulting from inter-band and intra-band effects. The inter-band effects are induced by changes in the total free-carrier concentration inside the conduction and valence bands caused by stimulated emission, absorption, spontaneous emission and nonradiative recombination. These usually occur on a 0.1-1 nanosecond scale [Mor94]. Referring to the above table, inter-band effects are the dominant nonlinearities at bit-rates of 10 and 40Gb/s (bit-rates used for the work described in this thesis).

The SOA intra-band effects are due to changes in the free-carrier concentration within a band and occur on a sub-picoseconds scale (see, for example, [Occ02a] and references therein). Referring to the above table, intra-band effects are the dominant nonlinearities at bit-rates of 160Gb/s and higher.

2.2 Characterisation of SOA gates

An SOA gate is as optically controlled intensity modulator exploiting SOA nonlinearities for switching. However, in contrast to digital electrical switches, such as flip-flops, which have a bi-stable (on-off) transfer function, SOA gates operate with an analogue transfer function [Dur96]. When compared to an electrically controlled optical modulator such as an EAM or an InP-MZ, SOA gates show a dependence of the switching properties on the input optical signal characteristics. For this reason the characterisation of an SOA gate strongly depends on its functionality. The applications of SOA gates in fibre transmission systems include 3R regeneration, wavelength conversion and demultiplexing [Nol00]. To date, these functionalities are solved digitally in the electrical domain utilising electrical to optical converters, and thus their performance is assessed in terms of BER. The Bit Error Rate (BER) is the ratio of the number of bits incorrectly received to the total number of bits sent during a specified time interval and is used as a measure of the transmission system performance.

However, an SOA gate must be considered as an analogue component. Thus, it is necessary to develop specific measurement techniques to characterise their performance and to predict their effects on a transmission system.

Here a literature review of the approaches utilised in assessing the SOA gates properties for application to optical regeneration and wavelength conversion is given, including the contribution of the work described in this thesis.

2.2.1 Characterisation of SOA gates operating in back-to-back configuration

In characterising an optical modulator, such as an SOA gate, the parameters of interest are the modulated signal Optical Signal-to-Noise Ratio (OSNR), the switching frequency, the pulse shape and the extinction ratio.

Depending on the electrical receiver, to a certain signal OSNR corresponds a particular BER. Also, at a particular OSNR the receiver operates with a certain power sensitivity which depends on the input signal quality. It is a common practice in digital communication system to assess the quality of a signal by measuring the receiver sensitivity at a given OSNR and compare it to sensitivity measured at the same OSNR for a reference signal such as the transmitter output signal (also referred to as the "*back-to-back*" signal) [Hum91]. This measurement approach has been used to assess the quality of the SOA gate output signal with respect to the transmitter output signal, considered to have the highest signal quality in the system.

Measurement of the signal BER is sufficient if the SOA gate is used at the receiver front-end. This is the case for SOA gate used for all-optical demultiplexing which is usually performed prior to the electrical receiver. However, if the SOA gate output signal is used in further optical processing devices or for transmission then more detailed measurements are required, namely the signal Q-factor and chirp. This is the case for application of SOA gates to optical wavelength conversion and regeneration where the signal at the gate output is likely to be re-transmitted in a system where several SOA gates are cascaded. The Q-factor is a parameter used to assess the signal quality and is defined by the difference of the mean values of the two signal levels ($\mu_{1,0}$) divided by the sum of the noise RMS values (standard deviations) at the two signal levels ($\sigma_{1,0}$). Assuming Gaussian noise distributions for both signal levels, the signal Q-factor can be expressed as [Agr02]:

$$Q = \frac{|\mu_1 - \mu_0|}{\sigma_1 + \sigma_0} \qquad (2\text{-}3)$$

For the case of optical 3R regeneration the assessment of the regenerative properties (signal retiming and reshaping) of the SOA gate is also required. To date, most of the optical regenerators proposed have been assessed in terms of the receiver sensitivity penalty at high OSNR introduced by the regenerator on the transmitter output signal; this includes [Lav02] [Leu01] [Phi98] [Gav04a]. Relevant experimental results are summarised in Table 2-2. However, this measurement only assesses the effect of pattern-dependent distortion on the regenerated output signal BER at certain switching frequency.

To demonstrate the SOA gate regenerative properties would require to show an improvement of the signal Q-factor or receiver sensitivity at low OSNR with respect to the reference transmitter signal. In particular, to claim 3R regeneration functionalities both optical retiming and reshaping have to be demonstrated. Assessment of the regenerator optical reshaping properties has been performed for most configurations and the most relevant results are summarised in Table 2-2.

Results in Table 2-2 include:

- The regenerator *Intensity jitter tolerance*; which is a measure of the intensity jitter (RMS) present on the input signal which can be suppressed by regeneration without incurring in a BER penalty.
- The *extinction ratio improvement*; which is a measure of the regenerated signal extinction ratio with respect to the input signal extinction ratio.
- *The Q-factor improvement*; which is a measure of the regenerated signal Q-factor with respect to Q-factor of the distorted input signal. Together with the Q-factor, the error-free receiver sensitivity is also usually measured for the signal before and after the regenerator.

Measurements of the receiver sensitivity involve loading the transmitter output signal with optical noise to degrade the OSNR before the regenerator in order to compare the receiver sensitivity improvement of the regenerated signal, with respect to the input signal. Following this approach receiver sensitivity improvement after regeneration from signals with OSNR as low as 20dB has been demonstrated at 40Gb/s for the SOA-DI [Leu02], the UNI [Tsu02] and the PSSI [Gav05].

		SOA-DI	**DOM-MZ**	**UNI**	**PSSI**
Retiming	**Timing jitter tolerance (RMS)**	6ps [Leu01]		8.5ps [Tsu02]	10ps [chapter 5]
Reshaping	**Intensity jitter tolerance (RMS)**				3dB [Gav04a]
	Extinction ratio improvement	5dB [Leu02a]	8dB [Arm05]		3dB [Gav04a]
	3R Signal OSNR (dB/0.1nm)	45dB [Leu01]	36dB [Nie03b]	>30dB	36dB [chapter 5]
	Receiver sensitivity penalty (dB)	1dB [Leu01]	1dB [Lav02]	1dB [Tsu03]	1dB [Gav04a]
	Q-factor (dB) improvement	3dB [Leu02a]		1dB [Tsu02]	1.5dB [Gav05c]

Table 2-2 Summary of the experimental results for the characterisation of the noise suppression properties of 40Gb/s optical regenerators

The physical process behind the receiver sensitivity and signal Q-factor improvement was explained in [Mik96], to be a consequence of the noise compression introduced by the regenerator transfer function slope. However, the noise compression properties of the regenerator depend on the input signal extinction ratio [Ohl97]. This is because the slope of the transfer function, which ultimately determines the regenerator noise compression, varies nonlinearly with the input power. Theoretical calculations presented in this thesis show that a variation of less than 1dB in the input signal extinction ratio can significantly change the noise compression properties of the regenerator.

Thus, assessing the reshaping properties an SOA regenerator with noise loading experiments is possibly inaccurate if the input extinction ratio is not carefully optimised. To perform an accurate measurement a precise knowledge of the regenerator transfer function is necessary, so to estimate the optimum input extinction ratio and the expected noise compression. However, the transfer function can only be measured with accuracy using static pump-probe techniques, as described in [Idl96] [Arm05]; where "*static*" refers to the fact that the SOA is triggered by a continuous wave (CW) pump signal rather than by a PRBS (Pseudo-Random Bit Sequence) modulated RZ pulse train. Thus, the effects of patterning, which at high bit-rate significantly change the regenerator transfer function and switching contrast [Bis02b], can not be assessed, and the measured transfer function is only indicative of the regenerator performance.

Furthermore, in most of the experiments summarised in Table 2-2, the regenerator noise suppression ability is quantified by measuring the receiver sensitivity improvement after regeneration. However, a measurement of the receiver sensitivity does not clearly indicate whether the improvement in the signal quality comes from an extinction ratio enhancement or a compression of the noise. If a Q-factor measurement is taken then it would still be difficult to retrieve the signal extinction ration and noise level of the regenerated signal with accuracy because of the non Gaussian statistics of the regenerated signal noise [Ohm05] [Ohl97]. Nonetheless, it is important to quantify, individually, the improvement in both extinction ratio and noise suppression, to estimate the performance of a chain of cascaded regenerators [Gav05c].

For these reasons, noise loading measurements are not ideal to predict the performance of the regenerator in transmission or to compare different configurations.

More general results can be deduced when assessing the regenerator tolerance to timing jitter. This is because the tolerance to timing jitter fundamentally depends on the regenerator switching window which is determined for most configurations by the physical implementation of the interferometer rather than by the SOA nonlinearities.

Retiming experiments involve the artificial introduction of timing jitter on the regenerator input signal to compare the receiver sensitivity improvement after regeneration. Following this approach the receiver sensitivity improvement after regeneration from signals with up to 8ps RMS timing jitter has been demonstrated at 40Gb/s for most configurations. Measurements of the retiming abilities of the different configurations at 40Gb/s are also summarised in Table 2-2. The larger tolerance to timing jitter of optical gates with respect to an electrical receiver was explained in [Jin94] to be a consequence of the larger electro-optical bandwidth typical of an SOA gate regenerator.

2.2.2 Characterisation of SOA gates in transmission

The investigation of the cascadability properties of SOA gates is necessary to predict the performance of transmission with cascaded optical regeneration and wavelength conversion.

It was shown that the BER evolution in transmission with cascaded nonlinear gates depends on the SOA gate transfer function slope around the signal zero and one levels [Mor03]. Given that for different values of the input extinction ratio the transfer function shows a different slope, there is an optimum range for input signal extinction ratio where the noise suppression is maximised. Thus, the fundamental condition to cascade nonlinear gates is that the signal extinction ratio at the input of each gate is maintained within the optimum noise suppression range [Ohl97]. Under this condition, noise suppression is maximised for all gates in the chain.

The cascadability condition imposes an important requirement on the regenerator; signal reshaping has to be accomplished while performing the necessary extinction ratio enhancement to maintain cascadability. In fact, the extinction ratio of the regenerated signal degrades along the transmission span between cascaded SOA gates due to amplifier noise and fibre nonlinearities. Thus, the SOA gate regenerator must compensate for the span extinction ratio degradation to maintain cascadabilty.

To date, the cascadability properties have been demonstrated for different configurations (UNI, DOM-MZI, PSSI). The relevant results are summarised in Table 2-3.

Scheme	TX signal	Spacing (km)	Distance (km)	Comments	Ref
MZI-DOM	2.5Gb/s NRZ	55 DSF	3850	SOA for wavelength conversion	[Lav98]
MZI-DOM	20Gb/s (2^7-1) PW = 6 ps	110 DSF	22000	2 cascaded MZI	[Lav00]
MZI-DOM	40Gb/s (2^{23}-1) PW = 12 ps	40 DSF	4000	2 cascaded MZI	[Lav01]
MZI-DOM	40Gb/s (2^{23}-1) PW = 12 ps	300 SMF	30000	SOA for wavelength conversion	[Lav03]
UNI	40Gb/s (2^7-1) PW = 4.5 ps	100 DSF	2000	wavelength conversion not required	[Thi99]
UNI	40Gb/s (2^7-1) PW = 6 ps	400 DSF	12000	2 cascaded UNI	[Has03]
UNI	40Gb/s (2^{23}-1) PW = 6 ps	200 DSF	30000	2 cascaded UNI	[Ino03]
SOA-DI	40Gb/s (2^{31}-1) PW = 6 ps	400 TWRS NZDSF	1000000	HNLF for wavelength conversion	[Leu02b]
PSSI	10Gb/s (2^{23}-1) PW = 20 ps	600 SMF	20000	SOA DI for wavelength conversion	[Gav05a]

Table 2-3 Summary of the experimental results for transmission with cascaded optical 3R regeneration

Several hundreds gates have been cascaded without affecting, in most cases, the receiver sensitivity or signal Q-factor. These experiments have demonstrated that, once the cascadability condition is satisfied, the transmission Q-factor is determined by the regenerator output Q-factor and is maintained unchanged over distance by the regenerator.

More recent studies, described in this thesis, have investigated the impact of noise on the cascadability properties of SOA gates [Gav05a]. This work led to demonstrate a further property of cascaded optical gates which relates the SOA gate regenerator output Q-factor to the inter-regenerator spacing. It was found that SOA gate regenerators operate with decreased output signal Q-factor when cascaded with longer inter-regenerator spacing. In fact, as described in chapter 3, there is a trade-off between the extinction ratio enhancement, and the noise suppression properties in an SOA gate. In particular, the reshaping ability of the SOA gate decreases when the SOA gate operates with increasing extinction ratio gain. Thus, over longer inter-regenerator spacing, where larger extinction ratio enhancement is required to maintain cascadability, the regenerator noise suppression decreases, and so does the output signal Q-factor. This trade-off was found to determine the maximum inter-regenerator spacing, and ultimately the regenerative ability of a cascaded SOA gate.

Thus, the SOA gate regenerator noise suppression properties have to be considered a function of the input signal extinction ratio but also of the regenerator extinction ratio gain. For this reason the noise suppression properties of an SOA gate must be measured in a cascaded experiment and can not be measured on a back-to-back configuration. In a transmission experiment with cascaded regenerators we ensure that the regenerator is providing the extinction ratio gain necessary to maintain cascadability. Furthermore, cascading regenerators we ensure that the extinction ratio is maintained at its optimum at the regenerator input where noise suppression is maximised. Under these experimental conditions the noise suppression of the regenerator can be optimally measured.

Experimental characterisation of the noise suppression ability of a regenerator in transmission with cascaded SOA gates is presented in this thesis, for the first time, to show that Q-factor improvement in the range of 3dB can be achieved with SOA gate regenerators with input OSNR of 20 (dB/0.1nm) [Gav05a]. This experimental technique is the most complete, of those proposed to date, to assess the regenerator noise suppression performance and is described in detail in chapter 6.

Summary

This chapter covered a review of the configurations proposed in the literature for high-bit rate (≥40Gb/s) all-optical processing based on XPM and XGM nonlinearities in SOA.

The fundamental trade-off in switching with SOAs as nonlinear elements is between large nonlinearities and speed. For this reason SOA gates can either be optimised to operate with large switching contrast, as in XPM configurations, or at fast switching speed, as in XGM configurations. The first finds applications in 40Gb/s all-optical regeneration and OTDM demultiplexing, while the second in analogue wavelength conversion at bit-rates of up to 160Gb/s.

Of all the XPM-gates, the DOM-MZI has been shown to have the shortest switching window which makes this configuration ideal for optical demultiplexing, whilst the polarisation discriminating interferometer configurations (UNI and PSSI) operate with enhanced switching contrast due to coupling asymmetries, which makes these configurations ideal for 3R regeneration. The PSSI configuration was proposed in this thesis and, to date, is the only configuration to have demonstrated multiple channel operation. The advantages of the PSSI over the UNI are in the simplicity of controlling the switching window, in the operating stability, and in the enhanced switching contrast due to the counter-propagating operations. Furthermore, the PSSI configuration does not require, as the UNI, polarisation insensitive SOA to operate, and thus can be used with advanced optical components such as SOA arrays for the investigation of multiwavelength optical processing [Mik01]. For this reason we will focus on the PSSI configuration in the investigation of the regenerative properties of XPM gates, which will be presented in chapter 5.

In the second part of this chapter, the experimental techniques proposed in the literature to characterise the SOA gate switching properties have been reviewed. To date, back-to-back measurements of the BER, Q-factor, chirp and switching window profile have been used to characterise demultiplexing, wavelength conversion and 3R regeneration with SOA gates. Similarly, the regenerative properties of SOA regenerators have been investigated in back-to-back configuration with noise loading experiments. However, due to the properties of the SOA analogue transfer function, it was discussed that back-to-back characterisation is not sufficient to predict the SOA regenerator performance in a transmission system with cascaded regenerators. This is because the regenerative properties of an SOA gate are a function of the input signal distortion characteristics, which can not systematically be reproduced in a back-to-back configuration. For this reason, in this thesis the regenerative properties of SOA gates are investigated with transmission experiments with cascaded optical regeneration. The results are discussed in chapter 6.

In the next chapter, the theoretical investigation of the reshaping and switching properties of SOA gates, including both XPM and XGM configurations, is presented.

Chapter 3 Assessment of the regenerative properties of optical switching with SOA nonlinearities

As described in chapter 2, SOA gates configurations can be classified in two groups; XGM configurations and XPM configurations. Most of the XGM and XPM gates proposed to date have been compared in terms of their switching speed, and not in terms of their reshaping properties, which, however, are of fundamental importance for application to optical signal regeneration. This chapter presents the comparison of the reshaping characteristics of XGM and XPM optical gates operating at high bit-rates.

In section (3.1) the transfer function of a general optical switch and the parameters relevant to the assessment of its regenerative properties are introduced. In particular, the concept of the transfer function slope is described to assess the gate optical reshaping abilities.

In section (3.2) the transfer function of both SOA gates based on nonlinear gain saturation (XGM) and on SOA-assisted interferometer configurations (XPM) is derived. The regenerative characteristics of both configurations are theoretically investigated by means of deriving the SOA gate transfer function slope. The approach proposed here allows to investigate the reshaping properties of the SOA gate as a function of the different the SOA physical parameters such as the α-factor, the small signal gain and the carrier recovery time.

In section (3.3) the impact of the SOA nonlinear effects dynamics on the gate switching characteristics is investigated. In particular, the penalties of operating with an ultra-short timing window on the gate switching contrast and noise compression properties are assessed.

In section (3.4) the cascadability properties of SOA-based regenerators are assessed on the basis of the transfer function characterisation.

In conclusion, this chapter provides the theoretical framework necessary to support the experimental investigation of the XGM and XPM gates regenerative properties presented in the following chapters.

3.1 Transfer function parameters of an all-optical gate

The switching characteristic of an optical gate in the absence of pattern-dependent effects are described by the static transfer function, which gives the relationship between the gate input to the output power. The transfer function can also be used to assess the reshaping properties of the optical gate when this is used for optical signal regeneration. Here, some of the important parameters of the transfer function relevant to signal regeneration are described.

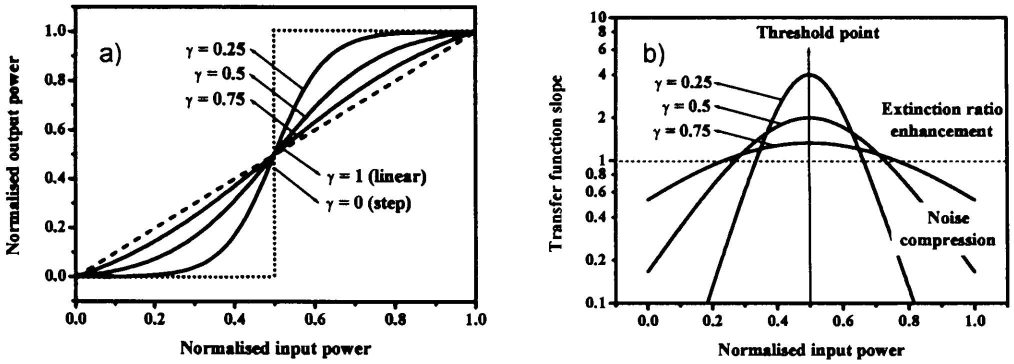

Figure 3-1 Transfer function (*tanh*) (a) and transfer function slope (b) for different γ-values

Figure 3-1(a) shows a general approximation of the transfer function of a bi-stable optical gate. The transfer function is approximated with a *tanh* function with nonlinear parameter γ [Ohl97]. The nonlinear parameter γ can be considered as the nonlinear coefficient of the material used for switching (SOA, fibre). The output power (P_{out}) is given by the simple relation: $P_{out} = T(P_{in})$, where $T(P_{in})$ is the transmittance of the gate which depends on the input power (P_{in}). At low input power the gate is virtually closed, at high input power the transmittance significantly increases and the gate is open. The $T(P_{in})$ function is defined, following [Ohl97]:

$$\begin{cases} T(P_{in}) = 1/2 + a\tanh[b(P_{in} - 1/2)] \\ T(0) = 0 \\ T'(1/2) = 1/\gamma \end{cases} \qquad (3\text{-}1)$$

For $\gamma = 1$, $T(P_{in})$ is a linear function with unit slope and for decreasing γ it evolves into an ideal step transfer function, which is achieved for $\gamma = 0$. The degree of nonlinearity of the optical switch, thus, increases with the parameter $(1 - \gamma)$.

Assessment of the reshaping ability of the optical gate involves the quantification of two fundamental parameters; the noise suppression and the signal extinction ratio enhancement or the extinction ratio gain of the optical gate. It will be shown here that both parameters can be quantified from optical gate transfer function slope.

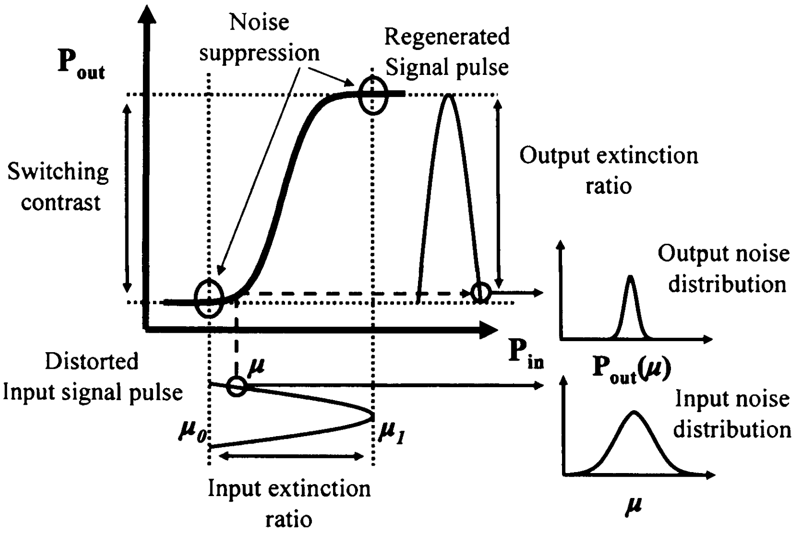

Figure 3-2 Noise compression with the nonlinear transfer function

With reference to Figure 3-2, the noise suppression performed by the optical gate transfer function at any point $\mu = P_{in}(t)$ on the input pulse intensity profile can be estimated by approximating the regenerator transfer function around μ with a linear function with slope Y, defined as:

$$Y_\mu = \left.\frac{dT}{dP_{in}}\right|_{P_{in}=\mu} \qquad (3\text{-}2)$$

Thus, the noise distribution function at the point $P_{out}(\mu)$ on the output pulse profile is the same as the noise distribution function at μ but the standard deviation σ_{out} is now given by:

$$\sigma_{out}^2 = Y_\mu^2 \sigma_{in}^2 \qquad (3\text{-}3)$$

Where σ_{in} is the standard deviation of the noise probability distribution function with mean μ. Thus, for example, the noise suppression around the input signal means values for the "*one*" (μ_1) and "*zero*" (μ_0) levels, will be given by:

$$\sigma_1^2 = Y_1^2 \sigma_{\mu_1}^2 \text{ where } Y_1 = \frac{dT}{dP}(\mu_1) \qquad (3\text{-}4)$$

$$\sigma_0^2 = Y_0^2 \sigma_{\mu_0}^2 \text{ where } Y_0 = \frac{dT}{dP}(\mu_0) \tag{3-5}$$

It is particularly important to estimate the noise on the means of the signal levels as this is used to estimate the signal Q-factor. We will refer to the transfer function slope around the signal zero (Y_0) and one (Y_1) levels as the regenerator noise compression term/factor (Y_{NC}). For the case of the transfer function $T(P_{in})$ described in equation (3.1), $Y_{NC} = Y_0 = Y_1$.

The transfer function slope $Y(P_{in})$ can be calculated as the derivative with respect to the input power of the optical gate transfer function $T(P_{in})$, which for a *tanh* function is a $sech^2$ function. The linear slope of the transfer function $T(P_{in})$ is given by:

$$Y(P_{in}) = \frac{dT}{dP_{in}} = (1/\gamma) sech^2[a(P_{in} - 1/2)] \tag{3-6}$$

The slope $Y(P_{in})$ of the optical gate transfer function $T(P_{in})$ is shown in Figure 3-1(b). The point were the slope is maximum is defined as the slope at the threshold point, which is equal to $Y_{th} = 1/\gamma$.

The switching contrast and the nonlinear transfer function of an optical gate are frequently expressed in decibels (dB). The slope of the transfer function expressed in decibels (T_{dB}) is defined as the derivative of T_{dB} with respect to the input power expressed in dBm (P_{dBm}), and can be calculated as:

$$\begin{aligned} Y_{dB}(P_{dBm}) &= \frac{dT_{dB}}{dP_{dBm}} = \frac{d10\log(T(P_{in}))}{d10\log(P_{in})} = \frac{dT_{dB}/dP_{in}}{dP_{dBm}/dP_{in}} \\ &= \frac{10/\ln(10)\cdot 1/T(P_{in})\cdot dT/dP_{in}}{10/\ln(10)\cdot 1/P_{in}} = \frac{P_{in}}{T(P_{in})}\frac{dT}{dP_{in}} \end{aligned} \tag{3-7}$$

Figure 3-3 shows the transfer function and the transfer function slope expressed in dB for the case of $\gamma = 0.25$.

As shown in equation (3.3), a nonlinear optical gate performs regeneration by noise compression. Noise compression only occurs at the points on the transfer function where the slope (Y) is less than unity $Y(P_{in}) < 1$, or for the slope express in decibels (Y_{dB}) where $Y_{dB}(P_{in}) < P_{in}/T(P_{in})$.

Thus, the condition for operating the optical gate as a regenerator is that the input signal "*zero*" and "*one*" levels occur where the regenerator transfer function slope satisfy the above conditions.

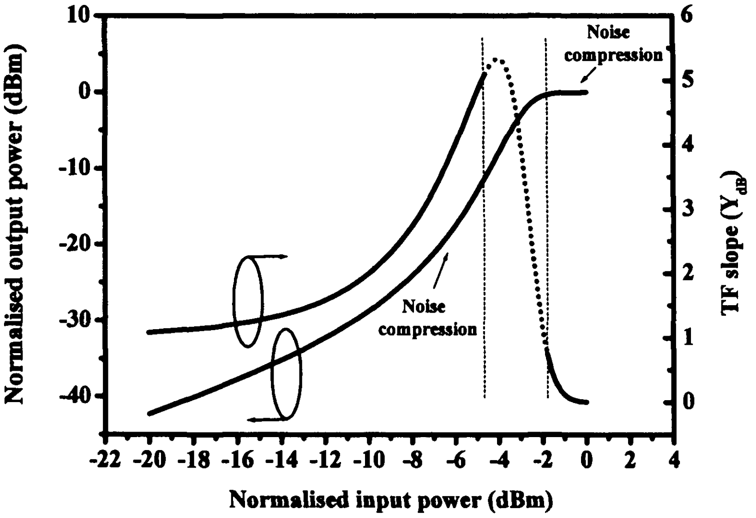

Figure 3-3 Transfer function (TF) and transfer function slope for $\gamma = 0.25$

Referring to Figure 3-1 (b), noise compression is performed continuously over the transfer function with different magnitudes except around the threshold point. A smaller nonlinear parameter γ corresponds to a smaller noise compression term and to a larger slope around the threshold point.

For the case of the transfer function expressed in dB, as shown in Figure 3-3, then noise compression is performed on the areas which correspond to the points on the transfer function where its slope $Y_{dB}(P_{in}) < P_{in}/T(P_{in})$ (solid segment of the TF slope).

The second important parameter is the regenerator extinction ratio enhancement, or extinction ratio gain. This refers to the ability of the regenerator to improve the input signal extinction ratio and is defined as the ratio of the output (ER_{out}) to the input (ER_{in}) signal extinction ratios:

$$ER_{in} = \mu_1/\mu_0 \tag{3-8}$$

$$ER_{out} = T(\mu_1)/T(\mu_0) \tag{3-9}$$

$$ER_{gain}dB = 10\log\left(\frac{ER_{out}}{ER_{in}}\right) \tag{3-10}$$

Thus, calculation of the extinction ratio gain requires the estimation of the gate input and output signal extinction ratio. The output extinction ratio is determined by the gate switching contrast which is related to the input extinction ratio by the transfer function. The input signal extinction ratio is here defined as the ratio between the two input power values (μ_1, μ_0) corresponding to particular transfer function slope values. Such definition is necessary because both the gate noise compression and the switching contrast are function of the input signal mean power levels. Therefore, when assessing the extinction ratio gain of a nonlinear gate, the input extinction ratio is calculated from the transfer function slope as the ratio between the two input power levels corresponding to a particular value of the transfer function slope. Throughout this thesis noise compression values equal to γ or to an order of magnitude smaller than the slope at the threshold point will be used to calculate the input signal extinction ratio.

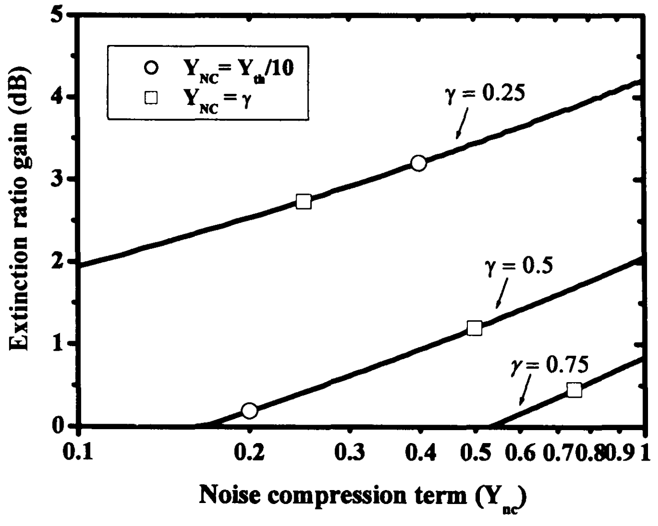

Figure 3-4 Trade-off between the extinction ratio gain and the slope around signal levels for different γ, (○) corresponds to the points where Y_{NC} is an order of magnitude smaller than the slope at the threshold point, (□) corresponds where Y_{NC} is equal to γ

Figure 3-4 shows the extinction ratio gain, given in equation (3-10), as a function of the noise compression term (Y_{NC}); the point (○) on the curve refers to where Y_{NC} is an order of magnitude smaller than the threshold slope, and the point (□) to where $Y_{NC} = \gamma$. Thus, for any given value of γ, there is a trade-off between the regeneration extinction ratio gain and noise compression term at the signal "*one*" and "*zero*" levels. In particular, the extinction ratio gain increases with the noise compression term. This trade-off is of particular importance when we consider transmission with cascaded regenerators, which will be described in section 3.4 of this chapter. Furthermore, for smaller values of the nonlinear parameter γ, the extinction ratio gain increases due to the sharper slope around the threshold point.

In conclusion, the fundamental difference between switching with a nonlinear transfer function, typical of optical gates, with respect to a step-like transfer function, typical of electrical gates, is that the output signal properties depend on the input signal characteristics (such as extinction ratio, signal Q-factor, pulse shape and power). In fact, both the noise level and the extinction ratio of the output signal are related to the input signal characteristics via the transfer function. In this chapter section, it as been shown that the transfer function slope can be used to investigate the reshaping performance of the optical gate. It has also been found that the fundamental conditions for an optical gate to operate as an optical regenerator are a noise compression factor smaller than unity ($Y_{NC} < 1$) and extinction ratio enhancement larger than unity ($ER_{gain}dB > 0$).

In the following sections of this chapter, the approach presented here is applied to compare the characteristics and reshaping properties of SOA gates based on XGM and XPM configurations.

3.2 Signal reshaping with SOA-based optical gates

The reshaping and cascadability properties of nonlinear optical gates have been investigated approximating the nonlinear transfer function with a *tanh* function [Ohl97]. This approach has shown to be appropriate to assess the reshaping ability of most optical nonlinear media such as fibre and semiconductor, whose transfer function resemble the *tanh* function.

However, this approximation precludes the analysis of the relationship between the SOA physical parameters and the transfer function characteristics. Yet, the SOA physical parameters will ultimately limit the performances of optical switching both in terms of the operating frequency and reshaping properties.

In this section, the impact of the SOA parameters, such as the α-factor the small signal gain and the recovery time, on the regenerative properties of SOA optical gates is theoretically investigated for both XGM and SOA-assisted interferometer (XPM) configurations. This is achieved using the transfer function slope to quantify the noise compression and signal reshaping properties as in [Ohl97], but here the slope is calculated directly from the SOA nonlinear transfer function, which depends on the SOA physical parameters, rather than from the general *tanh* approximation.

3.2.1 SOA nonlinearities

As described in chapter 2, most of the optical regenerator configurations investigated to date, utilise nonlinear effects in SOAs to achieve switching. These are the dependence of gain and phase of an SOA on a signal optical power.

The theory of nonlinear pulse propagation in an SOA is well known [Agr86]. The SOA response to an optical pulse, with pulse width (τ_p) larger than the SOA intra-band relaxation time ($\tau_p > 1ps$), is described by the carrier-density rate equation [Agr89]:

$$\frac{\partial N}{\partial t} = \frac{I}{qV} - \frac{N}{\tau_c} - \frac{g(N)}{h\omega_0}|A|^2 \tag{3-11}$$

N is the carrier density in the active region and is a measure of the gain per *cm* of the device, I is the effective injection current, q is the electron charge, V is the active volume of the SOA, g is the gain coefficient, $h\omega_0$ is the photon energy τ_c is the spontaneous carrier lifetime, and A is the slowly-varying envelope associated with the input optical field. The first term of equation (3-11) describes the pumping by the injection current, the second term accounts for the decrease of carrier density by radiative and nonradiative recombination, and the third term denotes the decrease of carrier density by stimulated emission. The power (P_s) and phase (φ_s) of the optical signal pulse propagating inside the amplifier can be derived from equation (3-11) as described in [Agr89]:

$$\frac{\partial P_s}{\partial z} = (g - \alpha_{\text{int}})P_s \tag{3-12}$$

$$\frac{\partial \varphi_s}{\partial z} = -\frac{1}{2}\alpha g \tag{3-13}$$

$$\frac{\partial g}{\partial t} = \frac{g_0 - g}{\tau_c} - \frac{gP_s}{E_{sat}} \tag{3-14}$$

Where g_0 is the small signal gain, E_{sat} the SOA saturation energy, α_{int} the SOA internal loss and α is the linewidth enhancement factor or α-factor [Hen82], which in a semiconductor optical amplifier is in the range of 3-8. The α-factor is defined as the ratio of the derivative of the real part of the refractive index with respect to the carrier density to the derivative of the gain with respect to the carrier density [Hen82]:

$$\alpha \equiv -\frac{4\pi}{\lambda}\frac{\partial n'/\partial N}{\partial g/\partial N} \tag{3-15}$$

where λ is the vacuum wavelength and n' the real part of the complex refractive index defined as $n = n' + j\,\lambda a/4\pi$ where a is the SOA absorption coefficient, related to the gain coefficient as $a = -g$. The absorption and the refractive index are related through the Kramers-Krönig (KK) relationship [Kit96] which in the following form gives the relationship between the refractive index and absorption [Leu99]:

$$n'(\omega) - 1 = \frac{c}{\pi} P \int \frac{a(\omega')}{\omega'^2 - \omega^2} d\omega' \tag{3-16}$$

where P indicates taking the principal value integral and ω is the frequency of the optical field. The KK relationship can be used to calculate the refractive index of a material by measuring its frequency-dependent absorption. Using the KK relationship an expression for the α-factor can be derived in terms of parameters which determine the SOA gain [Wes87].

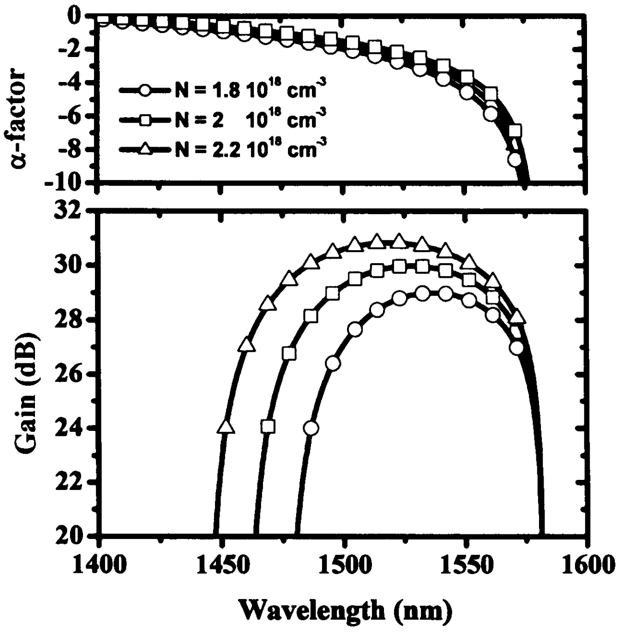

Figure 3-5 SOA Gain and α-factor as a function of wavelength for different carrier concentration levels N (cm^{-3}).

Figure 3-5 shows the calculated variation of the gain and α-factor as a function of wavelength for an InGaAsP device operating around 1.5μm. The device parameters values used in the calculations are; the temperature T = 300K, refractive index n = *3.5*, the energy band gap Eg = 0.785 eV, the effective electron mass $m_c/m_o = 0.06$, the effective hole mass $m_v/m_o = 0.4$ [Sve98].

In the spectral region of where the device has gain, the α-factor decreases with wavelength. It should also be noted that variation in the device carrier density (for example through a change in driving current) has a smaller effect on the α-factor than on the gain. The value of the α-factor depends on wavelength, carrier density, on the temperature and on the optical power coupled into the active region of the device [Leu99]. In chapter 4, measurements of the α-factor of different SOAs used in this work are presented.

The temporal evolution of the optical pulse inside the amplifier generally requires a numerical solution of equation (3-12)-(3.14) [Hod91] [Dur92]. However, if the ($\alpha_{int} \ll g$), it is possible to solve these equations in a closed form. This condition is often satisfied in practice. Thus, an expression for the power $P_{out}(t)$ and phase $\varphi_{out}(t)$ of the signal at the amplifier output can be obtained integrating equations (3-12)-(3-13) over the amplifier length L, for $\alpha_{int} = 0$:

$$P_{out}(t) = P_{in}(t)\exp[h(t)] \tag{3-17}$$

$$\varphi_{out}(t) = \varphi_{in}(t) - 1/2\,\alpha h(t) \tag{3-18}$$

Where $P_{in}(t)$ and $\varphi_{in}(t)$ are the power and phase of the input signal pulse. The integrated gain term h, which physically represents the integrated gain at each point of the pulse profile, can be expressed as the solution of the following ordinary differential equation:

$$\frac{dh}{dt} = \frac{g_0 L - h}{\tau_c} - \frac{P_{in}(t)}{E_{sat}}[\exp(h) - 1] \tag{3-19}$$

The analysis of the gain dynamics involves the numerical solution of the above equation. However, to derive the SOA gain and phase static transfer function, an expression for the $h(P_{in})$ as perturbed by a continuous wave (CW) signal is required. This is calculated from the steady state solution of equation (3-19) obtained for $(dh/dt = 0)$, and is given by:

$$h(P_{in}) = g_0 L - P(\exp[h(P_{in})] - 1) \tag{3-20}$$

where $P = P_{in}/P_{sat}$ and $P_{sat} = E_{sat}/\tau_c$. Equation (3-20) can be used in equations (3-17) and (3-18) to derive an analytical expression for the gain (G) and phase (φ) transfer function of the SOA perturbed by CW signal with power (P_{in}).

$$G = \exp[h(P_{in})] \tag{3-21}$$

$$\varphi = 1/2\,\alpha h(P_{in}) \tag{3-22}$$

In the following sections, the slope of the gain and phase transfer function, as expressed in equations (3-21) (3-22), are derived to investigate and compare the reshaping properties of XGM and XPM gates. The SOA parameters for the calculations presented in this chapter are E_{sat} = 1pJ, τ_c = 100ps and G_0 = 30dB unless specified otherwise.

3.2.2 Optical switching based on SOA gain nonlinearity

The principle of operation of an optical gate based on nonlinear gain saturation is shown in Figure 3-6.

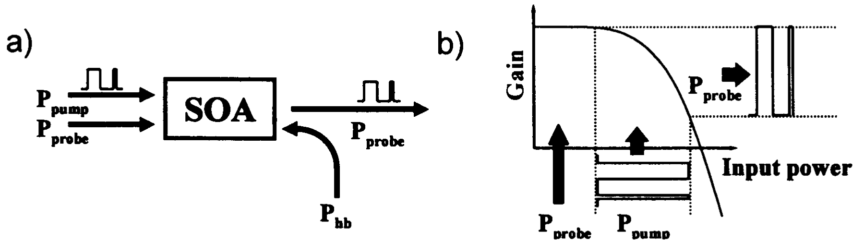

Figure 3-6 a) XGM gate configuration; b) Principle of optical switching with gain nonlinearity

The pump signal is an intensity modulated signal (RZ or NRZ), the probe is CW signal. The pump signal modulates the probe signal intensity varying the SOA gain saturation [Dur96]. In correspondence to large pump optical power the gain is saturated, the SOA transmittance is reduced at minimum and the gate is closed. However for low pump power the gain is unsaturated and the probe is amplified.

Figure 3-7 shows the SOA gain transfer function for different small signal gain values, calculated from equation (3-21). As the input power increases the gain saturates until it reaches transparency. The SOA gain transfer function shows bi-stable switching characteristics, which depend on the input power.

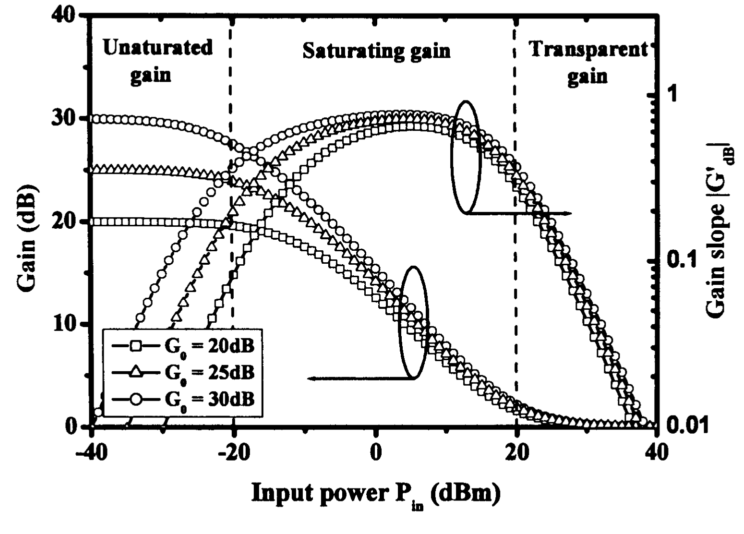

Figure 3-7 SOA Gain transfer function and gain transfer function slope magnitude for different small signal gain values (G_0)

Due to the nonlinear characteristics of the transfer function switching is accompanied by signal reshaping of the input signals. At low input power the unsaturated gain is responsible for the suppression of noise on the "*zero*" level of the input signal, at high input power the transparent gain is responsible for the suppression of noise on the "*one*" level of the input signal. The saturating part of the transfer function is responsible for the signal extinction ratio regeneration. To quantify the reshaping ability of gain dependent switching we use the slope of the $G(P_{in})$ function. This is derived differentiating equation (3-21) with respect to the input power normalized to the saturation power $P = P_{in}/P_{sat}$:

$$G' = \frac{dG}{dP} = \frac{G(1-G)}{1+PG} \text{ where } P = \frac{\log(G_0/G)}{G-1} \tag{3-23}$$

where G_0 is the SOA small signal gain defined as $G_0 = \exp(g_0 L)$. The derivation of equation (3-23)-(3-25) is given in appendix 1. The switching contrast and the nonlinear transfer function of an optical gate are frequently expressed in decibels (dB). The slope of the transfer function expressed in decibels (G_{dB}) is defined as the derivative of G_{dB} with respect to the normalised input power P, expressed in decibels (P_{dB}), and can be calculated as:

$$G'_{dB} = \frac{dG_{dB}}{dP_{dB}} = \frac{d10\log(G(P))}{d10\log(P)} = \frac{P}{G}\frac{G(1-G)}{1+PG} \tag{3-24}$$

Equation (3-24) shows that the slope is a function of G_0. The magnitude of the gain transfer function slope (G'_{dB}), as expressed in equation (3-24), is also shown in Figure 3-7 for different value of G_0. The gain slope curve is an order of magnitude smaller around the unsaturated and transparent gain regions with respect to the values around the saturating region of the gain. This ensures that the noise present on the pump signal levels is suppressed and not transferred on the probe signal during the process of wavelength conversion. Increasing G_0 sharpens the transfer function leading to an increase in the slope maximum.

The gain slope maximum, also defined as the slope at the threshold point, occurs around $G = \sqrt{G_0}$, and can be expressed as:

$$\left.\frac{dG_{dB}}{dP_{dB}}\right|_{G=\sqrt{G_0}} = \frac{-\log\left(\sqrt{G_0}\right)\left(\sqrt{G_0}-1\right)}{\sqrt{G_0}-1+\sqrt{G_0}\log\left(\sqrt{G_0}\right)} \tag{3-25}$$

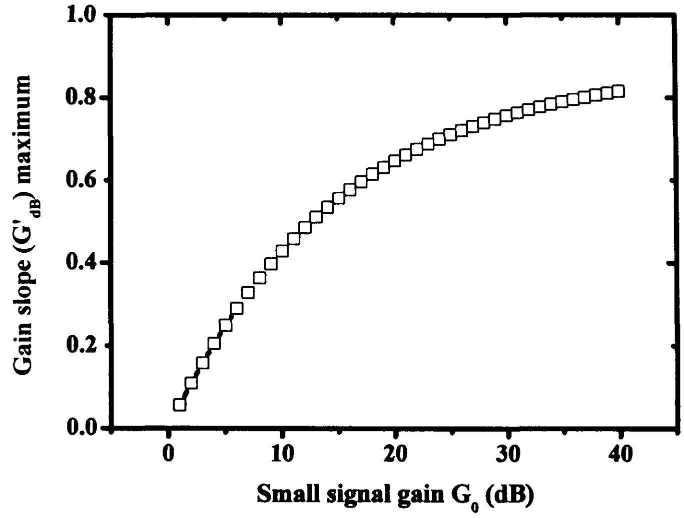

Figure 3-8 SOA gain transfer function slope (G'_{dB}) calculated at the threshold point as a function of G_0

Figure 3-8 shows the gain slope (G'_{dB}) calculated at $G = \sqrt{G_0}$ as a function of G_0. The gain slope increases with G_0, however never reaches unity. As described in section 3.1, if the slope at the threshold point is less than unity the SOA gate does not perform extinction ratio enhancement; thus, the probe signal has a smaller extinction ratio than the pump signal.

This suggests that, in XGM wavelength conversion, the noise present on the pump signal is compressed and not transferred to the probe signal, however the probe extinction ratio at the gate output is smaller with respect to the pump extinction ratio at the gate input. Thus, extinction ratio gain can not be achieved switching with gain based nonlinearity.

3.2.3 Optical switching with an SOA-assisted interferometer

Alternatively optical switching with an SOA can be achieved utilising nonlinear phase modulation effects. This is based on the use of an SOA in an interferometer which converts the nonlinear phase shift into intensity switching [Eis93]. The interferometer transfer function is:

$$P_{out} = 1/2\left[1-\cos(\varphi(P_{in}))\right] \qquad (3\text{-}26)$$

where $\varphi(P_{in})$ is the nonlinear phase shift induced in the SOA. The principle of operation of an optical gate based on phase nonlinearity in an SOA-assisted interferometer is shown in Figure 3-9.

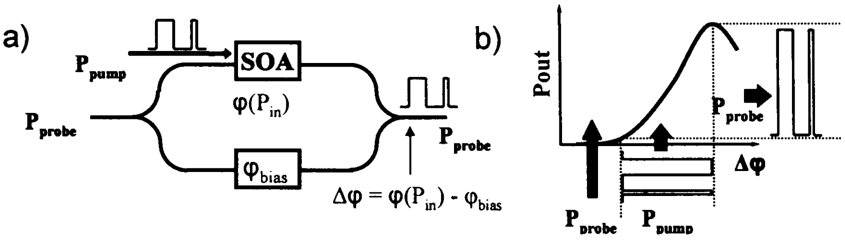

Figure 3-9 a) XPM gate configuration; b) interferometer transfer function

The pump signal modulates the SOA refractive index to generate a differential phase shift ($\Delta\varphi = \varphi(P_{in}) - \varphi_{bias}$, where φ_{bias} is the interferometer bias) between the two interfering probe components which is converted into intensity modulation by the interferometer. Corresponding to large pump optical power a differential phase shift ($\Delta\varphi$) of π radians is induced and the gate is open. However, for low pump power no differential phase shift is induced and the gate is virtually closed.

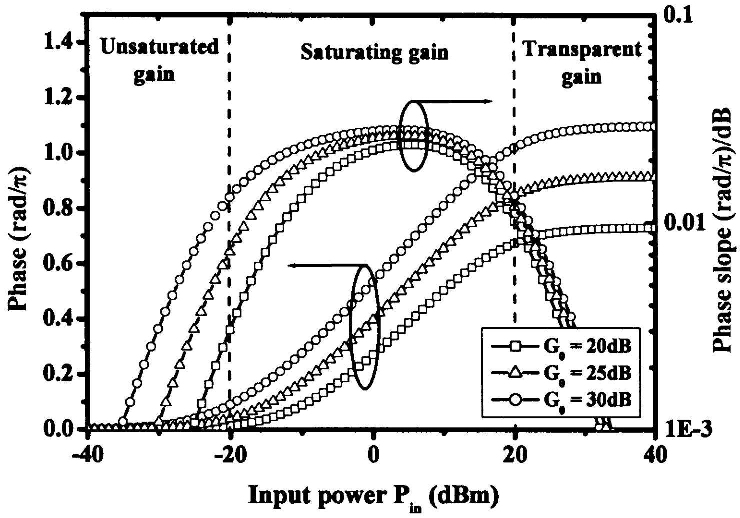

Figure 3-10 SOA Phase transfer function and phase transfer function slope (normalised to the α-factor) for different small signal gain values (G_0)

Figure 3-10 shows the SOA phase transfer function, normalised to the α-factor, for different small signal gain values, calculated from equation (3-22). As the input power increases the nonlinear phase shift increases until the gain reaches transparency. To quantify the efficiency of phase dependent switching, defined as the phase shift induced with respect to the input power, we use the slope of the $\varphi(P_{in})$ function. This is derived differentiating equation (3-22) with respect to the input power normalized to the saturation power $P = P_{in}/P_{sat}$:

$$\frac{d\varphi}{dP} = \left(-\frac{\alpha}{2}\right)\frac{(1-G)}{1+PG} \text{ where } P = \frac{\log(G_0/G)}{G-1} \tag{3-27}$$

The full derivation of equation (3-27)-(3-30) is given in appendix 1. The phase slope expressed in (rad/dB) is given by:

$$\frac{d\varphi}{dP_{dB}} = \frac{d\varphi}{d10\log(P)} = P\frac{\ln(10)}{10}\left(-\frac{\alpha}{2}\right)\frac{(1-G)}{1+PG} \tag{3-28}$$

Equation (3-28) shows that the slope is a function of G_0 and of the α-factor. The phase transfer function slope in (rad/π)/dB, normalised to the α-factor, is also shown in Figure 3-10 for different values of G_0. The phase slope curve is an order of magnitude smaller around the unsaturated and saturated gain region with respect to around the saturating region. Figure 3-11 shows the slope (rad/π)/dB of the phase curve calculated at $\varphi = \log(G_0)/2$ where the slope is close to its maximum, also defined as the slope at the threshold point.

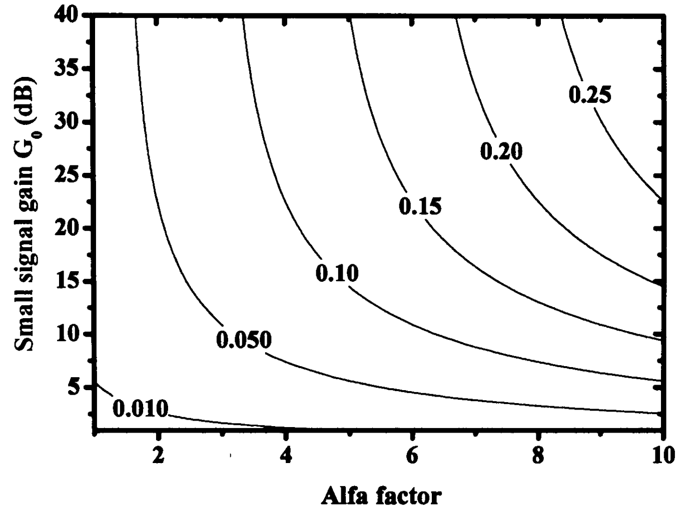

Figure 3-11 Phase slope calculated at the threshold point as a function of the α-factor and the small signal gain G_0

The phase slope increases with the small signal gain G_0 and the α-factor. A large slope is desirable as it increases the interferometer switching efficiency. This is defined as the derivative of the interferometer output power with respect to the input switching power. As shown in Figure 3-11, a phase slope of 0.1 (rad/π)/dB, which leads to a full π radians shift for an input power change of 10dB, can be achieved with realistic values of the α-factor and G_0. This suggests that switching with an SOA-assisted interferometer can be achieved with low input signal extinction ratios, and thus that extinction ratio gain is possible using an SOA-assisted interferometer configuration.

It is important to note that the results of Figure 3-11 do not refer to a specific practical device but rather are general results to show the impact of the α-factor and small signal gain on the phase slope, thus they cover a range of possible devices with different parameters. These results are intended to indicate the optimum range of parameters required for ideal regenerative properties but they may not be achievable with a single real/practical device.

Indeed, in a real device the gain and the α-factor are related, as described in section 3.2.1, through the Kramers-Kroning relation. Using this, Figure 3-5 shows that for a given carrier concentration, temperature and wavelength, a specific α-factor value has a corresponding small signal gain value. Thus, to assess the performance of a specific device the charaterisation of both gain and α-factor frequency response is essential. This can be either calculated as shown in [Wes87], or measured as described in chapter 4.

The switching efficiency and the reshaping properties of an SOA-assisted interferometer switching can be calculated differentiating the interferometer equation (3-26) with respect to the input power normalized to the saturation power $P = P_{in}/P_{sat}$. The SOA assisted interferometer slope can be expressed as:

$$T(P) = \frac{dP_{out}}{dP} = 1/2\sin(\varphi)\frac{d\varphi}{dP} \qquad (3\text{-}29)$$

where $d\varphi/dP$ is given in equation (3-27). The switching contrast and the nonlinear transfer function of an SOA-assisted interferometer are frequently expressed in decibels (dB).

Expressing both input and output power in decibels (P_{dB} and $P_{out_{dB}}$), then the transfer function slope can be expressed as:

$$T'_{dB}(P_{dB}) = \frac{dP_{out_{dB}}}{dP_{dB}} = \frac{d10\log(P_{out})}{d10\log(P)} = \frac{P}{P_{out}}\frac{dP_{out}}{dP} \tag{3-30}$$

Equation (3-29) shows that the interferometer transfer function slope is a function of the phase slope and is periodic with the nonlinear phase shift $\varphi(P)$. The interferometer transfer function and the transfer function slope (T'_{dB}), expressed in equation (3-30), are shown in Figure 3-12 for different value of the α-factor. The small signal gain is calculated from the α-factor value starting from the Kramers-Kronig relations, following [Wes87]. The device parameters used are those used for Figure 3-5, the carrier concentration is $N = 1 \times 10^{18}$ cm^{-1}.

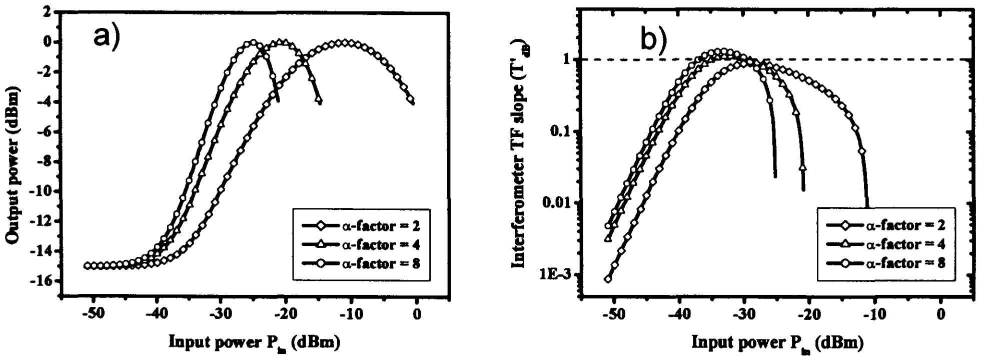

Figure 3-12 Interferometer transfer function (a) and transfer function slope (b) for different α-factor values

As shown in Figure 3-12(a), larger α-factor leads to a higher switching efficiency which decreases the input power change required for switching. As shown in Figure 3-12(b), for larger α-factor the maximum slope also increases to exceed unity for $\alpha >$ 2. The slope around the mean signal levels is an order of magnitude lower than at the threshold point. This ensures that the noise present on the pump signal levels is suppressed and not transferred on the probe signal.

An important figure of merit of any regenerator is the extinction ratio gain. This refers to the ability of the regenerator to improve the input signal extinction ratio and is defined, as in equation (3-10), as the ratio of the regenerator switching contrast to the input signal extinction ratio. If the SOA ASE [Sai87] (Amplifier Spontaneous

Emission) and phase and gain dynamic behaviour are neglected then the interferometer switching contrast is mainly limited by the physical implementation of the interferometer configuration [Leu98b], in particular of the optical discriminator used to select the "*ones*" form the "*zeros*". In the calculation of Figure 3-12 the interferometer maximum switching contrast was chosen to be 15dB.

Figure 3-13 shows the dependence of the SOA interferometer extinction ratio gain on the α-factor, calculated for different values of the switching contrast (SC). As discussed in section 3.1, when assessing the extinction ration gain of a nonlinear gate, the input extinction ratio is chosen as a function of the gate noise compression properties. In the calculation of Figure 3-13 the input extinction ratio is calculated from the transfer function slope as the ratio between the two input power levels corresponding to where the slope, as defined in equation (3-30), is an order of magnitude smaller with respect to its maximum. As shown in Figure 3-13 the extinction ratio gain becomes positive for the case of large switching contrasts (*SC* > 20dB). The small signal gain is calculated from the α-factor value starting from the Kramers-Kronig relations, following [Wes87]. The device parameters used are those used for Figure 3-5, the carrier concentration is $N = 1 \times 10^{18}$ cm^{-1}.

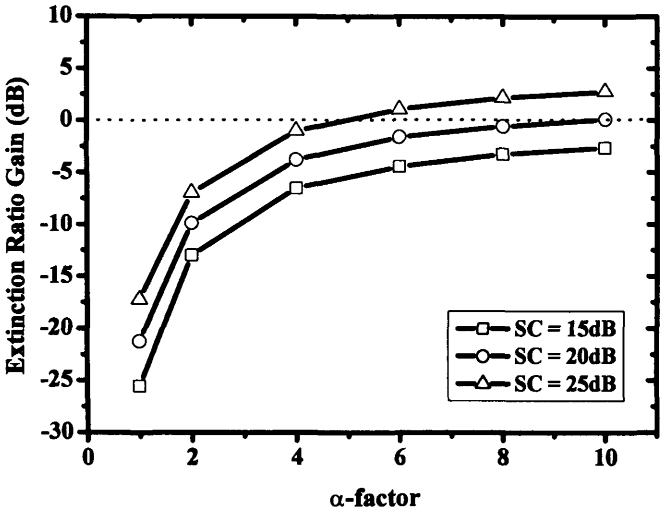

Figure 3-13 Extinction ratio gain as a function of the α-factor for different interferometer switching contrasts (SC)

In conclusion, due to the small transfer function slope of the interferometer around the input signal mean levels the noise present on the pump signal is compressed and not transferred to the probe signal; this is achieved while also performing extinction ratio enhancement of several dBs. The extinction ratio gain however depends significantly on the SOA gate switching contrast. In the next section, the parameters determining the limits of the switching contrast of an SOA gate, at high bit-rates, will be discussed.

3.3 SOA dynamics effects in high-bit rate switching

The transfer function allows for the analysis of the static behaviour of the optical gate. However, at high bit-rates ($\geq$ 10Gb/s), with bit periods exceeding of the SOA carrier lifetime ($\tau_c \approx 0.2 - 0.3ns$), the temporal behaviour of the SOA nonlinear effects can significantly degrade the SOA gate switching contrast due to intersymbol interference distortion, known as patterning [Wol98].

Experimentally, it was shown that the SOA switching frequency can be significantly increased, reducing patterning degradation, by clamping the SOA gain with an holding beam signal which constantly saturates the gain in the transparent region [Man94b] [Tsu98] [Dup00] [Ple02] or with a modulated holding beam signal [Bis02a] [Bis04] [Bor04].

Several approaches [Bis04] [Bis02b] have been proposed to assess the patterning penalty of switching at high bit-rates; these are mostly based on estimation of the gate optical switching window. However, this approach does not suit the assessment of the reshaping abilities [Uen04].

Here the effect of switching with a clamped SOA on the transfer function reshaping properties is investigated. This is achieved by assessing the impact of the holding beam signal on the transfer function slope, which was found to be an effective measure of the SOA gate noise compression properties. Both nonlinear switching based on nonlinear gain saturation (XGM) and SOA-assisted interferometer (XPM) configurations are considered.

3.3.1 High frequency switching with a clamped SOA

When switching at low frequencies, with periods longer than the recovery time of the SOA, the switching extinction ratio of a SOA-based interferometer is mainly limited by the physical implementation of the interferometer configuration, and principally ideal extinction ratios can be attained with asymmetric MZ configurations [Leu98b]. However, when switching at high frequencies, with periods smaller or in the range of the SOA gain recovery time, the dynamic effects of the SOA limit the gate switching contrast. Thus, estimation of the switching contrast requires evaluation of the SOA gain and phase dynamics. In this analysis the SOA intra-band carrier nonlinearities will not be considered.

The analysis of the gain and phase dynamics of an SOA perturbed by a strong optical pulse involves the numerical solution of equation (3-19). However, an analytical solution is also possible for the case of short optical pulses ($\tau_p < \tau_c$) saturating the SOA [Eis95]. For the analytical solution the saturating gain equation is given by:

$$g(t) = \frac{1}{1 - \left(1 - \frac{1}{G_0}\right)\exp\left(-\frac{E_{in}(t)}{E_{sat}}\right)} \tag{3-31}$$

The equation for the recovering gain is given by:

$$g(t) = G_0\left[\frac{G(t)}{G_0}\right]^{\exp[-t/\tau_c]} \tag{3-32}$$

The gain saturates following an exponential rising and recovers following an exponential decay determined by the carrier life-time (τ_c), which usually exceeds several hundred picoseconds. However, switching over shorter time scales (few picoseconds) was achieved saturating "*clamping*" the SOA with a CW holding beam signal [Tsu01]. The holding beam signal (P_{hb}) is launched at the SOA input as shown in Figure 3-6, thus the SOA now operates with 3 signals.

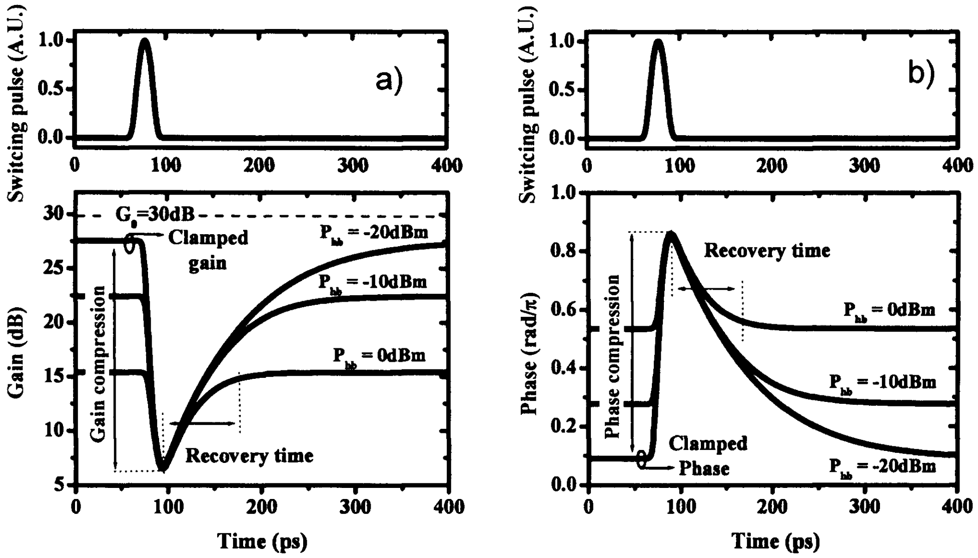

Figure 3-14 Gain (a) and phase (b) saturation by a 20ps pulse with 0dBm average power for different holding beam signal power (P_{hb})

Figure 3-14 shows the effect of the holding beam on the SOA gain recovery. This was calculated from equation (3-17) and (3-18) for an input signal pulse width of 20ps with 0dBm average power. The holding beam signal clamps the gain to a saturated level "*clamped gain*" preventing it from recovering back to its small signal value G_0. As shown in Figure 3-14(a), the gain is clamped to a lower level with larger holding beam power. As the optical pulse is injected into the SOA the gain is further saturated. After saturation the gain recovers back to its initial clamped value which depends on the holding beam power (P_{hb}). As a result, the "*10:90 recovery time*" ($\tau_{10:90}$) defined as the time required for the gain, exited by an optical pulse, to recover from 90% of its maximum saturation point to 10% of its initial value, is reduced with larger holding beam power. With reference to Figure 3-14(a) we refer to the gain saturated by the holding beam signal as the SOA "*clamped gain*", and to the gain saturation induced by the switching pulse as the "*gain compression*" [Sch03] [Occ02b]. The nonlinear phase dynamics, shown in Figure 3-14(b), follow the same behaviour. Similarly, we refer to the phase shift induced by the holding beam signal as the "*clamped phase*", and to the phase change induced by the switching pulse as the "*phase compression*".

When an SOA is used as the nonlinear element of an optical gate then the gain and phase compression determine the gate switching contrast. In XGM configurations, the switching contrast equals the SOA gain compression, while in XPM configurations the phase compression equals the maximum nonlinear phase shift term $\varphi(P_{in})$ in equation (3-26).

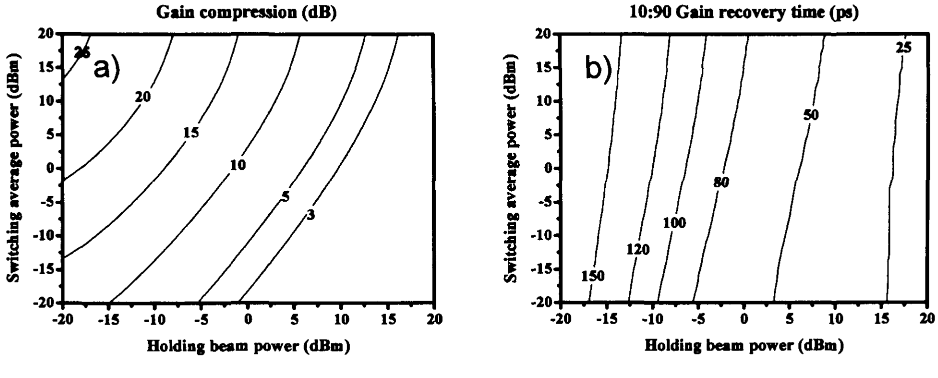

Figure 3-15 Gain compression (dB) (a) and the 10:90 recovery time (ps) (b) as a function of the holding beam and switching pulse average power

The gain saturation and recovery dynamics depend on the power of both the switching and the holding beam signal [Man94b] [Hil02]. Figure 3-15 shows the gain compression induced by a 20ps switching pulse and the corresponding gain recovery time, as a function of the holding beam and switching pulse average power. As the switching power increases the gain is further saturated, so the largest gain compression corresponds to the highest switching power; however, as the holding beam power increases the gain compression induced by the switching pulse decreases. Similarly, the 10:90 recovery time increases with larger switching power as the gain compression is higher, however it decreases with the holding beam power clamping the gain to lower values. Therefore, there is a trade-off between the gain compression and the gain recovery time which depends on the holding beam power.

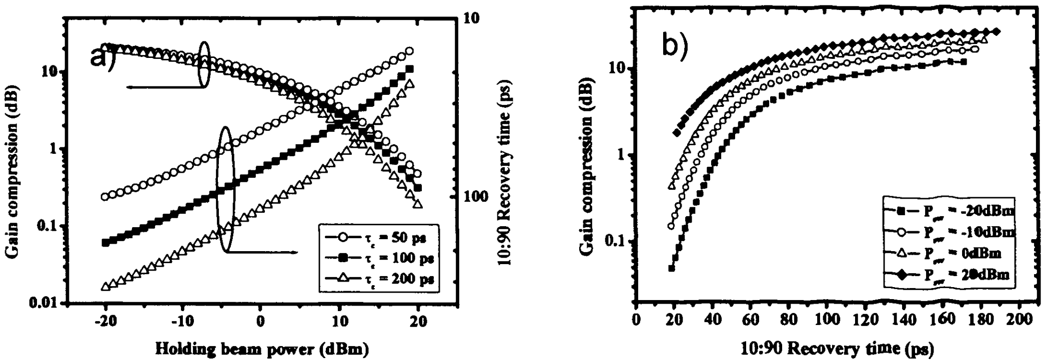

Figure 3-16 (a) Gain compression and 10:90 recovery time as a function of the holding beam power for different recovery time values (τ_c); (b) Gain compression a function of the effective recovery time for different switching power (P_{sw})

Figure 3-16(a) shows the gain compression induced by a 20ps pulse with 0dBm average power and the corresponding 10:90 recovery time, as a function of the holding beam power (P_{hb}), for different carrier lifetime values (τ_c). For a given τ_c, increasing the holding beam power decreases the effective recovery time and the gain compression. Decreasing τ_c does not significantly affect gain compression, however it strongly reduces the 10:90 recovery time.

The effect of the switching pulse power (P_{sw}) is also significant in this trade-off. The gain compression as a function of the effective recovery time is plotted in Figure 3-16(b) for τ_c = 100ps and for different average switching power levels. Increasing the switching power leads to a larger gain compression for a given τ_c value until the SOA gain becomes transparent to higher switching power. In conclusion, a decrease in the 10:90 recovery time corresponds to a reduction in gain compression and thus of the SOA gate switching contrast. However, as most SOA have a carrier lifetime in excess of 100ps, gain clamping is necessary to operate at high switching frequency ($\geq$ 10Gb/s).

So when estimating the SOA gain and phase transfer function it is also necessary to consider the effects of the holding beam power to have a realistic estimate of their characteristics and properties. In the following sections, the effect of gain clamping on the optical reshaping characteristics of XGM and XPM gates will be investigated.

3.3.2 Effect of gain clamping on the SOA nonlinearities

Clamping the SOA gain with a strong holding beam signal is necessary to reduce the gain recovery time and operate at high frequencies. However, the reshaping properties of SOA gates depend on the input optical power, thus it is important to assess the impact of the holding beam signal gain on the SOA gain and phase transfer function and transfer function slope.

The effect of clamping the SOA gain with a holding beam signal on the slope of the gain transfer function (G'_{dB}), defined in equation (3-24), can be estimated differentiating G_{dB} with respect to the switching signal power (P_{sw}), defined as $P_{sw} = P_{in} - P_{hb} = PP_{sat} - P_{hb}$:

$$\frac{dG_{dB}}{dP_{sw_{dB}}} = \frac{dG_{dB}}{dP_{dB}}\left(1 - \frac{P_{hb}}{P_{in}}\right) \qquad (3\text{-}33)$$

where $P_{sw_{dB}}$ is the switching signal power expressed in decibels, and dG_{dB}/dP_{dB} is given in equation (3-24). The derivation of equation (3-33)-(3-34) is also given in appendix 1.

Equation (3-33) shows that the gain transfer function slope decreases by a factor proportional to P_{hb}. Figure 3-17 shows the gain transfer function and slope magnitude, for different values of the holding beam signal power, calculated respectively from equation (3-21) and from equation (3-33). As the power of the P_{hb} signal increases the maximum value of the slope decreases. Furthermore, as the holding beam power increases the gain is clamped to lower values and the range of input power over which the slope is close to its maximum decreases, leading to a decrease in the SOA gate switching contrast.

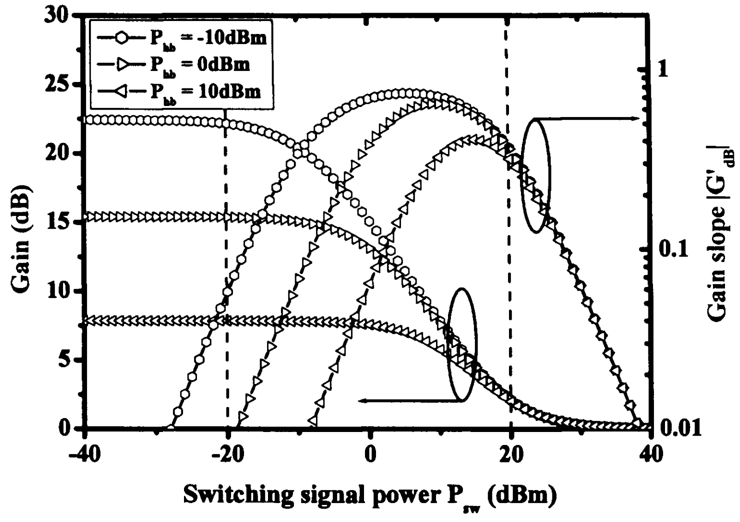

Figure 3-17 SOA gain transfer function and gain transfer function slope magnitude for different holding beam power P_{hb}

Figure 3-18 shows the gain transfer function slope calculated around its maximum value (slope at the threshold point), where $G = \sqrt{G_0}$, and the clamped gain as a function of the holding beam power.

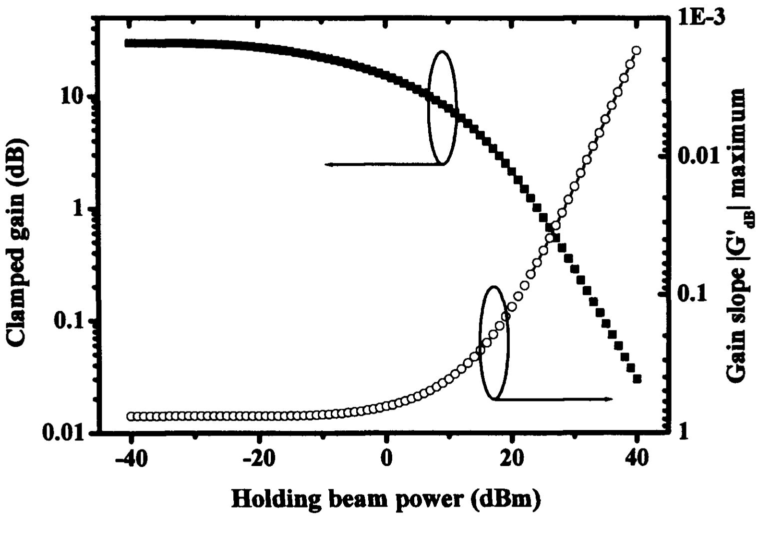

Figure 3-18 Clamped gain and gain transfer function slope at the threshold point (G_0 = 30dB) as a function of the holding beam power

As the holding beam power is increased the slope significantly decreases together with the clamped gain, reducing the switching contrast and thus the switching conversion efficiency. Thus, clamping the gain to reduce the SOA effective recovery time decreases gain compression and the slope of the gain transfer function. As a consequence, both the switching efficiency and the switching contrast of SOA gate decrease.

Similarly, the effect of clamping the SOA gain with a holding beam signal on the slope of the phase transfer function can be estimated differentiating $\varphi(P)$, defined in equation (3.22), with respect to the switching signal power (P_{sw}), defined as $P_{sw} = P_{in} - P_{hb} = PP_{sat} - P_{hb}$:

$$\frac{d\varphi}{dP_{sw_{dB}}} = \frac{d\varphi}{dP_{dB}}\left(1 - \frac{P_{hb}}{P_{in}}\right) \qquad (3\text{-}34)$$

where $d\varphi/dP_{dB}$ is given in equation (3-28). Equation (3-34) shows that the phase transfer function slope decreases by a factor proportional to P_{hb}.

Figure 3-19 shows the phase transfer function and slope (rad/π)/dB for different values of the holding beam power, calculated respectively from equation (3-22) and from equation (3-34). As the power of the P_{hb} signal increases the maximum value of the slope decreases.

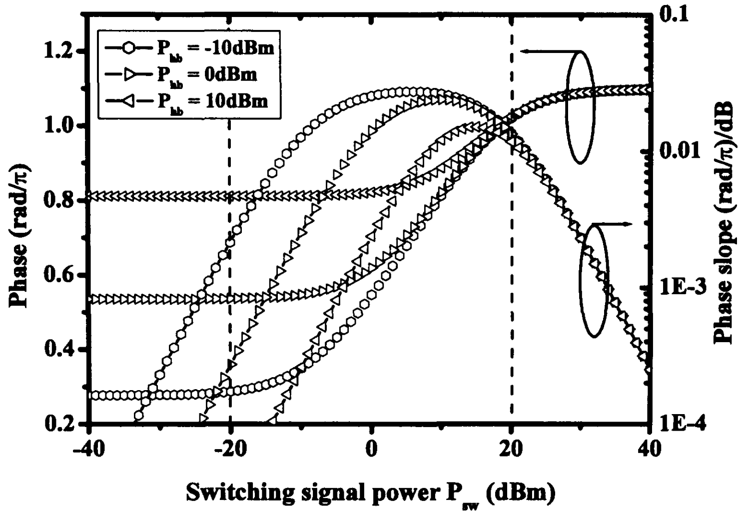

Figure 3-19 Phase transfer function and transfer function slope (rad/π) /dB (both normalised to the α-factor) for different holding beam power P_{hb}

Furthermore, as the holding beam power increases the phase shift induced by the switching input power decreases together with the range of input power over which the slope is close to its maximum. Figure 3-20 shows the slope (rad/π)/dB of the phase curve estimated at $G = \log(G_0/2)$ where the slope is close to its maximum (slope at the threshold point). The phase slope increases when the gain is clamped to high values and for large α-factor.

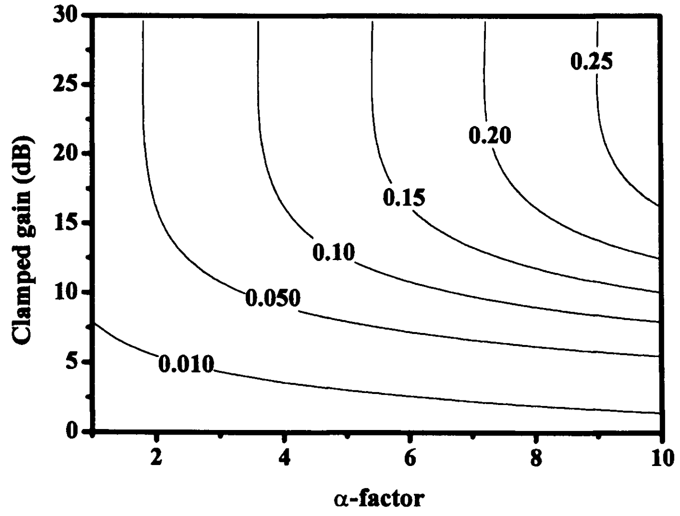

Figure 3-20 Phase transfer function slope (rad/π)/dB calculated at the threshold point (G_0 = 30dB)

Thus clamping the gain to reduce the SOA recovery time, decreases the nonlinear phase shift induced by the switching signal and the slope of the phase transfer function reducing the interferometer switching efficiency. In the next section the interferometer reshaping properties will be assessed.

It is important to note that, as in section 3.2.3, the results of Figure 3-20 do not refer to a specific practical device but rather are general results to show the impact of the α-factor and small signal gain on the phase slope, thus they cover a range of possible devices with different parameters. These results are intended to indicate the optimum range of parameters required for ideal regenerative properties but they may not be achievable with a single real/practical device. To assess the performance of a specific device the charaterisation of both gain and α-factor frequency response is essential. This can be either calculated as shown in [Wes87], or measured as described in chapter 4.

3.3.3 Interferometer switching with a gain clamped SOA

Reducing the recovery time by clamping the SOA gain leads to a decrease in the nonlinear phase transfer function slope and of the total phase shift. This significantly affects the transfer function characteristics of the interferometer which relies on the nonlinear phase shift for switching. The effect of a holding beam power on the interferometer transfer function slope (T'_{dB}) can be calculated differentiating equation (3-26) with respect to P_{sw}:

$$T'_{dB} = \frac{dP_{out_{dB}}}{dP_{sw_{dB}}} = \frac{dP_{out_{dB}}}{P_{dB}} \cdot \left(1 - \frac{P_{hb}}{P_{in}}\right) \tag{3-35}$$

where $dP_{out_{dB}} / dP_{dB}$ is given in equation (3-30). The derivation of equation (3-35) is also given in appendix 1.

Equation (3-35) shows that the interferometer transfer function slope decreases by a factor proportional to P_{hb}. Figure 3-21 shows the interferometer transfer function and transfer function slope for a clamped SOA for different α-factor values. The holding beam power is usually chosen to reduce the SOA effective recovery time to allow for operation at a certain bit-rate. However, in Figure 3-21, the P_{hb} was chosen so that the maximum phase compression (φ_{max}) induced by the switching signal (P_{sw}) was π radians for all cases investigated, in order to compare the effect of different α-factor on the transfer function slope. The small signal gain is calculated from the α-factor value starting from the Kramers-Kronig relations, following [Wes87]. The device parameters used are those used for Figure 3-5, the carrier concentration is $N = 1 \times 10^{18}\ \mathrm{cm}^{-1}$.

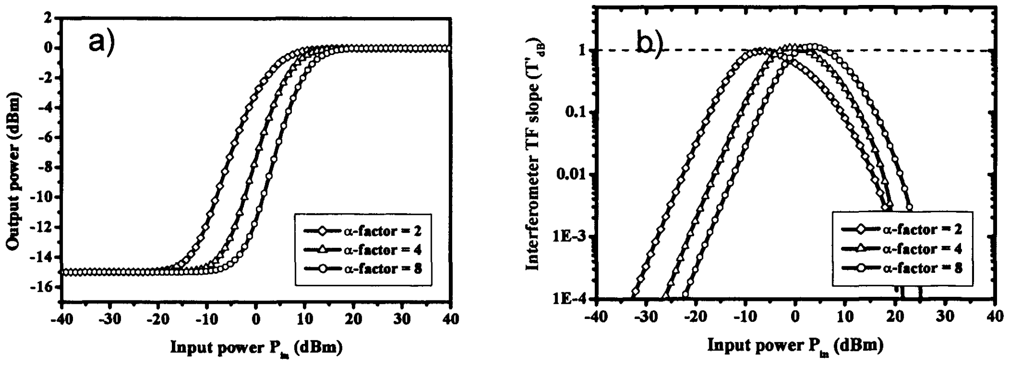

Figure 3-21 Interferometer transfer function (a) Interferometer transfer function (TF) slope (b) for different α-factor values, $\varphi_{max} = \pi$ and SC = 15dB

The case of $\varphi_{max} = \pi$ radians corresponds to clamping the SOA gain to operate with the shortest recovery time and the maximum switching contrast. The maximum slope value marginally increases with larger α-factor and is an order of magnitude larger with respect to the slope around the signal levels. However, the slope maximum value (slope at the threshold point) is not significantly larger than unity. This leads to strong noise suppression on the signal level but modest extinction ratio regeneration. Larger extinction ratio improvement can be achieved by "*biasing*" the interferometer [Uen02]. The differential phase shift in the interferometer equation (3-26) can be expressed as:

$$P_{out} = 1/2\left[1-\cos\left(\Delta\varphi\left(P_{in}\right)\right)\right] \tag{3-36}$$

$$\Delta\varphi = \varphi\left(P_{in}\right) - \varphi_{bias} \tag{3-37}$$

With reference to Figure 3-9, the term φ_{bias} refers to the relative phase delay between the interfering components when no switching occurs $\varphi(P_{in}) = 0$.

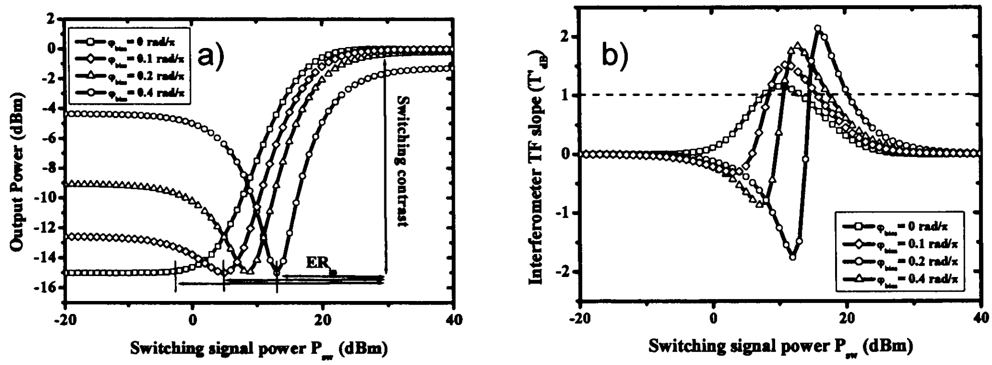

Figure 3-22 Interferometer transfer function (a) Interferometer transfer function slope (b) for different interferometer phase bias levels, $\varphi_{max} = \pi$, α-factor = 4 and SC = 15dB

Figure 3-22 shows the interferometer transfer function and slope for a clamped SOA for different values of the interferometer phase bias. The SOA gain is clamped so that the gain compression induced by the P_{sw} signal only leads to a maximum phase shift of $\varphi_{max} = \pi$ radians, and the α-factor is 4. As the phase bias is increased the interferometer transfer function slope increases exceeding unity at the threshold point. When the interferometer is biased the transfer function slope significantly increases, however the slope around the signal zero level, corresponding to the transfer function slope minima, also increases. Furthermore as shown in Figure 3-22(a) for the case of

$\varphi_{max} = \pi$ radians, the interferometer output switching contrast and the input signal extinction ratio (ER_{in}) required for switching decrease with higher phase bias levels. This significantly affects the extinction ratio gain of the optical gate.

Assuming that the holding beam power is sufficient to clamp the SOA gain to fully recover over the switching period and, thus, that no pattern-dependent effects is present, than we can estimate the interferometer extinction ratio gain from equation (3-10). The interferometer switching contrast, and thus the output signal extinction ratio, corresponding to a π radians shift was chosen to be $ER_{out} = 15$dB.

The input extinction ratio is calculated from the interferometer transfer function slope (T') as the difference between the two power levels corresponding to where the slope equal a particular noise compression value (Y_{NC}). Figure 3-23 shows the interferometer extinction ratio gain (dB) as a function of the interferometer phase bias and noise compression term.

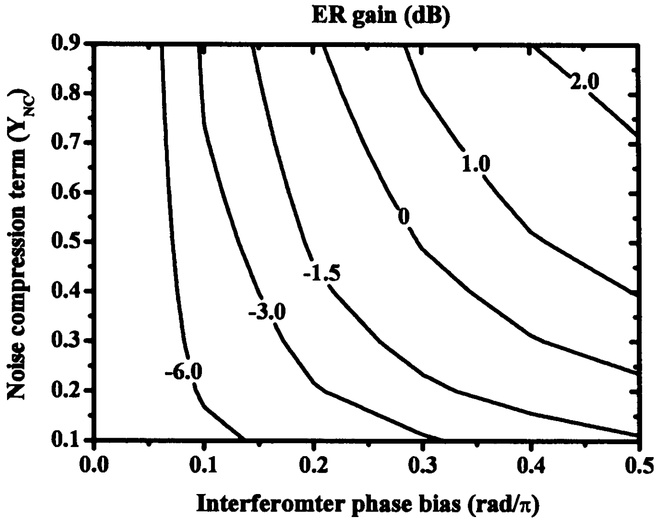

Figure 3-23 Interferometer extinction ratio gain as a function of the noise compression factor (Y_{NC}) and of the interferometer phase bias for $\varphi_{max} = \pi$, $G_0 = 30$dB, α-factor = 4 and $ER_{out} = 15$dB

The extinction ratio gain increases with increasing values of the interferometer phase bias. However, it can be seen that there is a trade-off between the extinction ratio gain and noise compression. Operating with larger phase bias level allows for larger extinction ratio gain but also reduces the interferometer noise compression term in particular around the signal "zero" level, as visible in Figure 3-22. The case just investigated assumed that the SOA gain was clamped to maximise the recovery time at the cost of operating with a limited maximum phase compression of π radians. As a consequence, an increase in the interferometer phase bias corresponds to a decrease in the switching contrast. However if the interferometer is operated with larger phase margin, then the switching extinction ratio penalty can be minimised. Figure 3-24 refers to the case of a $\varphi_{max} = 1.5\pi$ radians. The interferometer switching contrast does not decrease significantly with larger phase bias levels. Furthermore, the maximum interferometer transfer function slope is larger with respect to the case of $\varphi_{max} = \pi$ radians of Figure 3-22(b).

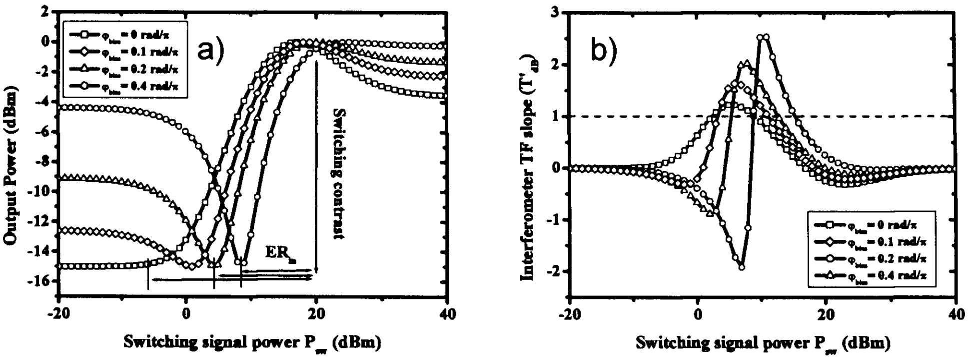

Figure 3-24 Interferometer transfer function (a) Interferometer transfer function slope (b) for different interferometer phase bias levels, $\varphi_{max} = 1.5\pi$, α-factor = 4 and SC = 15dB

Figure 3-24(a) shows the interferometer extinction ratio gain (dB) as a function of the interferometer phase bias and noise compression term for the case of $\varphi_{max} = 1.5\pi$ radians. Figure 3-24(b) shows the interferometer switching contrast as a function of the interferometer phase bias for different φ_{max} values.

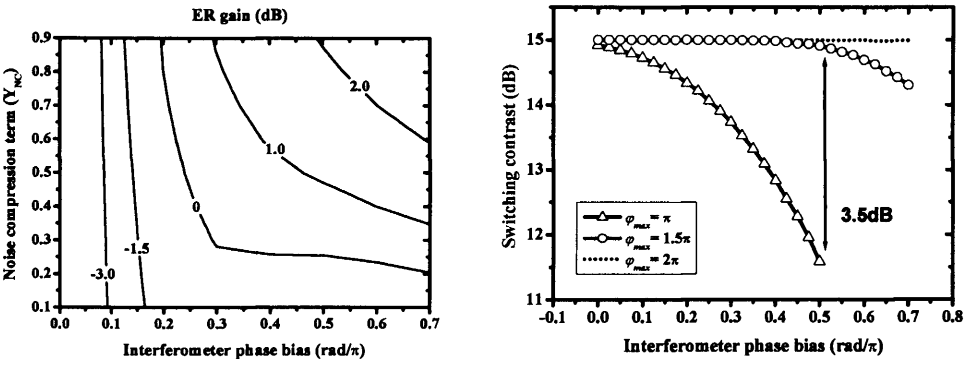

Figure 3-25 (a) Interferometer extinction ratio gain as a function of the noise compression factor (Y_{NC}) and of the interferometer phase bias for $\varphi_{max} = 1.5\pi$, G_0 = 30dB, α-factor = 4 and ER_{out} = 15dB; (b) Interferometer switching contrast as a function of the phase bias

Extinction ratio gain can be achieved for noise compression term (Y_{NC}) values greater than 0.2. Operating with $\varphi_{max} > \pi$ radians allows to minimise the penalty on the switching contrast occurring at large interferometer phase bias levels. However, clamping the SOA to a higher gain level to increase the nonlinear phase shift form π to 1.5π radians, implies a reduction in the switching speed given the trade-off between nonlinearity and recovery time described earlier.

3.4 Cascadability properties of SOA-based regenerators

The ultimate application of an optical regenerator is in a transmission system, where 3R optical regenerators concatenated between EDFA fibre links are used to reduce the noise accumulation, as shown in Figure 3-26.

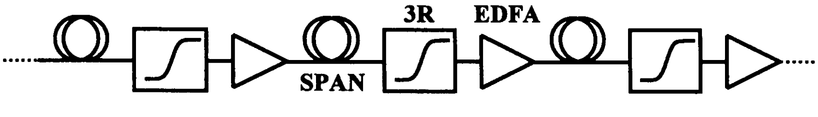

Figure 3-26 Transmission system with concatenated optical regenerators

It was shown that, assuming that each regenerator stage operates identically, then the noise accumulation along transmission depends on the regenerator transfer function slope around the input signal "*zero*" and "*one*" mean levels [Mor03], and that even a moderate slope ($Y_{NC} \approx 0.4$) can increase the transmission distance by an order of magnitude [Ohl97].

Given that the regenerator transfer function slope is a function of the input signal mean power levels, then to maintain constant regenerative properties along a chain of concatenated regenerators is necessary that the extinction ratio at the input of each regenerator is maintained constant. This condition determines an important requirement on the regenerator; signal reshaping has to be accomplished while performing the necessary extinction ratio enhancement to maintain cascadability. However, as descried in this chapter, there is a trade-off when using an SOA-assisted interferometer between the regenerator extinction ratio gain and the noise compression factor.

Having shown that extinction ratio gain can be achieved with a noise compression factor as low as 0.2 and realistic SOA parameters, it is now important to assess the impact of the noise compression term on the noise accumulation in a transmission link with cascaded optical regenerators. It was shown that the BER after N regenerators can be calculated as [Mor03]:

$$BER_N \cong \frac{1}{\sqrt{2\pi Q_0^2/F_n}} N \sqrt{\frac{1-Y_{NC}^2}{1-Y_{NC}^{2N}}} \exp\left(-\frac{1}{2}\frac{Q_0^2}{F_n}\frac{1-Y_{NC}^2}{1-Y_{NC}^{2N}}\right) \qquad (3\text{-}38)$$

where Q_0 is the transmitter output signal Q-factor and F_n is the noise figure of the optical amplifiers cascaded between regenerators in the transmission link, and Y_{NC} is the noise compression term as defined in section 3.1. For the case of an SOA-assisted interferometer the noise compression term around the input signal "*zero*" level is larger that around the "*one*" level ($Y_0 > Y_1$), as shown in Figure 3-22, and thus we can approximate $Y_{NC} \approx Y_0$.

The BER accumulation in the transmission system with concatenated optical regenerators, as shown in Figure 3-26, is plotted in Figure 3-27 for different Y_0 values as calculated from equation (3-38).

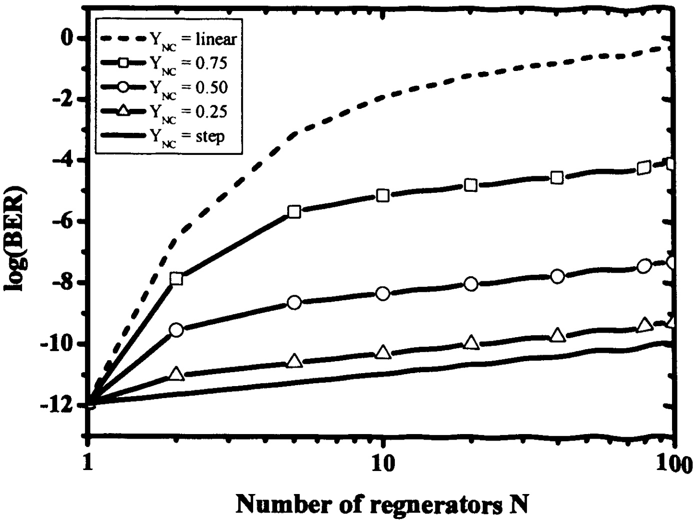

Figure 3-27 BER versus number of regenerators for a span ($Q_0^2/F_n = 9$)

Lower BER occurs for smaller Y_{NC} slope. For a large number of cascaded links, even a moderate reshaping may significantly improve the maximum transmission distance with respect to the un-regenerated link (linear case). Furthermore, for Y_{NC} smaller than 0.25 the optically regenerated link approaches the performance of a regenerated link with ideal step-function repeaters.

Summary

This chapter presented an investigation of the reshaping properties of optical gates based on XGM and SOA-assisted interferometer (XPM) configurations. It was shown that by deriving analytical equations for the slope of the SOA nonlinear gain and phase saturation we can relate the regenerative properties of optical gates to the SOA physical parameters. This approach was used to theoretically investigate the impact of the SOA parameters, such as the α-factor the small signal gain and the recovery time, on the reshaping properties of optical gates based on XGM and SOA-assisted interferometer configurations.

Several original results were obtained with this approach and presented in this chapter. It was found that optical switching based on XGM leads to a strong noise suppression ($Y_{NC} \leq 0.1$), however extinction ratio regeneration can not be achieved with gain base nonlinearity. Thus optical signal regeneration operating on SOA gain nonlinearity trades-off noise suppression on the signal levels with extinction ratio degradation.

It was also found that the advantageous features of an SOA-assisted interferometer with respect to an XGM gate are the extinction ratio enhancement and the noise reduction which are due to the interferometer transfer function. Extinction ratio gain of up to 3dB can be achieved with realistic SOA parameters (α-factor = 4, G_0 = 30dB) while maintaining a noise compression factor as low as $Y_{NC} = 0.2$.

The effects of operating at high bit-rate on the SOA transfer function are also investigated to show that operating at high switching frequencies is possible by clamping the SOA gain with a holding beam signal, as previously demonstrated in [Man94]. Here, however, we observe that the transfer function slope, which is the measure of the regenerator noise compression, is decreased by a factor proportional to the clamping power and thus the regenerative properties are significantly reduced.

Following the approach presented in [Ohl97], the characterisation of transfer function cascadability is also briefly investigated as function of the SOA physical parameters.

In the following chapters, we will investigate the reshaping properties of XGM and XPM configurations experimentally.

Chapter 4 Switching with SOA gain nonlinearity: wavelength conversion

As discussed in the previous chapter the nonlinear gain and phase saturation in SOA can be used for switching at high bit-rate. When characterising the SOA nonlinearities for application to optical switching, the fundamental parameter to quantify is the magnitude of the gain and phase change as a function of the recovery time, as this determines the achievable switching contrast of the SOA gate at a given operating frequency.

The first part of this chapter presents the experimental characterisation of the inter-band nonlinear effects dynamics of the SOA used in the all-optical processing experiments presented in this and later chapters. Inter-band effects due to carrier depletion are the strongest among the nonlinear effects in a SOA and are the key nonlinearities used for switching up to 40Gb/s. Both the SOA phase gain, an chirp temporal responses are investigated; analysis of the gain dynamics has application in the wavelength conversion experiment presented in this chapter, while the phase dynamics has application in the interferometer switching experiments presented in the following chapter.

In the second part of this chapter, optical switching based on SOA gain nonlinearity is investigated for applications in high bit-rate wavelength conversion (40Gb/s). The performance of different techniques for XGM-based wavelength conversion in SOAs is experimentally investigated at 10 and 40Gb/s and compared to the SOA characterisation experimental results.

In the last part of this chapter, the work on wavelength conversion is extended by looking at techniques for simultaneous multi-channel wavelength conversion using an integrated SOA array. To date, no configuration has shown multi-channel simultaneous wavelength conversion at high bit-rates (≥10Gb/s). However, this functionality has potential applications for connecting WDM networks operating with different operating bands or channel spacing [Sak98] [Kan99]. Here, we demonstrate for the first time, multi-channel wavelength conversion of 10Gbit/s WDM channels with a single integrated optical component, demonstrating the potential for large scale monolithic integration for optical processing applications for WDM networks.

4.1 SOA experimental characterisation

SOA characterisation involves both the assessment of the static and the dynamic gain and phase transfer function. The static transfer function shows the gain saturation characteristics with injected optical power, giving information on the gain transfer function, which determines the SOA gates switching contrast. Conversely, the dynamic transfer function, shows the time scale of the nonlinear gain and phase recovery time, which determines the SOA gate switching frequency.

4.1.1 SOA Static transfer function measurements

The characterisation of the SOA nonlinear saturation involves the measurements of both the phase and gain transfer function. The static gain transfer function can be measured using a pump and probe technique, as described in [Dre02]. The phase transfer function, instead, can be derived from the gain as described in [Hen82] measuring the SOA α-factor [Har83] [Sto91], or alternatively measured directly using an SOA-assisted interferometer [Sch03]. The experimental set-up used in this work to measure the SOA gain transfer function is shown in Figure 4-1.

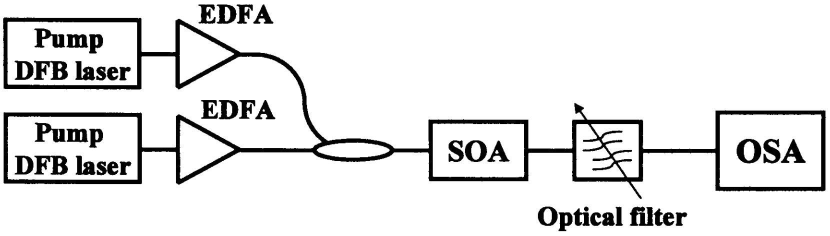

Figure 4-1 SOA gain transfer function measurement experimental set-up

The SOA gain transfer function was measured from the probe signal wavelength (λ_{probe} = 1550nm), while the pump signal (λ_{pump} = 1555nm) was used to clamp the SOA gain at different gain level. The pump and probe signals were generated using Distributed Feedback Lasers (DFB). Polarisation controllers were used because of the SOA PDG (Polarisation Dependent Gain), which was less than 0.5dB. The probe signal power at the SOA output was measured with an Optical Spectrum Analyser (OSA) set to 1nm resolution for the measurement. The SOA driving current used for all experiment presented in this chapter is 250mA unless specified.

Figure 4-2 (a) shows the SOA gain transfer function measured on a 1mm long bulk SOA driven with 250mA. The SOA is a commercially available component designed, manufactured and packaged by Kamelian [Kam05], and was used for all characterisation experiments presented in this chapter. The measured curves are fitted with the results of a numerical calculation following the model in [Agr89].

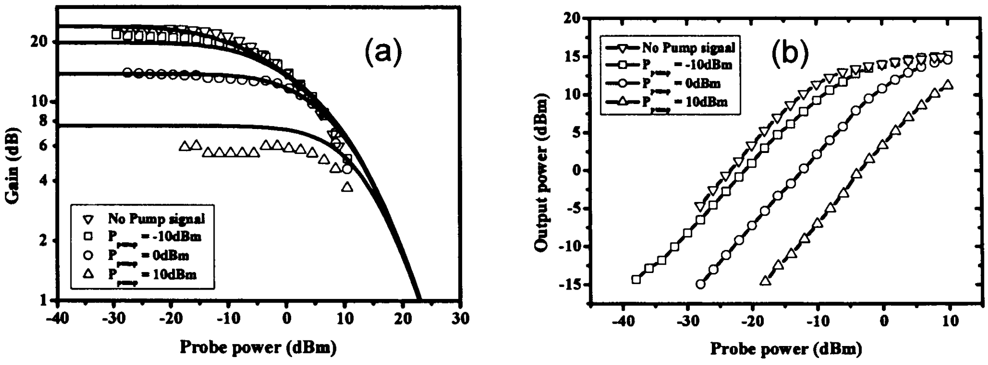

Figure 4-2 SOA gain (a) and output power (b) transfer function measured for different pump powers

The simulation parameters used were $E_{sat} = 1\text{pJ}$, $\tau_c = 20\text{ps}$ and $G_0 = 24$. For low input power the SOA gain is equal to the small signal gain value, measured to be 24dB. When the probe power is large enough to deplete the carrier density the gain saturates. As the pump power is increased the small signal gain is clamped to a lower value. Figure 4-2 (b) shows the measured SOA output power transfer function corresponding to the gain curves of Figure 4-2 (a). The output power increases with the probe power until it reaches the saturation level, measured to be 15dBm.

The characterisations of the other SOAs used in the optical processing experiments presented in this thesis are reported in appendix 2. Figure 4-3 shows the SOA gain transfer function slope around its maximum (the threshold point) ($G_0/2$), extrapolated from the measurements of Figure 4-2 (a) for different probe power levels.

The slope maximum occurs around $G = \sqrt{G_0}$ where G_0 is the SOA small signal clamped gain also shown in Figure 4-3. As predicted by equation (3.22) the slope of the SOA gain transfer function and the small signal clamped gain value decrease with larger probe power.

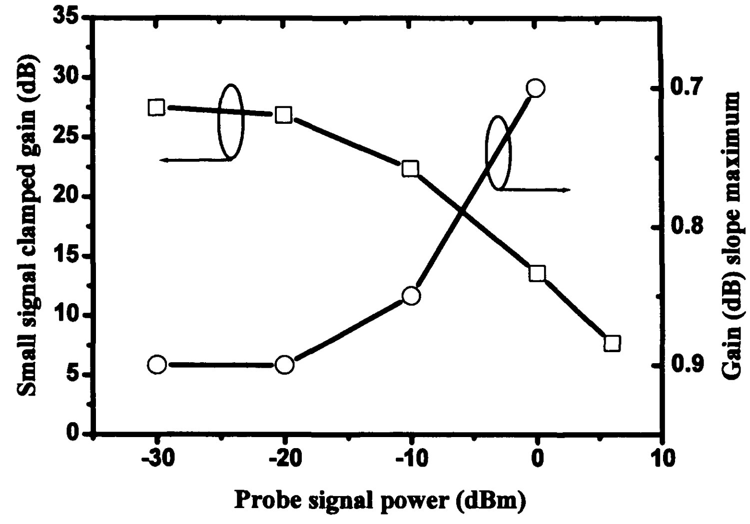

Figure 4-3 SOA Clamped gain and gain slope measured at the threshold point for different probe power levels

The gain and the phase transfer function are simply proportional to each other via a single linewidth enhancement factor (α-factor) due to the carrier density charge [Hen82]. Thus, estimation of the magnitude of the phase static transfer function requires measuring the SOA α-factor.

4.1.2 SOA gain and phase dynamics and α-factor measurements

The nonlinear optical responses of an SOA are known to originate from several processes, each occurring at a distinct time scale ranging from 100fs for spectral hole burning to 0.1-1ns for carrier recombination [Mor94]. To date, pump and probe techniques have been proposed to measure the SOA dynamics with ultra-short femtoseconds pulses [Kes87] [Hul91] [Occ02a] and high repetition rates [Sch03]. However, in these experiments, phase and gain dynamic are not measured simultaneously but from two different experimental configurations. This increases the error margin for the estimation of the gain and phase change magnitude especially for the ultra-fast nonlinearities which are significantly small. More recently, spectrogram techniques have been proposed to obtain, from a single measurement, the temporally-resolved transmission and phase of the SOA, by measuring the optical spectrum of a probe pulse as a function of the delay between the modulation and the probe pulse [Kan04]. This approach was used in this work to characterise the phase and gain dynamics and the α-factor of the SOAs used in the optical processing experiments presented in this thesis. The experimental set-up for the spectrogram measurements is shown in Figure 4-4.

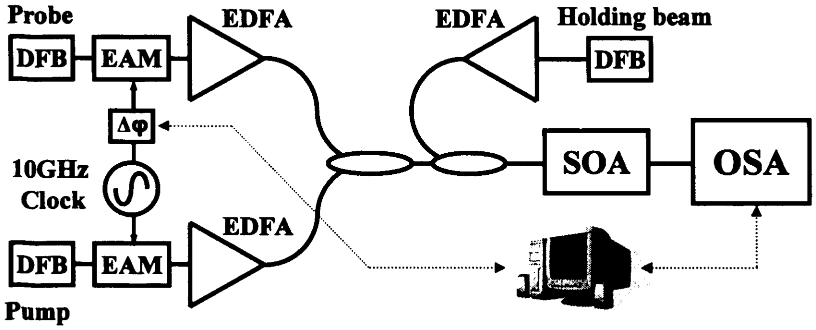

Figure 4-4 Spectrogram measurement experimental set-up

The pump (λ_{pump} = 1550nm) and probe (λ_{probe} = 1545nm) signals were 10GHz RZ pulse trains with 12ps and 20ps pulse durations (FWHM), respectively, and with an extinction ratio of 15dB, generated by modulating EAMs with a 10GHz sinusoidal signal. The pump signal power was 6dBm and the probe signal power was -14dBm. A DFB laser (λ_{hb} = 1552nm) generated the holding beam signal used to clamp the SOA gain to different values. A voltage-controlled phase shifter was used to vary the temporal delay (Δφ) between the pump and probe. The propagation of the pump pulse induced a gain and phase modulation which is measuring by recording the optical spectrum of the modulated probe pulse as a function of the optical frequency and relative delay between the modulation and probe pulse. The amplitude and the phase of the SOA response and of the probe pulse can then be simultaneously retrieved from this measurement using an iterative numerical procedure [Kan93]. The SOA used in the experiment is 1mm long bulk Kamelian SOA driven with 250mA [Kam05].

Figure 4-5 shows the measured SOA gain, phase and chirp dynamics for different holding beam power levels. The chirp, which is the variation of the optical signal frequency with time, is here calculated from the instantaneous phase change as shown in equation (4-3). As expected, the pump pulse depletes the SOA carrier decreasing the gain for the probe signal, then the gain recovers. As the holding beam power is increased the SOA gain is further saturated, consequently the gain depletion induced by the pump signal decreases together with the modulation imparted on the probe signal. The change in gain is accompanied by a nearly proportional change in phase.

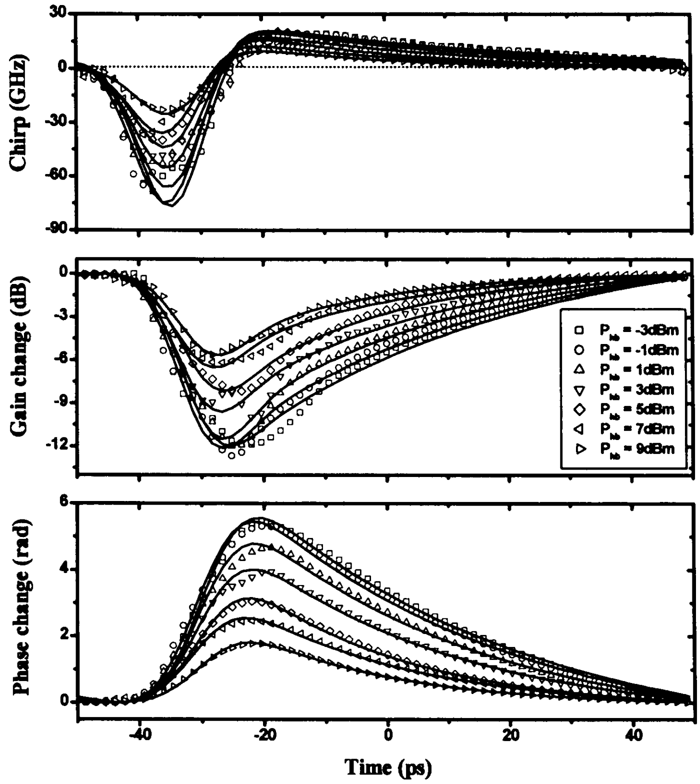

Figure 4-5 Gain, phase and chirp of the SOA for different holding beam powers

However, as previously observed [Kan04], the change in phase is delayed by typically 5ps relative to the changes in amplitude. Furthermore, the phase and gain recovery responses appear not to be proportional to each other with a single α-factor as the proportionality constant. The measurement of the chirp shows an initial red-chirp during the gain saturation phase followed by a blue-chirp during the gain relaxation phase. The experimental results were fitted with a phenomenological model [Hul91] describing the impulse response of the SOA when stimulated by an optical pulse with intensity I_p:

$$g(t) = \left[a_0 e^{-t/t_0} + a_1 e^{-t/t_1} + a_2 \delta(t)\right] \otimes I_p \tag{4-1}$$

$$\varphi(t) = \left[b_0 e^{-t/t_0} + b_1 e^{-t/t_1} + b_2 \delta(t)\right] \otimes I_p \tag{4-2}$$

$$\Delta f(t) = \frac{1}{2\pi}\frac{\partial \varphi}{\partial t} = \frac{1}{2\pi}\frac{\partial\left[\alpha \ln\left(\frac{G(t)}{G_0}\right)\right]}{\partial t} \tag{4-3}$$

The first two terms of both the phase and gain impulse response represent the lifetime associated with carrier depletion and carrier heating. The delta function represents the instantaneous effects such as TPA (travelling photon absorption), resulting in carrier depletion, and the Kerr effect which gives rise to a negative phase change [Hul91].

Each term corresponds to a different physical process, to which can be associated a α-factor and a recovery time value. The α-factor relates the amplitude response to the phase response and is defined for each process as the ratio between the phase and gain coefficients of the corresponding exponential term. The α-factor associated with the carrier depletion is given by $\alpha = \alpha_0 = 2b_0/a_0$ and is equal to 5.2 for the device characterised in this experiment. The α_0 parameter is usually referred to as the SOA α-factor [Agr98].

The recovery time indicates the time duration of each process, and is defined for each process as the time constant in the argument of the corresponding exponential, which in this fitting is identical for both the phase and gain curves. The α-factor and the recovery time can be similarly defined for the other nonlinear processes. The α-factor does not depend on power, however the carrier depletion recovery time does. Figure 4-6 shows the maximum dynamic gain (ΔG) phase (Δφ) and chirp (Δf) change induced by the pump pulse, and the effective recovery time (τ_{eff}) as a function of the holding beam power.

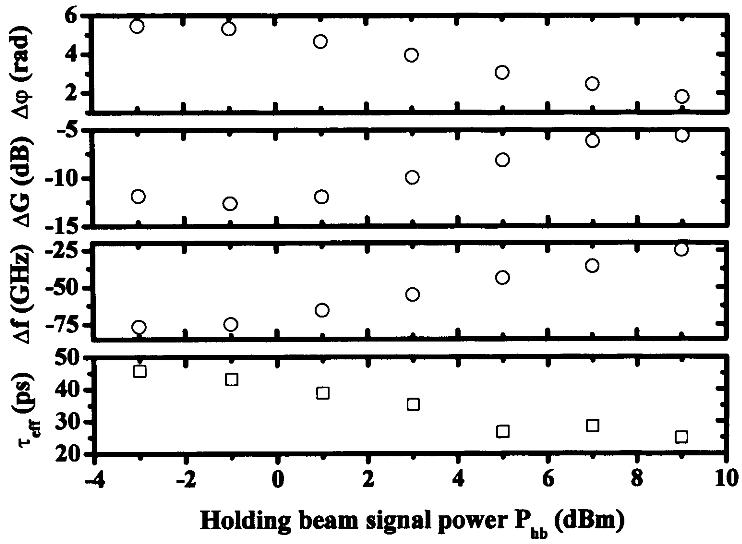

Figure 4-6 SOA dynamics characterisation for different holding beam signal power levels

The SOA effective recovery time (τ_{eff}) is the measure of the carrier depletion recovery time and corresponds to the term t_0 in the argument of the first exponential term of equation (4-1). τ_{eff} is related to the SOA carrier lifetime τ_c as [Man94]:

$$\tau_{eff} = \tau_c \tau_h / (\tau_c + \tau_h) \qquad (4\text{-}4)$$

which at high powers will be dominated by the holding beam recovery time τ_h defined:

$$1/\tau_h = P_{hb} / E_{sat} \qquad (4\text{-}5)$$

The 10:90 recovery time is related to τ_{eff} as $\tau_{10:90} = \log(9)\tau_{eff} = 2.2\tau_{eff}$. As shown in Figure 4-6, an increase in the holding beam power corresponds to a decrease in the dynamic gain and phase change and, thus, in the recovery time.

The effective α-factor (α_{eff}), defined as the ratio of the maximum phase to gain change estimated directly form the measurement as $\alpha_{eff} = \Delta\varphi/\Delta G$ is equal to 4. The effective α-factor (α_{eff}) is a measure of the contribution to XPM of all nonlinear processes, and in these measurements it is found smaller than α_0 parameter. This is because of the negative phase shift arising from the Kerr effect associated with the α_2 parameter ($\alpha_2 = 2b_2/a_2$) reduces the effective cross phase modulation induced by the carrier depletion and heating processes. Figure 4-7 shows the wavelength dependence of the effective α-factor, the recovery time and the maximum dynamic gain and phase change. The holding beam signal power was 6dBm.

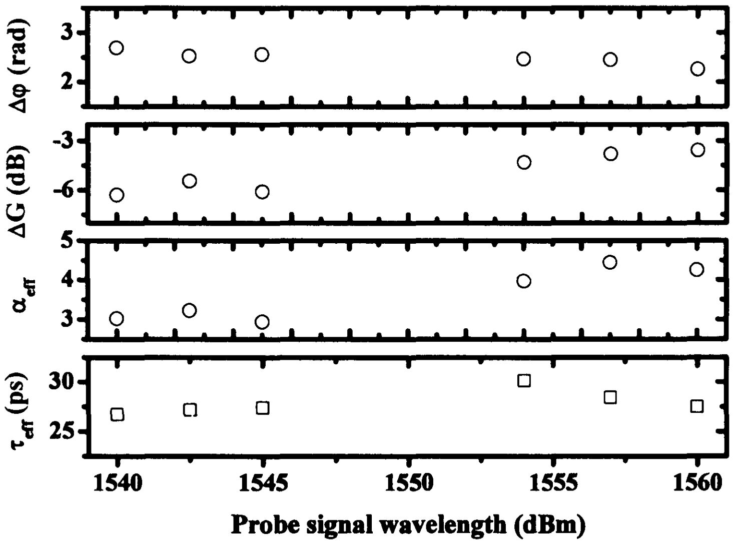

Figure 4-7 SOA dynamics characterisation for different pump wavelengths

The α-factor, as the SOA small signal gain, increases as a function of the wavelength, changing by a factor of 2 over the entire C-band (1530-1570nm). The recovery time, however, is not similarly affected by wavelength.

When characterising an SOA for application to optical switching at a certain bit-rate, the fundamental parameter to quantify is the gain and phase change magnitude as a function of the recovery time. In fact, it is necessary, for switching with PRBS sequences, that the gain and phase change recovers fully over the bit period to avoid pattern dependent distortion. This occurs when the SOA gain and phase temporal response extends over the bit slot. The relationship between the gain and phase change magnitude and the recovery time depends on the saturated small signal gain, which is a function of the holding beam power, and is plotted in Figure 4-8 for the SOA under test. The results are extrapolated form the spectrogram measurements plotted in Figure 4-6.

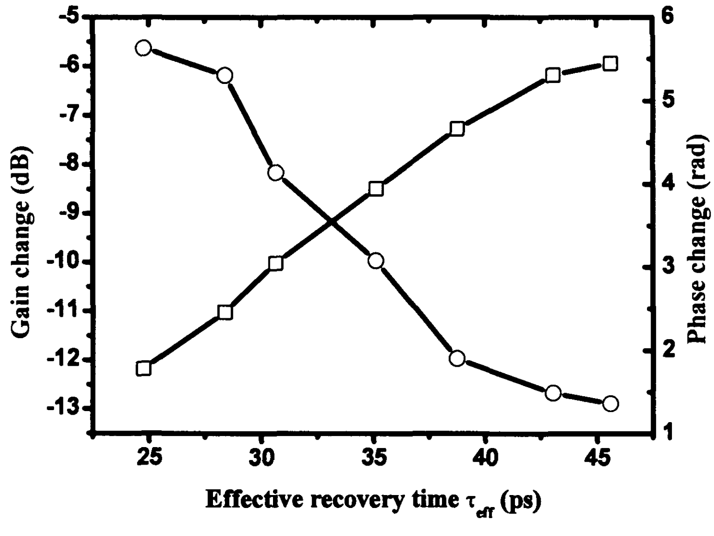

Figure 4-8 Dynamic gain and phase saturation as a function of the effective recovery time

From the characterisation measurements results that the SOA under test is expected to perform intensity switching based on gain saturation at 10GHz with switching contrast in excess of 13dB and at 40GHz with switching contrast in excess of 5dB. If we take advantage of XPM based non-linearity with an SOA-assisted interferometer configuration, switching with π radians contrast would be achieved with recovery time of 30ps, leading to switching frequency in excess of 30GHz.

4.2 Optical switching based on gain nonlinearity

The basic principle for optical switching with SOA gain nonlinearity was described in section (3.2.2). In an XGM-based wavelength converter, the pump signal modulates the probe signal intensity, varying the SOA gain saturation [Dur96]. The inter-band carrier lifetime, usually in the range between 0.1 to 1 ns, limits the maximum switching frequency and, thus, the operating bit-rate of the wavelength converter, which is expected to be less than 10GHz.

However, it was shown that by means of reshaping the wavelength converted pulses with optical off-set filtering [Ell98] or with a pulse delay interferometer [Leu00] the operating bit-rate could be significantly increased exceeding 40Gb/s. To date, the highest bit-rate performance for all-optical wavelength conversion has been achieved through Cross Gain Modulation (XGM) in an SOA followed by a bit-delay interferometer (SOA-DI), which demonstrated up to 160Gb/s operation [Leu05]. However, due to the fact that most published experiments use different SOAs, it remains unclear whether the improvement in the operating bit-rates reported has been enabled by SOA with a faster recovery time or rather by a significantly more efficient configuration. Here, the performance of XGM-based wavelength conversion in SOA and in an SOA-DI configuration was experimentally investigated at 10 and 40Gb/s and compared to the SOA characterisation experimental results.

4.2.1 10Gb/s wavelength conversion experiments

The simplest configuration for wavelength conversion consists in co-propagating a modulated pump signal and the CW probe signal through the SOA with a filter at the output to select the wavelength converted channel. Figure 4-9 shows the experimental set-up used to investigate 10Gb/s wavelength conversion.

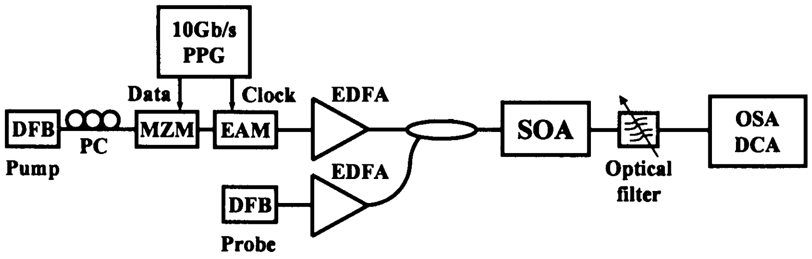

Figure 4-9 10Gb/s wavelength conversion experimental set-up

The pump signal was a 10 Gbit/s (PRBS 2^{31}-1) RZ signal with a 20ps pulse width (FWHM) and an extinction ratio of 15dB, generated cascading a Mach-Zehnder Modulator (MZM) and an Electro-Absorption Modulator (EAM) modulator driven with a 10Gb/s Pulse Pattern Generator (PPG). The 10Gb/s transmitter is described in detail in appendix 3. The probe signal wavelength was 1545nm and the pump signal wavelength was 1550nm. The SOA used in the experiment is 1mm long bulk Kamelian SOA driven with 250mA (characterisation in section 4.1). Figure 4-10 shows the eye diagrams and the spectra of the wavelength converted signal pulses at the SOA output for different pump switching power (P_{pump}) for the case of a probe power of -3dBm (a) and 7dBm (b), which was the maximum pump power we could launch in the SOA. The eye diagrams were obtained using a Digital Communication Analyser (DCA) with 40GHz optical bandwidth.

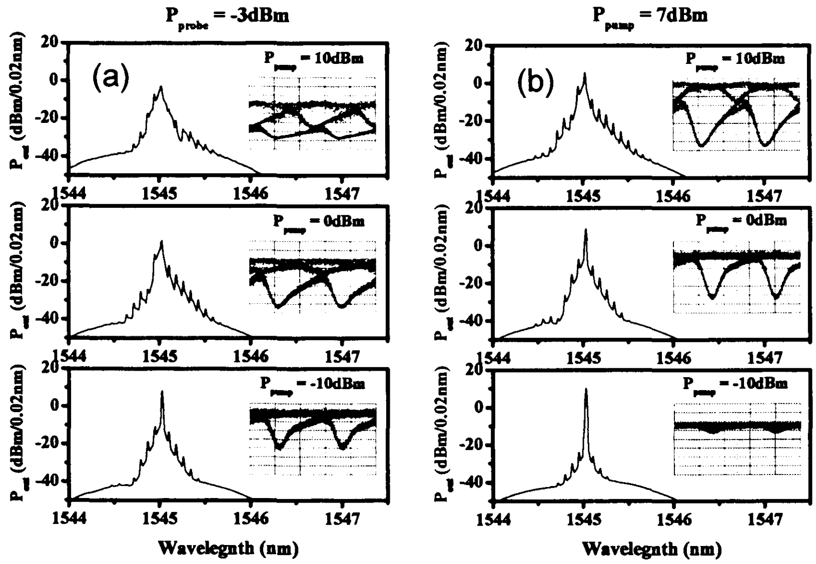

Figure 4-10 Spectra and eye diagrams of the 10Gb/s wavelength converted signal for different pump powers (P_{pump}) and for probe powers of -3dBm (a) and 7dBm (b)

As wavelength conversion occurs through gain depletion, the wavelength converted signal polarity is inverted and the pulse shape determined by the SOA gain recovery tail. For the case of larger probe power (7dBm), the SOA small signal gain is clamped to a lower value, consequently the gain recovery time decreases resulting in shorter wavelength converted pulses. For the case of a smaller probe power (-3dBm), the gain recovery time increases and pattern-dependent distortion was observed on the wavelength converted signal pulses. For a given probe power, the modulation depth of the wavelength converted signal increases with the pump power. However, for large pump power Self Gain Modulation (SGM) distortion present on the pump pulse [Agr89] is also transferred onto the wavelength converted pulses, significantly degrading the pulse shape. This is evident from the large pedestals in the wavelength converted pulses generated at large pump power, as shown in Figure 4-10. Thus, when operating the wavelength converter the probe power should be chosen to clamp the SOA recovery time to the desired bit period while the optimum pump power should be chosen to maximise the gain modulation depth whilst avoiding pump SGM distortion to transfer on the wavelength converted pulses.

The probe signal is cross-gain modulated and also cross-phase modulated (chirped) by the pump signal in the SOA, as described in section 4.1.2. The chirp acquired by the probe signal during the interaction with the pump signal is also visible in the multi-peak asymmetric profiles of the spectra of Figure 4-10. Referring to the results of Figure 4-5 for the chirp pulse profile of the probe signal, it can be seen that the leading edge of the probe pulse is shifted towards lower frequencies (red-shift) by the pump pulse raising edge, whereas the probe pulse trailing edge is shifted towards the higher frequencies (blue-shift) by the pump pulse falling edge.

It has been shown that by means of optical filtering the phase modulation associated with both the red-shifted and blue-shifted side-band of the probe spectrum can be converted into intensity modulation, improving the switching power efficiency and the wavelength converted pulse quality [Leu03] [Nie03]. These techniques are usually referred to as wavelength conversion based on pulse reshaping optical filtering (PROF) [Leu04]. In the course of the work described in this chapter two wavelength conversion techniques based on optimised filtering were investigated; the first relies on the use of an SOA with a hyperbolic off-set filter the second with a MZ filter.

4.2.2 Wavelength conversion based on off-set filtering

It has been shown that passing the chirped wavelength converted signal though a filter whose transmission varies linearly with frequency sharpens the transitions between the "*ones*" and "*zeros*" [Mah97] [Ell98]. This enhancement in speed only occurs if the slope of the filter has the same sign as the pulse phase factor [Mah97].

Figure 4-11 shows the principle of patterning suppression with off-set filtering.

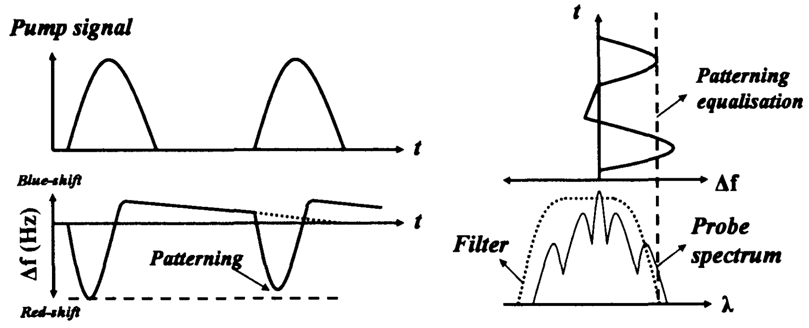

Figure 4-11 Patterning suppression with off-set filtering

As described earlier, pattern-dependent distortion is the variation of the wavelength converted pulse peak intensity due to the interference between adjacent bits caused by the SOA gain recovery time. A variation in the peak power of the wavelength converted signal pulses corresponds to a variation in the chirp. Figure 4-11 shows the chirp evolution in time for the case of two successive pump pulses. As shown in the characterisation result of Figure 4-5, the blue chirp induced by the first pump pulse will extend exceeding the bit period (for $T \leq 100$ps) causing a pattern dependent variation in the red-frequency shift (longer wavelengths) induced by the second pump pulse. Thus, the variation in the wavelength converted pulses peak power is associated with the longer wavelength components of its spectrum. By using a filter off-set from the centre wavelength, the spectral broadening induced by XPM over the longer wavelength can be minimised and thus patterning reduced.

This was investigated using the experimental configuration of Figure 4-9, by detuning the filter central frequency carefully so to place the signal spectrum near the red edge of the filter, where the hyperbolic filter function is nearly linear with negative slope. The eye diagram and spectrum of the wavelength converted signal at the SOA output and after off-set filtering are shown in Figure 4-12 (a). The wavelength converted signal eye diagram at the SOA output shows pulse shape distortion, which is significantly suppressed after off-set filtering. With the filter tuned to probe wavelength the optimum pump power was 7 dBm and the probe power was 8 dBm. However with off-set filtering, the optimum pump power was only -2 dBm. Thus, switching with off-set filtering is more power efficient, than XGM-based switching. This is because significant spectral broadening due to XPM can be observed at lower power, as shown in Figure 4-10, owing to the significant phase-gain coupling parameter (α-factor) of the SOA. The extinction ratio of the converter output is marginally improved with off-set filtering, and in this experiment was measured to be 10.2 dB, which is in the range of what predicted by the characterisation measurement for the dynamic gain change presented in Figure 4-8.

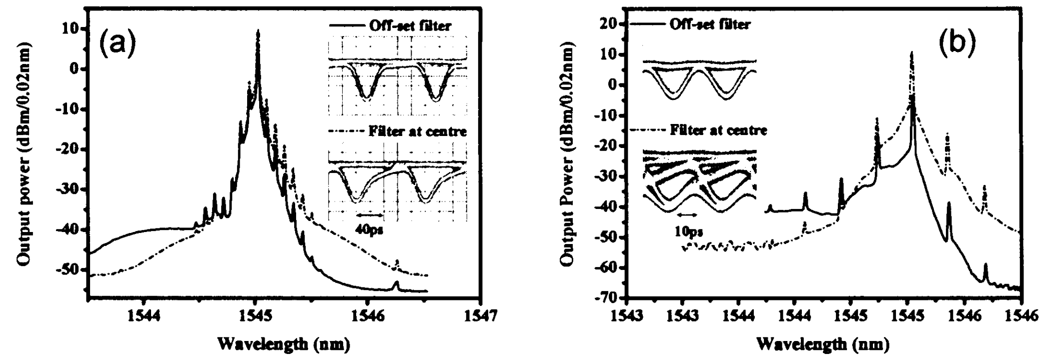

Figure 4-12 10Gb/s (a) 40Gb/s (b) Wavelength converted signal spectrum and eye diagram with off-set filtering

Wavelength conversion based on off-set filtering was also investigated at 40Gb/s. The pump signal was a 40 Gbit/s (PRBS 2^{31}-1) RZ signal with 12ps pulse width (FWHM) and with an extinction ratio of 15dB, generated by cascading a MZ and an EAM modulator driven with a 40Gb/s PPG. The pump wavelength was 1550nm and the probe wavelength was 1545nm. The details of the generation of the pump signal are given in appendix 3. The eye diagram of the wavelength converted signal and the optical spectrum at the SOA output and at the filter output were shown in Figure 4-12 (b). Again, the filter central frequency was carefully tuned so as to place the signal spectrum near the red edge of the filter to minimise patterning. It was found experimentally that the optimum filter centre frequency was 1544.5nm. The wavelength converted signal at the SOA output shows severe pattern-dependent distortion, which is significantly suppressed with off-set filtering. The eye diagram was recorded using a 65GHz photodetector with 7.4ps rise time. With the filter tuned to the probe wavelength (1545nm), the optimum pump power was 7dBm and the probe power was 8 dBm. However with the filter off-set to 1544.5nm, the optimum pump power was 2dBm and the probe power was 6dBm, which again is significantly less than the optimum power for switching without off-set filtering. The extinction ratio of the wavelength converted signal was measured to be 5dB and the pulse width 11.95ps.

When operating at 40Gb/s the switching power of both pump and probe signal are significantly increased with respect to the 10Gb/s experiment. Larger probe power is necessary to clamp the SOA recovery time close to 25ps rather than 100ps. However, this leads to an increase in the pump power required for switching. When optimising the probe power, there is a trade-off between the wavelength converted extinction ratio and the recovery time. The extinction ratio of the wavelength converted signal after off-set filtering was measured as a function of different probe power, and the results are shown in Figure 4-13.

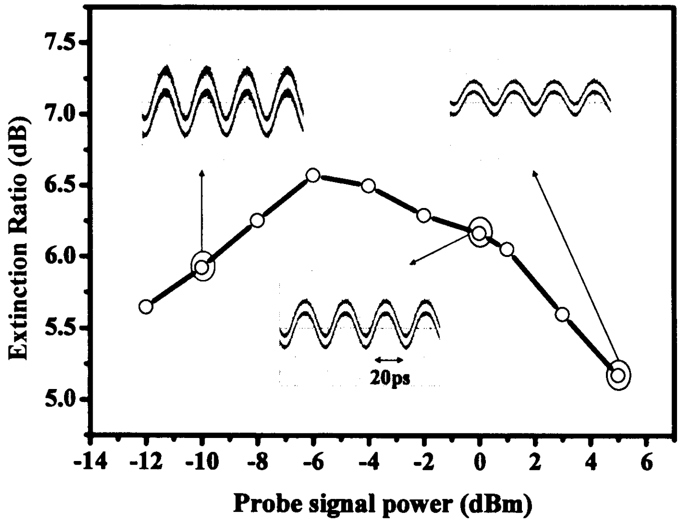

Figure 4-13 Extinction ratio of the 40GHz wavelength converted signal as function of the probe power

To maximise the gain switching contrast at 40GHz, the pump signal pulsewidth needs to be considerably smaller than the bit period (25ps). Thus, the pump signal was replaced with a 40GHz RZ signal with 1ps pulsewidth (FWHM), generated from a fibre ring laser with an extinction ratio in excess of 20dB, and launched into the SOA with an average power of 0dBm. The pump wavelength was 1554nm and the probe wavelength was 1547nm. As the probe power increases (from -15 to +5dBm) the recovery time shortened decreasing ISI (Inter-Symbol Interference) and, thus, improving the probe extinction ratio. For probe power equal to -6dBm the ISI is minimum, which corresponds to the point where the gain is fully recovered over the switching period. Further increase in the probe power depletes the gain and reduces the switching contrast. The maximum probe extinction ratio was 6.5dB, which exceeded by more than 1dB the switching contrast expected from the SOA characterisation results of Figure 4-8.

On the basis of the characterisation measurements of Figure 4-8, we conclude that off-set filtering allows for an enhancement of the SOA switching contrast at 10 and 40Gb/s. Experimentally it was found that switching contrast of in excess of 5 dB could be achieved with switching window of 12ps (FWHM), which is a factor of 2 higher than what observed from the characterisation measurements of section 4.1. This is because, with off-set filtering, the pattern dependent distortion is compensated rather than by clamping the device with large probe power to reduce the recovery time, by filtering the red-shifted components of the spectrum induced. However, the XPM induced spectral broadening occurs at significantly lower switching power levels than XGM gain depletion, owing to the large SOA α-factor. Thus, the observed switching contrast enhancement should be attributed to the larger gain available, resulting from the lower input power required to operate with off-set filtering.

However, both for the case of 10 and 40Gb/s switching the extinction ratio for the wavelength converted signal is significantly reduced with respect to the pump signal. This was expected from the gain transfer function slope measurement of Figure 4-3.

4.2.3 Wavelength conversion based on MZ filtering (SOA-DI)

Switching based on XGM in SOA has the fundamental disadvantage of signal polarity inversion. However, it was shown that passing the chirped XGM wavelength converted signal though a MZ filter can restore the signal polarity and pulse shape [Uen98]. As shown in Figure 4-10, much of the wavelength converted signal power is in the optical carrier, which caries the DC content of the polarity inverted wavelength converted signal. Thus, signal polarity can be restored using a MZ filter to transmit both sidebands of the probe spectrum while suppressing the probe carrier. Figure 4-14 shows the experimental set-up used to characterise wavelength conversion based on MZ filtering.

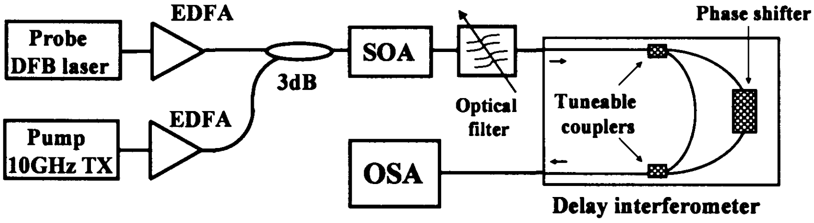

Figure 4-14 SOA-DI wavelength conversion experimental set up

As the differential delay between the 2 arms of the MZ interferometer is in the range of the pulsewidth, the MZ filter is usually referred to as a bit-delay interferometer (DI) [Leu01]. The delay between the two arms of the DI used in the experiments is 20ps giving a free spectral range of 50GHz, which ensure operation of up to 40Gb/s. The DI used in the experiments is described in detail in [Doe03]; it operates with a thermo-optic phase shifter in one arm and two voltage tuneable couplers. Figure 4-15 shows the measured transmittance of one MZI device for a fixed phase voltage.

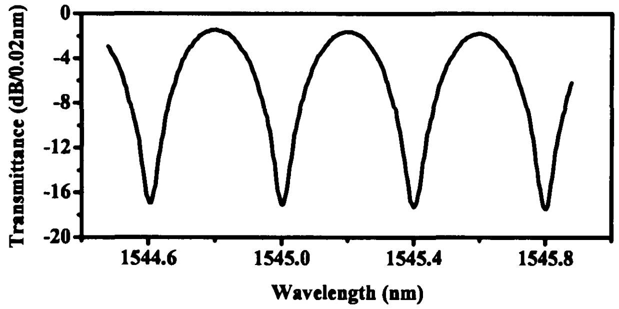

Figure 4-15 Delay interferometer transmittance over wavelength

To measure the wavelength converter transfer function it was necessary to use a time varying pump signal, as the DI suppresses the probe wavelength, filtering only the sidebands generated by XGM. In the experiment a 10GHz pulse train (FWHM = 20ps) was used as the pump signal. The CW probe signal wavelength was 1545nm, and the pump signal wavelength was 1550nm. The SOA used in the experiment is 1mm long bulk Kamelian SOA driven with 250mA (characterisation in section 4.1). An optical filter (bandwidth = 1nm) was used to select the probe wavelength at the DI output. The transfer function measured at the output of the optical filter and of the DI is shown in Figure 4-16.

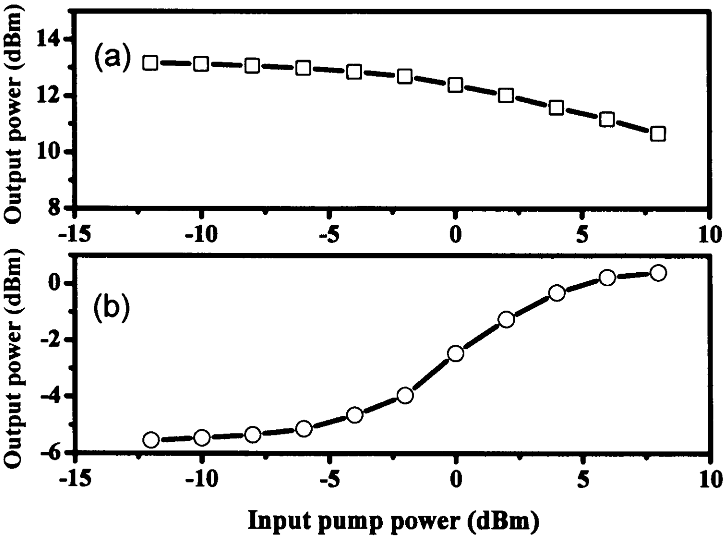

Figure 4-16 SOA-DI transfer function at the filter (a) and DI (b) output

The wavelength converted signal polarity is inverted at the filter output, and subsequently at the DI output. Thus, at the DI output wavelength conversion is achieved preserving signal and logic polarity.

The slope of the transfer function can not be estimated with accuracy following this measurement due to the limited extinction ratio of the pump signal. In fact as the pump power is increased also the SOA gain is further clamped by the pump pulse tails, which reduces the gain slope and the effective nonlinear gain change.

To assess the BER performance of the SOA-DI wavelength converter, a 10Gb/s (PRBS 2^{31}-1) RZ signal with a 20ps pulse width (FWHM) and with an extinction ratio of 15dB was used as the pump signal. The pump signal was generated cascading a

MZ and EAM modulator driven with a 10Gb/s PPG as described in appendix 3. The average pump signal power was 7dBm the probe power was 3dBm.

The measured spectrum of the probe signal at the DI output when the pump is not injected together with the spectral profile of the DI is shown in Figure 4-17 (a). The DI frequency response was adjusted by means of the phase shifter so to suppress the probe wavelength. The measured spectra of the probe signal at the filter output (b) and at the DI output (c) are also shown in Figure 4-17 when the probe was modulated by the pump signal.

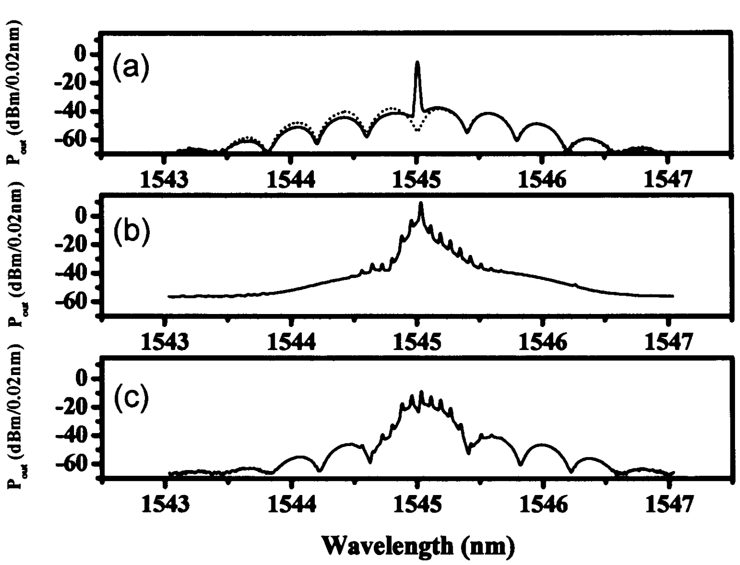

Figure 4-17 Spectrum of the probe signal at the DI output when the pump is not injected, and at the filter (b) and DI output (c) when the pump is injected

The sidebands of the probe signal at the filter output were filtered by the passband of the DI filter while the carrier was attenuated by 15dB. As a consequence, the signal polarity was reversed however the average power was attenuated from 12.3dBm at the filter output to -1.3dBm at the DI output. The OSNR of the wavelength converted signals was measured to be higher than 30dB with 0.07nm resolution bandwidth.

The BER was measured for the wavelength converted signal with respect to the pump signal back-to-back, and the results are shown in Figure 4-18. Figure 4-18 also shows the eye diagrams at the filter and DI output measured with a 30GHz pin pre-amp. The 10Gb/s optical receiver used in this experiment is described in appendix 3.

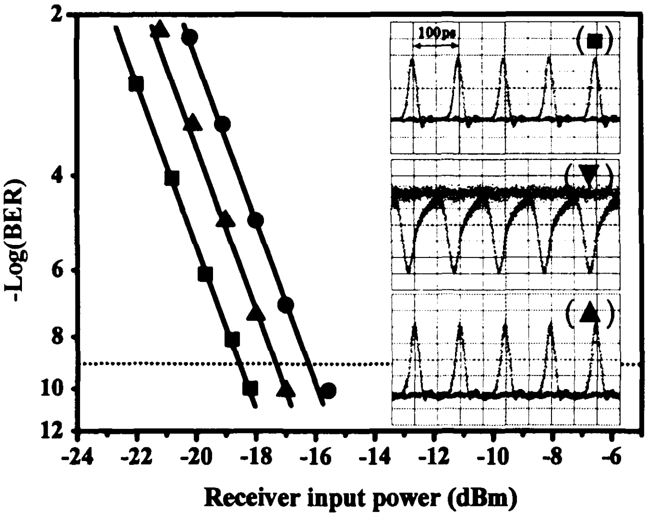

Figure 4-18 BER and eye diagrams of the wavelength converted signal at filter output (▼), at the DI output (▲) with respect to the 10G/s (PRBS 2^{31}-1) pump signal measured back to back (■)

It can be seen from the eye diagrams of Figure 4-18 that, due to the finite recovery time of the SOA, the probe signal at the filter output exhibits asymmetric pulse shape and long tails which spread into the following bit slots, resulting in ISI. The signal modulation shows also opposite logic polarity. The wavelength converted signals then propagate through the DI which compresses and reshapes the pulses, suppressing ISI and restoring the signal polarity [Leu01]. The DI compresses the probe pulses by taking a controllable portion of the input pulse energy at each time instant and, with a controllable phase, adding it ±20ps away, equivalent to approximately the tail of the wavelength converted pulse which exceeds the pump pulse width [Doe03].

From the bit error rate measurements, it can be seen that a power penalty of 1 dB was measured at BER = 10^{-9} for the SOA-DI wavelength converted signal with respect to the back-to-back pump signal. The sensitivity penalty is attributed to the lower signal extinction ratio of wavelength converted signal compared to the pump signal. The extinction ratio of the wavelength converted signal pulses was measured to be 10.5 dB, considerably less than the pump signal ($ER_{pump} \approx 15$dB). A power penalty of 2 dB was measured at BER = 1E-9 for the probe signal at the filter output without the DI. The enhancement in receiver sensitivity of 1dB is due to the suppression of ISI (Inter-Symbol Interference) distortion performed by the DI.

Wavelength conversion based on the SOA-DI was also investigated at 40Gb/s. The pump signal used for this experiment was a 40Gb/s (PRBS 2^{31}-1) RZ signal with a 12ps pulse width (FWHM) with an extinction ratio of 15dB. The pump wavelength was 1550nm and the probe wavelength was 1545nm. At the SOA-DI input, the average pump power was 7dBm and the probe power was 8dBm. The details of the 40Gb/s transmitter and receiver are given in appendix 3.

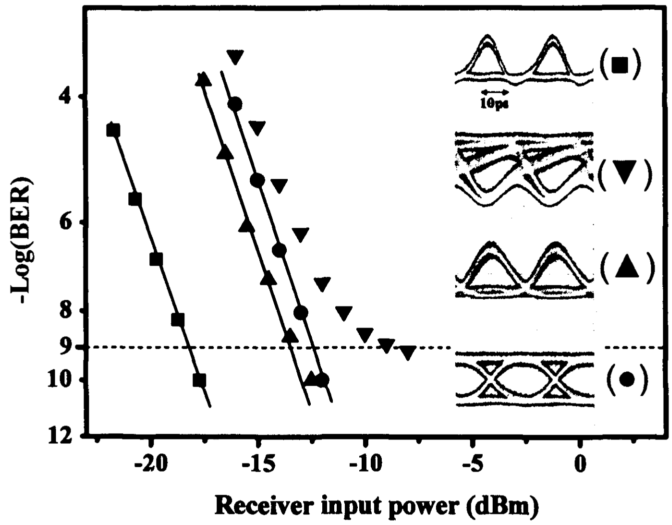

Figure 4-19 BER and eye diagrams of the wavelength converted signal at the filter output (▼), at the DI output for RZ format (▲) and NRZ format (●), with respect to the 40G/s (PRBS 2^{31}-1) pump signal back-to-back (■)

BER measurements were taken for the wavelength converted signal with respect to the pump signal back-to-back, and are shown Figure 4-19. The eye diagrams after the filter and DI output detected with a 65 GHz pin pre-amp were also measured and are shown in the same figure. Referring to the eye diagrams, each pulse of the probe signal at the filter output spreads over 3 bit slots due pattern-dependent distortion.

As described earlier, the DI can be used to either compress or disperse the probe pulses by ±20ps, equivalent to approximately one 40Gb/s bit slot. Compressing the probe pulses leads to a minimisation of the pattern-dependent distortion while maintaining the RZ signal format, dispersing the pulse by 20ps leads to the conversion of the signal format to NRZ. From the BER measurements, it can be seen that a power penalty of 6 dB was measured at BER = 10^{-9} for the RZ wavelength converted signal at the SOA-DI output with respect to the pump signal. The pulse width of the wavelength converted signal is 13ps and the extinction ratio was 6dB. The BER sensitivity penalty is attributed to a significant decrease in the signal extinction ratio through wavelength conversion due to the presence of strong pattern-dependent distortion. As the DI range is 20ps, ISI suppression is only limited to two adjacent bit, however the pattern dependent distortion exceeding 2 bit is left uncompensated. This is visible in the double railing around the "*zero*" level of the wavelength converted signal eye diagram at the DI output in Figure 4-19. A power penalty of 5.5 dB was measured at BER = 10^{-9} for the NRZ wavelength converted signal at the SOA-DI output with respect to the pump signal. The pulse width of the wavelength converted signal was 20ps and the extinction ratio is 6dB. A further sensitivity penalty of 9dB with evidence of an error floor, was measured fro the wavelength converted signal at the filter output without the DI, due to the uncompensated ISI. The OSNR of the wavelength converted signals was measured to be higher than 30dB with 0.07nm resolution bandwidth.

On the basis of the characterisation measurements of Figure 4-8, it can be concluded that the SOA-DI configuration allows for an enhancement of the SOA switching contrast at 10 and 40Gb/s. Experimentally it was found that switching contrast of 6 dB could be achieved with switching window of 12ps (FWHM), which is a factor of 2 higher than what observed from the characterisation measurements of section 1.2. This is because, in an SOA-DI configuration pattern-dependent distortions are compensated rather than by clamping the device with large probe power to reduce the recovery time, by compressing the wavelength converted signal pulses in the time domain. Thus, the observed switching contrast enhancement should be attributed to the minimisation of ISI, resulting in a larger wavelength converted signal extinction ratio. However, both for the case of 10 and 40Gb/s switching the extinction ratio for the wavelength converted signal is significantly reduced with respect to the pump signal, due to XGM being the dominant switching nonlinearity.

4.3 Multi-channel regenerative wavelength conversion

Large WDM systems operating in the S-band (1460-1530 nm), C-band (1530-1565 nm) and L-band (1565-1625), have been proposed to increase the transmission capacity [Gro02]. Multi-channel all-optical wavelength conversion is expected to be a key technique for connecting networks with different operating bands or channel spacing [Sak98] [Kan99]. High-capacity WDM networks also require all-optical 3R regeneration to minimize the accumulation of transmission impairments and achieve long transmission distances. Most of the techniques for all-optical 3R regenerative wavelength conversion demonstrated to date operate on a single channel, thus not offering a scalable solution for multiwavelength transmission networks.

To date, simultaneous multi-channel wavelength conversion has been demonstrated with an integrated SOA-array [Ito01]. However, due to limitation inherent in the SOA gain recovery time, the operating frequency was 2.5Gb/s. In this work, it is proposed to take advantage of broadband properties of the DI to simultaneously enhance the operating bit-rate of multi-channel wavelength conversion in an SOA array.

Firstly, the experimental demonstration of simultaneous multi-channel regenerative wavelength conversion of 10Gbit/s WDM channels, using a multi-channel optical equaliser [Doe03] and an array of discrete SOA is described. Then, the experiments are repeated using a novel monolithically-integrated wavelength selector SOA array module, to demonstrate simultaneous multi-channel L-band to C-band regenerative wavelength conversion of 10Gbit/s WDM channels with a single integrated optical component. The scheme is simple and can be fully monolithically integrated (SOA array + DI) for operation at higher bit-rate.

4.3.1 WDM wavelength conversion with SOA-DI configuration

Figure 4-20 shows the principle of operation of the scheme, when used as multi-channel wavelength converter. This consists of an array of SOAs followed by a multi-channel optical equalizer [Doe03]. The equaliser was originally designed to eliminate inter-symbol interference (ISI) in fibre transmission although here its function was to increase the switching speed of the SOAs, as described below. The optical equaliser is made up of two identical Mach-Zehnder interferometers connected in series with a single-mode waveguide.

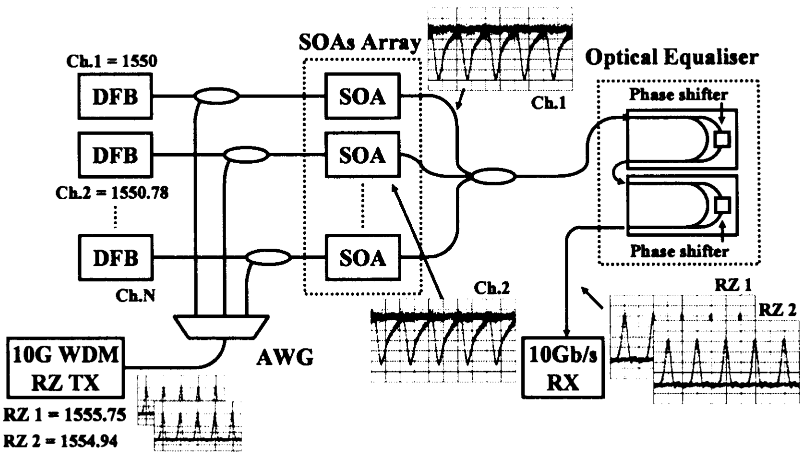

Figure 4-20 Multi-channel wavelength converter experimental set-up

Each MZI filter has a variable coupler and a free spectral range of 50GHz and was described in more detail in section 4.2.3. The equaliser operates simultaneously on multiple wavelength channels on a 50GHz grid, or an integer multiple thereof. The advantage of using two MZI filters compared to a single device is an extended pulse compression range, which with two devices is extended to 40ps. Each MZI filter reshapes either the pulse leading or falling edge by a maximum of 20ps.

A set of DFB lasers was used to generate the CW signals for the wavelength converter and each was coupled directly to a single SOA. The multi-channel RZ-modulated data signal was launched into the wavelength converter through an AWG which optically demultiplexed each WDM signal and routed it to a selected SOA. Thus, each SOA in the array was only reached by a single CW and data signal. As the RZ input signal enters an SOA, the gain and, thereby, the refractive index of the SOA are modulated. This encodes the phase and amplitude information on the co-propagating CW light. Due to the finite recovery time of the SOA the wavelength converted signal exhibits asymmetric pulse shape and long tails which spread into the following bit slots causing ISI (Inter-Symbol Interference), as well as opposite logic polarity. The wavelength converted signals then propagate though the equaliser which compresses and reshapes the pulses, suppressing ISI due to the finite recovery time of the SOA and restores the signal polarity [Leu01]. Selecting the CW wavelengths to match the equaliser free spectral range channels allowed the use of a single equaliser to simultaneously reshape all the wavelength converted signals. Due to large bandwidth of the equaliser, the proposed scheme is able to simultaneously operate across a wide wavelength range (tens of nm).

Firstly, two-channel simultaneous wavelength conversion was investigated. The two SOAs used in the experiment had low polarisation sensitivity (approx 0.5 dB) and 30dB small-signal gain, similar to the devices described in section 4.1. Although for the initial experiments discrete devices were used for simplicity, these were replaced, in later experiments (section 4.3.2), with an integrated SOA array module. The two RZ data signals were generated by modulating DFB lasers using electro-absorption modulators (EAM) driven with 30ps electrical pulses to give 20ps FWHM RZ signal pulses with 10 GHz repetition rate; the wavelengths of the data signals were λ_1 = 1555.75nm and λ_2 = 1554.94nm. The data signals were modulated by a 10Gb/s pseudo-random bit sequence with word length of $2^{31}-1$ using a Mach-Zehnder modulator (MZM). The wavelengths of the two DFB lasers used to drive the SOAs with CW light were λ_{cw1} = 1550nm and λ_{cw2} = 1550.784nm.

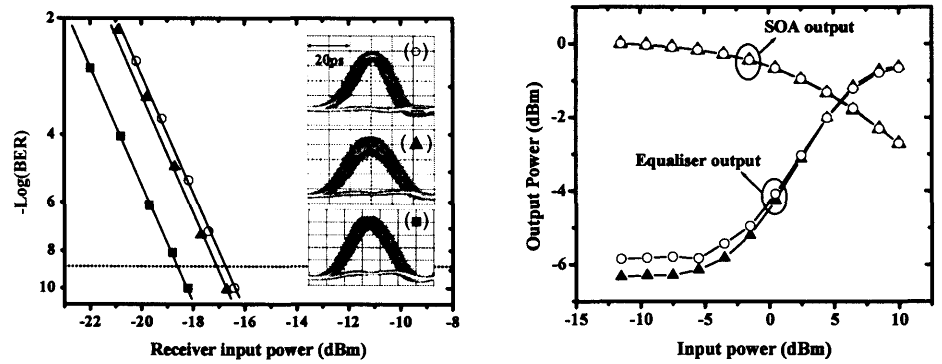

Figure 4-21 (a) BER and eye diagrams for two-channel simultaneous wavelength conversion; (b) Transfer function measured for the two wavelength converted channels: (■) Data back-to-back, (○) Ch.1 wavelength converted signal, (▲) Ch.2 wavelength converted signal

Figure 4-21 (a) shows the measured BER for the two simultaneously wavelength converted signals (Ch.1 and Ch.2), and the eye diagrams detected with 30GHz p-i-n pre-amp. A power penalty of 1.5 dB was measured for both channels with respect to the data signal, measured back-to-back. The average data signal power required to achieve optimal switching in the SOA was less than 6dBm. The OSNR of the wavelength converted signals was measured to be higher than 30dB with 0.07nm resolution bandwidth. To quantify the re-shaping capability of this scheme the extinction ratio of the wavelength converted signal pulses was measured and found to be higher than 10dB. Figure 4-21 (b) shows the transfer function measured for both signal channels simultaneously, showing similar performance for both channels.

The retiming capability of this scheme for application in multi-channel 3R regeneration was also investigated. For this, the CW light sources were replaced with synchronised optical clock pulses, generated by modulating the DFB lasers with an EAM to reshape the 20ps optical clock pulses prior to launching these into the SOAs. Figure 4-22 (a) shows the BER measurements and the eye diagrams for the two simultaneously regenerated signals (Ch.1 and Ch.2). A penalty of less than 1dB for both channels was measured with respect to the back-to-back data signal.

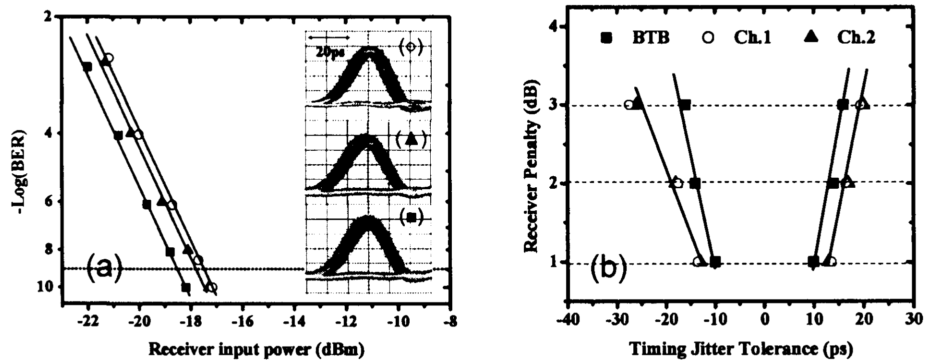

Figure 4-22 (a) BER and eye diagrams for two-channel simultaneous 3R regenerative wavelength conversion; (b) retiming window; (■) Data back-to back, (○) Ch.1 regenerated signal, (▲) Ch.2 regenerated signal

To investigate the retiming ability of the regenerator a timing offset between the clock and data signals was introduced and the BER of the regenerated signal measured. A penalty-free timing window of 20ps was measured for the regenerated signals, confirming the scheme tolerance to timing jitter. This range is fundamentally limited by the MZI delay timing window. However, when compared to the detection window of the receiver this shows a retiming improvement of 8ps within the 1dB penalty operating point. The measurements for retiming are summarised in Figure 4-22 (b), where the results for the measured error-free regenerator timing window are shown for different receiver penalties.

4.3.2 WDM wavelength conversion with an integrated SOA array-DI configuration

The initial measurements with discrete SOAs, described in the previous section, have demonstrated that the broadband equaliser can be used for simultaneous multi-channel pulse reshaping of RZ wavelength converted signals. Following these measurements the experiments were repeated using an integrated SOA-array rather than discrete components. The packaged fibre-pigtailed module, shown in Figure 4-23 (a), consists of 22-channel SOA array monolithically integrated with two 22 channels WGR (Waveguide Grating Router), extending the design reported in [Zir94].

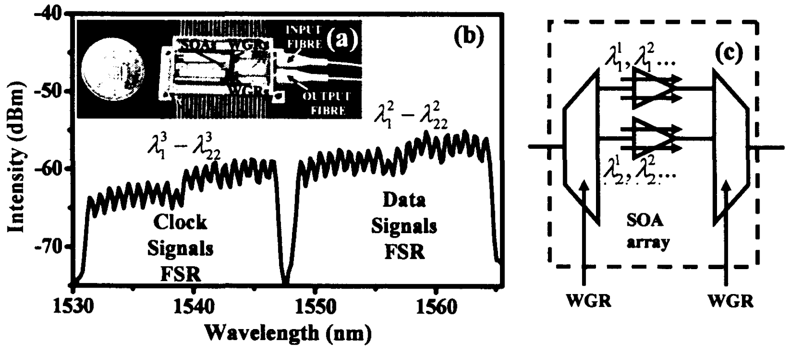

Figure 4-23 (a) Packaged 22-channel SOA-array module; (b) SOA-array ASE at the WGR output measured over 2 FSR for 20 channels operating simultaneously (SOA bias 75mA); (d) Optical circuit schematic

The SOAs are quantum well structures 1.6mm long spaced by 100μm [Joy99]; these are not yet designed for polarization independent operation and currently amplify TE polarized light predominantly. Figure 4.24(b) shows the SOA array amplified spontaneous emission (ASE) spectrum at the WGR output measured over 2 free spectral ranges (FSR) for 20 channels operating simultaneously (SOA bias 75mA). At 100mA operating current, the module exhibits fibre-to-fibre small-signal gain of 0-2 dB within the 1530-45 nm spectral range and of 3-4 dB within the 1550-65 nm spectral range for the best channels. The detailed characterisation of the SOA array module is given in appendix 4. The experimental set-up used to demonstrate simultaneous regenerative wavelength conversion of two signals is shown in Figure 4-24.

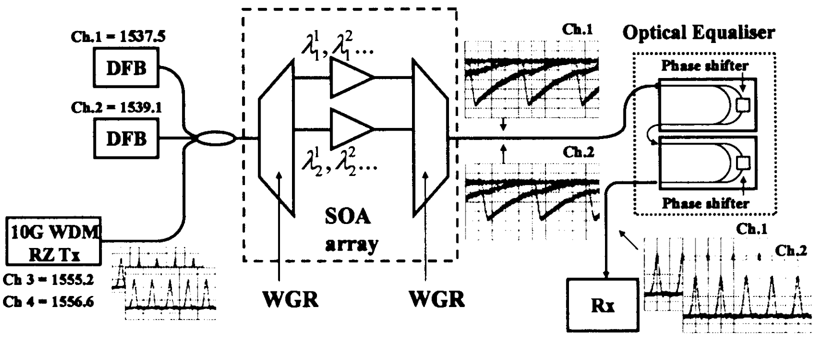

Figure 4-24 Multi-channel wavelength conversion with an SOA-array: principle of operation and experimental set-up

The use of two channels was limited by the availability of S-band laser sources and not by the device performance. The multi-channel wavelength converter consisted of the SOA array module as the multiwavelength non-linear element, followed by the multi-channel equaliser.

The two C-band RZ data signals were generated by modulating two external cavity tuneable laser sources (TL) lasing at $\lambda_1 = 1555.2$nm and $\lambda_2 = 1556.6$nm, with cascaded $LiNbO_3$ Mach-Zehnder (MZM) and electro-absorption modulators (EAM), driven by the data (word length 2^{31-1} PRBS) and clock outputs of the 10Gbit/s pattern generator (PPG), respectively, to generate 20ps FWHM pulses with 10GHz repetition rate. The two RZ S-band clock signals were generated by modulating the two S-band DFB lasers with an electro-absorption modulator (EAM), driven by the clock output of the 10Gbit/s pattern generator (PPG). This yielded 20ps FWHM pulses with 10GHz repetition rate. The data signal average power in the fibre at the input of the SOAs module was 6 dBm for both channels.

The data signals were launched into the SOA array via a 3dB coupler, so that the WGR demultiplexed each signal into a selected SOA in the array. The S-band CW signals were generated using two DFBs lasers lasing at $\lambda_3 = 1537.5$nm and $\lambda_4 = 1539.1$nm. The CW signals were TE polarised, using a polarisation controller, and launched at the input of the 3dB coupler into the SOA array and later routed in the equaliser. The data signal wavelengths were selected to match two channels within the 2nd Free-Spectral Range (FSR) (1550-65nm) of the SOA array module WGR. The CW signal wavelengths were selected to match the same two channels within the 1st FSR (1550-65nm) of the SOA array module WGR. Consequently each of the two SOA in the array, corresponding to the two selected WGR channels, was reached by one data and CW signal only. The two SOAs, corresponding to the two selected WGR channels, were simultaneously operating in the experiment and biased at a current of 180mA.

Operating the SOA array with the equaliser leads to a significant advantage compared to the previously reported configuration [Ito01]. In fact, the periodicity in wavelength of the equaliser MZI filters allows to suppress the ISI due to the slow carrier lifetime ($\tau_c \approx$ 500ps) simultaneously on all input wavelength converted signals. The MZI filters also compresses the wavelength converted signal pulsewidth and restores the signal polarity, as can be seen on the eye diagrams of Figure 4-24.

The BER was measured for the two simultaneously wavelength converted signals with respect to the data signals back-to-back, for both the case of CW clock signals and RZ clock signal; the results are shown in Figure 4-25.

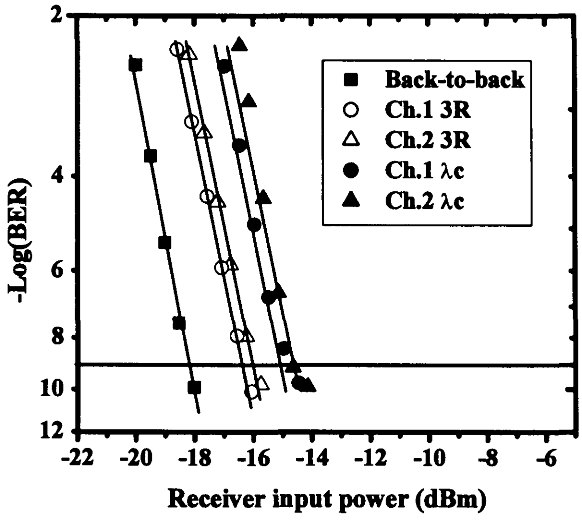

Figure 4-25 10Gb/s BER measurements (2^{31}-1 PRBS) and eye diagrams of the two simultaneously wavelength converted signals (λc); retimed signals (3R)

A penalty of less than 4dB was measured for channel 2 and 1 respectively for the case of CW probe signals; and of less than 3 dB for the case of RZ clock signals. This is mainly caused by residual patterning present on the wavelength converted signals at the equaliser output, which was more evident for the case of CW probe signals, and due to the OSNR degradation caused by the SOA-array ASE. The spectrum of the wavelength converted signals was measured using an optical spectrum analyser, and the results are shown in Figure 4-26.

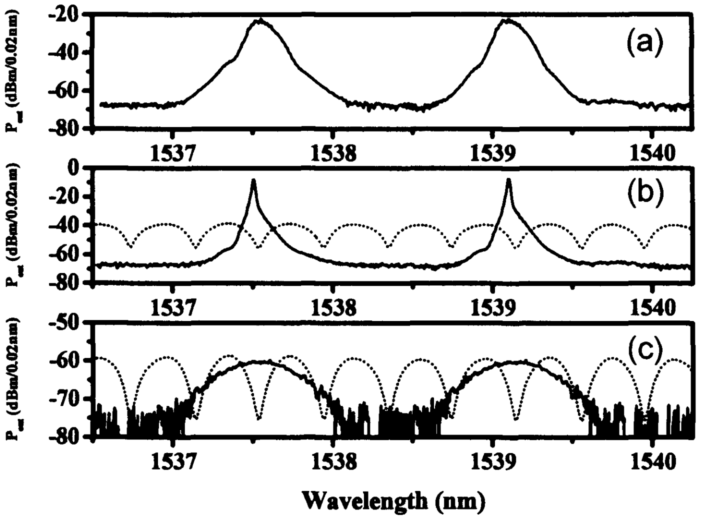

Figure 4-26 Spectrum of the wavelength converted signals at the optical equaliser output (a); at the SOA array output (b); SOA array output ASE power when the clock and data signals are not injected and DI frequency response in dotted line (c)

At the SOA array output most of the power of the wavelength converted signals is in the optical carriers. However the clock signal optical carriers are attenuated by 15dB at the optical equaliser output, where the pulse polarity is restored for both channels. The average optical signal-to-noise ratio as measured with 0.07nm resolution bandwidth at the output of the wavelength converter was larger than 38dB for both channels.

Summary

The first section of this chapter (4.1) presented the experimental characterisation of the dynamics and nonlinear responses of the gain, phase and chirp of the SOAs used in the optical processing experiments presented in this thesis. These results are key to predict the performance of both XGM and XPM-based optical gates.

From the characterisation measurements results, the tested SOA (1mm long bulk structure) can be expected to perform intensity switching based on gain saturation at 10GHz with switching contrast in excess of 13dB and at 40GHz with switching contrast in excess of 5dB. If an SOA-assisted interferometer configuration was used, switching with π radians contrast can be achieved with recovery time of 30ps which leads to switching frequency in excess of 30GHz.

The second section of this chapter (4.2) describes the experimental investigation of optical switching and reshaping properties of XGM gates for application to wavelength conversion. Both wavelength conversion based on XGM in SOA with off-set filtering and in an SOA-DI configuration have been investigated at 10 and 40Gb/s. On the basis of the SOA characterisation measurements, it can be concluded that both configurations allow for an enhancement of the SOA contrast at 10 and 40Gb/s switching frequencies. Experimentally, it was found that with both configurations a switching contrast in excess of 5 dB could be achieved with switching window of 12ps (FWHM), which is a factor of 2 higher than what observed from the gain characterisation measurements.

Finally, simultaneous wavelength conversion of 2 channels at 10Gbit/s was experimentally demonstrated, for the first time, using an integrated SOA array in a novel wavelength converter configuration. Wavelength conversion was obtained with low switching power demonstrating the potential for large scale monolithic integration for optical processing applications for WDM networks.

In the next chapter, the switching and regenerative properties of XPM configurations (SOA-assisted interferometer) will be experimentally investigated and related to the SOA characterisation measurements here described.

Chapter 5 Switching with an SOA-assisted interferometer: 3R regeneration and demultiplexing

The advantageous feature of an SOA-assisted interferometer compared to XGM configurations, is the ability to enhance extinction ratio [Dur94] [Idl95] of the input signal while reducing its noise [Mik96]. As shown in chapter 3, this property arises from the interferometer transfer function. However, when operating at bit-rates with a bit period shorter than the SOA recovery time, such as 40Gb/s, patterning can significantly degrade the switching performance of the SOA-assisted interferometer [Bis02b].

In the first part of this chapter a novel configuration for all-optical regeneration based on Polarisation Switching in an SOA-assisted Sagnac Interferometer (PSSI) will be described. The proposed scheme allows significantly enhance the switching frequency of the SOA, demonstrating error-free regeneration of 40Gb/s signal with long Pseudo-Random Bit Sequences (PRBS) using an SOA with carrier lifetime exceeding 250ps. The reshaping and retiming ability of the scheme are assessed experimentally at bit-rate of 10 and 40Gb/s, to show the largest distortion tolerance range published to date for optical regeneration.

In the second part of this chapter, the use of the PSSI scheme to demonstrate 40 to 10Gb/s demultiplexing is described. In particular the optical switching window temporal width and its relationship with the switching contrast are experimentally investigated.

In the last part of this chapter, multi-channel simultaneous regenerative wavelength conversion of 10Gb/s signals is demonstrated using an integrated SOA array in the PSSI configuration. To date, no other interferometer configuration has shown multiple channel simultaneous regenerative wavelength conversion, however, this functionality has potential applications in all-optical WDM networks.

5.1 All-optical 3R regeneration with PSSI

Error-free 3R regeneration at 40Gb/s with long PRBS has been demonstrated to date only in SOA-assisted MZ interferometer configurations, such as the DOM-MZI (2^{23}-1) [Lav01] and the UNI (2^{31}-1) [Phi98]. Unfortunately, these configurations require a temperature stabilisation circuit and a polarisation insensitive SOA such the UNI or a hybrid or integrated structure with multiple SOAs such as the DOM-MZI. Furthermore it seems that in more simple configurations such as the TOAD [Xu05] or Michelson interferometer [Dan98], pattern-dependence of the SOA limits the operation to 10Gb/s with short PRBS.

As shown in chapter 2, polarisation discriminator interferometers such as the UNI, operate with an enhanced tolerance to pattern-dependent distortion induced by the SOA. This feature allowed the UNI to perform all-optical regeneration at bit-rates of up to 80Gb/s [Kel98]. However, because of the linear interferometer geometry, the UNI operates with a fixed non-tuneable switching window and requires active phase stabilisation techniques to minimise temperature-dependent phase fluctuations. Both parameters are of fundamental importance to ensure stable operations and to maximise the retiming ability of the regenerator, especially for operation at high bit-rates [Jin94] [Gav01]. Furthermore, tuneability of the regenerator switching window is desirable in RZ-based bit-rate transparent optical networks [Blu03]. The UNI also require a polarisation independent SOA to operate. This precludes to use the UNI with an SOA array, which can enable multi-channel optical processing functionalities [Mik03a] [Gav03c] but usually has large polarisation dependent loss (PDL).

To address these problems, a simpler new all-optical regenerator configuration based on polarisation switching in a fibre Sagnac interferometer (PSSI) is proposed and described in this chapter. The PSSI configuration exhibits the same tolerance to pattern-dependent distortion as the UNI, however it allows for temperature stable operation, and tuneablility of the regenerator switching window. Furthermore, the PSSI can also work with a polarisation sensitive SOA; these unique features allowed to operate this configuration with an integrated SOA array to perform, for the first time, multiple wavelengths signal regeneration as described in section 5.3.

Experimental investigation of the regenerator noise suppression properties was also carried out at 10 and 40Gb/s and the results are described in this chapter.

5.1.1 Principle of operation of regeneration with PSSI

The regenerator principle of operation and configurations are shown in Figure 5-1. As briefly described in chapter 2, the PSSI regenerator consists of a 4-port polarisation beam splitter (PBS) with two arms forming a fibre loop which incorporates an SOA.

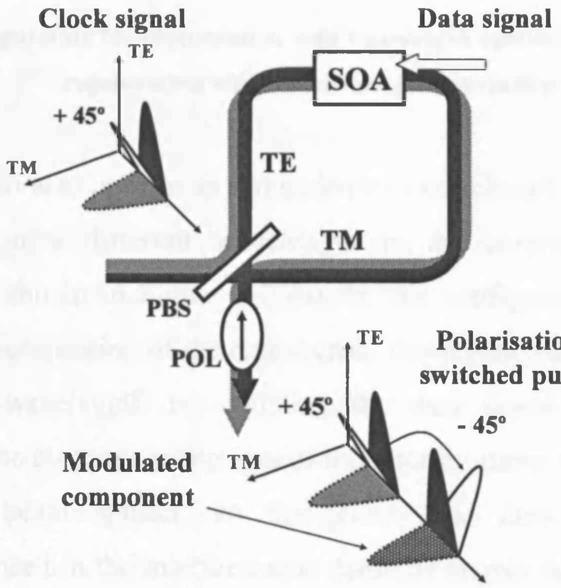

Figure 5-1 Principle of operations for polarisation switching in a Sagnac interferometer

A local pulse source provides an optical clock signal launched 45° polarised at the input of the polarisation beam splitter (PBS), used to split the signal into two orthogonally polarised pulses which counter-propagate in the loop and recombine at the output port of the polarisation beam splitter, to later interfere in a polariser (POL). As in a conventional TOAD scheme, described in chapter 2, the SOA is offset from the loop centre, so that the clock pulses are separated in time, and do not overlap as they travel through the SOA. The data signal pulse, synchronised to the local clock signal, is coupled into the co-propagating arm of the interferometer, so to reach the SOA immediately after the counter-propagating clock pulse and just before the co-propagating pulse has passed through it. The co-propagating pulse experiences nonlinear cross phase and intensity modulation, induced in the SOA by the data pulse, which causes the two clock pulses to recombine to a different polarisation state at the polarisation beam splitter output. Consequently the regenerator output signal is reshaped and retimed according to the quality of the clock signal and modulated with the information sequence encoded on the data signal.

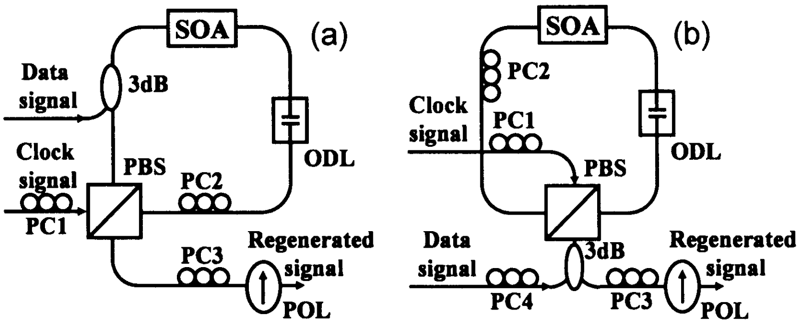

Figure 5-2 (a) Configuration for regeneration with wavelength conversion; (b) configuration for regeneration without wavelength conversion

The regenerator can also operate as a regenerative wavelength converter by coupling the data signal on a different wavelength in the co-propagating arm of the interferometer, as shown in Figure 5-2 (a). In this configuration the regenerator is insensitive to the polarisation of the data signal. The regenerator can be configured to retain the input wavelength by coupling the data signal, on the same clock wavelength, into the co-propagating arm of the interferometer from the output port of the polarisation beam splitter, so that clock and data signals co-propagate orthogonally polarised in the interferometer arms, as shown in Figure 5-2 (b). In this configuration the regenerator is sensitive to the polarisation of the data signal, which requires to be linearly polarised at the regenerator input. In both configurations, a polarisation controller (PC1) is used to tune the clock signal polarisation and therefore the power of the co-propagating and counter-propagating clock components at the SOA input, two more (PC2) (PC3) are similarly used before the polariser. As discussed in chapter 2, these coupling asymmetries give to the configuration an enhanced tollerance to pattern distortion and high switching contrast. A fourth polarisation controller (PC4) is used in the regeneration without wavelength conversion configuration to linearly polarise the data signal at the regenerator input.

The advantages of using a Sagnac interferometer over a linear interferometer geometry [Phi98] are in the simplicity of controlling the switching window and in the operating stability. The regenerator optical switching window can be easily tuned by controlling the position of the SOA in the fibre loop mirror using an optical delay line (ODL). The regenerator is inherently stable as the counter-propagating clock pulses split and recombine in the same beam splitter after travelling through the same fibre, including all random phase shifts induced by temperature effects on fibre, difficult to compensate in the linear geometry. Furthermore, it was shown [Top99] that nonlinear cross modulation between counter-propagating wavelengths is weaker than for the case of co-propagating wavelengths due to spatially localised nonlinearities in the SOA. The cross gain modulation imparted on a co-propagating wavelength was shown to be more than twice as strong as on a counter-propagating wavelength [Fen02]. Thus, using a counter-propagating configuration enhances the differential phase shift between the interfering clock components with respect to the case of a co-propagating configuration such as the UNI. As described in chapter 3, increasing the differential phase shift between the interfering clock components leads to a larger regenerator switching contrast.

However, the use of a counter-propagating switching configuration also has limitations, as described in chapter 2 for the case of the TOAD. First, the PSSI is expected to have a more asymmetric switching window with respect to the co-propagating configurations such as the DOM-MZI and the UNI. The switching window of counter-propagating configurations is characterised by a steep slope for the leading edge and a flatter slope for the trailing edge, as shown in Figure 2-3. The steep slope originates from the phase change seen by the clock pulse component co-propagating with the data pulse. The flatter slope results from the counter-propagating component, and depends on the length of the SOA. The consequence of an asymmetric switching window is a decreased timing jitter tolerance for the regenerator, which is maximised by operating with a flat-top shape of the switching window [Jin94]. However, as has been shown [Sch02], the counter-propagating Sagnac configuration operating with an 800μm long SOA can also generate flat-top switching window at switching frequency of 10GHz (≈30ps) and 40GHz (≈5ps) and, thus, a certain tolerance to jitter is also expected for this configuration.

A second important characteristic of a counter-propagating configuration is the dependence of the switching window width on the SOA length. As described in chapter 2 for the TOAD scheme, the propagation time through the SOA should be less than half of the switching window width to avoid the interaction of multiple data pulses with a single counter-propagating clock pulse component. This implies that, for example, to generate 25ps switching window width (required for 40Gb/s) 1mm long (or less) SOA should be chosen to avoid cross pulse interference.

This can be a limiting factor for application to optical signal demultiplexing where the optical switching window width is not limited by the SOA inter-band recovery time, and thus could lie in the sub-picoseconds range. Nonetheless, switching window of

4ps and 250Gb/s demultiplexing have been demonstrated with 500μm long SOA in TOAD [Gle94]. However, for 3R regeneration, which is the application for which the PSSI configuration is intended, the limiting factor in scaling to switching frequencies higher than 40Gb/s is the recovery time of the SOA and not the SOA length limiting the switching window width. In fact, as shown in chapter 4, a nonlinear phase shifts of π radians, as required for 3R regeneration, was achieved with recovery time close to 30ps in a 1mm long SOA. The characterisation measurement reported in this thesis for longer SOAs (varying between 1 to 2.5mm) has not demonstrated an increase in the SOA recovery time. Thus, the restrictions imposed by the SOA length do not have an impact on 3R regeneration applications, but they do for application to signal demultiplexing.

Finally, for application to wavelength conversion, where 3R regenerative capabilities are not required, and thus, the SOA-assisted interferometer can be operated with nonlinear phase shift of less than π radians, than the SOA length has to be considered. However, whether the extinction ratio penalty due to operating the SOA-assisted interferometer with a limited phase shift or the SOA length is the limiting factor is yet to be investigated and can be the subject of future work.

5.1.2 PSSI transfer function measurements

As described in chapter 3, the transfer function gives a qualitative indication of the regenerator cascadability and reshaping properties. To date, only the transfer function of the dual SOA MZI regenerator has been experimentally characterised using a pump and probe technique [Idl96]. This is based on monitoring the modulation induced on a CW probe signal by a CW pump saturating one of the two SOA in the MZ arms. However, this measurement method can not be applied for configuration utilising a single SOA as a differential phase shift can not be induced by a CW pump signal. Thus, to measure the transfer function of the proposed regenerator, it is necessary to use a time varying pump signal to induce a differential phase shift in the counter-propagating components of the probe signal.

The measured transfer function is, however, specific to a particular bit-rate (10GHz in this experiment) due to the time dependent gain dynamics of the SOA. The experimental set-up used to measure the regenerator transfer function is shown in Figure 5-3.

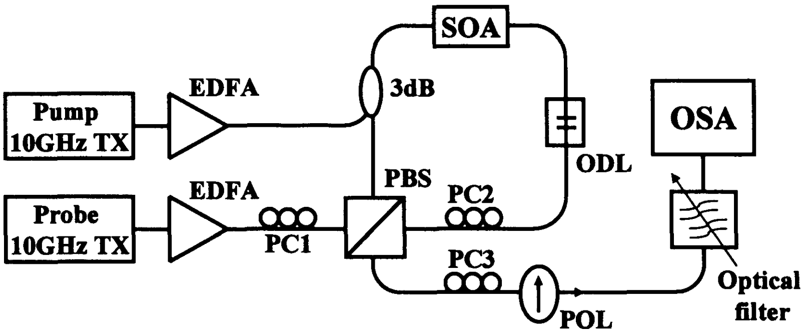

Figure 5-3 Interferometer transfer function measurement experimental set-up

In the experiments described in this work, the pump signal and the probe signal are 10GHz pulse trains with a pulse width of 20ps (FWHM), generated cascading a MZM and an EAM modulator driven with a 10Gb/s PPG; the probe signal wavelength was 1545nm, and the pump signal wavelength was 1550nm. The pump and probe pulse source are described in details in the appendix 3. EDFAs are used to boost the probe and pump power at the regenerator input. The SOA used in the experiment is a 1mm long bulk Kamelian SOA (characterisation in chapter 4.1). The transmitted optical power of the injected probe was measured at the two outputs of the regenerator as the pump power was varied, using an optical spectrum analyser (OSA) with resolution of 1 nm. An optical filter was used to select the probe for the pump signal at the OSA input.

Figure 5-4 shows the transfer function measured at the TE and TM outputs of the polarisation beam splitter for two different SOA bias current levels.

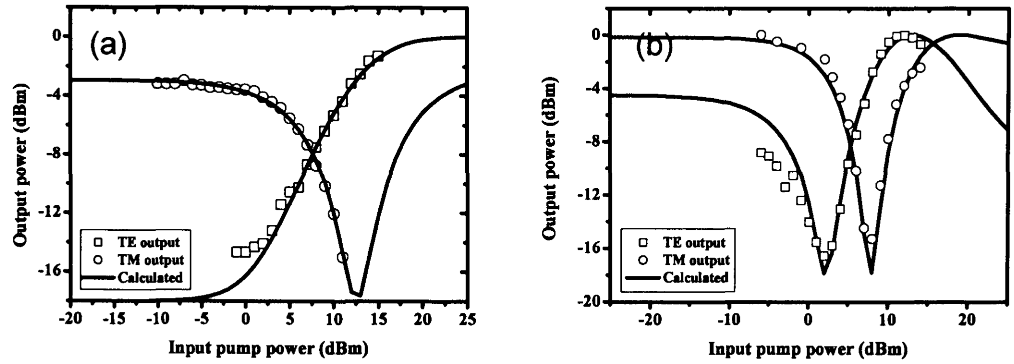

Figure 5-4 Interferometer transfer function TE and TM outputs, for the case of the I_{soa} = 150mA (a) and I_{soa} = 250mA (b)

Figure 5-4 (a) shows the transfer function measured driving the SOA with smaller bias current (I_{soa} = 150mA), corresponding to a measured small signal gain of 20 dB, the probe signal power at the interferometer PBS input was 3 dBm. Figure 5-4 (b) shows the transfer function measured driving the SOA with larger bias current (I_{soa} = 250mA), corresponding to a measured small signal gain of 27 dB, the probe signal power at the interferometer PBS input was 0 dBm. As expected, in both cases the interferometer bias differs by $\pi/2$ radians between the TE and TM outputs. The experimental results were fitted by numerically calculating for the interferometer transfer function using the model described in chapter 3. The SOA parameters used for the numerical calculations are α-factor = 5, τ_c = 150ps, E_{sat} = 1pJ, G_0 = 30dB for Figure 5-4 (a), G_0 = 20dB for Figure 5-4 (b). For the numerical calculations the probe power was optimised until the best fitting with the experimental results could be achieved, and the interferometer phase bias was maintained identical for both cases ($\varphi_{bias} \approx 0$). From the numerical calculations, it is estimated that the maximum SOA nonlinear phase shift, for the transfer function of Figure 5-4 (a), is close to π radians, while for Figure 5-4 (b) is close to 2.2 π radians. The larger phase shift available, in the case of Figure 5-4 (b), increases the range for which the SOA phase shift is linearly related to the input power. As shown in the figure, this gives rise to a sharper transfer function slope and to sharper transitions around the transfer function maximum and minimum point. Thus, increasing the driving current increases the small signal gain and also the effective phase shift, which can significantly reshape the regenerator transfer function. The switching extinction ratio is about 16dB for the measurements at 10Gb/s. This is not limited by the polarisation beam splitter extinction ratio which is larger than 20 dB, but possibly by the SOA ASE and the gain and phase recovery times.

However, it is important to notice that both the switching extinction ratio and the slope of the transfer function can not be estimated with accuracy with this measurement technique due to the limited extinction ratio of the pump signal. In fact, as the pump power is increased also the SOA gain is further clamped by the pump pulse tails reducing the gain slope and the effective nonlinear gain change. None the less, it is evident that the slope of the transfer function of Figure 5-4 (a) is significantly smaller than the slope of the transfer function of Figure 5-4 (b), which leads to a larger extinction ratio gain for the later case, as predicted by the theoretical model presented in chapter 3.

The interferometer transfer function shape does not only depend on the SOA characteristics, but also on the interferometer bias, which, as described in chapter 3 and in [Uen02], can significantly alter the regenerator reshaping capability. The regenerator utilises a polarizer as an optical discriminator, and thus the interferometer bias level can be adjusted by varying the polarisation state of the probe pulses prior to the polarizer using a polarisation controller (PC3) as shown in Figure 5-1. Figure 5-5 shows the interferometer transfer function for different values of the interferometer phase bias for two different operating conditions. Figure 5-5 (a) shows the transfer function measured driving the SOA with smaller bias current (I_{soa} = 150mA), corresponding to a measured small signal gain of 20 dB, the probe signal power at the interferometer PBS input was 3 dBm. Figure 5-5 (b) shows the transfer function measured driving the SOA with larger bias current (I_{soa} = 250mA), corresponding to a measured small signal gain of 30 dB, the probe signal power at the interferometer PBS input was -2 dBm.

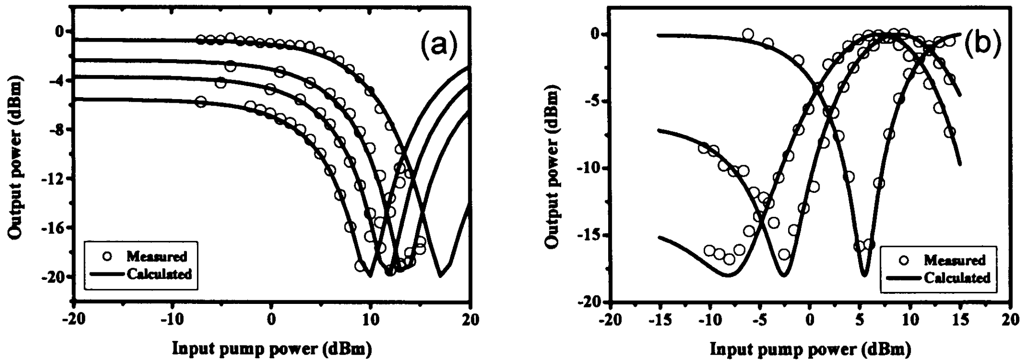

Figure 5-5 Interferometer transfer function for different bias levels, for the case of the I_{soa} = 150mA (a) and I_{soa} = 250mA (b)

For both cases, increasing the interferometer bias levels significantly increases the transfer function slope, but also sharpens the transitions around the transfer function maxima and minima. In regeneration terms this leads to an enhanced extinction ratio gain but also to a decreased noise reshaping ability especially around the signal "*zero*" level. The SOA parameters for the numerical calculations used to fit the experimental results are α = 5, τ_c = 150ps, E_{sat} = 1pJ, G_0 = 30dB for figure 6 (a), G_0 = 20dB for Figure 5-5 (b). From the numerical calculations, it is estimated that the SOA maximum nonlinear phase shift, for the transfer function of Figure 5-5 (a) is close to 2.5π radians, while for Figure 5-5 (b) is close to π radians. Therefore, the interferometer output switching extinction ratio decreases with larger phase biases for the case of Figure 5-5 (a), where only a π radians phase shift is available, however is unchanged for the case of Figure 5-5 (b) where a larger phase shift is available. This is because, as the phase bias is increased, the interferometer transfer function is shifted to operate over a higher input power range, however for the case of Figure 5-5 (a) the SOA is already fully saturated and no phase shift is available for switching.

It is important to notice that by varying the interferometer bias, the regenerator threshold, defined as the input power where the transfer function slope is maximum, is also changed. This is because by varying the interferometer bias both the "*zero*" and "*one*" level of the transfer function occur at different input powers.

This has important implications in how to operate the regenerator. Setting the threshold in the middle of the input signal eye diagram is optimum for regeneration of OSNR degraded signals, where distortion occurs on both signal levels. However, setting the threshold closer to either of the signal levels of the input signal pulses allows to optimise the tolerance of the regenerator to amplitude fluctuation around the "*zero*" or the "*one*" signal level. This can be beneficial when regenerating signal with pattern-dependent distortion as caused by fibre nonlinearity [Gav04a].

Furthermore, as shown in both Figure 5-4 and Figure 5-5, to operate the interferometer as a regenerator it is critical to match the means of input signal levels to the points on the interferometer transfer function where the slope is minimum. Thus, the interferometer performs noise suppression if the input signal extinction ratio matches the regenerator switching contrast.

5.1.3 10Gb/s regeneration experimental demonstration

The experimental set-up used to demonstrate 10Gb/s optical regeneration is shown in Figure 5-6. Data and clock signals were generated by modulating DFB (Distributed Feedback Laser) lasers using electro-absorption modulators (EAM) driven with 30ps electrical pulses to shape 16ps FWHM RZ signal pulses with 10 GHz repetition rate; the wavelength of the data signal was λ_d = 1555nm and of the clock signal λ_c = 1550nm. The data signal was modulated with a 10Gb/s pseudo-random bit sequence with word length of $2^{31}-1$ using a Mach-Zehnder modulator (MZM). The details of the 10Gb/s transmitter and receiver used in this experiment are given in appendix 3.

Both regeneration with wavelength conversion and without wavelength conversion was investigated by operating the regenerator in the two different configurations described in Figure 5-2.

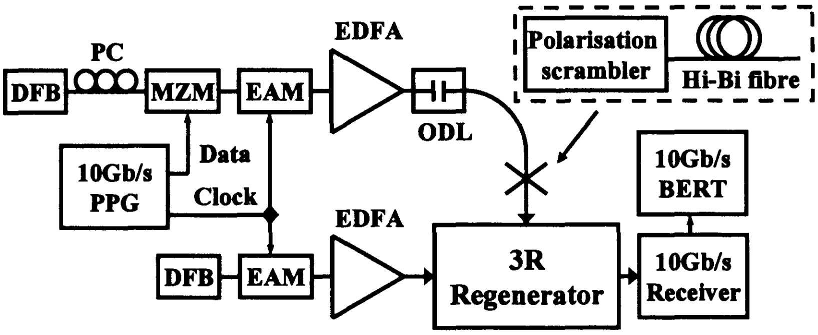

Figure 5-6 10Gb/s regeneration BER experimental set-up

For regeneration without wavelength conversion a single DFB laser ($\lambda_d = \lambda_c =$ 1555nm) was used for both data and clock transmitters. The SOA used in the experiment is a low polarisation-dependent 2.6mm long bulk Lucent SOA [Dre02] (characterisation in appendix 2), driven with 360mA bias current, although similar results are obtained also with a low polarisation-dependent 1mm long bulk Kamelian SOA [Tom03] (characterisation in chapter 4.1), used for the previous transfer function characterisations. Regeneration was achieved with low power levels; the data signal average power was 2dBm for regeneration with wavelength conversion and 0dBm for regeneration without wavelength conversion. BER was measured for both regenerator configurations and is plotted with respect to the data signal measured back-to-back in Figure 5-7.

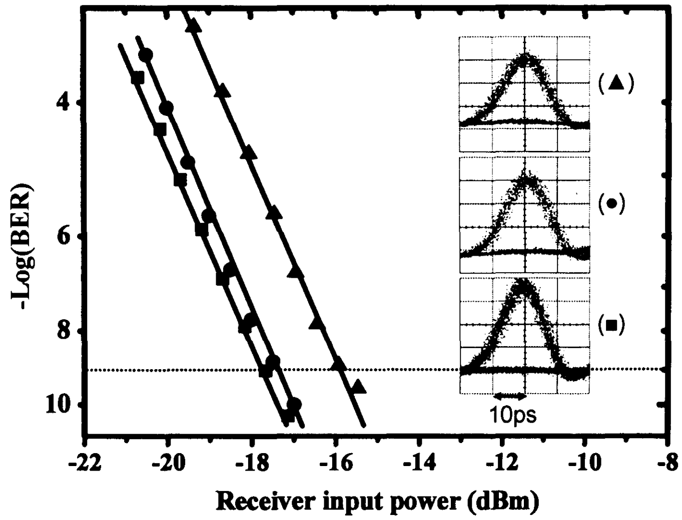

Figure 5-7 BER measurements (PRBS 2^{31}–1) for 10Gb/s regeneration without wavelength conversion (▲), with wavelength conversion (●) and data signal back-to-back (■)

In the experiment, an error-free (BER = 10^{-9}) penalty of less than 0.5dB was measured for regeneration with wavelength conversion, and of less than 2dB for regeneration without wavelength conversion. The increased penalty for regeneration without wavelength conversion is a result of internal reflections of the data pulses at the SOA facets, which contribute to the signal at the regenerator output with parasitic reflections. The eye diagrams of the input signal and of the regenerated signal for both regenerator configurations are also shown in Figure 5-7 as observed with a 50GHz PIN detector, showing clear and open eye, with no sign of patterning effects. To minimise patterning effect and enable regeneration of long pattern lengths without additional penalties, it was necessary to enhance the effective recovery time of the SOA. This was practically achieved by optimising the power in the two clock components (by means of PC1), allowing the counter-propagating pulse to determine the carrier density evolution of the SOA rather then the following switching pulse. The average optical signal-to-noise ratio (OSNR) of the regenerated signal measured at the output of the regenerator without optical filtering and with a 0.07nm resolution bandwidth was 40dB for wavelength conversion at 1557nm, as shown in Figure 5-8.

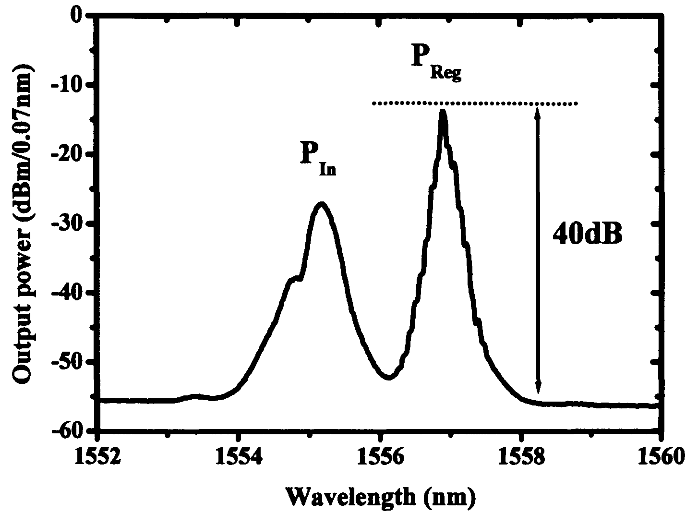

Figure 5-8 Spectrum of the data and regenerated signal

10Gb/s retiming experimental investigation: To date, most of the investigated all-optical 3R regenerators have demonstrated back-to-back operation, however tolerance to RZ pulse timing jitter has not been studied at 10Gb/s for most of the schemes proposed. Retiming at 10Gb/s was investigated previously only with a TOAD configuration [Wan01] to show a limited tolerance of regeneration to timing jitter; this was attributed to the patterning induced by timing to intensity jitter conversion within the generator switching window. However, timing jitter, defined as the rapid fluctuation of pulse-to-pulse mean time arrival induced by fibre nonlinearities [Mam99], polarisation mode dispersion [Kho05] or the Gordon Haus effect [Gor86], severely limits the achievable transmission distances of RZ signals [Kil02] [Mik03b]. Here we present the results of the experimental investigation of the retiming ability and timing jitter tolerance of the proposed regenerator.

To investigate the retiming ability of the regenerator a timing offset between the clock and data signals was introduced and the BER of the regenerated signal measured. The timing offset was controlled by delaying with an optical delay line (ODL), as shown in Figure 5-6, the clock signal with respect to the data signal at the regenerator inputs. The results are summarised in Figure 5-9, where the timing offset between clock and data signal is referred to as the regenerator timing jitter tolerance [Leu01].

Measurements were taken operating the scheme in the regenerative wavelength converter configuration. The error-free (BER < 1E^{-9}) penalty measured was less than 1dB within a 34ps timing window, and less than 2dB within a 43ps timing window corresponding to 43% of the bit period. When compared to the detection window of the receiver this shows a retiming improvement of 14ps within the 1dB penalty operating point. This shows the largest tolerance to timing jitter reported to date in literature for 10Gb/s regeneration, demonstrating that the resilience to patterning inherent to polarisation switching enhances the regenerator retiming ability.

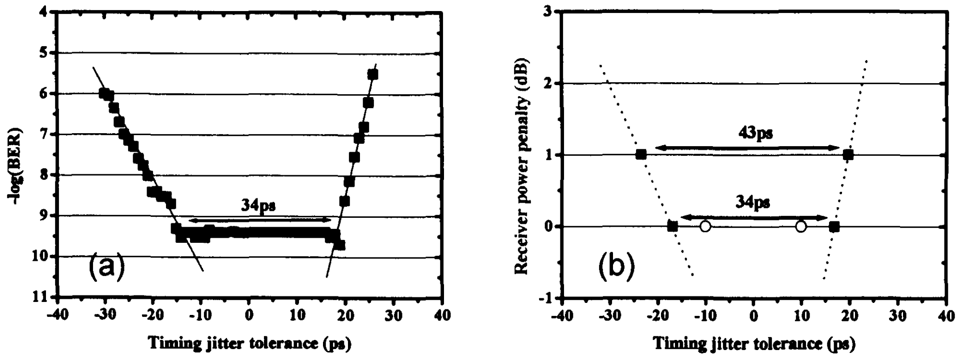

Figure 5-9 (a) BER of the regenerated signal as a function of the timing jitter tolerance; (b) retiming characteristics of the regenerator at the sensitivity point (■) with respect to the optical receiver (○)

Further to this measurement the ability of the regenerator to restore signal quality from a data signal corrupted by quasi-random signal jitter as encountered in real fibre transmission systems was investigated. With the regenerator optimised to operate with a 34ps optical switching window up to 18ps timing jitter restoration is expected, within 1dB operating penalty, for 16ps pulses [Jin94]. Quasi-random timing jitter was superimposed artificially on the data signal, by combination of a polarisation scrambler and high-birefringent (Hi-Bi) fibres of different length with PMD of 10, 15 and 21ps corresponding to different timing jitter levels, as shown in Figure 5-6. The BER measurements for regeneration from a jittered data signal for three different levels of timing jitter (10, 15 and 21ps) are plotted with respect to the data signal measured back-to-back in Figure 5-10. The BER measurements also show no polarisation dependent penalty. Eye diagrams of the jittered data signals and of the corresponding regenerated signals are also shown in Figure 5-10, for the three investigated cases. Full retiming was achieved, as can be seen from the eye diagrams, from up to 15ps of timing jitter with negligible penalties of less than 0.5dB with respect to the data signal measured back-to-back.

It should be noted that this corresponds to the penalty measured for regenerative wavelength conversion, showing that retiming was achieved with no further penalties on regeneration.

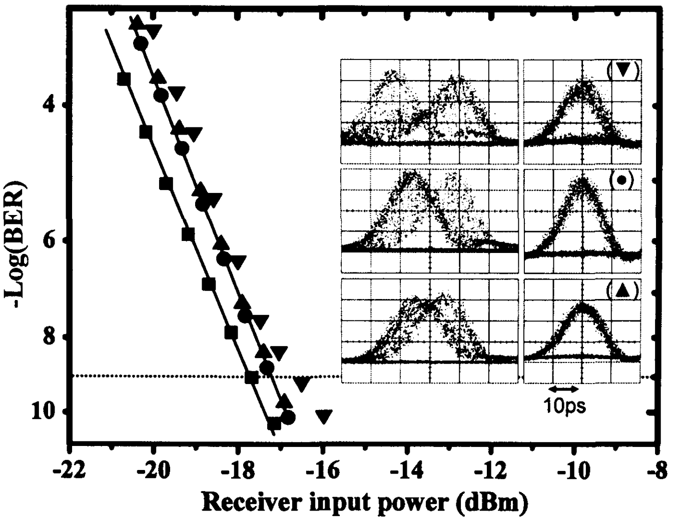

Figure 5-10 BER measurements (PRBS $2^{31}-1$) for 10Gb/s regeneration from jittered data signal; regeneration form 21ps jittered data signal (▼), regeneration from 15ps jittered data signal (●), regeneration from 10ps jittered data signal (▲), back-to-back (■)

Although for the case of 21ps timing jitter a penalty of 1dB was measured, the regenerated signal eye diagram is visibly affected by intensity jitter. This is induced on the regenerated signal by the fast modulation of the regenerator optical switching window caused by the data signal timing jitter, suggesting that the induced intensity jitter ultimately limits the regenerator tolerance to further timing jitter. Higher tolerance to timing jitter requires a wider optical switching window, however we observed the optical switching window to be limited to 34ps for the regenerator to operate within 1dB penalty.

5.1.4 40Gb/s regeneration experimental demonstration

To date, error-free regeneration at 40Gb/s has been demonstrated only in SOA-assisted MZ interferometer configurations, such as the DOM-MZ [Fis99] the UNI [Phi99] and the SOA-DI [Leu01]. However, it seems that pattern dependencies of the SOA limits operation to at 10Gb/s with short PRBS for most of the other reported SOA-based schemes such as the TOAD [Xu05] or MI [Dan98]. Here the operation of the PSSI regenerator, described in the previous section, is experimentally investigated at 40Gb/s to show negligible operating penalty with long PRBS sequences. This was the first demonstration of 40Gb/s regeneration with a single SOA in Sagnac fibre interferometer. The retiming and reshaping ability of the scheme is also investigated to assess the tolerance of the regenerator to different levels of timing and intensity jitter of the incident data signal.

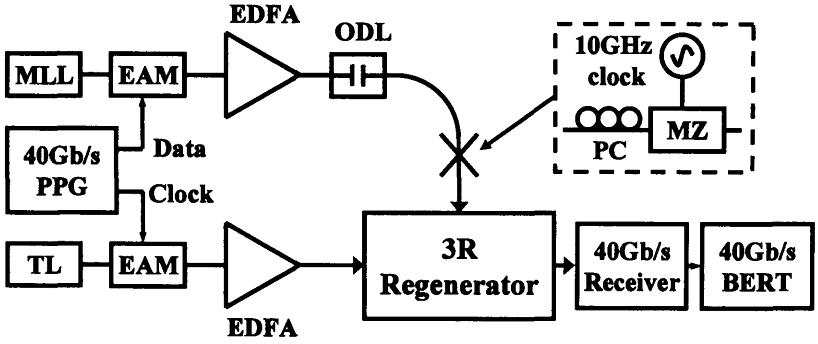

Figure 5-11 40Gb/s regeneration experimental set-up

The experimental set-up used to demonstrate 40Gb/s regeneration is shown in Figure 5-11. The RZ 40Gb/s data signal was generated by modulating the output of an OKI monolithically-integrated 40GH/z semiconductor mode locked laser, producing 6ps

FWHM optical sech-pulses at $\lambda_{DT} = 1547.5$, with a 40Gb/s 2^{31}-1 long PRBS using an electro-absorption modulator (EAM) driven by a 40Gb/s pulse pattern generator (PPG). The clock signal was generated by modulating the output of a tuneable laser (TL) lasing $\lambda_{CK} = 1549.5$, with an electro-absorption modulator (EAM) driven with a 40GHz electrical clock from the pulse pattern generator. The 40Gb/s receiver used in this experiment are described in details in appendix 3. The Lucent SOA used in the experiment is a low polarisation-dependent 2.6mm long bulk SOA [Dre02], driven with 500mA bias current (characterisation in appendix 2). Bit-error-rate (BER) measurement for regenerator with wavelength conversion is plotted with respect to the data signal measured back-to-back in Figure 5-12 (a).

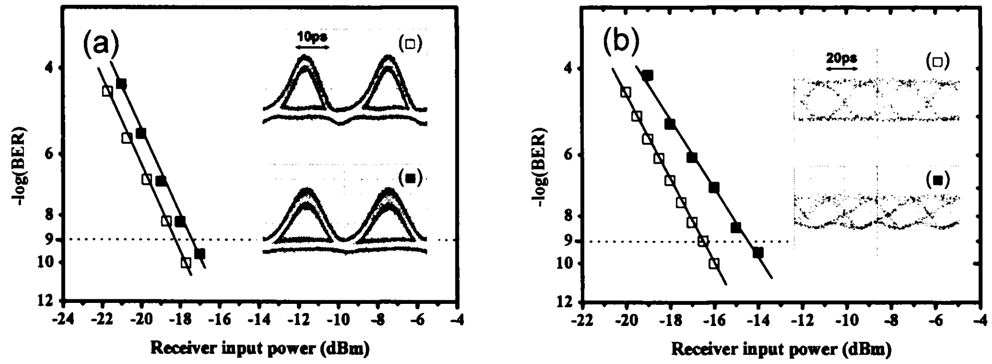

Figure 5-12 (a) BER measurements (PRBS 2^{31}–1) for 40Gb/s regeneration with wavelength conversion (■) and data signal back-to-back (□); (b) BER measurements (PRBS 2^{31}–1) for 40Gb/s NRZ to RZ signal format and wavelength conversion (■) and data NRZ signal back-to-back (□)

In the experiment, an error free (BER = 10^{-9}) penalty of less than 1dB was measured for regeneration with wavelength conversion. The eye diagrams of the input signal and of the regenerated signal are also shown in Figure 5-12 (a) as observed with a 50GHz PIN detector, showing clear and open eye, with no sign of patterning effects. The switching power in the fibre at the SOA input was 3dBm for the data signal and 4dBm for the clock signal, and the average OSNR of the regenerated signal was 36dB measured with 0.2nm resolution as shown in Figure 5-13.

When replacing the clock signal with a CW signal the regenerator operates as an RZ to NRZ signal format wavelength converter. Figure 5-12 (b) shows the results of the BER measurement for the RZ to NRZ wavelength converted signal plotted with respect to the NRZ data signal measured back-to-back. A penalty of less than 2dB was measured for the NRZ format and wavelength converted signal. The eye diagrams of the NRZ back-to-back signal and of the RZ to NRZ converted signal are also shown in Figure 5-12 (b) as observed with a 50GHz PIN detector.

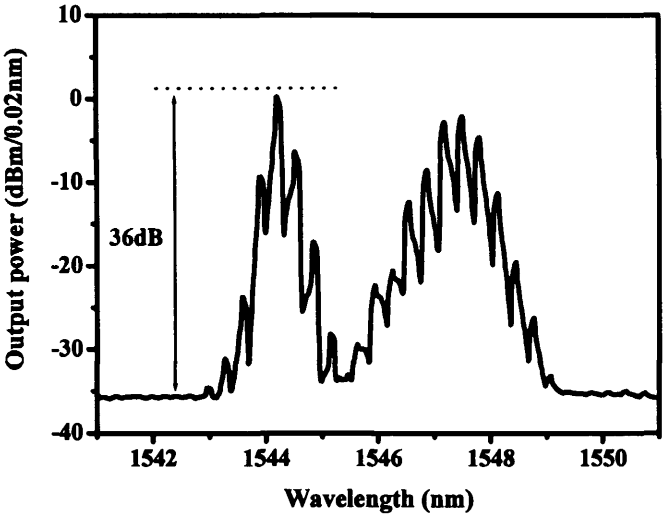

Figure 5-13 Spectrum of the data and regenerated signal

40Gb/s reshaping experimental investigation: To date, most of the investigated all-optical regenerators have been shown to be very efficient in retiming distorted signals and suppressing timing jitter [Leu01] [Tsu02], although tolerance to RZ pulse amplitude jitter has not been studied at 40Gb/s for most of the schemes proposed. However, amplitude jitter, defined as the rapid fluctuation of pulse-to-pulse peak power on the "*ones*" severely limits the achievable transmission distances of 40 Gb/s RZ signals. This amplitude jitter can be induced by nonlinear effects in fibre such as four wave mixing [Ess99] or by pattern-dependent distortion in SOA in-line amplifiers [Sal90] and wavelength converters [Bis02b]. Here we experimentally investigated for the first time, the patterning tolerance and the amplitude jitter cancellation properties the PSSI regenerator at 40Gb/s. Operating the Sagnac interferometer in polarisation diversity gives the significant advantage over the previously reported configuration [Sok93], of allowing the tuning of the regenerator switching threshold level. Optimising the discriminator threshold close to the zero level of the input pulses allows to minimise the amplitude fluctuation on the regenerated signal, enhancing the regenerator tolerance to amplitude jitter and patterning effects.

To investigate the regenerator tolerance to amplitude jitter, a quantifiable amount of distortion was imposed on the amplitude of the data signal pulses at the regenerator input. This was achieved by modulating the data signal pulses, as shown in Figure 5-11, with a 10GHz free running clock signal using a Mach-Zehnder (MZ) modulator, operating with a variable extinction ratio, corresponding to the fluctuation of amplitude introduced on the data pulses. The BER measurements on the back-to-back and regenerated signal were carried out using a 40 Gb/s receiver consisting of an EDFA pre-amplifier, a 50GHz photodetector followed by a 40GHz RF amplifier and a 40Gb/s error detector (BERT).

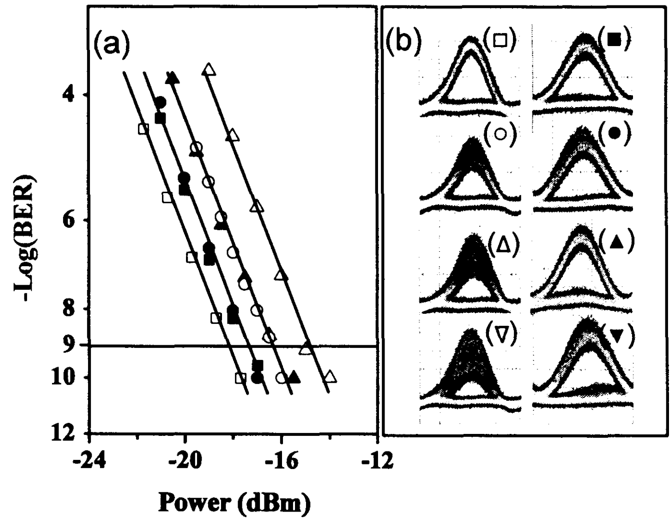

Figure 5-14 (a) BER measurements vs receiver power (PRBS $2^{31}-1$) for 40Gb/s regeneration from data signal for different level of peak-to-peak amplitude jitter (AJ); (b) Eye diagrams of the data signals with different level of peak-to-peak amplitude jitter 2dB (○), 3dB (△), 4dB (▽), back-to-back (□) (left trace) and corresponding regenerated signals (right trace)

The BER measured with respect to the receiver input power for regeneration from the data signal distorted by different levels of peak-to-peak amplitude jitter are plotted with respect to the data signal measured back-to-back in Figure 5-14 (a).

The switching power in the fibre at the SOA input was 3dBm for the data signal and 4dBm for the clock signal, and the average OSNR of the regenerated signal was 36dB measured with 0.2nm resolution.

When no amplitude jitter is present the already good quality of the data signal can not be further improved, resulting in a penalty for the regenerated signal with respect to the data back-to-back of less than 1dB. A penalty of 1dB and 1.8 dB was measured for regeneration from a data signal distorted by amplitude jitter of 2 dB and 3 dB respectively, with respect to the data signal back-to-back. An improvement in the receiver sensitivity of 1.5 dB was measured after regeneration for the amplitude jitter value of 3dB.

The BER measurements with respect to the decision threshold for regeneration of the data signal with different levels of peak-to-peak amplitude jitter are plotted in Figure 5-15 together with the back-to-back data signal, for comparison.

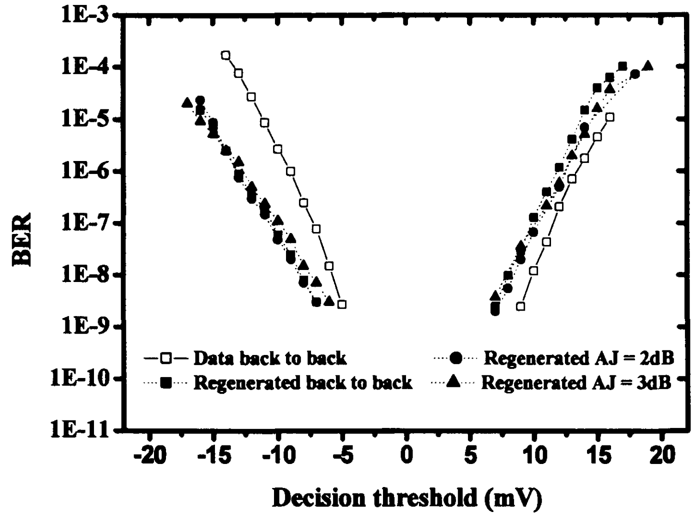

Figure 5-15 BER measurements vs decision threshold (2^{31-1} PRBS) for 40Gb/s regeneration from data signal for different level of peak-to-peak amplitude jitter (AJ)

Regeneration for all values of amplitude jitter of up to 3dB was achieved with no reduction of the threshold-voltage window within which the BER is below 10^{-9}. This shows that the regenerator suppresses amplitude jitter on the peaks of the pulses "*ones*", representative of pattern-dependent distortion, fully restoring the signal eye opening. The eye diagrams measured with a 50GHz photodetector for the data signals back-to-back and distorted by different level of peak-to-peak amplitude jitter and the corresponding regenerated signals are shown in Figure 5-14 (b). It can be seen that for all values of amplitude jitter of up to 3dB the regenerated signal eye opening was fully restored, confirming the measurements for the decision threshold window of Figure 5-15. For amplitude jitter level above 3dB the regenerated pulses were fully reshaped and the peak powers equalised, although an increase of noise on the "*zero*" level of the regenerated pulses can be seen. This is attributed to the decrease in the extinction ratio of the regenerator optical switching window when triggered by the low power pulses in the input sequence, suggesting that this ultimately limits the regenerator tolerance to further amplitude jitter.

The optimisation of the regenerator threshold also has a key role in determining the tolerance to intensity jitter. The transfer function of Figure 5-16 shows the operating point of the regenerator as optimally tuned for pulse reshaping. The transfer function was measured as described in section 5.1.2.

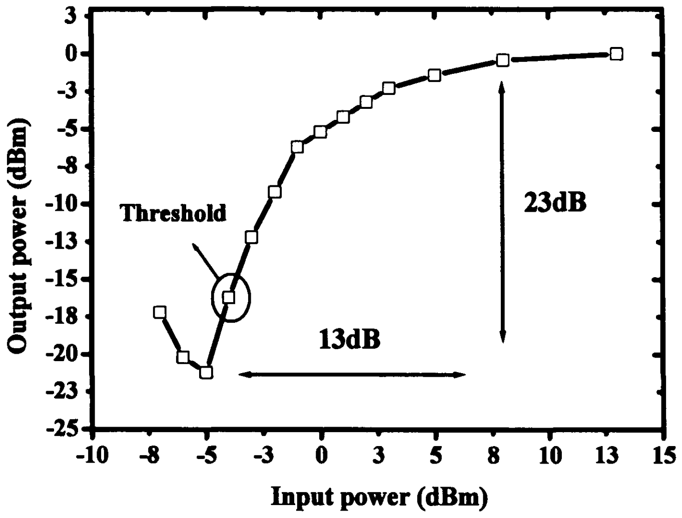

Figure 5-16 Regenerator transfer function as optimised for pulse reshaping experiments

The regenerator threshold, defined as the point at which the transfer function slope is maximum, was tuned close to the "*zero*" level of the input signal. As a consequence the regenerator operated with a large extinction ratio gain, as the steepest part of the interferometer transfer function lies on the linear part of the SOA phase transfer function. Around the signal "*one*" level the interferometer transfer function lies on the saturated part of the SOA transfer function, significantly increasing the tolerance margin of the regenerator to noise on the peak of the data signal pulse. In conclusion, the experimental results showed that the tuneability of the optical threshold is a fundamental feature which allows the equalisation of the regenerated pulses and significantly increases the regenerator tolerance to amplitude jitter and pattern-dependent effects.

40Gb/s retiming experimental investigation: Retiming at 40Gb/s was investigated previously with UNI [Tsu02] and SOA-DI [Leu01] configurations to show that optical regeneration has a larger jitter tolerance than a standard 40Gb/s electrical receiver. Here the retiming ability of the proposed regenerator is investigated following the same approach presented for the 10Gb/s experiments, to show the largest tolerance to timing jitter reported to date in literature for 40Gb/s regeneration. To investigate the retiming ability of the regenerator a timing offset between the clock and data signals was introduced and the BER of the regenerated signal measured. The timing jitter tolerance measured for BER lower than 10^{-9} was 9ps, which shows a retiming improvement of 2ps when compared to the detection window of the receiver. The regenerator timing window measured allowing for 1dB and 2dB receiver sensitivity penalty was 10ps and 12ps respectively. The later corresponds to approximately 50% of the bit period.

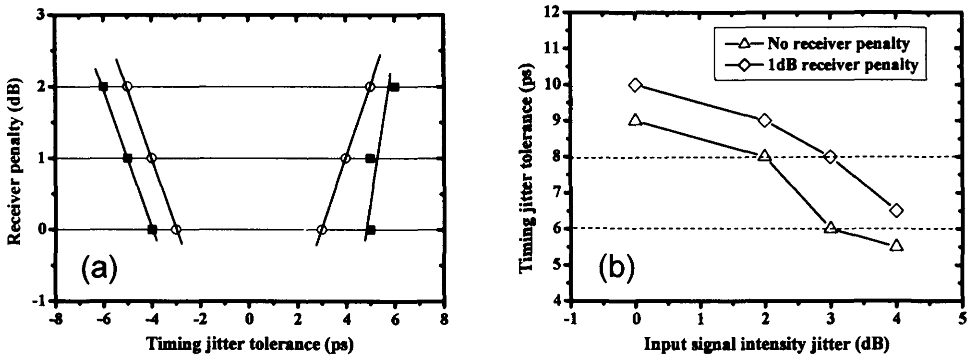

Figure 5-17 (a) Retiming characteristics of the regenerator (■) with respect to the optical receiver (○); (b) Regenerator timing jitter tolerance for different input signal intensity jitter levels

The measurements for retiming are summarised in Figure 5-17 (a) with respect to the receiver timing window for different error-free receiver sensitivity power penalties. Figure 5-17 (b) shows the regenerator timing window, for BER less than 10^{-9}, measured on the regenerated signal when the data signal was impaired by different level of intensity jitter. For large intensity jitter level the regenerator timing window is significantly reduced. This is attributed to the decrease in width of the flat top of regenerator optical switching window as consequence of the intensity jitter present on the data signal triggering the regenerator.

5.2 40Gb/s all-optical demultiplexing with PSSI

All-optical demultiplexing has been demonstrated with several SOA-assisted interferometer configurations, such as integrated MZ or the UNI and TOAD. For applications as optical demultiplexing, the generation of short (<6ps for 160Gb/s operations) and tuneable optical switching window is a fundamental requirement. A short switching window is necessary for operations at high bit-rates and tuneability is desirable for reconfiguring the demultiplexer for operations at different bit-rate or with different pulsewidth. To date the shortest switching window (200fs at 10GHz) has been demonstrated utilising the DOM-MZI configuration [Nak98] and the UNI [Nak98b]. However the only configurations to allow for tuneable switching window are the DOM-MZI and the TOAD interferometer. The TOAD has the advantage, over a MZ configuration, of requiring a single SOA for switching. However, error-free operations with long PRBS has not been demonstrated at 40Gb/s with the TOAD configuration, due to pattern-dependent distortion and limited switching extinction ratio [Hal99]. These limitations can be overcome operating the Sagnac interferometer in a polarisation switching configuration (PSSI).

In this section, we will investigate the demultipexing and switching window properties of the PSSI configuration at 40Gb/s.

Experimental set-up and results: The experimental set-up used to demonstrate 40 to 10Gb/s all-optical demultiplexing is shown in Figure 5-18.

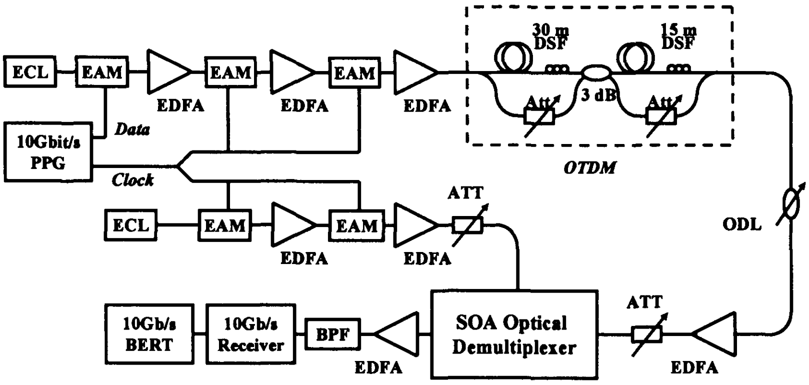

Figure 5-18 40 to 10Gb/s demultiplexing experimental set-up

The data signal was generated modulating an external-cavity-laser (ECL) at λ=1550nm with cascaded EAMs (electro-absorption-modulator) to shape 12ps RZ pulses with 10GHz repetition rate encoded with 2^{31}-1 PRBS, passively interleaved, using a fibre OTDM multiplexer, to 40Gb/s. The control signal was similarly generated modulating an ECL at λ=1555 nm using cascaded EAMs to shape 12ps RZ pulses with 10GHz repetition rate.

When operating the interferometer as a demultiplexer the 40Gb/s signal is launched in the clock port and the control signal is launched in the data port of the Sagnac interferometer as depicted in Figure 5-2 (a). The SOA used in the experiment is a low polarisation-dependent 2.6mm long bulk Lucent SOA described in [Dre02] (characterisation in appendix 2). The BER was measured for the demultiplexed signal at the PSSI output and for the 10Gb/s baseline on back-to-back; the results are shown in Figure 5-19. The eye diagrams of the 40Gb/s back-to-back and of the demultiplexed signal, recorded with 50GHz photodiode, are also shown in Figure 5-19.

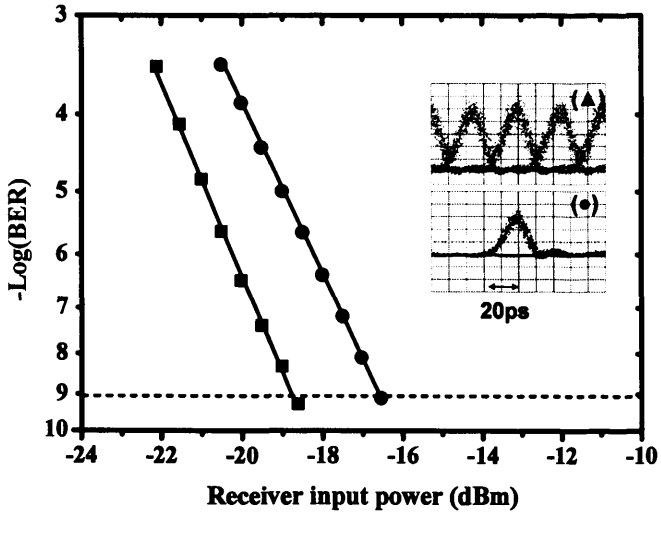

Figure 5-19 BER (2^{31}-1PRBS) measurements and eye diagrams: 40Gb/s back-to-back signal (▲), 10Gb/s baseline (■), demultipexed signal (•)

A low penalty of only 2dB (at BER=10^{-9}) was measured on the demultiplexed signal. The switching power (in the fibre at the SOA input) of the control signal was 1.5dBm, and the bias current of the SOA was 360mA. The optical switching window of the demultiplexer, defined as the temporal transmission or transfer function of the optical demultiplexer subsequent to the injection of the optical control pulse, was measured to have a temporal width of 12ps. To measure the switching window shape, the data signal was replaced with a 10GHz probe signal with 12ps pulse width, generated from data transmitter bypassing both the encoder and the optical multiplexer. An optical delay line was used to delay the control pulses with respect to the probe pulses.

The switching window was obtained by measuring the power of the probe pulses with an OSA (1nm resolution) at the demultiplexer output as a function of the time delay between the data and control pulses. It is important to notice that the result of this measurement is the convolution of the probe with the switching window of the demultiplexer. Figure 5-20 (a) shows the switching window measured for the 40 to 10Gb/s demultiplexing experiments.

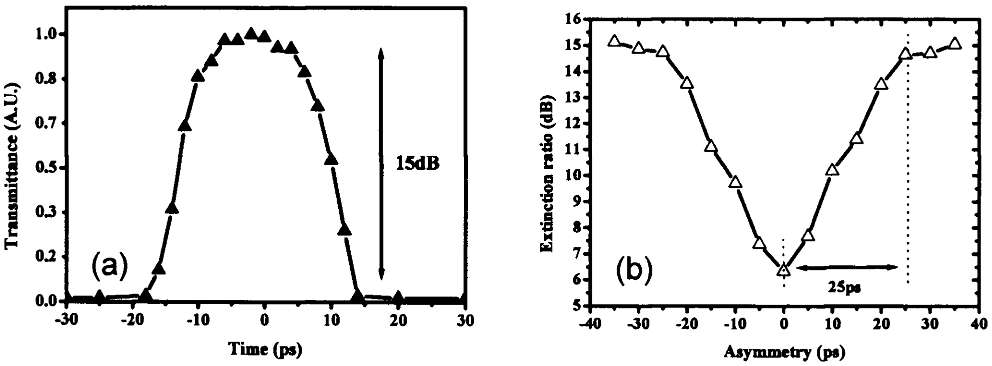

Figure 5-20 (a) Optical switching window measured with 12ps pulses; (b) Extinction ratio as a function of SOA asymmetry

Taking into account that the probe pulse width is 12ps, the effective demultiplexer switching window temporal duration is ≈ 12ps (FWHM). Figure 5-20 (b) shows the switching contrast measured for different SOA loop asymmetry. As demonstrated in [Die01], in a Sagnac interferometer the switching window increase linearly with the SOA loop asymmetry. Thus, decreasing the SOA loop asymmetry decreases both the optical switching window temporal duration and the switching contrast ratio. The reason for this behaviour is that the highest switching contrast is obtained when one probe pulse sees an almost unsaturated SOA while the other probe pulse experiences a highly saturated SOA, condition which occurs for large SOA loop asymmetry.

5.3 Multi-channel all-optical 3R regeneration with PSSI

As described is section 4.3, multi-channel 3R regeneration is expected to be a key functionality in large WDM optical networks.

In chapter 4, we have demonstrated a configuration for multi-channel wavelength conversion based on an SOA array followed by an optical equaliser. The advantage of this technique was the simplicity of the configuration which potentially could be monolithically integrated. However, to date, only SOA-assisted interferometer configurations have demonstrated 3R regenerative capability at high bit-rate.

Most of the SOA-assisted interferometer techniques proposed for all-optical 3R regeneration operate on a single channel. A possible solution to scale from single channel to multi-channel operation is to use integrated SOA array to simultaneously process multiple wavelengths [Ito01]. However, for this application the regenerator configuration has to be as simple as possible. Thus, configurations utilising a single SOA per channel should be considered to reduce the complexity of the optical integrated circuit.

To date, the PSSI and the UNI are the only interferometer configurations to have shown high bit-rate (40Gb/s) regeneration with a single SOA. An important requirement to operate a UNI is that the SOA must be polarisation insensitive. However to date, SOA arrays have been shown to have strong polarisation dependence due to the integration process. On the contrary, the PSSI configuration can operate with polarisation sensitive components such as the SOA array with no further penalty.

In this section we report on the experimental demonstration of simultaneous multi-channel L-band to C-band 3R regenerative wavelength conversion of 10Gbit/s WDM channels, using polarisation switching in a Sagnac interferometer and a novel monolithically-integrated wavelength selector SOA array module.

Experimental set-up and results: The multi-channel regenerative wavelength converter proposed in this work is based on a novel configuration, using polarisation switching in a fibre Sagnac interferometer, similar to the recently proposed single-channel scheme [Gav02], however here the single SOA was replaced with an integrated module to operate over multiple wavelengths. The packaged fibre-pigtailed module, described in detail in appendix 4, consists of 22-channel SOA array monolithically integrated with 2X22 channel WGRs (Waveguide Grating Router) extending from the design reported in [Zir94].

The experimental set-up used to demonstrate simultaneous regenerative wavelength conversion of two signals is shown in Figure 5-21.

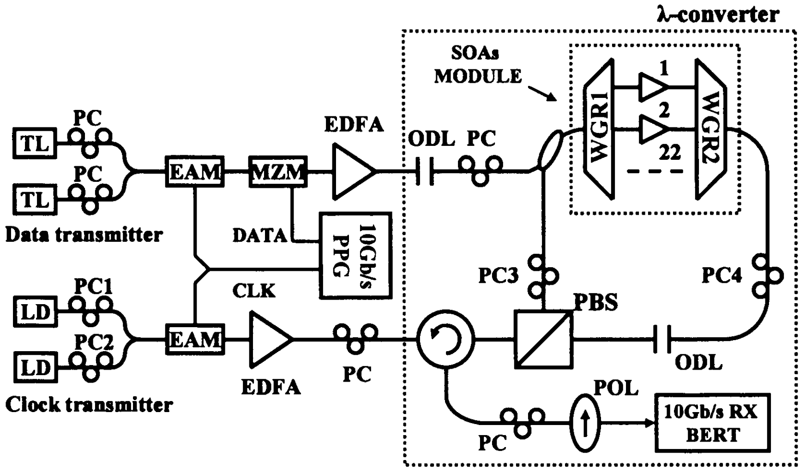

Figure 5-21 Experimental setup for 2 channels 10Gb/s wavelength conversion

The use of two channels was limited by the availability of L-band laser sources and not by the device performance. The multi-channel wavelength converter consists of a 3-port polarisation beam splitter (PBS) with two arms forming a fibre Sagnac interferometer which incorporates the SOA array module as the multiwavelength non-linear element. The two L-band RZ data signals were generated by modulating two external cavity tuneable laser sources (TL) lasing at λ_1 = 1574.8nm and λ_2 = 1576.5nm, with cascaded $LiNbO_3$ Mach-Zehnder (MZM) and electro-absorption modulator (EAM) driven by data (word length 2^{31}-1 PRBS) and clock outputs of the 10Gbit/s pattern generator (PPG) respectively, to generate 20ps FWHM pulses with 10GHz repetition rate.

The data signals were launched into the SOA array via a 3dB coupler in the co-propagating arm of the interferometer, so that the WGR demultiplex each signal into a selected SOA in the array. The two C-band RZ clock signals were similarly generated by modulating two DFB lasers lasing at λ_3 = 1556.8nm and λ_4 = 1558.4nm, to shape 20ps FWHM pulses at 10GHz repetition rate. The clock signals were launched 45° polarised at the input of the 3-port polarisation beam splitter, used to split each signal into two orthogonally-polarised components which counter-propagate in the fibre interferometer, recombine in the PBS and are routed via an optical circulator (OC) to interfere in a polarizer (POL). The data signal wavelengths were selected to match two channels within the 3rd FSR (1566-81nm) of the SOA array module WGR. The clock signal wavelengths were chosen to match the same two channels within the 2nd FSR (1550-65nm) of the SOA array module WGR. Consequently each of the two SOAs in the array, corresponding to the two chosen WGR channels, is reached by one data and clock signal only.

As in a conventional TOAD scheme, an optical delay line (ODL) is used to offset the SOA array from the loop centre, so that the counter-propagating components of each clock signal are differentially cross phase modulated by one data signal, and thus recombine to a different polarisation state at the polariser input. A C-band filter was used to select the wavelength converted signals form the input L-band data signals at the wavelength converter output. Consequently the wavelength converted signals are reshaped and retimed accordingly to the clock signal quality, and shifted in wavelength from L-band to C-band.

Operating the Sagnac interferometer in polarisation diversity leads to a major advantage when operated with the SOA array module with respect to the formerly reported configuration [Sok93]. The polarisation state of each clock signal at the interferometer input can be individually adjusted using the polarisation controllers PC1 and PC2, to equalise the power of the interfering components of each clock signal at the interferometer output before the polariser. This allows to maximise the switching contrast of the wavelength converter for both channel simultaneously [Zho99].

Furthermore using the polarisation controllers PC3 and PC4 to linearly polarise light through the SOA array allows to operate the interferometer in polarisation diversity also using polarisation sensitive SOAs. For operation in real networks all-optical synchronisation of data and clock signal is required, and this can be achieved using the multiwavelength all-optical clock recovery technique, previously demonstrated using a similar SOA array module [Mik01a].

Figure 5-22 shows the eye diagrams and the bit error rate (BER) measured for the two simultaneously wavelength converted signals with respect to the data signals back-to-back. The data signal average power in the fibre at the input of the SOAs module was 6 dBm for both channels. The two SOAs corresponding to the two selected WGR channels were simultaneously operating in the experiment and biased at a current value of 180mA.

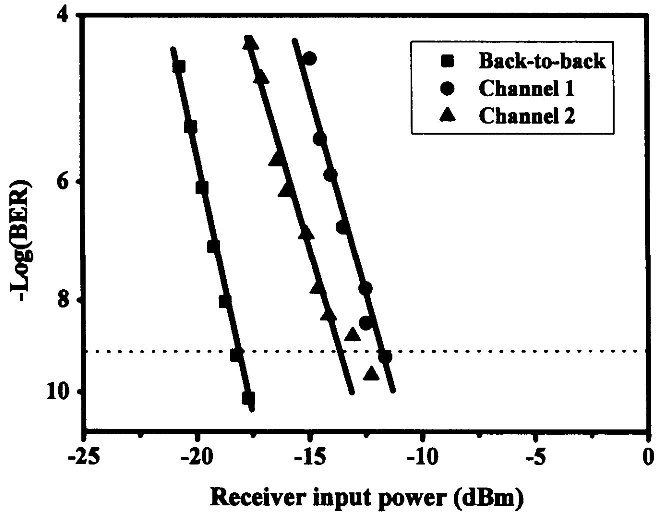

Figure 5-22 10Gb/s BER measurements (2^{31}-1 PRBS) and eye diagrams of the two simultaneously wavelength converted signals

A penalty of 5 and 6 dB was measured for channel 2 and 1 respectively; this is mainly caused by the high reflectivity at the coupling interface between the fibre pigtails and the WGR of the SOA array module and is expected to be significantly lower in future devices optimized for lower reflectivity. The spectrum of the wavelength converted signals is shown in Figure 5-24.

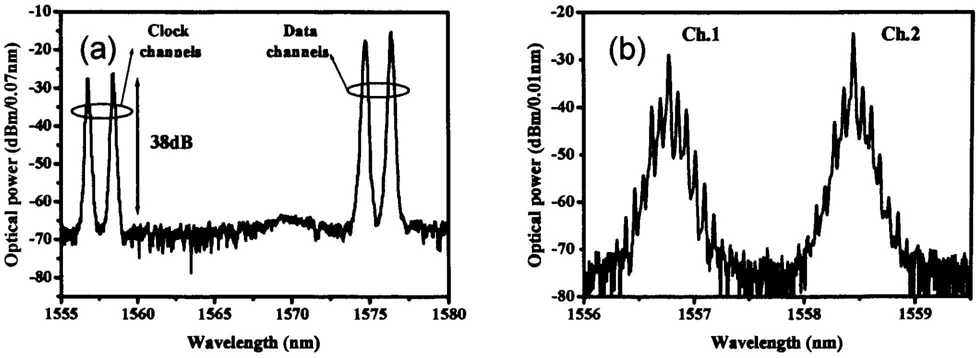

Figure 5-23 (a) Spectrum of both the data and clock signals at the PSSI output; (b) Spectrum of the two wavelength converted signals

The average optical signal-to-noise ratio as measured with 0.07nm resolution bandwidth at the output of the wavelength converter was larger than 38dB for both channels.

Summary

The work in this thesis has allowed to demonstrate, for the first time, all-optical 3R regeneration using fast polarisation switching in an SOA-assisted fibre Sagnac interferometer (PSSI). With the PSSI configuration, switching is achieved by polarisation rotation induced by nonlinear phase and gain modulation in the SOA. As described in the chapter 2, the use of polarisation rotation can minimise the effect of patter-dependent distortion which limits most of the other regenerator configurations to operate with short PRBS at 40Gb/s.

The performance of the regenerator operating with wavelength conversion and retaining the input wavelength was experimentally investigated at 10Gb/s, and 40Gb/s, using a bulk SOA with carrier lifetime exceeding 250ps, to show lower operating penalty with long PRBS. The regenerative properties have also been investigated experimentally. The error-free regenerator timing window was measured to be 43% of the bit period at 10Gb/s and 28% at 40Gb/s. This is the largest tolerance to timing jitter reported to date in literature for 10 and 40Gb/s regeneration.

The proposed scheme operates with an adjustable optical threshold which enhances its tolerance to amplitude jitter and patterning effects. The investigation of the regenerator reshaping capability demonstrated regeneration from up to 3dB amplitude jitter peak-to-peak achieved with a penalty of 1.8dB, while maintaining a retiming window of 6ps. Regeneration tolerance to amplitude jitter larger than 3dB peak-to-peak was found to be limited by the decrease of the regenerator extinction ratio.

All-optical 40Gb/s demultiplexing based on the PSSI gate was also experimentally demonstrated for the first time, to show error-free demultiplexing achieved with only 1.5dBm switching power. The demultiplexer switching contrast was measured to be 15dB for a switching window of 12ps (FWHM).

Finally, Simultaneous 3R regenerative wavelength conversion of 2 channels at 10Gbit/s was experimentally demonstrated for the first time using an integrated SOA array in the PSSI configuration. Wavelength conversion was obtained with low switching power demonstrating the potential for large scale monolithic integration for optical processing applications for WDM networks.

In the next chapter, the noise suppression ability of the PSSI will be investigated. Furthermore the PSSI configuration will also be used in transmission experiments to investigate the cacadability properties of SOA-assisted interferometer regenerators.

Chapter 6 Experimental investigation of transmission with all-optical 3R regeneration

In optically amplified linear systems, the main source of noise is the accumulation of the ASE of the optical amplifier [Ber95]. This degrades the signal OSNR which ultimately limits the maximum achievable transmission distance. Optical regenerators have been proposed to compensate for signal distortion along the link and increase the transmission distance.

In the previous chapter a novel optical regenerator configuration, named PSSI, was introduced and its retiming properties experimentally investigated. In this chapter, experimental results on the investigation of the noise suppression and cascadability properties of optical regeneration using the PSSI interferometer configuration are described.

As shown in chapter 3, an optical regenerator based on an SOA-assisted interferometer configuration can perform both noise compression and extinction ratio enhancement, improving the input signal Q-factor. The extinction ratio enhancement was found to be the necessary condition to cascade a chain of optical regenerators due to the nonlinear transfer function characteristics [Ohl97]. However, as described in chapter 3, a trade-off exists between the regenerator extinction ratio enhancement and its noise suppression properties. For this reason it is important to assess the regenerator noise suppression properties while this is cascaded in a chain.

First the study of the signal Q-factor improvement of a single optical regenerator at 10 and 40Gb/s in presence of signal noise distortion is described. As part of these experiments the enhancement of error free transmission distance with the use of a single regenerator placed at the transmission end prior to the electrical receiver was also explored.

Then, the regenerator signal Q-factor improvement in a transmission experiment with periodically cascaded optical regenerators was investigated. It was show that error rate accumulation can be significantly reduced in transmission with cascaded optical regenerators and ultra-long transmission distances achieved.

6.1 10Gb/s transmission with optical regeneration at the receiver

Optical regeneration of OSNR distorted signals has been demonstrated at 10Gb/s using 2R and 3R SOA-based regenerators [Wol00a] [Arm05]. These experiments have shown that optical regeneration can improve the signal OSNR and reshape the input signal improving the Q-factor and, thus, the receiver sensitivity.

An advantage of increasing the receiver sensitivity is to potentially increase the maximum transmission distance between electronic repeaters. Furthermore, quantification of the regenerator Q-factor improvement is indicative of the maximum spacing between cascaded optical regenerators.

However, most characterisation experiments of the noise suppression properties of optical regeneration have been performed on back-to-back by artificially degrading the OSNR at the regenerator input in order to assess the effect on the regenerated signal Q-factor, and the impact on the transmission distance has not been considered. Experiments on an EAM based 2R regenerator have shown that by positioning an optical regenerator at the receiver of a 10Gb/s dispersion managed soliton system (DMS) significantly improved the maximum error-free transmission distance [Cho00].

Here, the OSNR regenerative properties of a 3R SOA-based optical regenerator have been quantified utilising a fibre transmission loop. By positioning the regenerator at the transmission link end prior to the receiver it was possible to characterise, for the first time, the relationship between the regenerator output signal Q-factor and the input signal OSNR. Furthermore, the experiments allowed to investigate the effect of having an optical regenerator prior to the electrical receiver on the maximum error free transmission distance in an RZ system operating at 10Gb/s.

Experimental set-up and results: Figure 6-1 shows the experimental set-up for the 10Gb/s transmission experiments with the optical regenerator at the receiver.

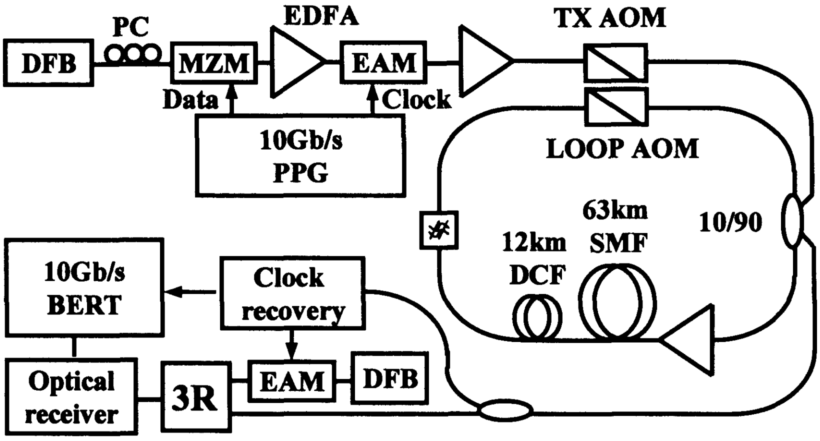

Figure 6-1 Transmission experiments with all-optical regeneration at the receiver

The loop transmission amplifier span consisted of 63km standard single mode fibre (SMF) link fully compensated by 12km of dispersion compensating fibre (DCF). An optical filter, with 1nm bandwidth, was also used at the span end to reduced the OSNR accumulation and avoid spectral burning [Luo98] [Mik03]. A single EDFA was used to compensate for the span loss which is 21dB.

The transmitted signal was a 10 Gbit/s (PRBS 2^{31}-1) RZ signal with a 20ps pulse width (FWHM) and with an extinction ratio of 15dB, generated cascading a MZ and an EAM modulator driven with a 10Gb/s PPG. The 10Gb/s transmitter and receiver are described in appendix 3. The transmitter wavelength was 1550nm and the launch power into the fibre span was 0dBm, ensuring that the transmission was in the linear regime, and thus OSNR limited. At the loop output the transmitted signal is regenerated and then routed to the optical receiver. The regenerator and optical clock recovery circuit is shown in Figure 6-2.

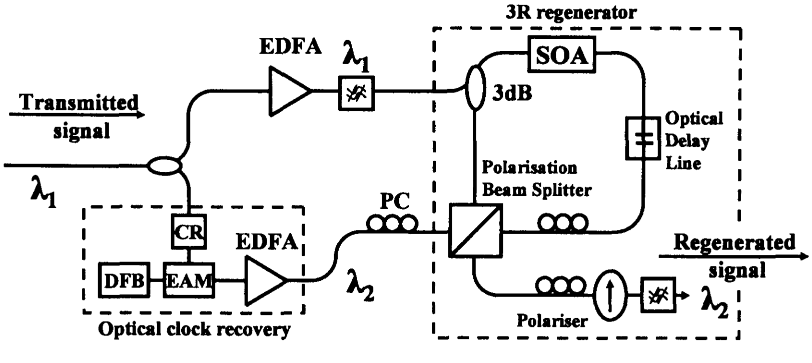

Figure 6-2 3R regenerator and optical clock recovery circuit

The SOA used in the PSSI regenerator is a 1nm long bulk Kamelian SOA (characterisation in chapter 4.1). The clock recovery circuit, based on a high-Q filter, was used to synchronise the BERT and to drive an EAM to generate the optical clock for the 3R regenerator. The regenerator optical clock signal wavelength was 1545nm, and the pulse width was 20ps.

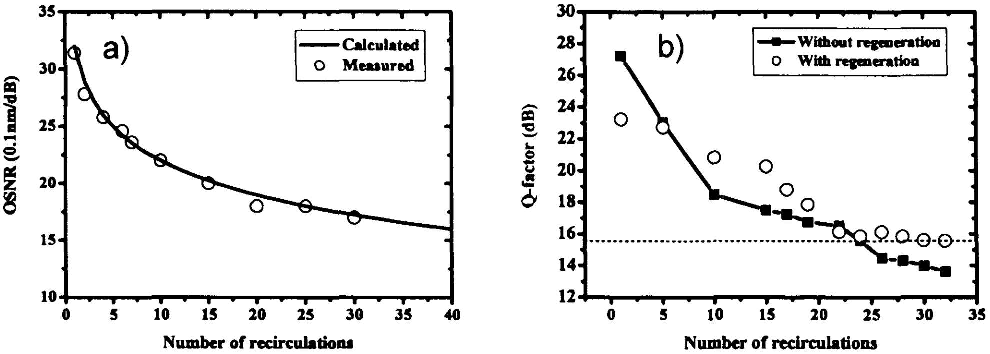

Figure 6-3 (a) OSNR accumulation measured with distance (75km per recirculation); (b) Q-factor (dB) measured with distance with (○) and without (■) regeneration at the receiver

The OSNR accumulation was measured as a function of the number of recirculations in the loop utilising an OSA with 0.1nm resolution. Figure 6-3 (a) shows the OSNR accumulation calculated as a function of the number of recirculations in the loop [Kam02], together with the experimentally measured values. Due to the high span loss the OSNR degraded rapidly reaching the 20dB/0.1nm after 15 spans. The evolution of the Q-factor measured as a function of the transmission distance is shown in Figure 6-3 (b) for transmission with and without regeneration prior to the optical receiver. The optical regenerator enhances the signal Q-factor allowing to improve the maximum error-free transmission distance from 1900km to 2300km. In order to minimise the effect of polarisation dependent OSNR variation in the loop the Q-factor was measured at the regenerator input and output without re-optimising the polarisation of the signal transmitted in the loop.

To quantify the improvement of the regenerator on the transmitted signal, the amplitude margin, or threshold window, defined by the voltage decision level for a constant BER of 10^{-9}, was measured as a function of the transmission distance and shown Figure 6-4 (a).

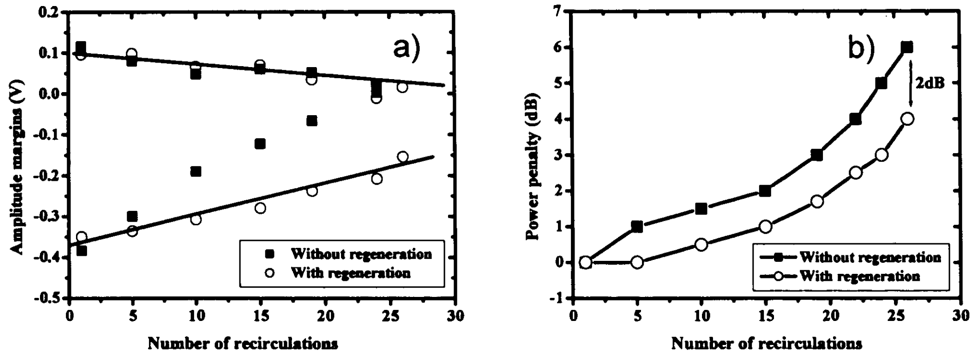

Figure 6-4 Amplitude margin (a) and receiver sensitivity penalty (b) measured as a function of transmission distance with (○) and without (■) regeneration at the receiver

The upper and lower curves represent the amplitude noise in the "*zeros*" and "*ones*", respectively. Without regeneration, the accumulation of the EDFA ASE noise in the "*ones*" limits the maximum error-free transmission distance to 25 recirculations. The regenerator effectively allows this distance to extend to 32 recirculations by compressing the noise on the "*ones*", enhancing the signal extinction ratio and, thus, the eye opening.

As shown in Figure 6-3 (b) the optical regenerator can improve the sensitivity of the electrical receiver, and thus the signal Q-factor by up to 2dB, when this operates with low input signal OSNR (18dB/0.1nm), close to the receiver noise limit. At low input OSNR the electrical receiver noise can significantly degrade the signal BER [Ber93]. However the optical regenerator can enhance the signal eye opening which minimises the impact of receiver noise on the BER, thus increasing the maximum error-free transmission. Furthermore, the regenerator can improve the BER due to the larger timing jitter, dispersion and PMD tolerance with respect to the electrical receiver, as demonstrated in chapter 5, this improvement can occur at both low and high OSNR.

The improvement in the amplitude margin leads to an enhancement in the receiver sensitivity, which depends on the signal extinction ratio. At high OSNR (after few recirculations) a sensitivity improvement does not necessary correspond to an improvement in BER, especially because the signal Q-factor is significantly larger than the measured BER and thus the presence of an error-floor can not be excluded.

Figure 6-4 (b) shows the receiver power penalty with respect to back-to-back measured as a function of distance for transmission with and without regeneration prior to the optical receiver. The regenerator receiver sensitivity enhancement increases with the transmission distance, and thus with decreasing OSNR at the regenerator input. This is because at low OSNR the receiver noise, timing jitter, PMD and residual dispersion have a stronger impact on the measured BER.

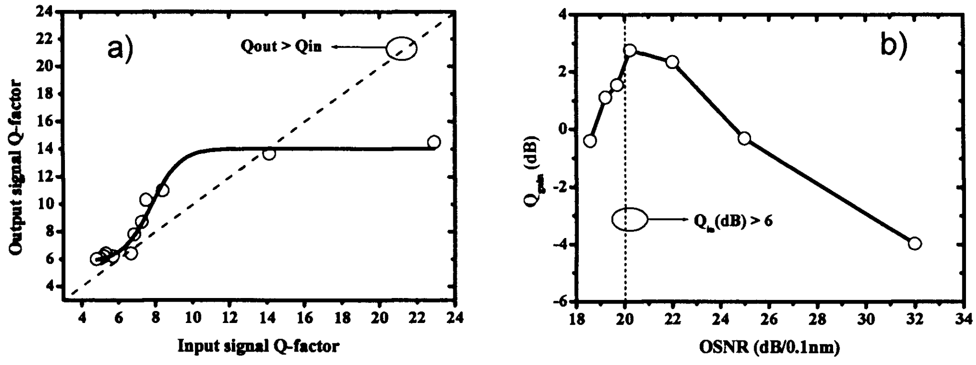

Figure 6-5 (a) Regenerated with respect to input signal Q-factor; (b) Q_{gain} (dB) as a function of regenerator input signal OSNR

Figure 6-5 (a) shows the linear Q-factor before and after regeneration derived from the results of Figure 6-3 (b). For input signal Q-factor values in excess of the maximum regenerator back-to-back signal Q-factor (Q = 14) no improvement can be observed. As the input signal Q-factor degrades below 14 as a result of the EDFA noise cumulated in transmission the regenerated signal Q-factor begins to exceed the input. This improvement can be quantified introducing the regenerator Q-factor gain or Q-gain parameter defined as the ratio between the Q-factor of the signal at the regenerator output and at the input.

$$Q_{gain} = \frac{Q_{out}}{Q_{in}} \qquad (6\text{-}1)$$

Figure 6-5(b) shows the Q-gain as a function of the regenerator input signal OSNR. The maximum Q-gain was measured to be 2.7dB and was achieved close to the receiver OSNR limit for BER $\approx 10^{-9}$, which occurs when the regenerator input signal OSNR $\approx$ 20dB/0.1nm corresponding to a Q-factor of 6. It is important to note that a Q-factor improvement does not necessary correspond to an improvement in BER, as presence of and error-floor for BER lower than 10^{-9} can not be excluded. The Q-gain increases with decreasing OSNR, however we find that there is an optimum input signal Q-factor, corresponding to 17.5dB, for which the regenerator Q-gain is maximum before decreasing with the input Q-factor. Figure 6-6 (a) shows the BER as a function of the receiver input power for the regenerated signal after 32 recirculations corresponding to the maximum achievable error-free transmission distance with optical regeneration.

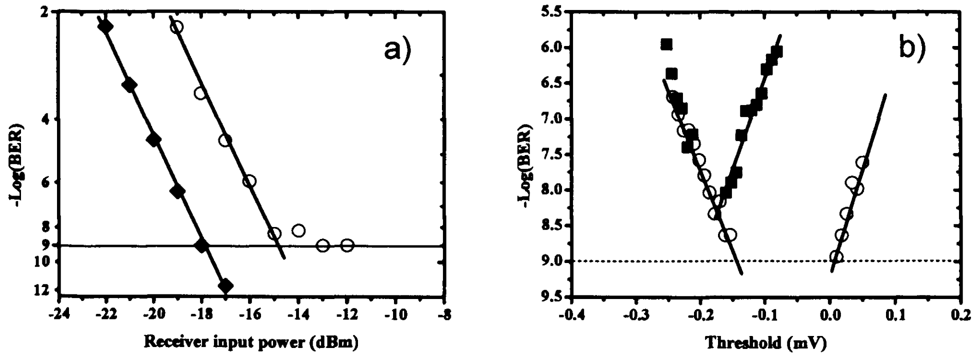

Figure 6-6 (a) Regenerated signal (o) after 32 spans with respect to regenerated signal back-to-back (♦); (b) BER as a function of the threshold voltage after 26 recirculation (■) and with optical regeneration (o)

Error-free operation was achieved after 32 recirculations, however an error-floor appeared around 10^{-9}, which prevented further increase of the error-free transmission. Figure 6-6 (b) shows the threshold window after 26 recirculation, corresponding to the maximum error-free transmission distance achievable without optical regeneration, for transmission with (o) and without (■) regeneration prior to the optical receiver. The extinction ratio enhancement provided by the optical regenerator significantly opens the amplitude margin most importantly without introducing an error-floor. This clearly shows that BER improvement can be achieved with the regenerator, which under the condition of low OSNR, outperforms the electrical receiver.

In conclusion, we find that at high input OSNR, corresponding to a signal Q-factor in excess of the regenerator back-to-back Q-factor, the regenerator does not improve the signal quality. For the case of lower input OSNR, corresponding to a signal Q-factor smaller than the regenerator back-to-back Q-factor, the regenerator could improve the input signal Q-factor with a Q-gain of up to 2.7dB. This led to the improvement of the receiver sensitivity for BER = 10^{-9}. For the case of input OSNR corresponding to the receiver OSNR limit for error-free operation the regenerator improved the signal Q-factor the receiver sensitivity and the BER. We explain the improvement of BER mainly as a result of the larger tolerance to timing jitter, PMD and residual dispersion. The optical regenerator and receiver function effectively as an improved "*decision circuit*" for the transmission system which is limited by accumulation of ASE noise in the "*ones*" and timing jitter. This becomes particularly effective for input signal OSNR close to the receiver sensitivity for error-free operations. In the next section the cascadability properties of the PSSI regenerator are investigated.

6.2 Investigation of transmission with cascaded all-optical 3R regenerators and variable inter-regenerator spacing

As described in chapter 2, various 3R (re-timing, re-shaping and re-amplifying) regenerative wavelength converter schemes have been proposed and demonstrated, and transmission with cascaded SOA-based optical regenerators has been investigated in loop experiments to prove the feasibility of achieving ultra-long transmission [Ref. in chapter 2]. To date all the loop experiments reported used a constant inter-regenerator spacing. Varying the inter-regenerator spacing, however, changes the amount of accumulated noise and allows for the assessment of the cascaded regenerator noise suppression performance. A condition necessary to ensure cascadability is that the input signal extinction ratio at each regenerator stage must be maintained [Olh97], implying a trade-off between noise suppression and cascadability.

In this work, this trade-off was identified and studied experimentally by cascading optical SOA-based 3R regenerators, at a distance of 20000km, with variable inter-regenerator spacing from 150 to 750km in novel reconfigurable fibre loop test-bed [Mik03a]. The experiments were carried out at 10Gb/s to provide larger margins in the transmission experiments in order to focus on the principles which determine cascadability of the SOA-based regenerator.

First the design rules and the principle of operation of the novel reconfigurable loop test-bed (*DR^2FL*) will be described in detail, then the transmission results will be discussed.

6.2.1 Principle of operation of the Dynamically Reconfigurable Recirculating Fibre loop (DR^2FL)

The schematic diagram of the DR^2FL is shown in Figure 6-7. As in a standard loop [Ber95] the optical signal is launched into the transmission span using an AOM switch. At the output of the transmission span a coupler is used to split the signal into two different paths with an AOM in each; the first is a bypass path and the second path contains the optical regenerator (3R). A second coupler is used to recombine the two arms and route the signal back into the transmission span. By controlling the operating states of the AOMs in each path the transmitted signal can be routed to the regenerator after a desired number of recirculations through the loop transmission span. The loop transmission amplifier span consists of a standard 63km SMF link whose dispersion is fully compensated by 12km of dispersion compensating fibre (DCF), with a total length of 75km and span loss of 21dB.

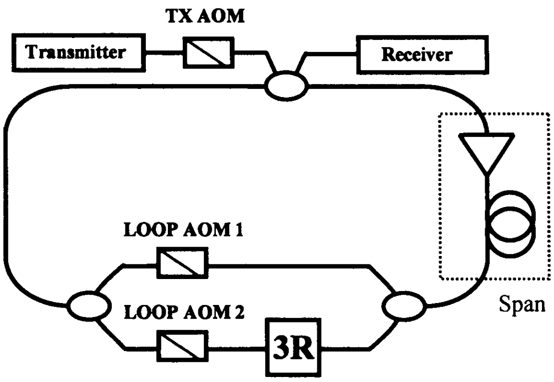

Figure 6-7 DR²FL loop set-up

The OSNR degradation of a 10Gb/s signal transmitted over a chain of N spans consisting of an EDFA and the 75km link, is given by [Kam02]:

$$OSNR = 58 + P_{in} - NF - L_{sp} - 10\log N_{amp} \tag{6-2}$$

where N_{amp} is the number of cascaded EDFAs, P_{in} is the average launch power per channel at the input of the transmission fibre in dBm, NF is the noise figure of the amplifier and L_{sp} is the 75km span loss, both in dB. The equivalent noise figure of a link operating with an additional in-line amplifier to compensate for the loss of a dispersion compensating fibre, is given by [Kam02]:

$$NF_{DC} = NF\left(1 + P_{in}^{A}\frac{\alpha_1}{P_{DCF}}\right) \tag{6-3}$$

where P_{DCF} is the average power at the DCF input, P_{in}^{A} is the average EDFA input power and α_l is the DFC insertion loss. Thus, the impact on OSNR of the loss of a DCF can be minimised using a dispersion compensating device with large input power tolerance. Figure 6-8 shows the impact on the OSNR accumulation from the presence of the additional amplification stage compensating for the DCF loss. An improvement of 75 spans for 20dB OSNR point is achieved operating with an additional EDFA at the DCF input. In this calculation the power at the fibre input was 0dBm.

When designing a transmission experiment in any loop, and in particular in a *DR^{2}FL* loop, it is important to assess the impact of the presence of the extra loop components (couplers and AOMs) on the transmission performance. This can be estimated including the loop components loss in the calculation of the OSNR degradation with distance.

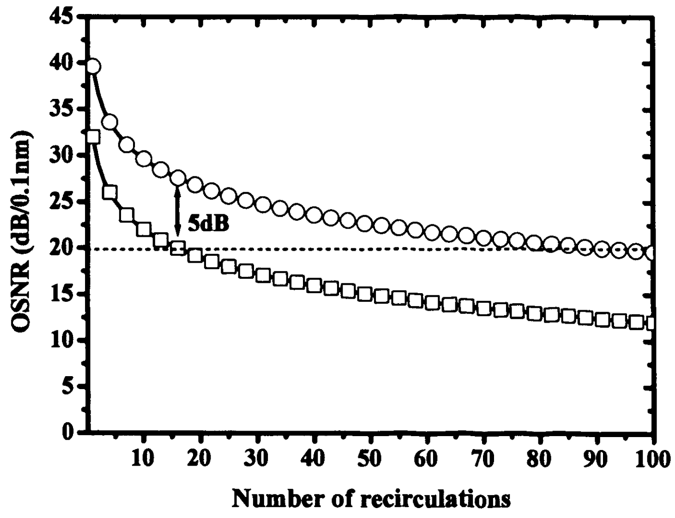

Figure 6-8 OSNR accumulation for a 75km link with DCF operating with a single EDFA at the fibre input (□) and with an additional EDFA at the DCF input (○)

For the case of the DR^{2}FL span the L_{sp} loss consisted of the SMF fibre, the dispersion compensating fibre and the reconfigurable loop optical components. In designing the span it was necessary to make sure that the loss of the reconfigurable loop optical components (couplers and switches) has the minimum impact on the OSNR accumulation, which should only depend on the fibre and dispersion compensator loss. Figure 6-9 shows the possible configurations for the DR^{2}FL loop spans.

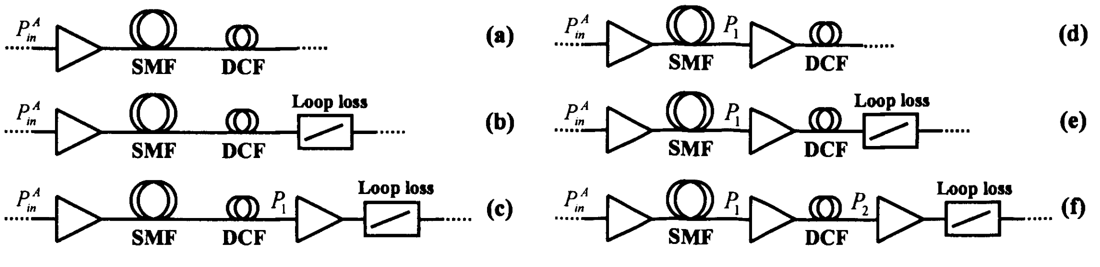

Figure 6-9 DR^{2}FL span configurations

The link (SMF+DCF) operating with an EDFA at the fibre input corresponds to the configurations (a, b, c) with an additional EDFA at the DCF input to (d, e, f). Configuration (a, d) corresponds to the ideal link operations, where the loop components are not considered. In configuration (c, f) the link operates with an additional EDFA for the compensation of the loop loss components, while in configuration (b, e) the loop components loss is not compensated.

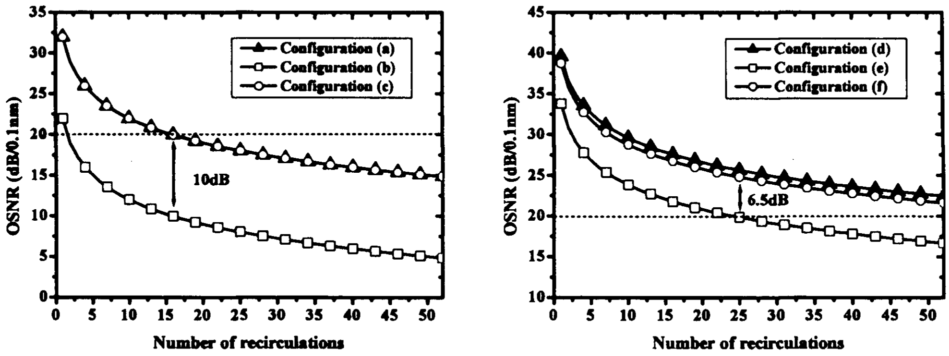

Figure 6-10 OSNR accumulation for the different span (75km link length) configurations of Figure 6-9

Figure 6-10 shows the impact on the OSNR accumulation of the loop components for the different span configurations presented in Figure 6-9. The impact on the noise figure of an in-line amplifier from the presence of an additional amplification stage, configuration (c), used to compensate for the loss of an additional optical component can be calculated as [Kam02]:

$$NF_2 = NF\left(1 + P_{in}^{A}\frac{\alpha_{loop}}{P_{loop}}\right) \qquad (6\text{-}4)$$

where P_{loop} is the average power at the loop input. For configuration (d), where two additional amplifiers are used to compensate for the DCF and loop components loss, the equivalent noise figure can be calculated to be:

$$NF_3 = NF\left[1 + P_{in}^{A}\left(\frac{\alpha_{loop}}{P_{loop}} + \frac{\alpha_{DCF}}{P_{DCF}}\right)\right] \qquad (6\text{-}5)$$

When the loop components loss is not compensated with a dedicated EDFA, as in configuration (b) and (e), then the OSNR accumulation is significantly decreased from its ideal evolution with distance represented by curves (a) and (d). However, for the case of (c) and (f) the OSNR accumulation is not affected by the presence the loop components. Under this condition, the transmission experiments with the DR^{2}FL have the same validity of a more conventional fibre recirculating loop.

6.2.2 10Gb/s transmission with cascaded optical 3R regeneration experimental set-up

The optical 3R regenerator used in the experiment is shown in Figure 6-11. The regenerator consisted of 3 units; the PSSI interferometer, an SOA-DI wavelength converter and the optical clock recovery. The PSSI interferometer was used to perform optical retiming ad reshaping.

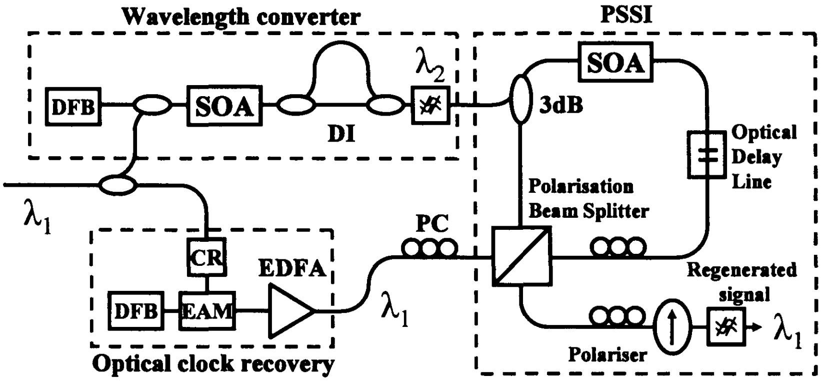

Figure 6-11 3R regenerator set-up

As described in chapter 5, the PSSI configuration operates with wavelength conversion. Thus, the regenerator included a wavelength converter so that the input wavelength (λ_1) was maintained at the output of the regenerator. The wavelength converter utilises cross gain modulation in an SOA followed by a delay interferometer (DI) to reshape the wavelength converted pulses [Leu01]. The SOA-DI wavelength converter is described in details in chapter 4.2.3. The regenerator requires an optical clock to retime the input signal; this is generated using a high-Q filter-based electrical clock recovery (CR) circuit. The recovered electrical clock was used to drive an electro-absorption modulator (EAM) which generated 10GHz 20ps optical pulses synchronised to the incoming transmitted signal.

The transfer function of the wavelength converter at the SOA and DI output is was measured, as described in section 4.2.3, and the results are shown in Figure 6-12 (a). The slope of the transfer function is significantly less than 1, thus the wavelength converter performs a first stage of noise compression but decreases the input extinction ratio. The PSSI transfer function is shown in Figure 6-12 (b) for two different interferometer bias levels.

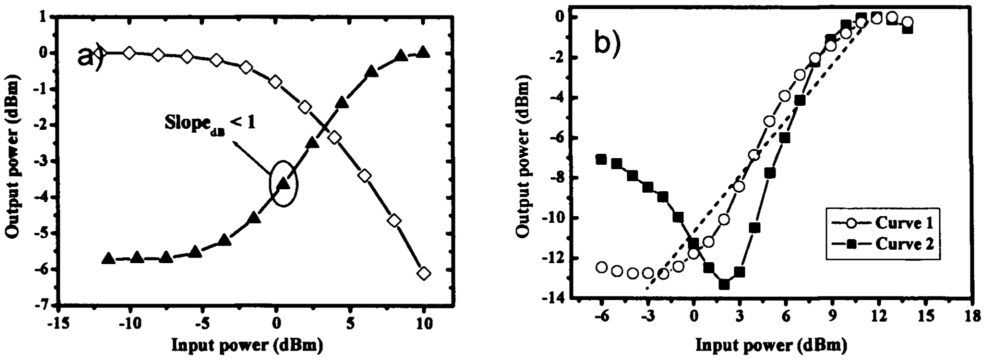

Figure 6-12 (a) Transfer function of the wavelength converter at SOA (▲) and DI output (◊); (b) Regenerator transfer function for two different interferometer bias level (○, ■)

The PSSI configuration exploits the optically induced phase shift provided by the SOA. As described in section 3.3.3, when using the nonlinear phase response of an SOA in an interferometer the phase bias of the interferometer can be adjusted to obtain different regenerator transfer functions. The regenerator transfer function labelled curve 1 shows strong reshaping of fluctuations around the "*zero*" and "*one*" levels, however the extinction ratio is only just maintained, as shown by the reference linear transfer function. To cascade a chain of regenerators it is necessary that the regenerator improves the input signal extinction ratio. This is required to ensure that extinction ratio of the input signal to each regenerator is maintained within the optimum noise suppression levels of the regenerator transfer function. In this experiment the signal extinction ratio degradation is caused by both the wavelength converter and the fibre span. The required extinction ratio gain is obtained by adjusting the PSSI interferometer phase bias, as described in section 3.3.3, to produce the measured regenerator transfer function labelled curve 2 in Figure 6-12 (b). In this case the output extinction ratio is improved by 3dB after the PSSI regeneration, but the suppression of the noise fluctuations on the "*zero*" of the signal level is reduced with respect to curve 1. Thus, as described in chapter 3, there is a trade-off between the regenerator noise suppression and extinction ratio improvement and, therefore, an optimal spacing for cascaded regenerators. To investigate the cascadability and the maximum spacing between regenerators the reconfigurable loop test-bed was used, as shown in Figure 6-13.

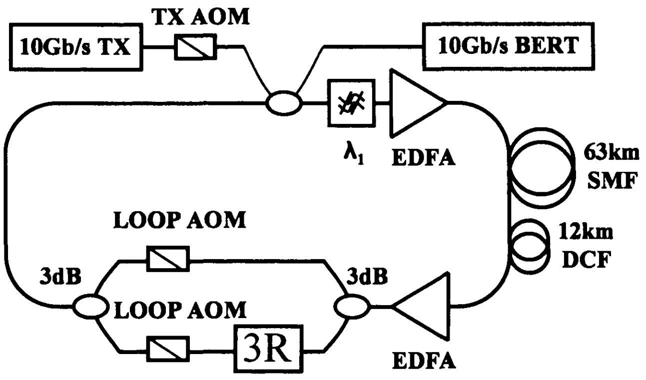

Figure 6-13 Reconfigurable loop test-bed

The loop transmission amplifier span consisted of a 1nm bandwidth optical filter and a standard SMF link whose dispersion is fully compensated by dispersion compensating fibre (DCF), with a total length of 75km and span loss of 21dB. An EDFA was used to compensate for the span loss and a further EDFA compensates for the loss of the reconfigurable loop components. As described in section 6.2.1, in this configuration, the span EDFA is the dominant contributor to the OSNR accumulation. The transmitter generates a 10Gb/s RZ signal with 20ps FWHM pulses, encoded with $2^{23}-1$ PRBS. Transmitter and receiver are described in details in appendix 3. The transmitter wavelength is 1550nm and the launch power into the fibre span was 0dBm, ensuring that the transmission was in the linear regime.

Without 3R regeneration the maximum error-free transmission distance was OSNR limited and measured to be 2250km.

The regenerator was then placed in the loop and cascaded with different spacing over a distance fixed at 20000km (chosen to allow convenient BER measurement time). Figure 6-14 shows the Q-factor measured as a function of transmission distance for different inter-regenerator spacing from 150 to 750km (2-10 inter-regenerator spans). The Q-factor is extrapolated from the signal BER measured to values as low as BER $< 10^{-9}$. The Q measurements show that error-free transmission (BER $< 10^{-9}$) over 20000km with $Q^2 \geq 18$dB can be maintained with a maximum of 600km between regenerators, and a total of 33 cascaded regenerators.

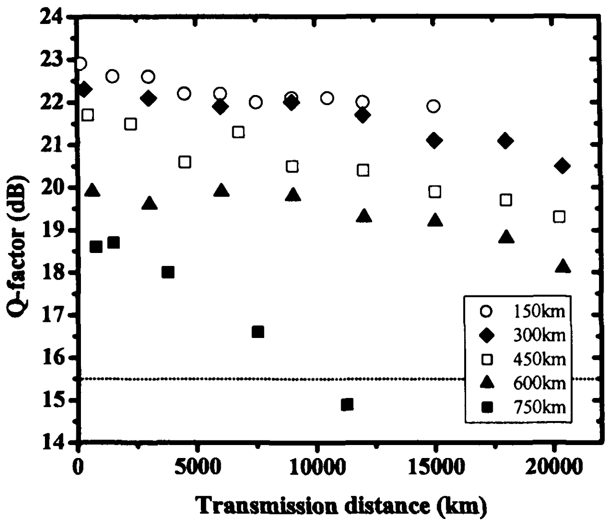

Figure 6-14 Experimental Q-factor evolution with transmission distance for different inter-regenerator spacing

The regenerator noise suppression ability in cascaded transmission can be quantified by the parameter Q-gain, which is defined as the ratio between the Q-factor of the signal at the regenerator output and at the input, for a single regenerator within a cascaded chain. In these experiments it was measured after a transmission distance of 10000km for different inter-regenerator spacing and is shown in Figure 6-15 (a).

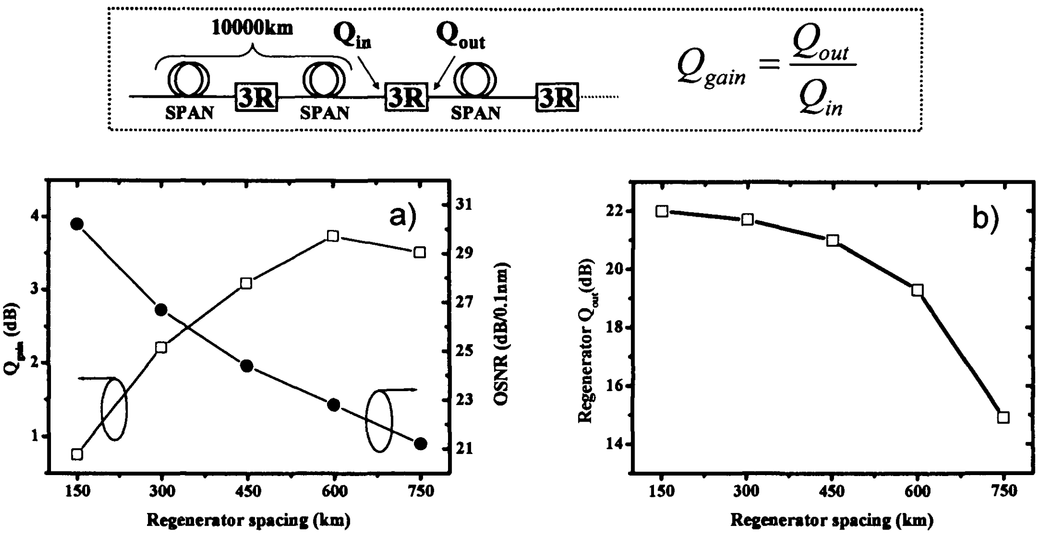

Figure 6-15 (a) Regenerator Q-gain measured after 10000km and OSNR at the regenerator input for different inter-regenerator spacing; (b) Regenerator Q_{out} measured after 10000km for different inter-regenerator spacing

For larger inter-regenerator spacing the regenerator operates with higher Q-gain, to compensate for the larger OSNR degradation associated with a longer span. For a spacing of up to 300km the Q-gain fully compensates for the span degradation, restoring the Q-factor to the value measured back-to-back at the regenerator output (Q-factor = 22dB). For spacing of 450 and 600km, the regenerator Q-gain is sufficient to suppress the accumulated noise over the span and to ensure that the extinction ratio condition for cascadability is maintained, however the regenerated signal Q-factor decreases. The regenerator Q-gain reached a maximum value of 3.8dB for a spacing of 600km. For a spacing of 750km, the accumulation of distortion over the inter-regenerator span, measured to cause a deterioration of the signal Q-factor = 4dB, exceeds the regenerator Q-factor improvement range resulting in the maximum achievable error-free transmission distance of 7500km. The regenerated signal output Q-factor decreases when the regenerator operates with larger Q-gain. Figure 6-15 (b) shows the regenerator output Q-factor (Q_{out}) measured after a transmission distance of 10000km for different inter-regenerator spacing. The regenerated signal output Q-factor dropped by up to 3dB when the spacing increases from 150km to 600km. A change in the Q-factor is caused by a variation in the signal extinction ration or/and in the noise level around the signal "*one*" and "*zero*" levels.

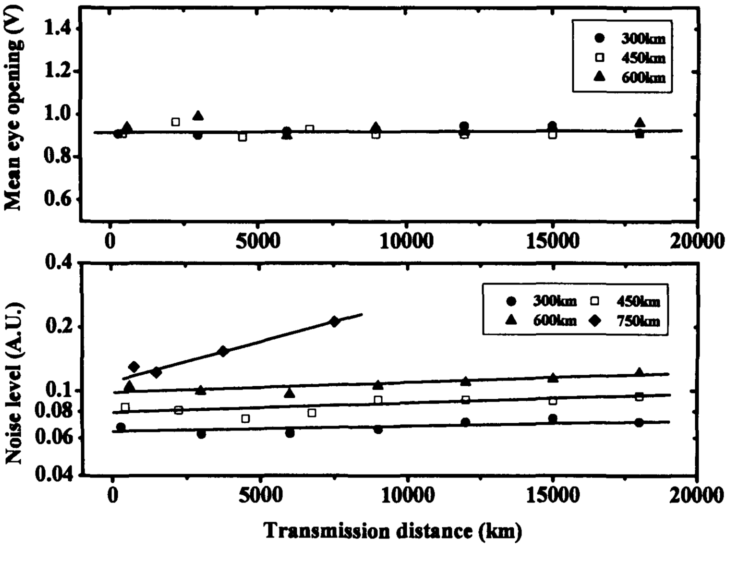

Figure 6-16 Mean eye opening and noise level of the transmitted signal for different inter-regenerator spacing

Figure 6-16 shows the signal mean eye opening and the noise level, both derived from the Q-factor measurements plotted in Figure 6-14 as a function of distance for transmission with different inter-regenerator spacing.

The transmitted signal mean eye opening, defined as the difference between the mean of the "*zero*" and "*one*" level, does not significantly vary with distance. This demonstrates that the regenerator satisfies the fundamental condition for cascadability, which is to maintain the signal extinction ratio at each regenerator input constant, to operate the regenerator with optimal noise suppression. For the case of inter-regenerator spacing equal to 10 spans (750km) the extinction gain is not sufficient to maintain cascadability and the transmission Q-factor quickly degrades. We also observed that at the beginning of transmission the regenerated signal extinction ratio slightly oscillates causing the Q-factor to vary until the steady state is reached. At this point the transmitted signal extinction ratio is matched to the regenerator switching contrast.

Furthermore, the mean eye opening does not vary significantly with different spacing, suggesting that the regenerator operates with the same contrast ratio. Thus the change in Q-factor with larger spacing has to be attributed to a change in the signal noise level.

Figure 6-16 shows the noise level, proportional to the sum of the standard deviation of the noise around the signal "*one*" and "*zero*" level, over distance for different inter-regenerator spacing. It is important to notice that since the regenerator operates with logic inversion the noise statistical characteristics on the "*one*" and "*zero*" signal levels are averaged with the number of cascade. The noise level after the first regenerator drops with larger spacing, which causes the regenerator output signal Q-factor to decrease. After the first regenerator the noise level of the transmitted signal marginally increase with distance. In particular, the slope of the linear fittings for the noise level measurements with distance present similar slope at different inter-regenerator spacing, suggesting that the regenerator operates with a similar noise compression factor. Since for a given inter-regenerator spacing the extinction ratio does not vary with distance then each regenerator in the chain operates with the same noise compression factor. The noise compression term (Y_{NC}), was defined in chapter 3, as the slope of the regenerator transfer function around the signal "*zero*" or "*one*" mean levels.

The regenerator output Q-factor and the noise compression term are related as:

$$Q_{3R} = \frac{\mu_1 - \mu_0}{\sigma_{3R_1} + \sigma_{3R_0}} = \frac{\mu_1 - \mu_0}{Y_{NC}\left(\sigma_{IN_1} + \sigma_{IN_0}\right)} \qquad (6\text{-}6)$$

where σ_{IN} refers to the regenerator input signal standard deviation and the σ_{3R} to the regenerates signal standard deviation while μ is the mean of the signal "*one*" and "*zero*" level. The noise compression term can be estimated from the slope of the linear fitting of the Q-factor versus distance measurements shown in Figure 6-14. The noise compression term is plotted for the different inter-regenerator spacing in Figure 6-17 (a). As described in chapter 3 the noise compression term is a function of the interferometer bias which is also determines the regenerator extinction ratio gain.

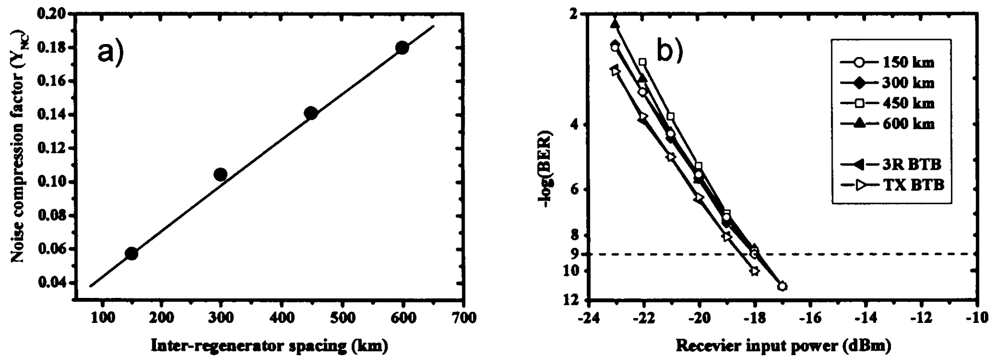

Figure 6-17 (a) Noise compression term at different inter-regenerator spacing; (b) BER curves measured at 20000km for transmission with different inter-regenerator spacing

The nose compression term slightly increases with larger spacing due to the fact that at larger spacing the regenerator requires more extinction ratio gain to compensate for the larger signal extinction ratio degradation caused by the longer span. Figure 6-17 (b) shows the BER curves measured after 20000km for different inter-regenerator spacing, showing error-free (BER < 1E-9) transmission with receiver sensitivity penalty of less than 1dB with respect to the transmitter signal measured back-to-back. It is important to notice that the BER has increased as a function of distance proportionally to the decrease of the Q-factor. However, since the Q-factor was as low as 22dB no sensitivity penalty could be measured at BER of 10^{-9}.

In conclusion, an error-free 10Gb/s transmission with all-optical cascaded 3R regeneration over 20000km was achieved, for input OSNR ranging from 30 to 23 dB/0.1nm, resulting in a maximum spacing of 600km. It was demonstrated that the proposed optical regenerator can operate with a noise compression factor as low as $Y_{NC} < 0.2$ for regenerator input signal OSNR > 23 (dB/0.1nm). As theoretically predicted in [Olh97], for $Y_{NC} < 0.2$ the BER can be approximated to linearly accumulate with distance as in an ideal electrical repeater.

It was found that the regenerator noise compression factor increased with the inter-regenerator spacing. This is because at longer spacing the regenerator must compensate for larger extinction ratio degradation and trades off noise compression with extinction ration gain as theoretically predicted in chapter 3. This demonstrated that the maximum inter-regenerator spacing is limited by the regenerator trade-off between noise suppression and maintenance of the extinction ratio required for cascadability.

It is believed that the proposed experimental technique is the most complete, as proposed to date, to assess the regenerator noise suppression performance. In fact, due to the physical characteristics of the SOA-assisted interferometer regenerator noise suppression is maximised at a unique input extinction ratio which corresponds to the regenerator switching contrast. Only cascading regenerators it was possible to ensure that the extinction ratio was maintained at its optimum at the regenerator input. Under these experimental conditions the noise suppression of the regenerator could be optimally measured. Comparison of the results of Figure 6-5 (a) and Figure 6-15 (a) demonstrates that the larger Q-gain was measured with the cascaded loop experiments where regenerator input signal extinction ratio is optimal.

Furthermore, as previously mentioned the regeneration noise suppression characteristics and extinction ratio gain are related. In a transmission experiment with cascaded regenerators it was possible to make sure that the regenerator is also providing the extinction ratio gain necessary to maintain cascadability. Under these experimental conditions the noise suppression of the regenerator can be optimally measured for a given extinction ratio gain.

6.3 Fibre launch power margin in a 40Gb/s transmission with optical regeneration

The regenerative properties of 40Gb/s 2R and 3R optical regenerators to OSNR distortion has been experimentally investigated to show that optical regeneration can improve the signal Q-factor and, thus, the receiver sensitivity [Wol00b] [Tsu02]. In section 6.2, it was shown that the regenerator Q-gain contributes significantly to determine the inter-regenerator spacing. Thus, a detailed investigation of the Q-gain has to be performed to assess the cascadability properties of optical regenerators.

Most of regeneration characterisation experiments presented in the literature have been performed back-to-back by artificially degrading the OSNR at the regenerator input in order to assess the effect on the regenerated signal Q-factor. However, when operating at 40 Gb/s not only the fibre span length but also the power of the signal propagating in the fibre determines the accumulation of signal distortion due to nonlinear effects [Ess99].

In this work, the impact of fibre launch power on the regenerator Q-gain was investigated utilising a transmission loop. This was achieved by positioning the optical regenerator at the transmission link output prior to the electrical receiver. Results give indication of the inter-regenerator spacing in a 40 Gb/s transmission system for applications to transmission with cascaded optical regenerators. The enhancement of error-free transmission distance with the use of a single regenerator at the receiver is also demonstrated.

Experimental set-up and results: Figure 6-18 shows the experimental set-up for the 40Gb/s transmission experiments with the optical regenerator at the receiver. As the transmission margins at 40Gb/s are significantly lower than at 10Gb/s [Mik03a] the loop span now included an additional EDFA prior to the DCF to mitigate the OSNR accumulation with distance. The transmitted signal was a 40 Gbit/s (PRBS 2^{31}-1) RZ signal with a 9ps pulse width (FWHM) and with an extinction ratio in excess of 15dB, generated by cascading two EAM modulator driven with a 40Gb/s PPG. The 40Gb/s transmitter and receiver are described in appendix 3.

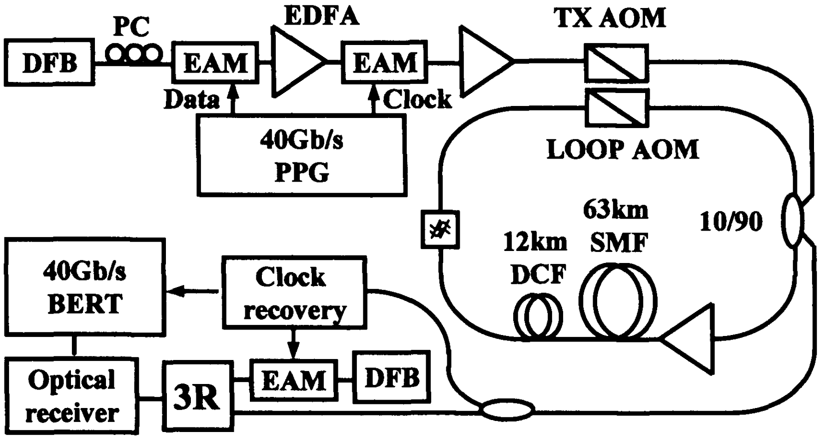

Figure 6-18 40Gb/s Transmission experiments with all-optical regeneration at the receiver

At the loop output the transmitted signal was regenerated and then routed to the optical receiver. The receiver consisted of EDFA pre-amplified photo-detector and a 40 Gb/s Error detector. The regenerator was set-up to operate in wavelength conversion configuration as shown in Figure 6-2. A clock recovery circuit, based on a high-Q filter, was used to synchronise the BERT and to generate the optical clock for the 3R regenerator driving an EAM with a 40GHz sinusoid. The regenerator optical clock signal wavelength is 1545nm, is and the pulse width is 9ps.

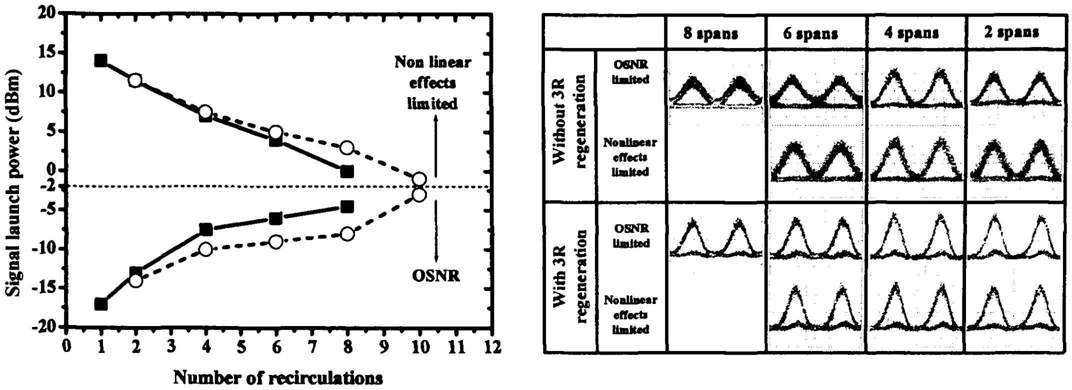

Figure 6-19 Maximum error free transmission distance as a function of the power launched into the fibre span and eye diagrams for transmission with (○) and without (■) regeneration at the receiver

Figure 6-19 shows the maximum error free (BER < 10^{-9}) transmission distance as a function of the power launched into the fibre span with and without the optical 3R regenerator prior to the receiver. The eye diagrams of the transmitted and regenerated signal at different transmission distances are also shown in Figure 6-19. The optimum launch power in the fibre for longest error-free transmission distance was found to be P_{fibre} = -2dBm. At lower launch powers, when the maximum transmission distance is limited by OSNR degradation, the major signal impairment is the Amplifier Spontaneous Emission (ASE) signal beat noise which results in an increased amplitude noise of the signal "*ones*" as shown in Figure 6-19. The optical regenerator was able to effectively suppress this amplitude noise, as shown in the optically regenerated signal eye diagrams, and to enhance by the 3.5 dB the error-free power margin at 8 recirculations. At higher launch powers, when the error-free transmission distance is limited by the optical nonlinearities, signal impairments arise from both amplitude noise and increased timing jitter as seen in Figure 6-19. The optical regenerator operated with a switching window of 12ps, providing a margin for the suppression of timing jitter 4ps larger then the electrical receiver, as described in section 5.1.4. Signal improvement is clearly visible in the regenerated signal eye diagrams, and leads to a 3dB increase in the receiver error-free power margins.

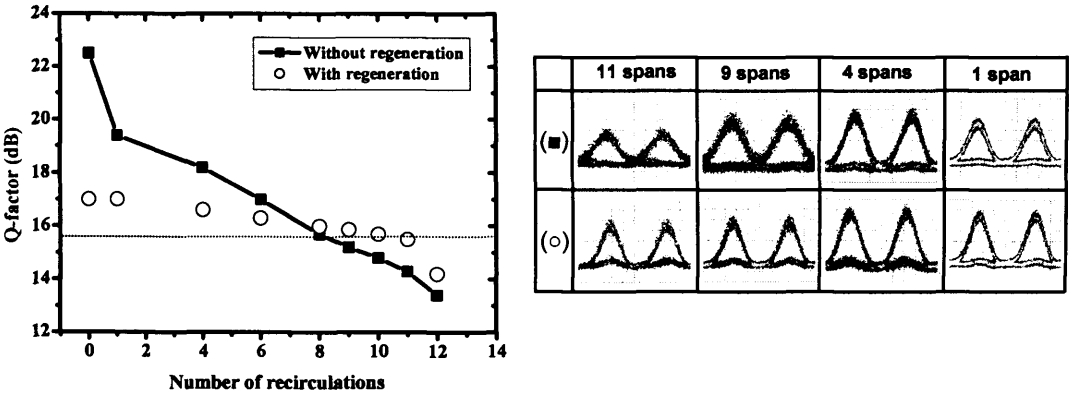

Figure 6-20 Q-factor (dB) and eye diagrams for transmission with (o) and without regeneration at the receiver (■) for fibre launch power of -2dBm

Figure 6-20 shows the evolution of the Q-factor measured as a function of the transmission distance for transmission with (o) and without (■) regeneration prior to the electrical receiver for fibre launch power of -2dBm. This was found to be the optimum fibre transmission launch power as shown in Figure 6-19. The optical regenerator enhances the signal Q-factor allowing to improve the maximum error-free transmission distance from 8 to 10 recirculations. In order to minimise the effect of polarisation dependent OSNR variation in the loop, the Q-factor was measured at the regenerator input and output without re-optimising the polarisation of the signal transmitted in the loop. The enhancement in the maximum transmission distance is mainly due to the suppression of timing jitter.

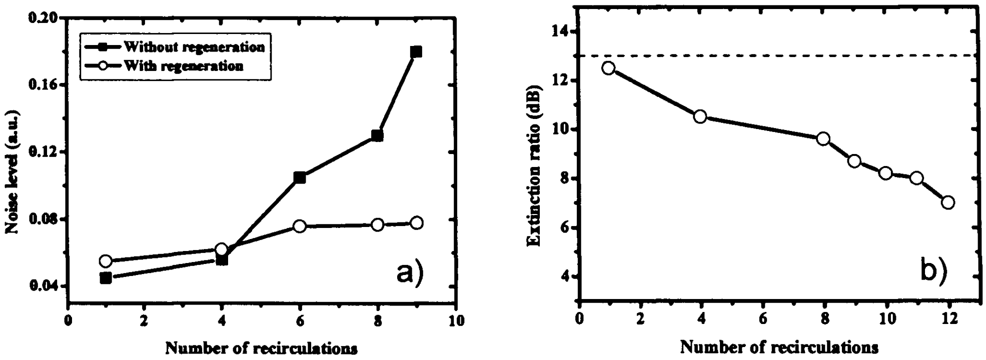

Figure 6-21 Transmitted signal noise level (a) and extinction ratio (b) with (○) and without regeneration at the receiver (■) for fibre launch power of -2dBm

Figure 6-21 shows the transmitted signal noise level, or noise variance, and extinction ratio, derived from the Q-factor measurement of Figure 6-20, as a function of distance for transmission with (○) and without (■) regeneration, for fibre launch power of -2dBm. The Q-factor improvement introduced by the regenerator, shown in Figure 6-20, is a consequence of the suppression of noise around the signal levels. However, the decrease of the regenerated signal Q-factor with distance is due to a decrease in the extinction ratio.

Figure 6-22 (a) shows the Q-factor before and after regeneration extrapolated from the results of Figure 6-20.

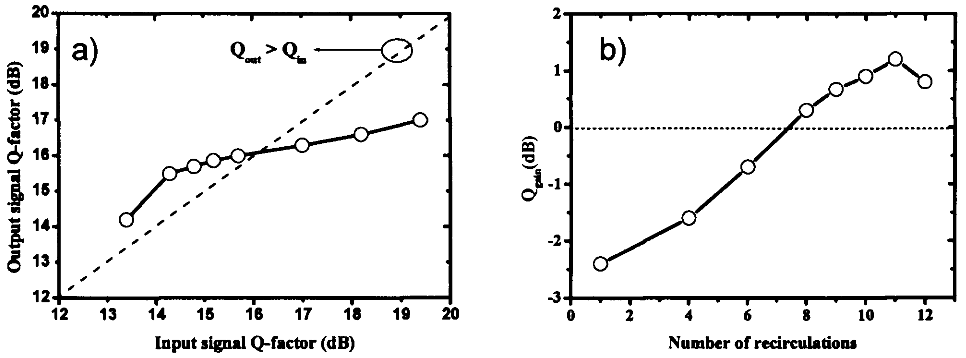

Figure 6-22 (a) Regenerated signal Q-factor with respect to input signal Q-factor; (b) Q_{gain} (dB) as a function of the number of recirculations

For input signal Q-factor values in excess of the maximum regenerator signal Q-factor (17dB) no improvement can be observed on the regenerated signal. As the input signal Q-factor degrades below 16dB as a result of the EDFA noise cumulated in transmission the regenerated signal Q-factor exceeds the input. This improvement can be quantified introducing the regenerator Q-factor gain, as defined in equation (6.1). Figure 6-22 (b) shows the Q-gain measured as the number of recirculation is increased at a fixed fibre launch power of -2dBm.

The maximum Q-gain was measured to be 1.5dB and this was achieved close to the receiver OSNR limit for BER $\approx 10^{-9}$, which occurred when the regenerator input signal OSNR $\approx$ 20dB corresponding to a Q-factor of 15.6dB, and allows to increase the error-free transmission distance by 2 recirculation. The Q-gain increases with decreasing OSNR, however we find that there is an optimum input signal Q-factor, corresponding to 15.2dB, for which the regenerator Q-gain is maximum before decreasing with the input Q-factor. As mentioned earlier, a Q-factor improvement enhances the receiver sensitivity but not necessary corresponds to an improvement in BER, due to the possible presence of and error-floor. Figure 6-23 shows the threshold window (defined as the BER as a function of the receiver threshold voltage), measured after 10 recirculation, corresponding to the maximum error-free transmission distance achievable without optical regeneration, for transmission with (○) and without (■) regeneration prior to the optical receiver.

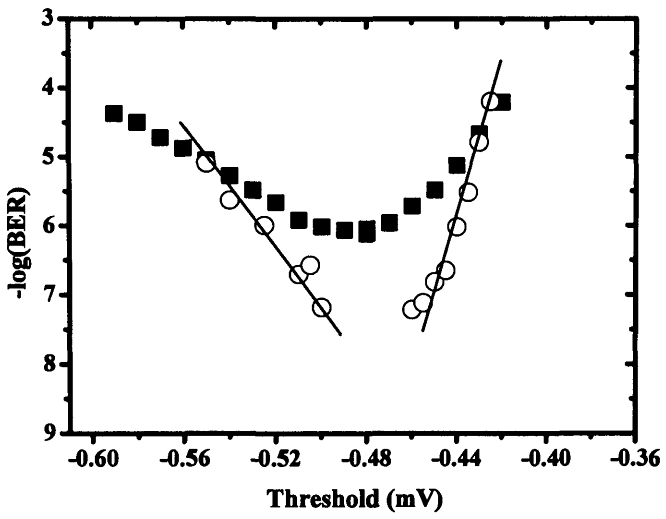

Figure 6-23 BER as a function of the threshold voltage after 10 recirculations (■); with optical regeneration (○)

The Q-factor improvement provided by the optical regenerator corresponds to an increase of the amplitude margins around to BER = 10^{-9} achieved most importantly without introducing an error-floor in the BER. This shows that, as observed for the 10Gb/s experiments in section 6.1, BER improvement can be achieved with the optical regenerator which, under the condition of low OSNR, outperforms the electrical receiver.

In conclusion, it was found that the regenerator can enhance the error-free receiver sensitivity both for OSNR limited and nonlinear limited transmission. In particular, we show that the use of an optical regenerator before the electrical receiver increases the power margin by up to 6.5 dB at 40Gb/s.

At the optimum launch power (-2dBm) the regenerator improved the signal Q-factor at low OSNR operating with a maximum Q-gain of 1.5dB for input signal OSNR of 20dB, and the maximum error-free transmission distance by 2 recirculations. The improvement of BER can be explained to occur mainly as a result of the larger tolerance of the optical regenerator to timing jitter, PMD and residual dispersion.

Summary

First, the noise suppression performance of a single optical regenerator placed at the end of a transmission link prior to the electrical receiver was investigated. These experiments have demonstrated that optical regeneration can improve the signal Q-factor both at 40 and 10Gb/s, enhancing the extinction ratio, compressing the noise distributions around the signal levels and suppressing timing jitter.

The concept of Q-gain was introduced to quantify the improvement in Q-factor between the regenerator input and output signal. It was found that the regenerator Q-gain depends on the input signal Q-factor and that the maximum Q-gain occurs at low OSNR. Q-gain of 3dB were measured at 10Gb/s for input signal OSNR $\approx$ 20(dB/0.1nm) and of 1.5dB at 40Gb/s s for input signal OSNR $\approx$ 21(dB/0.1nm).

The dependence of the regenerated signal Q-factor on the input signal Q-factor is a fundamental difference between electrical and optical repeater. In an electrical repeater, in fact, the output and input signal Q-factor are independent; however in an optical regenerator these are related by the optical nonlinear transfer function. Therefore, to fully assess the reshaping properties of optical 3R regenerators it is necessary to measure the regenerator Q-gain while is cascaded.

The transmission experiments with cascaded optical regeneration, presented this chapter, have demonstrated that the BER accumulation with distance for electrically and optically repeated systems can be almost identical. Error-free 10Gb/s transmission with all-optical cascaded 3R regeneration over 20000km was achieved for input OSNR ranging from 30 to 23 (dB/0.1nm), resulting in a maximum inter-regenerator spacing of 600km. The optical regenerator operated with a noise compression factor of less than 0.2 at OSNR of 23 (dB/0.1nm) and with an output Q-factor larger than 16dB.

Thus, it can be concluded that the fundamental difference between an electrically repeated system and the optically repeated systems investigated in this thesis is the relationship between the transmission Q-factor (repeater output signal Q-factor) and the error-rate accumulation. In an electrically repeated system the BER accumulation depends on the inter-repeater spacing but not on the transmission Q-factor. However, as demonstrated in this chapter, in an optically regenerated link there is a relationship between the transmission signal Q-factor and the inter-regenerator spacing. In particular with longer inter-regenerator spacing the transmission Q-factor decreases. Furthermore, for the case of optically regenerated links, the maximum inter-regenerator spacing was found to be limited by the regenerator trade-off between noise suppression and maintenance of the extinction ratio required for cascadability.

Chapter 7 Summary and conclusions

Several configurations have been proposed, over the last decade, to implement optical gates exploiting SOA nonlinearities. However, only more recently the development of highly nonlinear SOA has lead to a new class of optical devices potentially capable of truly operating at ultra-fast frequencies up to an order of magnitude larger than common electronic processing gates.

Because of their high operating frequency, SOA gates have been proposed to replace the bit-level processing functionalities to date implemented electronically, such as optical demultiplexing, 3R regeneration and wavelength conversion at bit-rates of 40Gb/s and beyond. However, differently to digital electrical switches, such as flip-flops, which have a bi-stable transfer function, the SOA gates operate with an analogue transfer function. This has particular implications for applications to 3R optical regeneration. As a consequence of the analogue transfer function:

- SOA gates regenerators are expected to operate with smaller margins to input signal distortion, and thus to show less regenerative abilities than electrical regenerators. However, to date, a complete quantification of the regenerator tolerance to input signal distortion, including both timing jitter and intensity jitter, has not yet been experimentally reported for 40Gb/s operations.
- Transmission with cascaded optical regenerators can have significantly different properties with respect to a system employing electrical regeneration. However, to date, an analysis of the relationship between the SOA gate regenerative properties and the properties of a transmission system (signal Q-factor, BER accumulation and OSNR evolution) employing optical regenerators has not been experimentally investigated.

A second important characteristic of SOA gates, with respect to electrical processing devices, is their ability of simultaneously process multi-wavelength signals. However, to date, this property remains unexploited in all configurations proposed in literature.

In this thesis novel SOA gates configurations for applications to wavelength conversion, regeneration and demultiplexing for bit-rates of up to 40Gb/s and capable of simultaneous multi-channel operations have been described. The switching, regenerative and cascadability properties has also been assessed both theoretically and experimentally at bit-rates of 10 and 40Gb/s using novel measurement techniques based on a multiple span recirculating loop. The work developed in this thesis was presented as follows.

In **Chapter 3** a theoretical comparison of the switching and reshaping properties of SOA gates based on XGM configurations with respect to those based on XPM configurations (SOA-assisted interferometers) was presented. In particular, the impact of the SOA physical parameters, such as the α-factor the small signal gain and the recovery time, on the SOA gate switching transfer function properties was investigated.

It was found that optical switching based on XGM nonlinearities leads to a strong noise suppression and ultra-fast time response, however extinction ratio regeneration can not be achieved with gain based nonlinearity. Thus XGM techniques are better suited for wavelength conversion rather than signal 3R regeneration. On the contrary, we find that SOA-assisted interferometers can perform extinction ratio enhancement and the noise reductions due to the interferometer transfer function. These properties make SOA-assisted interferometers more suitable for optical 3R regeneration. It was also found that a trade-off exists between the noise suppression properties and the extinction ratio gain in an SOA-assisted interferometer which depends on the interferometer bias. Calculations have shown that extinction ratio gain in excess of 5 dB can be achieved with realistic α-factor (5-6) and small signal gain values (30dB), while maintaining a low noise compression factor (Y_{NC}).

Thus, to predict the SOA gates reshaping and switching properties for application to high bit-rate 3R regeneration and wavelength conversion is necessary to quantify the SOA gain and phase recovery time and the α-factor.

In **chapter 4,** detailed experimental measurements of the inter-band dynamics of both phase and gain nonlinearity in highly nonlinear SOA with different lengths was presented. When characterising an SOA for application to optical switching at a certain bit rate, the fundamental parameter to quantify is the gain and phase change magnitude as a function of the recovery time. Our results show the interrelationship between the phase, gain and chirp temporal evolution acquired by a probe signal in the SOA excited by a short optical pulse. The wavelength dependency of SOA nonlinearities was also considered. From these measurements it is possible to derive the relationship between the switching contrast and the switching frequency of any SOA gate configuration.

The nonlinear SOAs characterised in this thesis are expected to perform intensity switching based on gain saturation at 10GHz with switching contrast in excess of 13dB and at 40GHz with switching contrast in excess of 5dB. If we take advantage of XPM based non-linearity with an SOA-assisted interferometer configuration, switching with π-contrast (ideal switching contrast) is achieved with recovery time of 30ps which leads to switching frequency in excess of 30GHz. Therefore, these results suggest that to operate at frequency in excess of 40GHz it is necessary to work with SOA gate configurations which take advantage of the different SOA nonlinearities simultaneously. Based on the nonlinear SOA characterisation results, we investigated SOA gate configurations for 40Gb/s operations.

The experimental investigation of the switching properties of XGM gates was also described in chapter 4. Two different XGM configurations for application to 10 and 40Gb/s wavelength conversion were experimentally assessed and their performance compared to the SOA characterisation measurements. Both wavelength conversion based on an SOA with off-set filtering and on the SOA-DI configuration were investigated; these configurations take advantage of both nonlinear gain and chirp modulation, and thus possibly can exceed the switching frequency limits imposed by the SOA gain recovery time.

Experimentally it was found that with both configurations a switching contrast in excess of 5 dB could be achieved with switching window of 12ps (FWHM), which is a factor of 2 higher than what observed from the gain characterisation measurements. We attribute this enhancement to the chirp to intensity conversion performed by the DI or by the off-set filter. However, the extinction ratio penalty and the limited noise suppression ability of inherent with XGM configuration limit their applications to wavelength conversion.

A significant advantage of the SOA-DI configuration is the broadband periodic characteristics of the DI filter. Using a monolithically integrated SOA array and a single DI interferometer simultaneous wavelength conversion of 2 at 10Gbit/s channels was experimentally demonstrated and the reshaping properties assessed.

In **chapter 5** the properties of XPM configurations (SOA-assisted interferometers) for application to 10 and 40Gb/s 3R regeneration were experimentally investigated. A fundamental limit to operate XPM configurations at high bit-rates is pattern-dependent distortion. To overcome pattern-dependent distortion, a novel configuration based on XPM and XGM induced polarisation rotation in a SOA-assisted Sagnac interferometer (PSSI) was proposed. 3R optical regeneration with the PSSI configuration was demonstrated at 40Gb/s with 2^{31}-1 PRBS utilising an SOA with a carrier lifetime exceeding 250ps.

The regenerative properties of the PSSI configuration were also investigated experimentally at 10 and 40Gb/s. The error-free regenerator timing window was measured to be 43% of the bit period at 10Gb/s and 28% at 40Gb/s, which is the largest timing jitter cancellation demonstrated to date for optical regeneration. The investigation of the regenerator tolerance to intensity jitter was also carried out to demonstrate regeneration from up to 3dB amplitude jitter peak-to-peak. This also shows the large tolerance to pattern-dependent distortion inherent with the PSSI configuration.

Other optical processing functionalities with the PSSI configuration were also demonstrated and the results presented in chapter 5. All-optical 40 to 10Gb/s demultiplexing was also experimentally demonstrated to show error-free operation achieved with only 1.5dBm switching power. The demultiplexer switching contrast was measured to be 15dB for a switching window of 12ps (FWHM).

Finally, Simultaneous 3R regenerative wavelength conversion of 2 channels at 10Gbit/s was experimentally demonstrated for the first time using an integrated SOA array in the PSSI configuration, demonstrating the potential for large scale monolithic integration for optical processing applications for WDM networks.

In **Chapter 6** the experimental investigation of cascadability and reshaping properties, which is both signal noise compression and extinction ration improvement, of the PSSI optical regenerator at 10 and 40Gb/s was presented.

First the noise compression ability of the regenerator was investigated. The experiments involved loading the transmitter output signal with optical noise to degrade the OSNR before the regenerator in order to compare the receiver sensitivity and Q-factor improvement of the regenerated signal with respect to the input signal. Q-factor improvement of up to 1.5dB was measured at 40Gb/s and of 2.8dB at

10Gb/s. It was also demonstrated that utilising an optical regenerator prior to the electrical receiver can enhance the receiver sensitivity allowing to increase the error free transmission distance of up to 150km at 40Gb/s in an SMF link.

The regenerator cascadability properties were then investigated. In particular, this work was focused on assessing the regenerator noise suppression properties in transmission. For this purpose, a novel reconfigurable multi-span recirculating fibre loop was developed to perform transmission experiment with cascaded optical regeneration and variable inter-regenerator spacing. Varying the inter-regenerator spacing changes the amount of noise accumulated and allows for the assessment of the cascaded regenerator noise suppression performance. Error-free transmission at 10Gb/s over 20000km of standard single-mode fibre was demonstrated with inter-regenerator spacing range of 150-600km, corresponding to an OSNR range of 30-23 dB/0.1nm at the regenerator input. Results also demonstrated that:

- Regenerator's cascadability is achieved when the extinction ratio at the input of each regenerator is maintained constant. Thus, each regenerator performed the extinction ratio improvement necessary to compensate for the degradation of the span.
- The transmission signal Q-factor at the regenerator output depends on the regenerator noise compression factor and on the inter-regenerator spacing. The noise compression factor of the regenerator was measured in transmission to be less than 0.2 for inter-regenerator spacing of 600km.

The regenerator noise suppression properties in transmission were also investigated. The concept of Q-factor gain was introduced to quantify the Q-factor improvement introduced by the regenerator while it is cascaded; a Q-gain of up to 3.8dB was measured from an input OSNR of 21(dB/0.1nm). It is believed that this experimental technique is the most complete, proposed to date, to assess the regenerator noise suppression performance for application to transmission.

The research work presented in this thesis could be extended in the following areas:

- This thesis has focused on the investigation of the reshaping ability of optical regenerators in the presence of OSNR distortion. The investigation of the impact of fibre launch power on the inter-regenerator spacing in a 40 Gb/s transmission system with cascaded optical regenerators was investigated, however the impact of launch power on the maximum transmission distance is yet to be verified.
- A further application of optical regeneration could be in conjunction with more efficient digital modulation formats such as multilevel OOK, or analogue formats as BPSK. However this requires novel configurations capable of detecting also the phase information encoded on the input signal.
- The assessment of the regenerator tolerance to PMD distortion and to uncompensated dispersion in transmission is still to be addressed.

The switching properties of SOA gates based on inter-band nonlinearities have been extensively studied and applications to optical processing functionalities at up to 40GHz switching frequency demonstrated.

Future work should concentrate on scaling optical signal processing at frequency exceeding 40GHz, where intra-band nonlinearities are dominant. To date, literature on intra-band nonlinearities is limited to few experimental findings and observations [Mor87] [Hul91] [Occ02], however a detailed theoretical understanding of the physical processes involved supported by experimental measurements is not yet available. Detailed measurements of the dynamics and magnitude of intra-band effects in SOA could be performed with the characterisation experimental set-up described in chapter 3. Then configurations which optimally take advantage of the nonlinear characteristics of intra-band nonlinearity will have to be proposed and their performance assessed.

Chapter 8 Appendices

8.1 Appendix 1: SOA gate transfer function slope derivation

This appendix contains the derivation of the equations for the gain, phase and for the interferometer transfer function slope equations presented in chapter 3.

8.1.1 SOA gain transfer function slope derivation

The slope of the gain transfer function (G) can be derived differentiating equation (3-21) with respect to the input power normalized to the saturation power $P = P_{in}/P_{sat}$:

$$\frac{dG}{dP} = \frac{d\exp(h(P))}{dP} = \exp[h(P)]\frac{dh}{dP} \tag{8-1}$$

where $h(P)$ is given in equation (3.20) and the derivative of $h(P)$ with respect to P is:

$$\begin{aligned} \frac{dh}{dP} &= \frac{d(P\exp[h(P)-1])}{dP} \\ &= 1 - \exp(h) - P\exp(h)\frac{dh}{dP} \\ &= \frac{1-\exp(h)}{1+P\exp(h)} \end{aligned} \tag{8-2}$$

Thus, the gain slope is:

$$\frac{dG}{dP} = \exp[h(P)]\frac{dh}{dP} = \exp(h)\frac{1-\exp(h)}{1+P\exp(h)} \tag{8-3}$$

Given that $G(P) = \exp[h(P)]$, then equation (8-3) can be expressed in terms of the gain G, as:

$$\frac{dG}{dP} = \frac{G(1-G)}{1+PG} \tag{8-4}$$

The term P is derived rearranging equation (3-20):

$$P = \frac{g_0L - h}{\exp[h(P)]-1} = \frac{\log(G_0)-\log(G)}{\exp[h(P)]-1} = \frac{\log(G_0/G)}{G-1} \tag{8-5}$$

Chapter 8 Appendices

8.1 Appendix 1: SOA gate transfer function slope derivation

This appendix contains the derivation of the equations for the gain, phase and for the interferometer transfer function slope equations presented in chapter 3.

8.1.1 SOA gain transfer function slope derivation

The slope of the gain transfer function (G) can be derived differentiating equation (3-21) with respect to the input power normalized to the saturation power $P = P_{in}/P_{sat}$:

$$\frac{dG}{dP} = \frac{d\exp(h(P))}{dP} = \exp[h(P)]\frac{dh}{dP} \tag{8-1}$$

where $h(P)$ is given in equation (3.20) and the derivative of $h(P)$ with respect to P is:

$$\begin{aligned} \frac{dh}{dP} &= \frac{d(P\exp[h(P)-1])}{dP} \\ &= 1-\exp(h) - P\exp(h)\frac{dh}{dP} \\ &= \frac{1-\exp(h)}{1+P\exp(h)} \end{aligned} \tag{8-2}$$

Thus, the gain slope is:

$$\frac{dG}{dP} = \exp[h(P)]\frac{dh}{dP} = \exp(h)\frac{1-\exp(h)}{1+P\exp(h)} \tag{8-3}$$

Given that $G(P) = \exp[h(P)]$, then equation (8-3) can be expressed in terms of the gain G, as:

$$\frac{dG}{dP} = \frac{G(1-G)}{1+PG} \tag{8-4}$$

The term P is derived rearranging equation (3-20):

$$P = \frac{g_0L-h}{\exp[h(P)]-1} = \frac{\log(G_0)-\log(G)}{\exp[h(P)]-1} = \frac{\log(G_0/G)}{G-1} \tag{8-5}$$

The slope of the gain transfer function expressed in decibels (G_{dB}) can be derived as follows:

$$\begin{aligned}\frac{G_{dB}}{P_{dB}} &= \frac{d10\log_{10}(G)}{d10\log_{10}(P)} = \frac{d[10\log_{10}(G)]/dP}{d[10\log_{10}(P)]/dP} \\ &= \frac{10/\ln(10)\cdot 1/G\cdot dG/dP}{10/\ln(10)\cdot 1/P} = \frac{P}{G}\cdot\frac{dG}{dP}\end{aligned} \qquad (8\text{-}6)$$

The gain transfer function slope at a particular value of G_{dB} can be expressed substituting P of (8.5) in equation (8.6):

$$\begin{aligned}\frac{dG_{dB}}{dP_{dB}} &= \frac{-G(G-1)^2}{(G-1)+G[\log(G_0/G)]}\cdot\frac{\log(G_0/G)}{G(G-1)} \\ &= \frac{-\log(G_0/G)(G-1)}{(G-1)+G\log(G_0/G)}\end{aligned} \qquad (8\text{-}7)$$

Thus, the slope of $G_{dB}(P)$ around $\sqrt{G_0}$ is given by:

$$\left.\frac{dG_{dB}}{dP_{dB}}\right|_{G=\sqrt{G_0}} = \frac{-\log\left(\sqrt{G_0}\right)\left(\sqrt{G_0}-1\right)}{\left(\sqrt{G_0}-1\right)+\sqrt{G_0}\left[\log\left(\sqrt{G_0}\right)\right]} \qquad (8\text{-}8)$$

The effect of clamping the SOA gain with a holding beam signal on the slope of the gain transfer function (G_{dB}), can be estimated differentiating G_{dB} with respect to the switching signal power (P_{sw}), defined as $P_{sw} = P_{in} - P_{hb} = PP_{sat} - P_{hb}$:

$$\frac{dG_{dB}}{dP_{swdB}} = \frac{dG_{dB}/dP}{(dP_{swdB})/dP} \qquad (8\text{-}9)$$

Given that:

$$\frac{dG_{dB}}{dP} = \frac{10}{\log(10)}\frac{1}{G}\frac{dG}{dP} \qquad (8\text{-}10)$$

$$\frac{dP_{swdB}}{dP} = \frac{d[10\log_{10}(PP_{sat}+P_{hb})]}{dP} = \frac{10}{\log(10)}\frac{1}{P\cdot P_{sat}-P_{hb}}P_{sat} \qquad (8\text{-}11)$$

Thus:

$$\begin{aligned}\frac{dG_{dB}}{dP_{sw_{dB}}} &= \frac{1}{G}\frac{dG}{dP}\left[\frac{PP_{sat}-P_{hb}}{P_{sat}}\right] = \frac{dG}{dP}\left[\frac{P}{G}-\frac{P_{hb}}{P_{sat}G}\right] \\ &= \frac{dG}{dP}\left[\frac{P}{G}-\frac{1}{P}\left(\frac{P\cdot P_{hb}}{G\cdot P_{sat}}\right)\right] = \frac{dG_{dB}}{dP_{dB}}\left[1-\frac{P_{hb}}{P_{in}}\right]\end{aligned} \qquad (8\text{-}12)$$

8.1.2 SOA phase transfer function slope derivation

The slope of the phase (φ) transfer function can be derived differentiating equation (3-22) with respect to the input power normalized to the saturation power $P = P_{in}/P_{sat}$:

$$\frac{d\varphi}{dP} = \frac{d(-\alpha/2\,h(P))}{dP} = -\frac{\alpha}{2}\frac{dh}{dP} \qquad (8\text{-}13)$$

Where dh/dP is given in equation (8-2). Expressing the phase slope in terms of the gain G:

$$\frac{d\varphi}{dP} = -\frac{\alpha}{2}\frac{(1-G)}{1+PG} \qquad (8\text{-}14)$$

The slope of the phase transfer function with respect to the input power, expressed in decibels, can be derived as follows:

$$\frac{d\varphi}{dP_{dB}} = \frac{d\varphi}{d10\log_{10}(P)} = \frac{d\varphi/dP}{d[10\log_{10}(P)]/dP} = \frac{d\varphi}{dP}P\frac{\ln(10)}{10} \qquad (8\text{-}15)$$

The effect of clamping the SOA gain with a holding beam signal on the slope of the phase transfer function, defined in equation (3-18), can be estimated differentiating φ with respect to the switching signal power (P_{sw}), defined as $P_{sw} = P_{in} - P_{hb} = PP_{sat} - P_{hb}$:

$$\frac{d\varphi}{dP_{sw\,dB}} = \frac{d\varphi/dP}{(dP_{sw\,dB})/dP} \qquad (8\text{-}16)$$

where $dP_{sw\,dB}/dP$ is given in equation (8-11), and $d\varphi/dP$ in equation (8-14):

$$\frac{d\varphi}{dP_{cw_{dB}}} = \frac{d\varphi}{dP}P\frac{\log(10)}{10}\left(\frac{PP_{sat} - P_{hb}}{P_{sat}}\right) = \frac{d\varphi}{dP_{dB}}\left(1 - \frac{P_{hb}}{PP_{sat}}\right) \qquad (8\text{-}17)$$

8.1.3 SOA-assisted interferometer transfer function slope derivation

The slope of the SOA-assisted interferometer transfer function can be derived differentiating equation (3-26) with respect to the input power normalized to the saturation power $P = P_{in}/P_{sat}$:

$$\frac{dP_{out}}{dP} = 1/2\sin(\varphi)\frac{d\varphi}{dP} \qquad (8\text{-}18)$$

Where dh/dP is given in equation (8-2). Expressing both input and output power in decibels, P_{dB} and $P_{out_{dB}}$ respectively, then the transfer function slope can be expressed as:

$$\frac{dP_{out_{dB}}}{dP_{dB}} = \frac{d10\log(P_{out})}{d10\log(P)} = \frac{dP_{out_{dB}}/dP_{out}}{dP_{dB}/dP_{out}} = \frac{dP_{out_{dB}}}{dP_{out}}\frac{dP_{out}}{dP_{dB}} \tag{8-19}$$

where $dP_{out_{dB}}/dP_{out}$ is given by:

$$\frac{dP_{out_{dB}}}{dP_{out}} = \frac{d[\log_{10}(P_{out})]}{dP_{out}} = \frac{1}{P_{out}}\frac{10}{\ln(10)} \tag{8-20}$$

and dP_{out}/dP_{dB} can be expressed, from equation (8-18), as:

$$\frac{dP_{out}}{dP_{dB}} = 1/2\sin(\phi)\frac{d\varphi}{dP_{dB}} \tag{8-21}$$

Thus,

$$\frac{dP_{out_{dB}}}{dP_{dB}} = \frac{1}{P_{out}}\frac{10}{\ln(10)}\left[1/2\sin(\varphi)\frac{d\varphi}{dP_{dB}}\right] \tag{8-22}$$

which can also be rearranged as:

$$\frac{dP_{out_{dB}}}{dP_{dB}} = \frac{P}{P_{out}}\left[1/2\sin(\varphi)\cdot\frac{d\varphi}{dP}\right] = \frac{P}{P_{out}}\frac{dP_{out}}{dP} \tag{8-23}$$

The effect of a holding beam power on the interferometer transfer function slope can be calculated as follows:

$$\frac{dP_{out_{dB}}}{dP_{sw_{dB}}} = \frac{dP_{out_{dB}}/dP}{dP_{sw_{dB}}/dP} = \frac{dP_{out_{dB}}}{dP}\frac{dP}{dP_{sw_{dB}}} \tag{8-24}$$

where:

$$\frac{dP_{out_{dB}}}{dP} = \frac{1}{P_{out}}\frac{10}{\ln(10)}\frac{dP_{out}}{dP} \tag{8-25}$$

$$\frac{dP_{sw_{dB}}}{dP} = \frac{10}{\ln(10)}\frac{P_{sat}}{PP_{sat} - P_{hb}} \tag{8-26}$$

Thus,

$$\frac{dP_{out_{dB}}}{dP_{sw_{dB}}} = \frac{PP_{sat} - P_{hb}}{P_{out}P_{sat}} \frac{dP_{out}}{dP} \tag{8-27}$$

which can be rearranged into:

$$\frac{dP_{out_{dB}}}{dP_{sw_{dB}}} = \frac{dP_{out_{dB}}}{P_{dB}} \left(1 - \frac{P_{hb}}{P_{in}} \right) \tag{8-28}$$

8.2 Appendix 2: SOAs characterisation

This appendix contains the characterisation of the SOA utilised in the experiments described in chapters 4-6. SOA characterisation involves both the assessment of the static and the dynamic gain and phase transfer function. The static transfer function shows the gain saturation characteristic with injected optical power. The dynamic transfer function instead, shows the time response of the SOA nonlinear gain and phase excited by a short (12ps) high intensity optical pulse. Furthermore the SOA α-factor and chirp were also measured. The experimental set-ups for these measurements are described in details in chapter 4.1.

8.2.1 Kamelian SOA

The SOA is a high confinement factor, 1mm long bulk structure designed, manufactured and packaged by Kamelian [Kam05]. The small signal gain is 24dB and the saturated output power 15dBm. The detailed characterization of this SOA is reported in chapter 4.

8.2.2 CIP (Centre for Integrated Photonics) SOA

The SOA is a high confinement factor, 1.1mm long bulk structure designed, manufactured and packaged at CIP [CIP05]. The small signal gain is 28dB and the saturated output power 15dBm.

SOA Static gain transfer function measurements: The experimental set-up for the measurements is shown in Figure 4-1. The SOA gain transfer function was measured at the probe signal wavelength (λ_{probe} = 1550nm), while the pump signal (λ_{pump} = 1555nm) was used to clamp the SOA gain at different levels.

Figure 8-1 (a) shows the SOA gain transfer function measured with a bias current of 250mA. The measured curves were fitted with the results of a numerical calculation following the model in [Agr89]. The simulation parameters used are E_{sat} = 1pJ, τ_c = 200ps and G_0 = 28dB. Figure 8-1 (b) shows the SOA output power measured with a bias current of 250mA. The SOA PDL was less than 1dB.

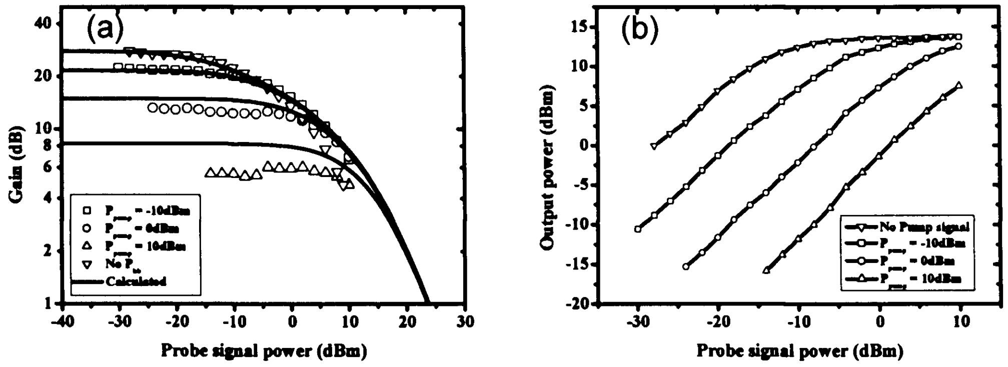

Figure 8-1 CIP SOA gain (a) and output power (b) transfer function measured for different pump powers

SOA gain and phase dynamics and α-factor measurements: The experimental set-up for the measurements is shown in Figure 4-4. The SOA gain dynamic transfer function and α-factor was measured at the probe signal wavelength (λ_{probe} = 1550nm), while the pump signal (λ_{pump} = 1545nm) was used to clamp the SOA gain at different gain level. The pump signal power was 6dBm and the probe signal power was -14dBm.

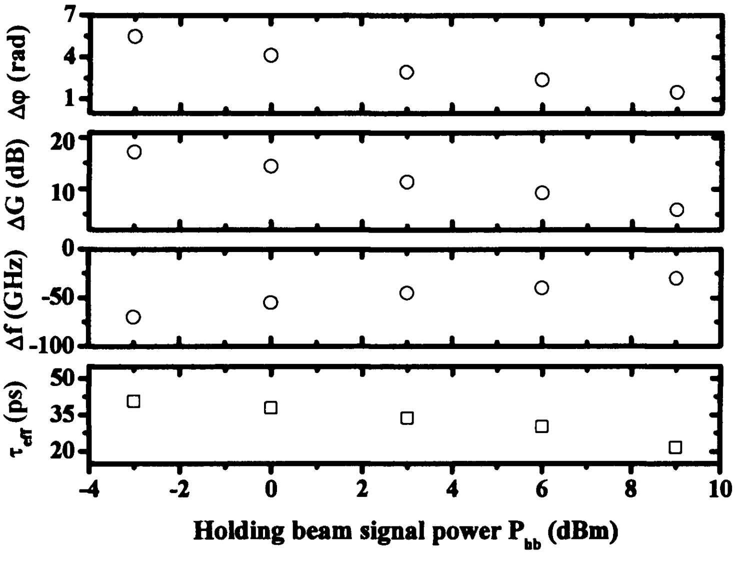

Figure 8-2 CIP SOA dynamics characterisation for different holding beam signal power levels

Following the terminology introduced in chapter 4; Figure 8-2 shows the maximum dynamic gain (ΔG) phase (Δφ) and chirp (Δf) change induced by the pump pulse, and the effective recovery time (τ_{eff}) as a function of the holding beam power. The effective α-factor (α_{eff}), defined as the ratio of the maximum phase to gain change estimated directly form the measurement as $\alpha_{eff} = \Delta\varphi / \Delta G$, is equal to 3 at the probe wavelength, while the α-factor (α_0) is equal to 4.5. Figure 8-3 shows the wavelength dependency of the effective α-factor, the recovery time and the maximum dynamic gain and phase change.

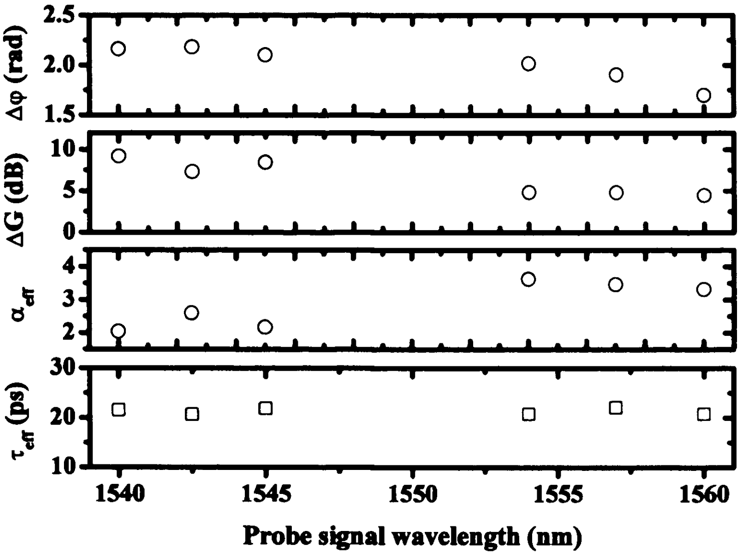

Figure 8-3 CIP SOA dynamics characterisation dependence on wavelength

8.2.3 LUCENT SOA

The SOA is a high confinement factor, 2.6mm long bulk structure designed, manufactured and packaged at Bell labs, Lucent technologies [Dre02]. The small signal gain is 18dB and the saturated output power 12dBm.

SOA Static gain transfer function measurements: The experimental set-up for the measurements is shown in Figure 4-1. The SOA gain transfer function was measured at the probe signal wavelength (λ_{probe} = 1550nm), for different SOA bias current levels (I_{bias}), the pump signal was disenabled.

Figure 8-4(a) shows the SOA gain transfer function measured for different bias current levels. Figure 8-4(b) shows the SOA output power measured for different bias current levels. The SOA PDL was 0.5dB at 400mA.

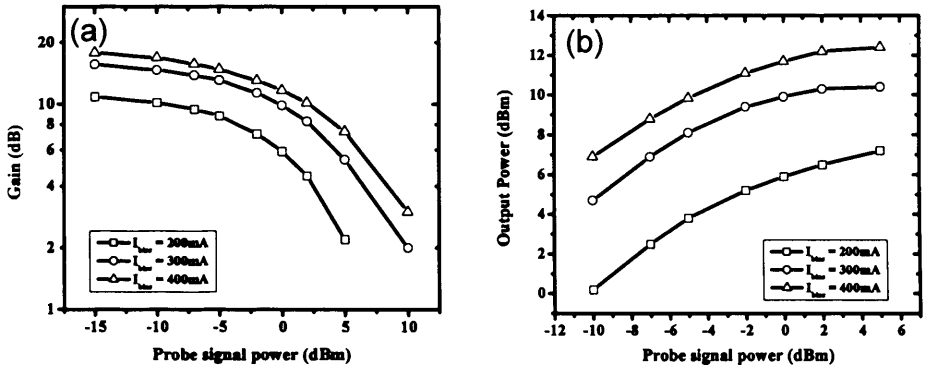

Figure 8-4 Lucent SOA gain (a) and output power (b) transfer function measured for different SOA bias current levels

SOA gain and phase dynamics and α-factor measurements: The SOA gain dynamic transfer function and α-factor were measured at the probe signal wavelength (λ_{probe} = 1550nm), while the pump signal (λ_{pump} = 1545nm) is used to clamp the SOA gain at different gain level. The pump signal power was 6dBm and the probe signal power was -14dBm.

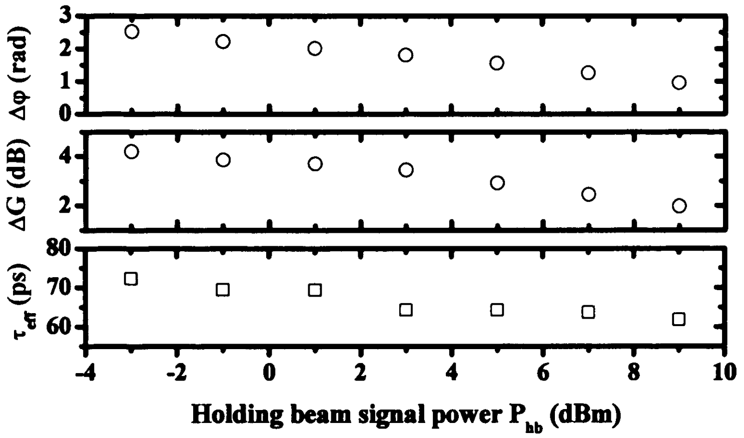

Figure 8-5 Lucent SOA dynamics characterisation for different holding beam signal power levels

Following the terminology introduced in chapter 4; Figure 8-2 shows the maximum dynamic gain (ΔG) phase (Δφ) change induced by the pump pulse, and the effective recovery time (τ_{eff}) as a function of the holding beam power. The effective α-factor (α_{eff}), defined as the ratio of the maximum phase to gain change estimated directly form the measurement as $\alpha_{eff} = \Delta\varphi/\Delta G$, is equal to 4.7, while α-factor (α_0) is equal to 6.

8.3 Appendix 3: 10 and 40Gb/s transmitter and receiver

In this appendix, the design of the 10Gb/s and 40Gb/s transmitter and receiver used in the experiments reported in chapter 4-6 is described in detail.

8.3.1 40Gb/s transmitter and receiver experimental set-up

40Gb/s EDTM RZ transmitter: The 40Gbit/s RZ signal was generated using a 40Gbit/s pulse pattern generator (PPG) as shown in Figure 8-6. The electrical signal from a 40Gbit/s PPG was used to drive a single electro-absorption modulator (EAM) which modulated the constant wavelength (CW) signal from the external cavity laser (ECL), with side-mode suppression of greater than 60dB. The resultant 2^{31}-1 PRBS 40Gbit/s NRZ optical signal had an extinction ratio of 16dB. The NRZ signal was fed into a second EAM driven by a 40GHz clock signal also obtained from the pattern generator, resulting in a RZ signal of pulsewidth 11.25ps (FWHM) as measured on an autocorrelator [Mik03a]. The extinction ratio of the TDM RZ signal, measured using an autocorrelator, was approximately 30dB [Mik03a]. The Q-factor of the RZ transmitter output signal is 24dB, and the OSNR 38 (dB/0.07nm).

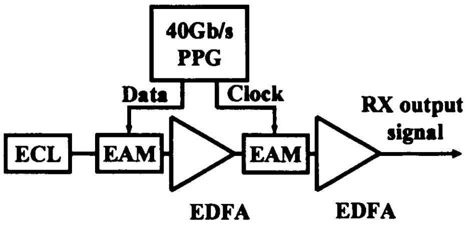

Figure 8-6 40Gbit/s ETDM RZ transmitter

40Gb/s receiver and clock recovery: The 40Gb/s RZ receiver consists of a data receiver and a clock recovery receiver as shown in Figure 8-7. The data receiver consists of a broadband photo-detector (3dB bandwidth = 60GHz) followed by a RF amplifier (3dB bandwidth = 45GHz) and a 40Gb/s electrical demultiplexer and BER counter. An optically pre-amplifier EDFA front end [Ber93], shown in Figure 8-8, was used at the photodetector input to enhance the receiver sensitivity.

The clock recovery receiver consists of a broadband photo-detector (3dB bandwidth = 60GHz) followed by of a 40G phase locked loop which generated a 20GHz clock directly from a 40Gb/s RZ input signal. A frequency doubler (20GHz to 40GHz) and a 40GHz RF amplifier (3dB bandwidth = 45GHz) was then used to synchronise the electrical demultiplexer to the incoming data signal. An optically pre-amplifier EDFA front-end was also used at the clock recovery photodetector input to enhance its sensitivity.

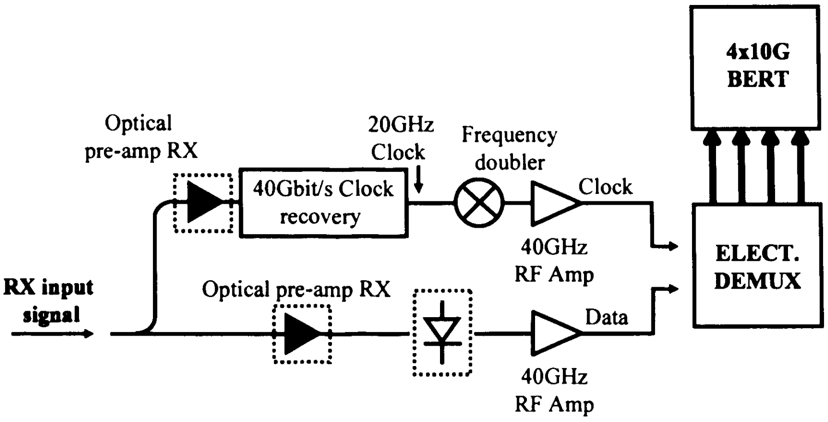

Figure 8-7 Electrical demultiplexer and receiver experimental set-up

The pre-amplifier EDFA front-end (PA-RX) is shown in Figure 8-8. It consists of a chain of 2 EDFAs with optical filters (hyperbolic shape with 1nm bandwidth) followed by two variable attenuators. The OSA is used to monitor the photodetector input signal power and OSNR.

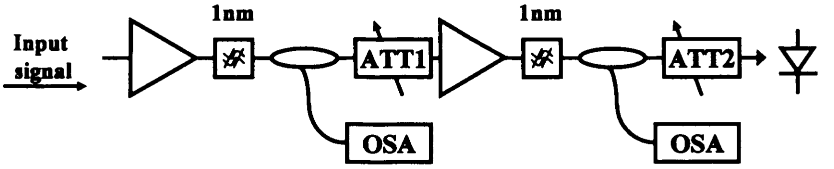

Figure 8-8 Optically pre-amplified front end experimental set-up (PA-RX)

The transmitter RZ signal spectrum, eye diagram and back-to-back BER measurement are show in Figure 8-9.

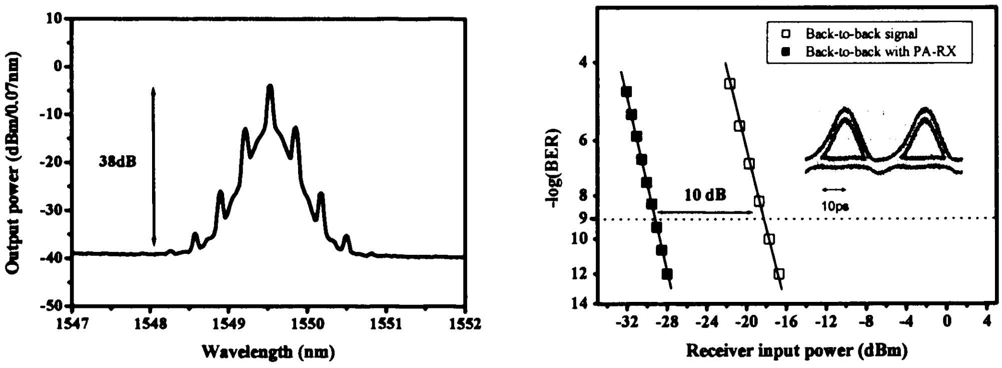

Figure 8-9 (a) 40Gb/s RZ signal OSNR; (b) Eye diagram and back-to-back BER measurements

8.3.2 10Gb/s Transmission systems experimental set-up

10Gb/s RZ transmitter: The 10Gbit/s RZ signal was generated using a 10Gbit/s pulse pattern generator (PPG) as shown in Figure 8-10. The electrical signal from a 10Gbit/s PPG was used to drive a Mach-Zehnder (MZI) which modulated a constant wavelength (CW) signal from the external cavity laser (ECL) with side-mode suppression greater than 60dB.

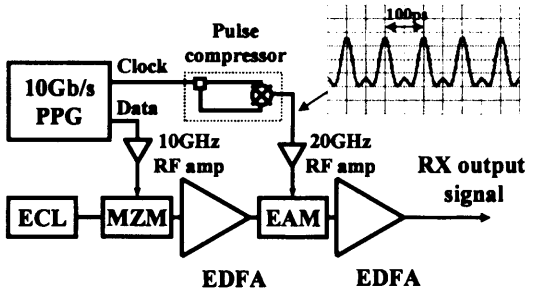

Figure 8-10 10Gbit/s ETDM transmitter

The resultant 2^{31}-1 PRBS 40Gbit/s NRZ optical signal had an extinction ratio of 15dB. The NRZ signal was fed into a second EAM driven by a 10GHz electrical signal obtained from the pattern generator and a pulse compressor [El197]. The resulting RZ optical signal had a pulsewidth 15ps (FWHM) and an extinction ratio of 18dB, as measured on an autocorrelator [Mik03a]. The Q-factor of the RZ transmitter output signal is 30dB, and the OSNR 45 (dB/0.02nm).

10Gb/s receiver and clock recovery: The 10Gb/s RZ receiver consists of a data receiver and a clock recovery receiver as shown in Figure 8-11. The data receiver consists of a broadband photo-detector (3dB bandwidth = 20GHz) followed by a RF amplifier (3dB bandwidth = 20GHz) and a 10Gb/s BER counter.

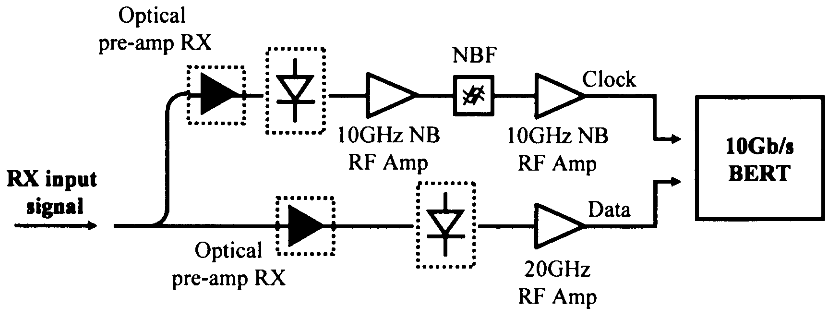

Figure 8-11 Electrical demultiplexer and receiver experimental set-up

The optically pre-amplifier EDFA front-end, shown in Figure 8-8, was used at the photodetector input to enhance the receiver sensitivity.

The clock recovery receiver consists of a broadband photo-detector (3dB bandwidth = 20GHz) followed by of a 10GHz narrow band filter (3dB BW = 30MHz) for clock recovery. An optically pre-amplifier EDFA front-end, shown in Figure 8-8, was also used at the clock recovery photodetector input to enhance its sensitivity. The transmitter RZ signal spectrum, eye diagram and back-to-back BER measurement are show in Figure 8-12.

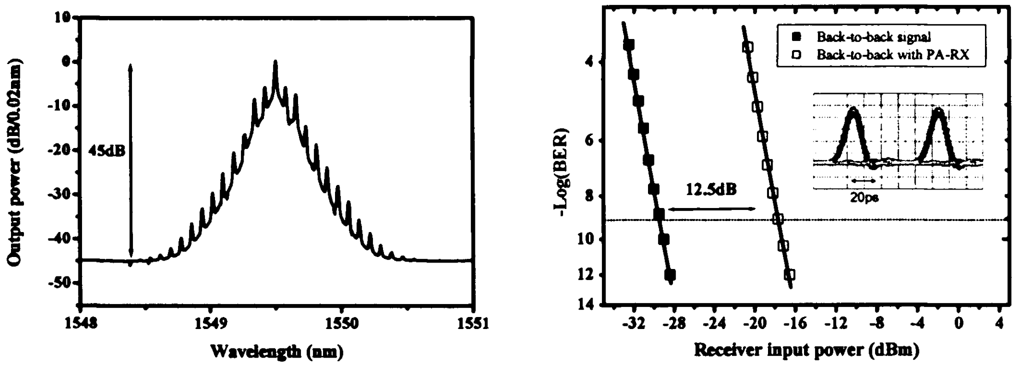

Figure 8-12 (a) 40Gb/s RZ signal OSNR; (b) Eye diagram and back-to-back BER measurements

8.4 Appendix 3: SOA array characterisation

This appendix contains the characterisation measurements performed on the SOA array used for the experiments presented in chapter 4 and 5. the SOA array module was designed manufactured and packaged by Bell Labs, Lucent technologies. The SOA array, described in details in chapter 4, consists of 22-channel SOA array monolithically integrated with 2X22 channels WGR (Waveguide Grating Router), extending the design reported in [Zir94]. The SOAs are quantum well structures 1.6mm long spaced by 100μm [Joy99]; these are not yet designed for polarization independent operation and currently amplify TE polarized light predominantly. The packaged fibre-pigtailed module used in the experiments presented in this thesis is shown in Figure 4-23(a). Figure 8-13 shows the SOA array amplified spontaneous emission (ASE) spectrum at the WGR output measured over 5 free spectral rages (FSR) (1530-1623nm) for 20 channels operating simultaneously (SOA bias 75mA).

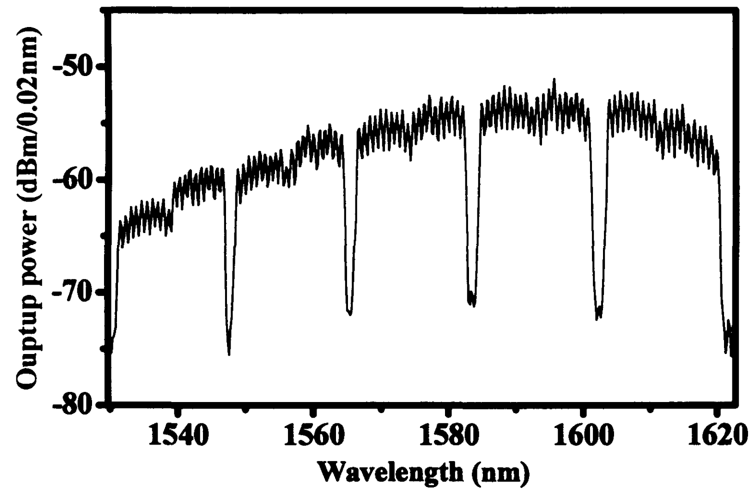

Figure 8-13 SOA array ASE at the WGR output measured over 5 FSR for 20 channels operating simultaneously (SOA bias 75mA)

Gain saturation and spectral profile measurements: The gain saturation or static gain transfer function was measured using the probe experimental set-up shown in Figure 8-14. To each WGR channel corresponds a single SOA in the array. Once a channel was selected and the probe wavelength tuned accordingly, then the input signal probe power was varied and the SOA output power was measured at the WGR output with an OSA (1nm resolution).

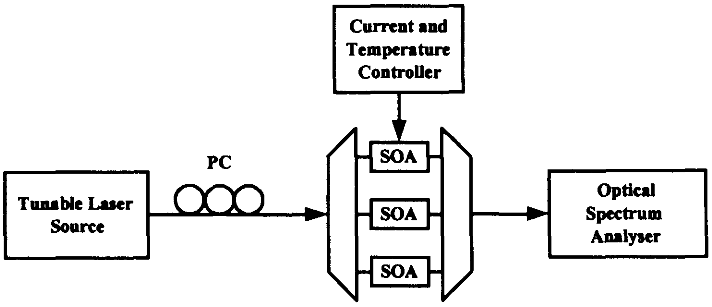

Figure 8-14 SOA gain transfer function measurement experimental set-up

Figure 8-15 shows the gain saturation transfer function of the SOA in the array corresponding the probe wavelength 1555.7nm measured for different SOA currents.

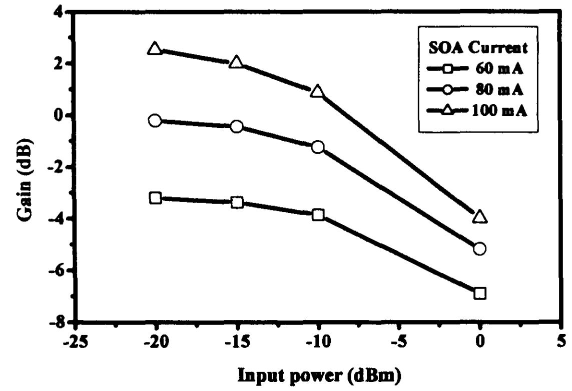

Figure 8-15 SOA gain transfer function measured for different SOA bias currents

Figure 8-16 shows SOA array spectral profile; this was obtained by measuring the gain characteristics of each individual SOA in the array with different input probe power. The SOA array PDL was measured to be 45dB. For bias currents of 100mA the SOA array module operates with gain over the C and L band.

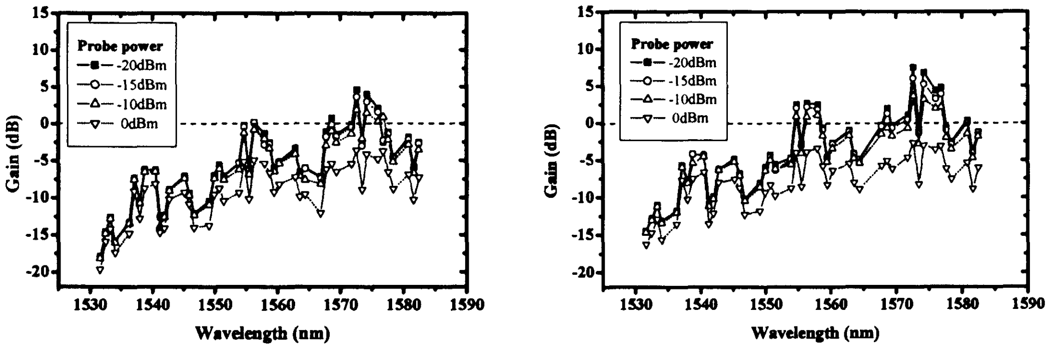

Figure 8-16 Gain spectral profile measured at 80mA (a) and 100mA (b) bias currents

SOA frequency response: Due to the complexity of the structure of the SOA array module, the gain dynamics can not be measured as described in chapter 4. Thus, to have an indication of the recovery time of the SOAs in the array, the gain frequency response was measured with a lightwave component analyser as shown in Figure 8-17.

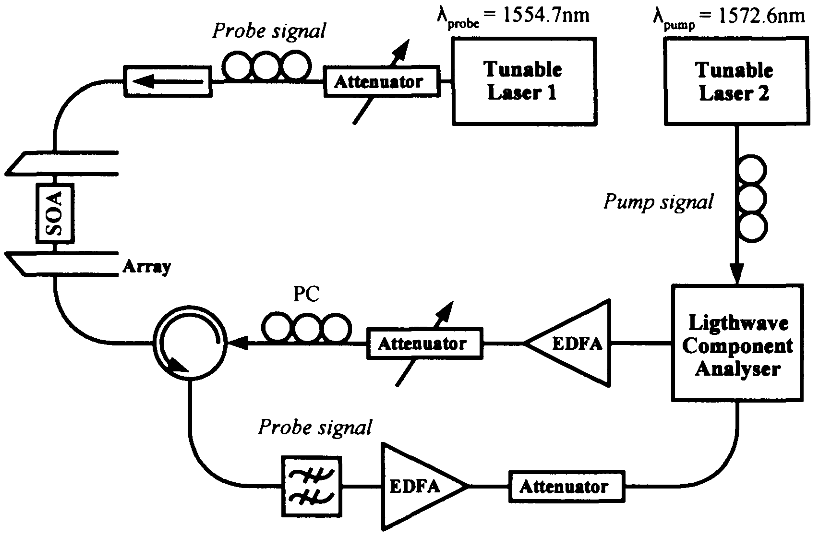

Figure 8-17 SOA frequency response experimental set-up

The pump and probe wavelength were tuned to the same WGR channel; the pump wavelengths is λ_{pump} = 1572.6.8, and the probe λ_{probe} = 1554.7. The pump power at the SOA input was +5dB and the probe power -5dBm. The pump and probe signals are routed by the WGR to the same SOA in the array corresponding the selected WGR channel.

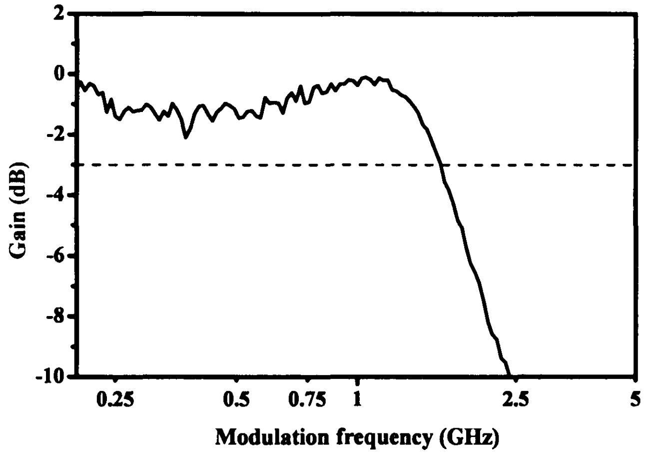

Figure 8-18 Frequency response of a selected SOA in the array

Measurement of the nonlinear modulation imparted by the pump signal into the probe signal in the SOA was obtained with a 20GHz ligthwave component analyser, and it is shown in Figure 8-18. The SOA gain recovery time, estimated from the 3dB bandwidth of the SOA frequency response [Mar97a], was 500ps.

8.5 Appendix 4: Glossary

3R	Re-shaping, Re-amplifying, Re-timing
AJ	Amplitude Jitter
AM	Amplitude Modulation
AOM	Acousto-Optic-Modulator
ASE	Amplifier Spontaneous Emission
ATT	Attenuator
AWG	Arrayed Waveguide Grating
BER	Bit-Error-Rate
BERT	Bit-Error-Rate Test-set
BPSK	Binary Phase Shif-Keying
CW	Continuous Wave
DCA	Digital communication analyser
DCF	Dispersion Compensating Fibre
DFB	Distributed Feedback Laser
DGF	Different Frequency Generation
DI	Delay Interferometer
DOM-MZI	Differential Operating Mode Mach-Zehnder Interferomter
DR^2FL	Dynamically Reconfigurable Recirculation Fibre Loop
EAM	Electro Absorption Modulator
ECL	External Cavity Laser
EDFA	Erbium Doped Fibre Amplifier
ETDM	Electrical Time-Division-Multiplexer
FBG	Fibre Bragg Grating
FSR	Free Spectral Range
FWHM	Full Width Half Maximum
FWM	Four-Wave-Mixing
HNLF	Highly Non-Linear Fibre
IFWM	Intra-channel Four-Wave-Mixing
ISI	Inter-Symbol-Interference
MEMS	Micro-Electro-Mechanical Systems
MI	Michelson Interferometer
MLL	Mode-Locked laser
MUX	Multiplexer
MZI	Mach-Zehnder interferometer
NF	Noise Figure
NRZ	Non-Return-to-Zero
NZDSF	Non-Zero Dispersion Shifted Fibre
OC	Optical Circulator

ODL	Optical Delay Line
OOK	On-Off Keying
OSA	Optical Spectrum Analyser
OSNR	Optical Signal-to-Noise Ratio
OTDM	Optical Time-Division-Multiplexer
PA-RX	Pre-Amplified Optical Receiver
PBS	Polarisation Beam Splitter
PC	Polarisation Controller
PDL	Polarisation Dependent Loss
PLL	Phase Locked Loop
PMD	Polarisation Mode Dispersion
PMF	Polarisation Mode Fibre
POL	Polariser
PPG	Pulse Pattern Generator
PRBS	Pseudo-Random Bit Sequence
PSSI	Polarisation Switching in Sagnac Interferometer
RMS	Root Mean Square
RX	Receiver
SBS	Stimulated Brillouin Scattering
SC	Switching Contrast
SMF	Standard Single Mode Fibre
SNR	Signal-to-Noise Ratio
SOA	Semiconductor Optical Amplifier
SPM	Self-Phase Modulation
SRS	Stimulated Raman Scattering
TE	Transverse Electric
TF	Transfer Function
TL	Tuneable Laser
TM	Transverse Magnetic
TOAD	Terahertz Optical Asymmetric Demultiplexer
TWRS	True Wave Reduced Slope
TX	Transmitter
UNI	Ultra-fast Nonlinear Interferometer
WDM	Wavelength Division Multiplexing
WGR	Waveguide Grating Router
XGM	Cross-Gain Modulation
XPM	Cross-Phase Modulation

Chapter 9 References

[Agr86] G. P. Agrawal and N. K. Dutta, "Long-wavelength Semiconductor laser", Van Nostrand Reinhold, New York, 1986

[Agr89] G.P. Agrawal and N.A. Olsson, "Self-phase modulation and spectral broadening of optical pulses in semiconductor laser amplifiers", IEEE Journal of Quantum Electronics, Volume 25, Issue 11, Nov. 1989, Pages: 2297 – 2306

[Agr95] G. P. Agrawal, "Nonlinear fiber optics", Academic Press, San Diego, 1995

[Agr02] G. P. Agrawal, "Fiber-optic communication systems", John Wiley & Sons Inc., New York, 2002

[Arm05] I. Armstrong, I. Andonovic, A.E. Kelly, S. Bonthron, J. Bebbington, C. Michie, C. Tombling, S. Fasham and W. Johnstone, "Hybridization platform assembly and demonstration of all-optical wavelength conversion at 10 Gb/s", Journal of Lightwave Technology, Volume 23, Issue 5, May 2005, Pages: 1852 – 1859

[Ber93] N.S. Bergano, F.W. Kerfoot and C.R. Davidsion, "Margin measurements in optical amplifier system", IEEE Photonics Technology Letters, Volume 5, Issue 3, March 1993, Pages: 304 – 306

[Ber95] N.S. Bergano and C.R. Davidson, "Circulating loop transmission experiments for the study of long-haul transmission systems using erbium-doped fiber amplifiers", Journal of Lightwave Technology, Volume 13, Issue 5, May 1995, Pages: 879 – 888

[Bis02a] S. Bischoff and L. Mork, "Reduction of pattern effects in SOA-based all-optical switches by using cross-gain modulated holding signal", in Proc. Lasers and Electro-Optics Conference (CLEO 2002), Long Beach (USA), 19-24 May 2002, Paper CWA53

[Bis02b] S. Bischoff, B. Lading and J. Mork, "BER estimation for all-optical regenerators influenced by pattern effects", IEEE Photonics Technology Letters, Volume 14, Issue 1, Jan. 2002, Pages: 33 – 35

[Bis04] S. Bischoff, M.L. Nielsen and J. Mork, "Improving the all-optical response of SOAs using a modulated holding signal", Journal of Lightwave Technology, Volume 22, Issue 5, May 2004, Pages: 1303 – 1308

[Blu03] D.J. Blumenthal, J.E. Bowers, L. Rau, H. Chou, S. Rangarajan, W. Wang, and H.N. Poulsen, "Optical signal processing for optical packet switching networks," Optical Communications, Volume 41, Number 2, Feb. 2003, Pages: S-23-S-29

[Boe05] C. Boerner, V. Marembert, S. Ferber, C. Schubert, C. Schmidt-Langhorst, R. Ludwig and H.G. Weber, "320 Gbit/s clock recovery with electro-optical PLL using a bidirectionally operated electroabsorption modulator as phase comparator", in Proc. Optical Fiber Communication Conference (OFC05), Anaheim (USA), 6-11 March 2005, Paper OTu03

[Bor04] C Bornholdt, J. Slovak and B. Sartorius, "Semiconductor-based all-optical 3R regenerator demonstrated at 40 Gbit/s", Electronics Letters, Volume 40, Issue 3, Feb. 2004, Pages: 192 – 194

[Bre97] D. Breuer and K. Petermann, "Comparison of NRZ and RZ modulation format for 40Gb/s TDM standard fibre systems", IEEE Photonics Technology letters, Vol.9, No.3, 1997, Pages: 398-400

[Bux98] A. Buxens, A.T. Clausen, H.N. Poulsen, K.S. Jepsen, K.E. Stubkjaer, C. Bornholdt, O. Brox, M. Mohrle, B. Sartorius, "40 to 10 Gbit/s demultiplexing using a self-pulsating DFB laser for clock recovery", in Proc. European Conference on Optical Communication (ECOC 1998), 20-24 Sept. 1998, Madrid (Spain), Volume 1, Pages: 507 - 508

[Che96] S. Chelles, F. Devaux, D. Meichenin, D. Sigogne, A. Ougazzaden and A. Carenco, "Polarization insensitive wavelength conversion by cross gain modulation in a strained MQW optical amplifier", in Proc. European Conference on Optical Communication (ECOC 1996), Oslo (Norway), 15-19 Sept. 1996, Paper ThB.2.5

[Cho00] P.S. Cho, P. Sinha, D. Mahgerefteh, and G.M. Carter, "All-optical regeneration at the receiver of 10-Gb/s RZ data transmitted over 30000 km using an electroabsorption modulator", IEEE Photonics Technology Letters, Volume 12, Issue 2, Feb. 2000, Pages: 205 – 207

[Chr98] A.R. Chraplyvy and R.W. Tkach, "Terabit/second transmission experiments", IEEE Journal of Quantum Electronics, Volume 34, Issue 11, Nov. 1998, Pages: 2103 – 2108

[CIP05] http://www.ciphotonics.com/

[Dag02] B. Dagens, A. Labrousse, S. Fabre, B. Martin, S. Squedin, B. Lavigne, R. Brenot, M. L. Nielsen and M. Renaud, "New modular SOA-based active-passive integrated Mach-Zehnder interferometer and frist stand mode 40Gb/s all-optical wavelgnth conversion in C-band", in Proc. European Conference on Optical Communication (ECOC 2002), 30 Sept. – 4 Oct. 2002, Copenhagen (Denmark), Paper PD3.1

[Dan96] S.L. Danielsen, C. Joergensen, M. Vaa, B. Mikkelsen, K.E. Stubkjaer, P. Doussiere and F.L. Pommerau, "Bit error rate assessment of 40 Gbit/s all-optical polarisation independent wavelength converter", Electronics Letters, Volume 32, Issue 18, 29 Aug. 1996, Page: 1688

[Dan98] S.L. Danielsen, P.B. Hansen, K.E. Stubkjaer, M. Schilling, K. Wunstel, W. Idler, P. Doussiere and F. Pommerau, "All optical wavelength conversion schemes for increased input power dynamic range", IEEE Photonics Technology Letters, Volume 10, Issue 1, Jan. 1998, Pages: 60 - 62

[Dav95a] D.A.O. Davies, "Small-signal analysis of wavelength conversion in semiconductor laser amplifiers via gain saturation", IEEE Photonics Technology Letters, Volume 7, Issue 6, June 1995, Pages: 617 – 619

[Dav95b] D.A.O. Davies, A.D. Ellis, T. Widdowson and G. Sherlock, "10 Gbit/s data switched semiconductor laser amplifier nonlinear loop mirror", Electronics Letters, Volume 31, Issue 2, 19 Jan. 1995, Pages: 111 - 112

[Die01] S. Diez, E. Hilliger, M. Kroh, C. Schmidt, C. Schubert, H. G. Weber, L. Occhi, L. Schares, G. Guekos and L. K. Oxenloewe, "Optimization of SOA-based Sagnac-interferometer switches for demultiplexing to 10 and 40 Gb/s", Optics Communications, Volume 189, Issues 4-6, March 2001, Pages: 241-249

[Doe03] C.R. Doerr, S. Chandrasekhar, P.J. Winzer, L.W. Stulz, A.R. Chraplyvy and R. Pafchek, "Simple multichannel optical equalizer for mitigating intersymbol interference", in Proc. Optical Fiber Communications Conference (OFC 2003), Atlanta (USA), 23-28 March 2003 Volume 3, Paper PD11

[Dor88] N.J. Doran and D. Wood, "Nonlineari-optical loop mirror", Optics letters, Volume 13, Number 1, Jan. 1988, Pages: 56-58

[Dot96] A. D'Ottavi, F. Martelli, P. Spano, A. Mecozzi, S. Scotti, R. Dall'Ara, J. Eckner and G. Guekos, "Very high efficient frou-wave mixing in a single semiconductor travelling-wave amplifier", Applied Physics Letters, Volume 68, Number 16, April 1996, Pages: 2186-2188

[Dre02] K. Dreyer, C.H. Joyner, J.L. Pleumeekers, C.A. Burrus, A. Dentai, B.I. Miller, S. Shunk, P. Sciortino, S. Chandrasekhar, L. Buhl, F. Storz and M. Farwell, "High-gain mode-adapted semiconductor optical amplifier with 12.4-dBm saturation output power at 1550 nm", Journal of Lightwave Technology, Volume 20, Issue 4, April 2002, Pages: 718 – 721

[Dup00] M.A. Dupertuis, J.L. Pleumeekers, T.P. Hessler, P.E. Selbmann, B. Deveaud, B. Dagens and J.Y. Emery, "Extremely fast high-gain and low-current SOA by optical speed-up at transparency", IEEE Photonics Technology Letters, Volume 12, Issue 11, Nov. 2000, Pages:1453 – 1455

[Dur92] T. Durhuus, B. Mikkelsen and K.E. Stubkjaer, "Detailed dynamic model for semiconductor optical amplifiers and their crosstalk and intermodulation distortion", Journal of Lightwave Technology, Volume 10, Issue 8, Aug. 1992, Pages: 1056 – 1065

[Dur94] T. Durhuus, C. Joergensen, B. Mikkelsen, R.J.S. Pedersen and K.E. Stubkjaer, "All optical wavelength conversion by SOA's in a Mach-Zehnder configuration", IEEE Photonics Technology Letters, Volume 6, Issue 1, Jan. 1994, Pages: 53 – 55

[Dur96] T. Durhuus, B. Mikkelsen, C. Joergensen, S. Danielsen and K.E. Stubkjaer, "All-optical wavelength conversion by semiconductor optical amplifiers", Journal of Lightwave Technology, Volume 14, Issue 6, June 1996, Pages: 942 – 954

[Eis89] G. Eisenstein, R. S. Tucker, J. M. Wiesenfeld, P. B. Hansen, G. Raybon, B. C. Johnson, T. J. Bridges, F. G. Storz, and C. A. Burrus; "Gain recovery time of traveling-wave semiconductor optical amplifiers", Applied Physics Letters, Volume 54, Issue 5, Jan. 1989, Pages: 454 – 456

[Eis92] M. Eiselt, "Optical loop mirror with semiconductor laser amplifier", Electronics Letters, Volume 28, Issue 16, July 1992, Pages: 1505 – 1507

[Eis93] M. Eiselt, W. Pieper and H.G. Weber, "Decision gate for all-optical data retiming using a semiconductor laser amplifier in a loop mirror configuration", Electronics Letters, Volume 29, Issue 1, Jan 1993, Page: 107

[Eis95] M. Eiselt, W. Pieper and H.G. Weber, "SLALOM: semiconductor laser amplifier in a loop mirror", Journal of Lightwave Technology, Volume 13, Issue 10, Oct. 1995, Pages: 2099 – 2112

[Ell95] A.D. Ellis, D.M. Patrick, D. Flannery, R.J. Manning, D.A.O. Davies, and D.M. Spirit, "Ultra-high-speed OTDM networks using semiconductor amplifier-based processing nodes", Journal of

Lightwave Technology, Volume 13, Issue 5, May 1995, Pages: 761 – 770

[Ell97] A. Ellis, "All optical networking beyond 10Gb/s; OTDM networks based on electro-optic modulators and fibre ring laser", PhD thesis submitted to the University of Aston, April 1997

[Ell98] A.D. Ellis, A.E. Kelly, D. Nesset, D. Pitcher, D.G. Moodie and R. Kashyap, "Error free 100 Gbit/s wavelength conversion using grating assisted cross-gain modulation in 2 mm long semiconductor amplifier", Electronics Letters, Volume 34, Issue 20, Oct. 1998, Pages: 1958 – 1959

[Ess99] R. J. Essiambre, B. Mikkelsen and G. Raybon, "Intra-channel cross-phase modulation and four-wave mixing in high-speed TDM systems", Electronics Letters, Volume 35, Number 18, 1999, Pages: 1576-1578

[Fen02] J.G. Fenn, M. Mazilu, A.G. Iglesias and A. Miller, "Ultrafast dynamics in semiconductor optical amplifiers with implications for interferometric switching", in Proc. Annual meeting of the IEEE Lasers and Electro-Optics Society (LEOS 2002), 10-14 Nov. 2002, Glasgow (Scotland), Volume 2, Paper WE3

[Fis99] S. Fischer, M. Dulk, E. Gamper, W. Vogt, E. Gini, H. Melchior, W. Hunziker, D. Nessetand and A.D. Ellis, "Optical 3R regenerator for 40 Gbit/s networks", Electronics Letters, Volume 35, Issue 23, 11 Nov. 1999, Pages: 2047 – 2049

[Gam98] P. Gambini, M. Renaud, C. Guillemot, F. Callegati, I. Andonovic, B. Bostica, D. Chiaroni, G. Corazza, S.L. Danielsen, P. Gravey, P.B. Hansen, M. Henry, C. Janz, A. Kloch, R. Krahenbuhl, C. Raffaelli, M. Schilling, A. Talneau and L. Zucchelli, "Transparent optical packet switching: network architecture and demonstrators in the KEOPS project", IEEE Journal on Selected Areas in Communications, Volume 16, Issue 7, Sept. 1998 Pages: 1245 – 1259

[Gav01] G. Gavioli and P. Bayvel, "Investigation and comparison of high-speed synchronisation techniques for optical packet networks", in Proc. Network and Optical Communications (NOC 2001), 10 June 2001, Ipswich (UK), Pages: 311-316

[Gav02] G. Gavioli and P. Bayvel, "A novel high-stability 3R all-optical regenerator based on polarisation switching in semiconductor optical amplifier", in Proc. European Conference on Optical Communication (ECOC 2002), 30 Sept. – 4 Oct. 2002, Copenhagen (Denmark), Paper We.7.3.2

[Gav03a] G. Gavioli and P. Bayvel, "Novel, 3R regenerator based on polarisation switching in a semiconductor optical amplifier-assisted fibre Sagnac interferometer", IEEE Photonics Technology Letters, Volume 15, Number 9, Sept. 2003, Pages: 1261-1263

[Gav03b] G. Gavioli, V. Mikhailov and P. Bayvel, "Novel, all-optical demultiplexer based on polarisation switching in a semiconductor optical amplifier", In Proc. Conference on Laser and Electro-Optics (CLEO 2003), 23-27 June 2003, Baltimore (USA), Paper CThQ7

[Gav03c] G. Gavioli and P. Bayvel, "Multichannel All-optical Regenerative Wavelength Conversion using an Integrated Semiconductor optical Amplifier Array", In Proc. Annual meeting of the IEEE Lasers and

Electro-Optics Society (LEOS 2003), 26-30 October 2003, Tucson (USA), Paper ThO5

[Gav04a] G. Gavioli and P. Bayvel, "Amplitude jitter suppression using a patterning–tolerant, all-optical 3R regenerator", Electronics Letters, Volume 40, Number 11, May 2004, Pages: 688 – 690

[Gav04b] G. Gavioli, V. Mikhailov and P. Bayvel, "Multichannel wavelength conversion and regeneration using an array of SOA and a multichannel optical equalizer", in Proc. 30th European Conference on Optical Communication (ECOC 2004), 5-9 September 2004, Stockholm (Sweden), Paper Tu4.4.4

[Gav05a] G. Gavioli, V. Mikhailov, B. Thomsen and P. Bayvel, "Investigation of Cascadability and Optimum Inter-Regenerator Spacing in Transmission with All-Optical 3R Regeneration", In Proc. Conference on Laser and Electro-Optics (CLEO 2005), 24-26 May 2005, Baltimore (USA), Paper CMQ5

[Gav05b] G. Gavioli, V. Mikhailov, B. Thomsen and P. Bayvel, "Investigation of fibre launch power margin in 40 Gb/s transmission with all-optical regeneration", in Proc. European Conference on Optical Communication (ECOC 2005), 25-29 Sept. 2005, Glasgow (Scotland), Paper Tu3.3.2

[Gav05c] G. Gavioli, V. Mikhailov, B. Thomsen and P. Bayvel, "Investigation of transmission with cascaded all-optical 3R regenerators and variable inter-regenerator spacing", Electronics Letters, Volume 41, Number 3, Feb. 2005, Pages: 146 – 148

[Ger97] D.F. Geraghty, R.B. Lee, M. Verdiell, M. Ziari, A. Mathur and K.J. Vahala, "Wavelength conversion for WDM communication systems using four-wave mixing in semiconductor optical amplifiers", IEEE Journal of Selected Topics in Quantum Electronics, Volume 3, Issue 5, Oct. 1997, Pages: 1146 – 1155

[Gle94] I. Glesk, J.P. Sokoloff, and P.R. Prucnal, "Demonstration of all-optical demultiplexing of TDM data at 250 Gbit/s", Electronics Letters, Volume 30, Issue 4, Feb. 1994, Pages: 339 – 341

[Gna96] A.H. Gnauuck, A.R. Chraplyvy, R.W. Tkach, J.L. Zyskind, J.W. Sulhoff. A.J. Lucero, Y.Sun, R.M. Jopson, F.Forghieri, R.M. Derosier, C.Wolf and A.R. Mc-Cormick; "One terabit/s transmission experiment", in Proc. Optical Fiber Communication Conference (OFC96), 25 Feb. - 1 March 1996, San Jose (USA), Paper PD20.1

[Gor86] J. P. Gordon and H. A. Haus, "Random walk of coherently amplified solitons in optical fiber transmission," Optics Letters, Volume 11, Oct. 1986, Pages: 665-667

[Gro02] D. F. Grosz, A. Agarwal, S. Banerjee, A. P. Kung, D. N. Maywar, A. Gurevich, T.H. Wood, C.R. Lima, B. Faer, J. Black and C. Hwu, "5.12 Tb/s (128 x 42.7 Gb/s) Transmission with 0.8 bit/s/Hz Spectral Efficiency over 1280 km of Standard Single-Mode Fiber Using All-Raman Amplification and Strong Signal Filtering", in Proc. European Conference on Optical Communication (ECOC 2002), 30 Sept. – 4 Oct. 2002, Copenhagen (Denmark), Paper PD4.3

[Hal99] K.L. Hall and B.S. Robinson, "Bit error rate characterization of 100 Gb/s all-optical demultiplexers", in Proc. Conference on Laser and

Electro-Optics (CLEO 1999), 23-28 May 1999, Baltimore (USA), Paper CTuW1

[Ham02] S.A. Hamilton, B.S. Robinson, T.E. Murphy, S.J. Savage and E.P. Ippen, "100 Gb/s optical time-division multiplexed networks", Journal of Lightwave Technology, Volume 20, Issue 12, Dec. 2002, Pages: 2086 - 2100

[Har83] C. Harder, K. Vahala and A. Yariv, "Measurement of the linewidth enhancement factor α of semiconductor lasers", Applied Physics Letters, Volume 42, Issue 4, Feb. 1983, Pages: 328-330

[Has93] T. Hasegawa, K. Inoue and K. Oda, "Polarization independent frequency conversion by fiber four-wave mixing with a polarization diversity technique", Photonics Technology Letters, IEEE, Volume 5, Issue 8, Aug. 1993, Pages: 947 – 949

[Has03] Y. Hashimoto, R. Kuribayashi, S. Najamura, K. Tajima and I.Ogura, "Transmission at 40Gbps with Semiconductor-based Optical 3R Regenerator", In Proc. European Conference on Optical Communication (ECOC 2003), 21-25 Sept. 2003, Rimini (Italy), Paper Mo4.3.3

[Hen82] C. Henry, "Theory of the linewidth of semiconductor lasers", IEEE Journal of Quantum Electronics, Volume 18, Issue 2, Feb. 1982, Pages: 259 – 264

[Hil02] M.T. Hill, E. Tangdiongga, H. de Waardt, G. D. Khoe and H. J. S. Dorren, "Carrier recovery time in semiconductor optical amplifiers that employ holding beams", Optics Letters, Volume 27, Number 18, Sept. 2002, Pages: 1625- 1627

[Hod91] T.G. Hodgkinson and R.P. Webb, "Carrier-density modulation effects in a traveling-wave semiconductor optical amplifier: communications theory analysis and experiment", Journal of Lightwave Technology, Volume 9, Issue 5, May 1991, Pages: 605 – 622

[Hul91] C. T. Hultgren and E. P. Ippen, "Ultrafast refractive index dynamics in AlGaAs diode laser amplifiers", Applied Physics Letters, Volume 59, Issue 6, Aug.1991, Pages: 635-637

[Hum91] P.A. Humblet and M. Azizoglu, "On the bit error rate of lightwave systems with optical amplifiers", Journal of Lightwave Technology, Volume 9, Issue 11, Nov. 1991, Pages: 1576 – 1582

[Idl95] W. Idler, M. Schilling, K. Daub, D. Baums, U. Korner, E. Lach, E. Laube and K. Wunstel, "Signal quality and BER performance improvement by wavelength conversion with an integrated three-port Mach-Zehnder interferometer", Electronics Letters, Volume 31, Issue 6, 16 March 1995, Pages: 454 – 455

[Idl96] W. Idler, K. Daub, G. Laube, M. Schilling, P. Wiedemann, K. Dutting, M. Klenk, E. Lach and K. Wunstel, "10 Gb/s wavelength conversion with integrated multiquantum-well-based 3-port Mach-Zehnder interferometer", IEEE Photonics Technology Letters, Volume 8, Issue 9, Sept. 1996, Pages: 1163 – 1165

[Ino03] R. Inohara, M. Tsurusawa, K. Nishimura and M. Usami, "Experimental verisfication for cascadeability of all-optical 3R regenerator utilizing two-stage SOA-based polarisation discriminator switches with estimated Q-factor over 20 dB at 40Gbit/s transmission", In Proc. European Conference on Optical Communication (ECOC 2003), 21-25 Sept. 2003, Rimini (Italy), Paper Mo4.3.2

[Ito01] T. Ito, I. Ogawa, Y. Suzaki, K. Magari, Y. Kawaguchi, Y. Suzuki, N. Ishihara, " Eight-channel Simultaneous Wavelength Conversion From Equal to Unequal Channel Spacing", IEEE Photonics Technology Letters, Volume 13, Number 10, Oct. 2001, Pages: 1106-1108

[Jah96] E. Jahn, N. Agrawal, H. Ehrke, R. Ludwig, W. Pieper and H.G. Weber, "Monolithically integrated asymmetric Mach-Zehnder interferometer as a 20 Gbit/s all-optical add/drop multiplexer for OTDM systems", Electronics Letters, Volume 32, Issue 3, Feb. 1996, Pages: 216 – 217

[Jin94] M. Jinno, "Effects of crosstalk and timing jitter on all-optical time-division demultiplexing using a nonlinear fiber Sagnac interferometer switch", IEEE Journal of Quantum Electronics, Volume 30, Issue 12, Dec. 1994, Pages:2842 – 2853

[Joy99] H. Joyner, C.R. Doerr, L.W. Stulz, M. Zirngibl and J.C. Centanni: "Low-threshold nine-channel waveguide grating router-based continuous wave transmitter", IEEE Journal of Lightwave Technology, 1999, Volume 17, Issue 4, Pages: 647-651

[Kam02] I. Kaminow and T. Koch, "Optical fiber telecommunications IVB", Academic Press, San Diego, 2002

[Kam05] http://www.kamelian.com/

[Kan93] D.J. Kane and R. Trebino, "Characterization of arbitrary femtosecond pulses using frequency-resolved optical gating", IEEE Journal of Quantum Electronics, Volume 29, Issue 2, Feb. 1993, Pages: 571 – 579

[Kan95] K.I. Kang, T.G. Chang, I. Glesk, P.R. Prucnal and R.K. Boncek, "Demonstration of ultrafst, all-optical, low control energy, single wavelength, polarisation independent, cascadable, and integrable switch", Applied Physics Letters, Volume 67, Issue 5, April 1995, Pages: 604 – 607,

[Kan99] J. Kani, T. Sakamoto, M. Jinno, K. Hattori, M. Yamada, T. Kanamori and K. Oguchi, "Novel 1470-nm-band WDM transmission and its application to ultra-wide-band WDM transmission", IEICE Transactions on Communications, Volume E82-B, Aug. 1999, Pages: 1131-1139

[Kan04] I. Kang and C. Dorrer, "Measurements of gain and phase dynamics of a semiconductor optical amplifier using spectrograms", in Proc. Optical Fiber Communications Conference (OFC 2004), 23-28 March, Atlanta (USA), Paper MF43

[Kav99] S. Kawanishi, H. Takara, K. Uchiyama, I. Shake and K. Mori, "3 Tbit/s (160 Gbit/s×19 channel) optical TDM and WDM transmission experiment", Electronics Letters, Volume 35, Issue 10, May 1999, Pages: 826-827

[Kaw97] S. Kawanishi, K. Okamoto, M. Ishii, O. Kamatani, H. Takara and K. Uchiyama, "All-optical time-division-multiplexing of 100 Gbit/s signal based on four-wave mixing in a travelling-wave semiconductor laser amplifier", Electronics Letters, Volume 33, Issue 11, May 1997, Pages: 976 - 977

[Kei99] G.E. Keiser, "A review of WDM technology and applications", Optical Fibre Technology, Volume 5, Issue 5, 1999, Pages: 3-39

[Kel99] A.E. Kelly, I.D. Phillips, R.J. Manning, A.D. Ellis, D. Nesset, D.G. Moodie, and R. Kashyap, "80 Gbit/s all-optical regenerative wavelength conversion using semiconductor optical amplifier based interferometer", Electronics Letters, Volume 35, Issue 17, Aug. 1999, Pages: 1477 - 1478

[Kes87] M. P. Kesler and E. P. Ippen, "Subpicosecond gain dynamics in GaAlAs laser diodes", Applied Physics Letters, Volume 51, Issue 22, Nov. 1987, Pages: 1765-1767

[Kho05] R. Khosravani, "Timing-jitter in high bit-rate WDM communication systems due to PMD-nonlinearity interaction", In Proc. Optical Fiber Communication Conference (OFC 2005), 6-11 March 2005, Anaheim (USA), Paper OFF7

[Kil02] R.I. Killey, V. Mikhailov, S. Appathurai and P. Bayvel, "Investigation of nonlinear distortion in 40-Gb/s transmission with higher order mode fiber dispersion compensators", Journal of Lightwave Technology, Volume 20, Issue 12, Dec. 2002, Pages: 2282 – 2289

[Kit96] C. Kittel, "Introduction to Solid State Physics", John Wiley & Sons Inc., New York, 1996

[Lav98] B. Lavigne, D. Chiaroni, L. Hamon, C. Janz and A. Jourdan, "Experimental analysis of SOA-based 2R and 3R optical regeneration for future WDM networks", in Proc. Optical Fiber Communication Conference (OFC 1998), , 22-27 Feb. 1998, San Jose (USA), Paper Th07

[Lav00] B. Lavigne, P. Guerber, C. Janz, A. Jourdan and M. Renaud, "Full validation of an optical 3R regenerator at 20 Gbit/s", In Proc. Optical Fiber Communication Conference (OFC 2000), 7-11 March 2000, Baltimore (USA), Paper ThF7

[Lav01] B. Lavigne, P. Guerber, P. Brindel, E. Balmefrezol and B. Dagens, "Cascade of 100 optical 3R regenerators at 40Gbit/s based on all-active Mach Zehnder interferometers", In Proc. European Conference on Optical Communication (ECOC 2001), 1-3 Oct. 2001, Amsterdam (Netherlands), Paper We.F.2.6

[Lav02] B. Lavigne, E. Balmefrezol, P. Brindel, B. Dagens, L. Pierre, P. Pecci, R. Brenot and O. Leclerc, "Operaion margins of 40Gb/s SOA-MZI used in differential scheme for optical 3R regneration" In Proc. European Conference on Optical Communication (ECOC 2002), 30 Sept. – 4 Oct. 2002, Copenhagen (Denmark), Paper PD 3.1

[Lav03] B. Lavigne, E. Balmefrezol, P. Brindel, B. Dagens, R. Brenot, L. Pierre, J. Moncelet, D. de la Grandiere, J. Remy, J. Bouley, B. Thedrez and O. Leclerc, "Low input power all-optical 3R regenerator based on SOA devices for 42.66 Gbit/s ULH WDM RZ transmissions with 23 dB span loss and all-EDFA amplification", In Proc. Optical Fiber Communications Conference (OFC 2003), 23-28 March 2003, Atlanta (USA), Paper PD15

[Lec03] O. Leclerc, B. Lavigne, E. Balmefrezol, P. Brindel, L. Pierre, D. Rouvillain and F. Seguineau, "Optical regeneration at 40 Gb/s and beyond", Journal of Lightwave Technology, Volume 21, Issue 11, Nov. 2003, Pages: 2779 – 2790

[Leu97] J. Leuthold, E. Gamper, M. Dulk, P.A. Besse, J. Eckner, R. Hess and H. Melchior, "Cascadable all-optical space switch with high and balanced extinction rations", in Proc. Optoelectronic and Communications Conference (OECC97), 8-11 July 97, Seoul (Korea), Pages: 184-185

[Leu98a] J. Leuthold, P.A. Besse, E. Gamper, M. Dulk, W. Vogt and H. Melchior, "Cascadable MZI all-optical switch with separate ports for data- and control-signals", in Proc. European Conference on Optical Communication (ECOC 1998), 20-24 Sept. 1998, Madrid (Spain), Volume 1, Pages: 463 - 464

[Leu98b] J. Leuthold, P.A. Besse, J. Eckner, E. Gamper, M. Dulk and H. Melchior, "All-optical space switches with gain and principally ideal extinction ratios", IEEE Journal of Quantum Electronics, Volume 34, Issue 4, April 1998, Pages: 622 - 633

[Leu99] J. Leuthold, "Advanced Indium-Phosphide waveguide Mach-Zehnder interferometer all-optical switches and wavelength converters", Hartung-Gorre, Zurich, 1999

[Leu00] J. Leuthold, C.H. Joyner, B. Mikkelsen, G. Raybon, J.L. Pleumeekers, B.I. Miller, K. Dreyer and C.A. Burrus, "100 Gbit/s all-optical wavelength conversion with integrated SOA delayed-interference configuration", Electronics Letters, Volume 36, Issue 13, 22 June 2000, Pages: 1129 – 1130

[Leu01] J. Leuthold, B. Mikkelsen, R.E. Behringer, G. Raybon, C.H. Joyner and P.A. Besse, "Novel 3R regenerator based on semiconductor optical amplifier delayed-interference configuration", Photonics Technology Letters, Volume: 13, Issue: 8, Aug. 2001, Pages: 860 – 862

[Leu02a] J. Leuthold, "Signal regeneration and all-optical wavelength conversion", in Proc. Annual Meeting of the IEEE Lasers and Electro-Optics Society (LEOS 2002), Glasgow (Scotland), 10-14 Nov. 2002, Volume 1, Pages: 107 – 108

[Leu02b] J. Leuthold, G. Raybon, Y. Su, R. Essiambre, S. Cabot, J. Jaques and M. Kauer, "40 Gbit/s transmission and cascaded all-optical wavelength conversion over 1000000 km", Electronics Letters, Volume: 38, Issue: 16, Pages :890 – 8921, Aug 2002

[Leu04] J. Leuthold, D.M. Marom, S. Cabot, J.J. Jaques, R. Ryf and C.R. Giles, "All-optical wavelength conversion using a pulse reformatting optical filter", Journal of Lightwave Technology, Volume 22, Issue 1, Jan. 2004, Pages: 186 – 192

[Leu05] J. Leuthold, L. Moller, J. Jaques, S. Cabot, L. Zhang, P. Bernasconi, M. Cappuzzo, L. Gomez, E. Laskowski, E. Chen, A. Wong-Foy and A. Griffin, "160 Gbit/s SOA all-optical wavelength converter and assessment of its regenerative properties", Electronics Letters, Volume 40, Issue 9, 29 April 2004, Pages: 554 – 555

[Lu00] L. Lu; Y. Dong; H. Wang; W. Cai and S. Xie, "Bit-error-rate performance dependence on pump and signal powers of the wavelength converter based on FWM in semiconductor optical amplifiers", IEEE Photonics Technology Letters, Volume 12, Issue 7, July 2000, Pages: 855 – 857

[Lud96] R. Ludwig, A. Ehrhardt, W. Pieper, E. Jahn, N. Agrawal, H. Ehrke, L. Kuller and H.G. Weber, "40 Gbit/s demultiplexing experiment with 10 GHz all-optical clock recovery using a modelocked semiconductor laser", Electronics Letters, Volume 32, Issue 4, Feb. 1996. Pages: 327 – 329

[Luo98] G. Luo, J.L. Zyskind, J.A. Nagel and M.A. Ali, "Experimental and theoretical analysis of relaxation-oscillations and spectral hole burning effects in all-optical gain-clamped EDFA's for WDM networks", Journal of Lightwave Technology, Volume 16, Issue 4, April 1998, Pages: 527 – 533

[Mah97] D. Mahgerefteh, P. Cho, J. Goldhar and G. l. Burdge, "Technique for suppression of patter dependence in a semiconductor-optical-amplifier wavelength converter", IEEE Photonics technology letters, Volume 9, Number 12, Dec. 1997, Pages: 1583-1585

[Mam99] P. V. Mamyshev and N.A. Mamysheva, "pulse-overlapped dispersion-managed data transmission and intra-channel four-wave mixing", Optics Letters, Volume 24, Number 21, 1999, Pages: 1454-1456

[Man94a] R.J. Manning, D.A.O. Davies, S. Cotter and J.K. Lucek, "Enhanced recovery rates in semiconductor laser amplifiers using optical pumping", Electronics Letters, Volume 30, Issue 10, May 1994, Pages: 787 – 788

[Man94b] R. Manning and D. Davies, "Three-wavelength device for all-optical signal processing," Optics Letters, 15 June 1994, Volume 19, Issue 12, Pages: 889-891

[Mar97a] D. Marcenac and A. Mecozzi, "Switches and frequency converters based on cross-gain modulation in semiconductor optical amplifiers", IEEE Photonics Technology Letters, Volume 9, Issue 6, June 1997, Pages: 749 - 751

[Mar97b] D.D. Marcenac, D. Nesset, A.E. Kelly, M. Brierley, A.D. Ellis, D.G. Moodie and C.W. Ford, "40 Gbit/s transmission over 406 km of NDSF using mid-span spectral inversion by four-wave-mixing in a 2 mm long semiconductor optical amplifier", Electronics Letters, Volume 33, Issue 10, May 1997, Pages: 879 – 880

[Mas90] J.F. Massicott, J.R. Armitage, R. Wyatt, B.J. Ainslie, S.P. and Craig-Ryan, "High gain, broadband, 1.6 μm Er^{3+} doped silica fibre amplifier", Electronics Letters, Volume 26, Issue 20, Sept. 1990, Pages: 1645-1646

[Max02] G. Maxwell, B. Manning, M. Nield, M. Harlow, C. Ford, M. Clements, S. Lucas, P. Townley, R. McDougall, S. Oliver, R. Cecil, L. Johnston, A. Poustie, R. Webb, I. Lealman, L. Rivers, J. King, S. Perrin, R. Moore, I. Reid and D. Scrase, "Very low coupling loss hybrid-integrated all-optical regenerator with passive assembly", In Proc. European Conference on Optical Communcation (ECOC02), 8-12 Sept. 2002, Copenhagen (Denmark), Paper PD-3.5

[Mik01] V. Mikhailov and P. Bayvel, "All-optical multiwavelength clock recovery using integrated semiconductor amplifier array module", Electronics Letters, Volume 37, Issue 4, Feb 2001 Pages: 232 – 234

[Mik03a] V. Mikhailov, "Investigation of high-speed wavelength-division-multiplexed (WDM) optical fibre transmission systems and devices using recirculating loop techniques", PhD thesis submitted to the University of London, 2003

[Mik03b] V. Mikhailov, R.I. Killey, S. Appathurai and P. Bayvel, "Investigation of intra-channel nonlinear distortion in 40Gb/s transmission over standard fibre", Fibre and Integrated Optics, Volume 22, Number 3, June 2003, Pages: 189-195

[Mik96] B. Mikkelsen, S.L. Danielsen, C. Joergensen, R.J.S. Pedersen, H.N. Poulsen and K.E. Stubkjaer, "All-optical noise reduction capability of interferometric wavelength converters", Electronics Letters, Volume 32, Issue 6, March 1996, Pages: 566 - 567

[Mik96] B. Mikkelsen, S.L. Danielsen, C. Joergensen, R.J.S. Pedersen, H.N. Poulsen and K.E. Stubkjaer, "All-optical noise reduction capability of interferometric wavelength converters", Electronics Letters, Volume 32, Issue 6, 14 March 1996 Pages: 566 – 567

[Mor87] Morris P. Kesler and E.R. Ippen, "Subpicosecond gain dynamics in GaAlAs laser diodes", Applied Physics Letters, Volume 51, Number 22, Nov. 1987, Pages: 1765-1767

[Mor94] J. Mørk and A. Mecozzi; "Response function for gain and refractive index dynamics in active semiconductor waveguides", Applied Physics Letters, Volume 65, Issue 14, 3 Oct. 1994, Pages: 1736-1738

[Mor96] T. Morioka, H. Takara, S. Kawanishi, O. Kamatani, K. Takiguchi, K. Uchiyama, M. Saruwatari, H. Takahashi, M. Yamada, T. Kanamori and H. Ono, "100Gb/s x 10 channel OTDM/WDM Transmission using a single super-continuum WDM source", in Proc. Optical Fiber Communication Conference (OFC96), 25 Feb. - 1 March 1996, San Jose (USA), Paper 21.1

[Mor03] J. Mork, F. Ohman and S. Bischoff, "Analytical expression for the bit error rate of cascaded all-optical regenerators", IEEE Photonics Technology Letters, Volume 15, Issue 10, Oct. 2003 Pages: 1479 – 1481

[Nak98a] S. Nakamura, Y. YUeno and K. Tajima, "Ultrafast (200fs) and high-repetition (10GHz) operations of symmetric Mach-Zehnder all-optical switch", in Proc. International Workshop on Femtosecond Technology (FST 1998), 13-14 Feb. 1998, Tsukuba (Japan), Page: 64

[Nak98b] S. Nakamura, Y. Ueno and K. Tajima, "Ultrafast (200-fs switching, 1.5-Tb/s demultiplexing) and high-repetition (10 GHz) operations of a polarization-discriminating symmetric Mach-Zehnder all-optical switch", IEEE Photonics Technology Letters, Volume 10, Issue 11, Nov. 1998, Pages: 1575 – 1577

[Nak00] M. Nakazawa, "Solitons for breaking barriers to terabit/second WDM and OTDM transmission in the next millennium", IEEE Journal of Selected Topics in Quantum Electronics, Volume 6, Issue 6, Nov. 2000, Pages: 1332 – 1343

[Nak01] S. Nakamura, Y. Ueno and K. Tajima, "168-Gb/s all-optical wavelength conversion with a symmetric-Mach-Zehnder-type switch", IEEE Photonics Technology Letters, Volume 13, Issue 10, Oct. 2001, Pages: 1091 – 1093

[Nak02] S. Nakamura, Y. Ueno and K. Tajima, "Error-free all-optical demultiplexing at 366Gb/s with a hybrid-integrated symmetric-Mach-Zehnder switch", in Proc. Optical Fiber Communication Conference (OFC02), 17-22 March 2002, Anaheim (USA), Paper FD3-1

[Nie03a] M.L. Nielsen, B. Lavigne and B. Dagens, "Polarity-preserving SOA-based wavelength conversion at 40 Gbit/s using bandpass filtering",

	Electronics Letters, Volume 39, Issue 18, 4 Sept. 2003, Pages: 1334 - 1335
[Nie03b]	M.L. Nielsen, M. Nord, M.N. Petersen, B. Dagens, A. Labrousse, R. Brenot, B. Martin, S. Squedin and M. Renaud, "40 Gbit/s standard-mode wavelength conversion in all-active MZI with very fast response", Electronics Letters, Volume 39, Issue 4, 20 Feb. 2003, Pages: 385 – 386
[Nol00]	H. Nolting, "All-optical signal processing devices for photonic networks: toward packet switching"; in Proc. working conference on Optical Network Design and Modelling (ONDM 2000), 7-8 Feb. 2000, Athens (Greece), Pages: 52-83
[Occ02a]	L. Occhi, Y. Ito, H. Kawaguchi, L. Schares, J. Eckner and G. Guekos, "Intraband gain dynamics in bulk semiconductor optical amplifiers: measurements and simulations", IEEE Journal of Quantum Electronics, Volume 38, Issue 1, Jan. 2002, Pages: 54 - 60
[Occ02b]	L. Occhi, "Semiconductor Optical Amplifiers made of Ridge Waveguide Bulk InGaAsP/InP: Experimental Characotirsation and Numerical Modelling of Gain, Phase, and Noise", PhD thesis No.14788, submitted to Eidgenossische Technische Hochschule (Zurich), 2002
[Ohl97]	P. Ohlen and E. Berglind, "Noise accumulation and BER estimates in concatenated nonlinear optoelectronic repeaters", IEEE Photonics Technology Letters, Volume 9, Issue 7, July 1997, Pages: 1011 – 1013
[Ohm05]	F. Ohman, B. Tromborg, J. Mork, A. Aurelius, A. Djupsjobacka, and A. Berntson, "Measurements and Simulations of nonlinear noise redistribution in an SOA", IEEE Photonics Technology Letters, Volume 17, Issue 1, Jan. 2005, Pages: 16 – 18
[Ona96]	H. Onaka, H. Miyata, G. Ishikawa, K. Otsuka, H. Ooi, Y. Kai, S. Kinoshita, M.Seino, H. Noshimoto and T. Chikama, "1.1 Tb/s WDM Transmission over a 150km 1.3μm zero-dispersion single mode fiber", in Proc. Optical Fiber Communication Conferece (OFC96), 25 Feb. - 1 March 1996, San Jose (USA), Paper 19.1
[Pat94]	D.M. Patrick and R.J. Manning, "20 Gbit/s wavelength conversion using semiconductor nonlinearity", Electronics Letters, Volume 30, Issue 3, Feb. 1994, Pages: 252 – 253
[Per94]	J.S. Perino, J.M. Wiesenfield and B. Glance, "Fibre transmission of 10 Gbit/s signals following wavelength conversion using a travelling-wave semiconductor optical amplifier", Electronics Letters, Volume 30, Issue 3, 3 Feb. 1994, Pages: 256 – 258
[Phi98]	I.D. Phillips, A.D. Ellis, J. Thiele, R.J. Manning and A.E. Kelly, "40 Gbit/s all-optical data regeneration and demultiplexing with long pattern lengths using a semiconductor nonlinear interferometer", Electronics Letters, Volume: 34, Issue: 24, Nov. 1998, Pages: 2340 - 2342,
[Pie96]	W. Pieper, K. Weich, R. Ludwig, E. Patzak and H.G. Weber, "All-optical polarisation and wavelength independent 3R signal regenerator", Electronics Letters, Volume 32, Issue 14, 4 July 1996, Pages: 1316 – 1318
[Ple02]	J.L. Pleumeekers, M. Kauer, K. Dreyer, C. Burrus, A.G. Dentai, S. Shunk, J. Leuthold and C.H. Joyner, "Acceleration of gain recovery in

semiconductor optical amplifiers by optical injection near transparency wavelength", IEEE Photonics Technology Letters, Volume 14, Issue 1, Jan. 2002, Pages: 12 - 14

[Pou97] A.J. Poustie, K.J. Blow and R.J. Manning, "Amplitude restoration and storage threshold in an all-optical memory", in Proc. European Conference on Optical Communications (ECOC 1997), 22-25 Sept. 1997, Edinburgh (Scotland), Pages: 69-71

[Ray92] G. Raybon, P.B. Hansen, U. Koren, B.I. Miller, M.G. Young, M. Newkirk, P.P. Iannone, C.A. Burrus, J.C. Centanni and M. Zirngibl, "Two contact, 1 cm long, monolithic extended cavity laser actively mode-locked at 4.4 GHz", Electronics Letters, Volume 28, Issue 24, Nov. 1992, Pages: 2220 – 2221

[Sai87] T. Saitoh and T. Mukai, "1.5 μm GaInAsP traveling-wave semiconductor laser amplifier", IEEE Journal of Quantum Electronics, Volume 23, Issue 6, Jun 1987, Pages: 1010 – 1020

[Sak98] T. Sakamoto, K. Hattori, M. Fukutoku, M. Fukui, M. Jinno and K. Oguchi, "Properties of gain-shifted EDFA (1580 nm-band EDFA) cascades in WDM transmission systems", in Proc. Optical Amplifier and Applications, 1998, Vail (CO), Pages: 88-91

[Sal90] A. A. M. Saleh and I. M. I. Habbab, "Effects of semiconductor-optical –amplifier nonlinearity on the performance of high-speed intensity-modulation lightwave system", IEEE Transaction on Communications, Volume 38, Number 6, June 1990, Pages: 839-846

[Sch01] C. Schubert, S. Diez, J. Berger, R. Ludwig, U. Feiste, H.G. Weber, G. Toptchiyski, K. Petermann and V. Krajinovic, "60-Gb/s all-optical demultiplexing using a gain-transparent ultrafast-nonlinear interferometer (GT-UNI)", IEEE Photonics Technology Letters, Volume 13, Issue 5, May 2001, Pages: 475 – 477

[Sch02] C. Schubert, J. Berger, S. Diez, H.J. Ehrke, R. Ludwig, U. Feiste, C. Schmidt, H.G. Weber, G. Toptchiyski, S. Randel and K. Petermann, "Comparison of interferometric all-optical switches for demultiplexing applications in high-speed OTDM systems", Journal of Lightwave Technology, Volume 20, Issue 4, April 2002, Pages: 618 – 624

[Sch03] L. Schares, C. Schubert, C. Schmidt, H.G. Weber, L. Occhi and G. Guekos, "Phase dynamics of semiconductor optical amplifiers at 10-40 GHz", IEEE Journal of Quantum Electronics, Volume 39, Issue 11, Nov. 2003, Pages: 1394 – 1408

[Sok93] J.P. Sokoloff, P.R. Prucnal, I. Glesk and M. Kane, "A terahertz optical asymmetric demultiplexer (TOAD)", Photonics Technology Letters, Volume 5, Issue 7, July 1993, Pages: 787-790

[Sto91] N. Storkfelt, B. Mikkelsen, D.S. Olesen, M. Yamaguchi and K.E. Stubkjaer, "Measurement of carrier lifetime and linewidth enhancement factor for 1.5-μm ridge-waveguide laser amplifier", IEEE Photonics Technology Letters, Volume 3, Issue 7, July 1991, Pages: 632 - 634

[Stu97] K.E. Stubkjaer, S.L. Danielsen, M. Vaa, B. Mikkelsen, C. Joergensen, H.N. Poulsen, K.S. Jepsen, A. Kloch and P.B. Hansen, "All-optical signal processing with semiconductor amplifiers", in Proc. Optoelectronic & Communications conference (OECC 97), 8-11 July 1997, Seoul (Korea), Pages: 426-427

[Suz93] M. Suzuki, H. Tanaka, N. Edagawa, K. Utaka and Y. Matsushima, "Transform-limited optical pulse generation up to 20-GHz repetition rate by a sinusoidally driven InGaAsP electroabsorption modulator", IEEE Journal of Lightwave Technology, Volume 11, Issue 3, Mar 1993, Pages: 468 - 473

[Sve98] O. Svelto, "Principles of Lasers", Plenum Press, New York, 1998

[Taj93] K. Tajima, "All-optical switch with switching-off time unrestricted by carrier lifetime", Japanese Journal of Applied Physics, Volume 32, Number 12A, Dec. 1993, Pages: L1746-L1749

[Taj95] K. Tajima, S. Nakamura and Y. Sugimoto, "Ultrafast polarisation-discriminating Mach-Zehnder all-optical switch", Applied Physics Letters, Volume 67, Issue 25, Dec. 1995, Pages: 3709-3711,

[Tak90] A. Takada and H. Miyazawa, "30 GHz picosecond pulse generation from actively mode-locked erbium-doped fibre laser", Electronics Letters, Volume 26, Issue 3, Feb. 1990, Pages: 216 – 217

[Thi99] H.J. Thiele, A.D. Ellis and I.D. Phillips, "Recirculating loop demonstration of 40 Gbit/s all-optical 3R data regeneration using a semiconductor nonlinear interferometer", Electronics Letters, Volume 35, Issue 3, Feb. 1999, Pages: 230 – 231

[Tol00] P. Toliver, R.J. Runser, I. Glesk and P.R. Prucnal, "Comparison of three nonlinear interferometric optical switch geometries", Optics Communications, Volume 175, 2000, Pages: 365-373

[Tom03] C. Tombling, C. Michie, I. Andonovic and A.E. Kelly, "Recent advances in semiconductor optical amplifiers", in Proc. Annual Meeting of the IEEE Lasers and Electro-Optics Society (LEOS 2003), 26-30 Oct. 2003, Tucson (USA), Volume 2, Pages: 892 - 893

[Top99] G. Toptchiyski, S. Kindt, K. Petermann, E. Hilliger, S. Diez and H.G. Weber, "Time-domain modeling of semiconductor optical amplifiers for OTDM applications", Journal of Lightwave Technology, Volume 17, Issue 12, Dec. 1999, Pages: 2577 – 2583

[Tsu98] M. Tsurusawa, M. Usami and Y. Matsushima, "New method for reduction of carrier lifetime in semiconductor optical amplifier using assist light", in Proc. International Conference on Indium Phosphide and Related Materials (IPRM 1998), 11-15 May 1998, Tsukuba (Japan), Pages: 258 – 261

[Tsu01] M. Tsurusawa, K. Nishimura and M. Usami, "Novel scheme for reducing the pattern effect in 40 Gbps SOA based all-optical switch utilizing transparent CW assist light", in Proc. IEEE International Conference On Indium Phosphide and Related Materials (IPRM 2001), Nara (Japan), 14-18 May 2001, Pages: 174 – 177

[Tsu02] M. Tsurusawa, K. Nishimura, R. Inohara and M. Usami, "Distinct regeneration capability of 40 Gbit/s signal impaired with amplitude noise and timing jitter using SOA-based all-optical polarization discriminated switch", in Proc. Optical Fiber Communication Conference (OFC 2002), Aneheim (USA), 17-22 Mar. 2002, Paper TuN4

[Tsu03] M. Tsurusawa, K. Nishimura, R. Inohara and M. Usami, "Operation margin of all-optical regenerator at 40-Gbit/s by SOA-based polarization discriminated switch", in Proc. Optical Fiber

Communication Conference (OFC 2003), Atlanta (USA), 23-28 Mar. 2003, Volume 2, Pages: 584-586

[Uen98] Y. Ueno, S. Nakamura, K. Tajima and S. Kitamura, "3.8-THz wavelength conversion of picosecond pulses using a semiconductor delayed-interference signal-wavelength converter (DISC)", IEEE Photonics Technology Letters, Volume 10, Issue 3, March 1998, Pages: 346 – 348

[Uen01] Y. Ueno, S. Nakamura and K. Tajima, "Penalty-free error-free all-optical data pulse regeneration at 84 Gb/s by using a symmetric-Mach-Zehnder-type semiconductor regenerator", IEEE Photonics Technology Letters, Volume 13, Issue 5, May 2001, Pages: 469 – 471

[Uen02] Y. Ueno, M. Takahashi, S. Nakamura, K. Suzuki, T. Shimizu, A. Furukawa, T. Tamanuki, K. Mori, S. Ae, T. Sasaki and K. Tajima, "Control scheme for optimizing the interferometer phase bias in a symmetric-Mach-Zehnder-type all-optical switch", IEEE Photonics Technology Letters, Volume 14, Issue 12, Dec. 2002, Pages: 1692 – 1694

[Uen04] Y. Ueno, "Theoretically predicted performance and frequency-scaling rule of a Symmetric-Mach-Zehnder optical 3R gating", Journal of Optical Commumincations, Volume 229, Jan. 2004, Pages: 253-261

[Usa98] M. Usami, M. Tsurusawa, Y. Matsushima; "Mechanism for the reduction of optical nonlinearity in semiconductor laser amplifier", Applied physics letters, Volume 72, Number 21, May 1998, Pages: 2657-2659

[Wan01] B.C. Wang, L.X.V. Baby, D. Zhou, R.J. Runser, I. Glesk and P.R. Prucnal, "Experimental study on the regeneration capability of the terahertz optical asymmetric demultiplexer", Optics Communications, Volume 199, Issues 1-4, 15 Nov. 2001, Pages: 83-88

[Wat98] S. Watanabe, S. Takeda and T. Chikama, "Interband wavelength conversion of 320 Gb/s (32×10 Gb/s) WDM signal using a polarization-insensitive fiber four-wave mixer", in Proc. European Conference on Optical Communication (ECOC 1998), 20-24 Sept. 1998, Rimini (Italy), Volume 3, Pages: 83 – 87

[Wes87] L.D. Westbrook and M.J. Adams, "Simple expression for the linewidth enhancement factor in direct-gap semiconductor", IEE Proceedings, Volume 134, Pt. J, Issue 4, Aug. 87, Pages: 209-214

[Wie93] J.M. Wiesenfeld, B. Glance, J.S. Perino and A.H. Gnauck, "Wavelength conversion at 10 Gb/s using a semiconductor optical amplifier", Photonics Technology Letters, IEEE Volume 5, Issue 11, Nov. 1993, Pages: 1300 – 1303

[Win05] P. J. Winzer, G. Raybon and M. Duelk, "107-Gb/s Optical ETDM Transmitter for 100G Ethernet Transport", in Proc. European Conference on Optical Communication (ECOC 1905), 25-29 Sept. 1998, Glasgow (Scotland), Volume 3, Pages: 83 – 87

[Wol98] D. Wolfson, S.L. Danielsen, C. Joergensen, B. Mikkelsen and K.E. Stubkjaer, "Detailed theoretical investigation of the input power dynamic range for gain-clamped semiconductor optical amplifier gates at 10 Gb/s", IEEE Photonics Technology Letters, Volume 10, Issue 9, Sept. 1998, Pages: 1241 – 1243

[Wol00a] D. Wolfson, T. Fjelde, A. Kloch, C. Janz, A. Coquelin, I. Guillemot, F. Gaborit, F. Poingt and M. Renaud, "Experimental investigation at 10 Gb/s of the noise suppression capabilities in a pass-through configuration in SOA-based interferometric structures", IEEE Photonics Technology Letters, Volume 12, Issue 7, July 2000, Pages: 837 - 839

[Wol00b] D. Wolfson, A. Kloch, T. Fjelde, C. Janz, B. Dagens and M. Renaud, "40-Gb/s all-optical wavelength conversion, regeneration, and demultiplexing in an SOA-based all-active Mach-Zehnder interferometer", IEEE Photonics Technology Letters, Volume 12, Issue 3, March 2000, Pages: 332 – 334

[Xu05] L. Xu, V. Baby, I. Glesk and P.R. Prucnal, "New description of transmission of an SOA-based Sagnac loop and its application for NRZ wavelength conversion", Optics Communications, Volume 244, Issues 1-6, 3 Jan. 2005, Pages: 199-208

[Yoo98] S.J.B Yoo, "Polarisation independent, multi-channel, multi-format wavelength conversion by difference-frequency generation in AlGaAs waveguides", In Proc. European Conference on Optical Communication (ECOC 1998), 20-24 Sept. 1998, Madrid (Spain), Volume 1, Pages: 653 - 654

[Zho99] D. Zhou, K. Il Kang, I. Glesk and P. R. Prucnal; "An Analysis of Signal-to-Noise Ratio and Design Parameters of a Terahertz Optical Asymmetric Demultiplexer"; Journal of Lightwave Technology, Volume 17, Number 2, February 1999, Pages: 298-307

[Zir94] M. Zirngibl and C.H. Joyner, "High performance, 12 frequency optical multichannel controller", Electronics Letters, Volume 30, Issue 9, Apr. 1994, Pages: 700-701